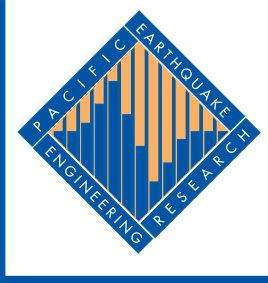

PACIFIC EARTHQUAKE ENGINEERING
RESEARCH CENTER

Performance Characterization of Bench- and Shelf-Mounted Equipment

Samit Ray Chaudhuri

and

Tara C. Hutchinson

Department of Civil and Environmental Engineering
University of California, Irvine

PEER 2005/05
AUGUST 2005

Performance Characterization of Bench- and Shelf-Mounted Equipment

Samit Ray Chaudhuri

and

Tara C. Hutchinson

Department of Civil and Environmental Engineering
University of California, Irvine

PEER Report 2005/05
Pacific Earthquake Engineering Research Center
College of Engineering
University of California, Berkeley

August 2005

ABSTRACT

It is now well recognized by the earthquake engineering community that even during a moderate seismic event extensive nonstructural damage may occur, resulting in a potential threat to life safety and significant economic losses. For equipment and building contents, the primary economic losses may be accrued due to operational failure or repair of the equipment and the associated downtime. In science laboratories or hospitals, equipment are generally placed on the surface of ceramic laboratory benches, which in turn are attached to the structural floor and ceiling systems. Therefore, the sliding response of the equipment and contents are greatly influenced by the acceleration amplification due to a support element (such as a bench-shelf system). This report addresses the above issues within a typical laboratory building. Experiments are conducted to determine the interface frictional behavior and the dynamic characteristics of typical bench-shelf systems. Large system-level shake table experiments are performed to study the bench-shelf and equipment response. Analytical simulations are conducted, and in general good comparison with respect to the experimental results is obtained. Finally, seismic fragility curves for sliding-dominated equipment are developed and provided in simplified form for design purposes. Results from this study are useful for estimating the vulnerability of equipment and contents within typical laboratory or hospital buildings.

ACKNOWLEDGMENTS

This work was supported primarily by the Earthquake Engineering Research Centers Program of the National Science Foundation under award number EEC-9701568 through the Pacific Earthquake Engineering Research (PEER) Center. Any opinions, findings, and conclusions or recommendations expressed in this material are those of the author(s) and do not necessarily reflect those of the National Science Foundation.

The UC Science Building Facilities and Silicon Graphics Incorporated donated hardware for the shake table experiments. Greatly appreciated are the helpful comments and suggestions by the UC Science Test Bed team: Professor Mary Comerio, the Manager; Dr. Paul Sommerville, who provided the ground motions; and Professors Nicos Makris, Khalid Mosalam, and Dr. Keith Porter. The support of the students and staff of the Structural Engineering Test Hall at UC Irvine, particularly Mr. Bob Kazanjy, development engineer, and Ms. Julie Thompson, PEER intern, are also appreciated.

CONTENTS

Page

ABSTRACT . . . iii

ACKNOWLEDGMENTS . . . iv

TABLE OF CONTENTS . . . v

LIST OF FIGURES . . . ix

LIST OF TABLES . . . xix

1 INTRODUCTION AND BACKGROUND . . . 1

1.1 Nonstructural Systems of Interest . . . 2

1.2 Scope of this Report . . . 3

2 PREVIOUS WORK AND MOTIVATION FOR SLIDING RESPONSE STUDIES 5

2.1 Introduction . . . 5

2.2 Literature Review . . . 5

2.3 Sliding Model Using Coulomb Friction . . . 6

2.4 Sliding Response Variability due to Uncertain Parameters (μ_s and μ_k) . . . 7

2.5 Results and Discussion . . . 8

2.6 Summary Remarks . . . 11

3 EQUIPMENT CHARACTERIZATION FOR SEISMIC RESPONSE PREDICTION . . . 13

3.1 Introduction . . . 13

3.2 Background . . . 13

3.3 Experimental Study . . . 14

3.3.1 Inclined Base Tests . . . 14

3.3.2 Horizontal Pull Tests . . . 16

3.4 Determination of μ_s and μ_k . . . 17

3.4.1 Inclined Base Test . . . 17

3.4.2 Horizontal Pull Tests . . . 18

3.4.3 Results and Discussion . . . 18

3.5 Summary Remarks . . . 23

4 DYNAMIC EXPERIMENTS AND RESULTS . . . 25

4.1 Introduction . . . 25

4.2 System-Level Shake Table Tests . . . 25

4.2.1 Equipment of Interest . . . 26

4.2.2 Earthquake Input Motions . . . 26

4.2.3 Instrumentation . . . 28

4.3 Shake Table Results and Discussion . . . 29

4.3.1 Observations during Shake Table Tests . . . 30

4.3.2 Equipment and Contents Measured Response . . . 30
4.3.3 Input Motion Amplification . . . 31
4.3.4 Other Observations from Shake Table Experiments . . . 32
4.4 Component-Level Bench-Shelf Dynamic Characterization . . . 33
4.4.1 Impulse (Tap) Excitation . . . 34
4.4.2 White Noise Excitation . . . 36
4.4.3 Earthquake Excitation . . . 36
4.4.4 Summary of Dynamic Characterization Results . . . 37
4.5 Numerical Modeling and Results . . . 38
4.5.1 Eigenvalue Analysis . . . 40
4.5.2 Acceleration Amplification . . . 41
4.6 Summary Remarks . . . 44
5 BARE SHAKE TABLE EXPERIMENTS . . . 45
5.1 Introduction . . . 45
5.2 Equipment Testing: Experimental Setup and Instrumentation . . . 46
5.3 Equipment Response: Uniaxial and Biaxial Tests . . . 47
5.4 Equipment Response: Analytical-Experimental Comparison and Discussion . . . 48
5.5 Chemical Glassware Testing: Experimental Setup and Instrumentation . . . 56
5.5.1 Seismic Response of Chemical Glassware: Results and Discussion . . . 58
5.6 Summary Remarks . . . 68
6 DEVELOPMENT OF SEISMIC FRAGILITY CURVES . . . 71
6.1 Introduction . . . 71
6.2 System and Parameters Considered . . . 72
6.2.1 Ground Motions Selected . . . 72
6.2.2 Numerical Model of a Representative Science Building . . . 72
6.3 Probabilistic Formulation . . . 74
6.4 Results and Discussion . . . 75
6.4.1 Effect of Variability of Support Structure . . . 79
6.5 Development of Simplified Fragility Curves . . . 81
6.6 Summary Remarks . . . 83
7 CONCLUSIONS AND FUTURE WORK . . . 85
7.1 Conclusive Findings . . . 85
7.2 Recommendations for Future Work . . . 86
REFERENCES . . . 87
APPENDIX A GROUND MOTIONS USED FOR MOCK-LABORATORY SHAKE TABLE TESTS . . . 91
APPENDIX B EXPERIMENTAL RESULTS . . . 101
B.1 Configuration 1 . . . 101
B.2 Configuration 2 . . . 114

B.3 Configuration 3 127
B.4 Configuration 4 140
APPENDIX C SUMMARY EQUIPMENT RESPONSE FROM BARE SHAKE TABLE STUDY 153

LIST OF FIGURES

Figure Page

1.1 Nonstructural equipment of interest: typical laboratory bench-shelf system and mounted equipment in the UC Science building (courtesy of Professor Mary Comerio). 3

1.2 Illustration of bench-mounted equipment analysis. 4

2.1 Free body diagram of a rigid unattached equipment resting on a bench-top. . . . 7

2.2 Response of rigid unattached equipment with μ_s = 0.4 and ϕ = 50%: (a) relative displacement and (b) relative velocity (Erzincan, Turkey, earthquake, scaled to a hazard level of 2% in 50 years). 9

2.3 Response of rigid unattached equipment subjected to Erzincan, Turkey, earthquake (scaled to a hazard level of 2% in 50 years), in terms of absolute relative (a) maximum displacement and (b) maximum velocity as a function of a range of μ_s and ϕ values. 10

2.4 Deviation in absolute maximum response of a rigid unattached equipment subjected to Erzincan, Turkey, earthquake (scaled to a hazard level of 2% in 50 years), in terms of relative (a) displacement and (b) velocity, as a function of a range of μ_s and ϕ values. 11

2.5 Coefficient of variation (COV) in absolute maximum response of a rigid unattached equipment subjected to Erzincan, Turkey, earthquake (scaled to a hazard level of 2% in 50 years), in terms of relative (a) displacement and (b) velocity as a function of a range of μ_s and ϕ values. 12

3.1 Equipment tested for this study: *Scientific equipment*– (a) Technicon autoanalyzer, (b) Eppendoff centrifuge, (c) large microscope, (d) small microscope; *Computer monitors*– (e) 38 cm diagonal (15″ standard) CRT monitor, (f) 43 cm diagonal (17″ standard) CRT monitor, (g) 48 cm diagonal (19″ standard) CRT monitor; and *Silicon Graphics Inc. (SGI) computer workstations*– (h) Indigo, (i) Indy, (j) Octane. 15

3.2 Photographs of the experimental setup for characterizing the frictional resistance of the equipment: (a) inclined base tests and (b) horizontal pull tests. . . . 17

3.3 Free body diagram for friction experiments performed: (a) inclined base test and (b) horizontal pull tests. 19

3.4 Experimental and parabolic fit to equipment displacement (Technicon autoanalyzer): (a) high velocity and (b) low velocity. 19

3.5 Experimental and parabolic fit to equipment displacement– large microscope: (a) high velocity and (b) low velocity. 21
3.6 Photographs of base conditions for select equipment: (a) Technicon autoanalyzer and (b) large microscope. 21
3.7 Ratio of frictional coefficients $\phi = \frac{\mu_k}{\mu_s}$ versus coefficient of static friction μ_s for the different tests conducted. 24

4.1 Plan layouts of the experimental configurations considered in this study: (a) single bench, longitudinal response, (b) single bench, transverse response, (c) double bench, longitudinal response, and (d) double bench, transverse response (all units in meters). 27
4.2 Photographs of bench-shelf systems on shake table, assembled: (a) single bench, subjected to transverse shaking – Configuration 2A and (b) double bench subjected to longitudinal shaking – Configuration 3A, and connection details: (c) during construction (hanging upper shelves and assembling bench), (d) base attachment condition and (e) connection of unistruts at lateral supports. 28
4.3 Elastic five percent damped acceleration response spectra for the earthquake motions used in this study: (a) GM-3–GM-6 and (b) GM-7–GM-10. 29
4.4 Photographs of final position of a piece of equipment due to simulated seismic loading: (a) pure translation for symmetric equipment, (b) translation and rotation of an unsymmetric equipment, and (c) only observed toppling failure of computer monitor. 30
4.5 Response of a small microscope subjected to GM - 10 in Configuration 1: (a) photograph of equipment and location of passive markers and (b) displacement of bench and relative x-direction displacement time history of the three passive markers placed on the microscope. 31
4.6 Maximum equipment movement (relative to bench surface) versus peak horizontal *bench* acceleration (PHBA) for the (a) analyzer, (b) small microscope, and (c) large microscope, and maximum equipment movement (relative to bench surface) versus peak horizontal *floor* acceleration (PHFA) for the (d) analyzer, (e) small microscope, and (f) large microscope. 32
4.7 Measured time history response at floor (input), bench surface, and shelf within Configuration 4, for base excitation GM - 6: (a) absolute displacement (full duration), (b) absolute displacement (from t = 2 – 5 seconds), (c) absolute acceleration (full duration), and (d) absolute acceleration (from t = 2 – 5 seconds). 33
4.8 Sample mode shapes for a nine-point hammer impact test on a typical bench-shelf system: (a) 1^{st} mode (longitudinal) and (b) 2^{nd} mode (transverse). 35
4.9 Low-amplitude hammer FRFs for Configuration 3, where impact is provided along the (a) longitudinal and (b) transverse directions. 35

4.10 Acceleration transfer functions generated from low-amplitude white noise (base excitation) for (a) Configuration 3 (shaking along longitudinal direction) and (b) Configuration 4 (shaking along transverse direction). 36

4.11 SDOF-fit analysis to earthquake input motion (GM - 3) to generate transfer functions: (a) Configuration 3 and (b) Configuration 4. 37

4.12 Photograph of a typical field laboratory environment. 39

4.13 Idealized lumped-mass model of a fixed-fixed bench-shelf system (all units in cm). 39

4.14 (a) First and (b) second fundamental frequencies, for the single and double bench-shelf systems in the *longitudinal* direction; (c) first and (d) second fundamental frequencies, for the single bench-shelf systems in the *transverse* direction; and (e) first and (f) second fundamental frequencies, for the double bench-shelf systems in the *transverse* direction. 42

4.15 Maximum acceleration amplification Ω for the fixed-fixed case: (a) bench level and (b) shelf level, and pinned-pinned case: (c) bench level and (d) shelf level (mass loading case (iv): bench loaded and shelf half loaded) and summary regression analyses for (e) fixed-fixed and (f) pinned-pinned cases. 43

5.1 Photographs of the bare shake table experiments (uniaxial as noted and biaxial-including vertical component): (a) equipment on bench-top surface and (b) glassware on shelf surface. 46

5.2 Photograph of sensors used in bare shake table experiments. 47

5.3 Photograph of digital measurement system used in bare shake table experiments: (a) camera layout surrounding experiments and (b) passive marker layout for typical equipment. 47

5.4 Maximum relative sliding displacement of *scientific equipment*: (a) Techtonic autoanalyzer, (b) Eppendoff centrifuge, (c) small microscope, and (d) large microscope, for uniaxial and biaxial bare shake table tests. 49

5.5 Maximum relative sliding displacement of *SGI CPUs*: (a) Indy, (b) Indigo, and (c) Octane for uniaxial and biaxial bare shake table tests. 50

5.6 Maximum relative sliding displacement of *computer monitors*: (a) large monitors (19″), (b) medium monitors (17″), and (c) small monitors (15″) for uniaxial and biaxial bare shake table tests. 51

5.7 Comparison of experimental and analytical equipment displacement – SGI Indy subjected to GM - 9. 51

5.8 Comparison of experimental and analytical equipment displacement – SGI Indy subjected to GM - 10. 52

5.9 Measured bench-top acceleration time histories for (a) GM - 9 and (b) GM - 10. 53

5.10 Comparison of experimental and analytical equipment sliding displacement subjected to GM - 10 (for $\mu_k = 1.1 \times 0.315$, $\mu_k = 0.315$ (mean), and $\mu_k = .9 \times 0.315$. 54

5.11 Shake table experimental results and analytical predictions of maximum relative displacement for the SGI Indy equipment: (a) measured relative displacement, (b) percentage deviation in measured relative displacement w.r.t. corresponding mean measured values for each ground motion, and (c) percentage error in predicted relative displacement w.r.t. measured relative displacement. . 55

5.12 Photographs of glassware tests using mock-shelf: (a) front view and (b) side view of assembly. 56

5.13 Photographs of glassware tested: (a) 500 mL flask, (b) 1000 mL flask, and (c) 1000 mL bottle. 57

5.14 Photographs of the bare shake table testing of glassware using shelf surface (uniaxial and biaxial): (a) all empty glassware (b) all water-filled glassware (c) mixed glassware (empty, filled with water and filled with gelatine conditions). . 57

5.15 Displacement response of glassware samples to GM - 10 (Tottori, Kofu 2% in 50 year) record: (a) 500 mL conical flask and (b) 1000 mL bottle. 58

5.16 Summary glassware maximum relative displacement response – *500 mL flask*: (a) empty and (b) water-filled condition. 59

5.17 Summary glassware maximum rocking rotation (rotation about y-axis) response – *500 mL flask*: (a) empty and (b) water-filled condition. 60

5.18 Summary glassware maximum in-plan rotation (rotation about z-axis) response – *500 mL flask*: (a) empty and (b) water-filled condition. 61

5.19 Summary glassware maximum relative displacement response – *1000 mL flask*: (a) empty and (b) water-filled condition. 62

5.20 Summary glassware maximum rocking rotation (rotation about y-axis) response – *1000 mL flask*: (a) empty and (b) water-filled condition. 63

5.21 Summary glassware maximum in-plan rotation (rotation about z-axis) response – *1000 mL flask*: (a) empty and (b) water-filled condition. 64

5.22 Summary glassware maximum relative displacement response – *1000 mL bottle*: (a) empty and (b) water-filled condition. 65

5.23 Summary glassware maximum rocking rotation (rotation about y-axis) response – *1000 mL bottle*: (a) empty and (b) water-filled condition. 66

5.24 Summary glassware maximum in-plan rotation (rotation about z-axis) response – *1000 mL bottle*: (a) empty and (b) water-filled condition. 67

5.25 Summary glassware maximum relative displacement response. Glassware are empty, filled with water and filled with gelatine conditions: (a) 1000 mL bottle subjected to uniaxial input, (b) 1000 mL bottle subjected to biaxial input, (c) 500 mL flask subjected to uniaxial input, and (d) 500 mL flask subjected to biaxial input. 68
5.26 Summary glassware maximum relative displacement response – *uniaxial and biaxial input condition*: (a) 1000 mL bottle and (b) 500 mL flask. 69

6.1 Example seismic fragility curves for damage measure DM = 5 cm and range of μ_s and ϕ values. 76
6.2 Effect of μ_s and ϕ on seismic fragility curves, considering different DMs: (a) 5 cm and (b) 10 cm. 76
6.3 Sample seismic fragility curves for damage measure = 50 cm/sec and range of μ_s and ϕ values. 78
6.4 Effect of μ_s and ϕ on seismic fragility curves (high and low bounds study), considering different maximum relative velocity DMs where: (a) DM = 30 cm/s and (b) DM = 50 cm/s. 79
6.5 Fragility curves for DM = 5cm, uncertain μ_s and ϕ, considering m , $m + \sigma$, $m - \sigma$, and deterministic approach (no uncertainties in μ_s and ϕ). 80
6.6 Effect of f_n on the fragility curves for a range of μ_s and ϕ values and considering different maximum relative displacement DMs where: (a) DM = 5 cm and (b) DM = 10 cm. 80
6.7 Effect of ζ_n on the fragility curves for a range of μ_s and ϕ values and considering different maximum relative displacement DMs where: (a) DM = 5 cm and (b) DM = 10 cm. 81
6.8 Parameters of the lognormal distribution, for varying relative maximum displacement magnitudes: (a)–(e) represent median $\tilde{m}$ and (f)–(i) represent coefficient of variation COV respectively for Categories 1–5, considering the mean and mean + standard deviation response. 83

A.1 50% in 50 years Morgan Hill Anderson Dam Down (transverse) (GM - 3) (a) 5% elastic acceleration response spectrum, (b) 5% elastic pseudo velocity response spectrum, (c) 5% elastic displacement response spectrum, (d) Fourier spectrum, (e) acceleration time history, (f) velocity time history, and (g) displacement time history. 92
A.2 50% in 50 years Morgan Hill Halls Valley (transverse) (GM - 4) (a) 5% elastic acceleration response spectrum, (b) 5% elastic pseudo velocity response spectrum, (c) 5% elastic displacement response spectrum, (d) Fourier spectrum, (e) acceleration time history, (f) velocity time history, and (g) displacement time history. 93

A.3 10% in 50 years Kobe, JMA, Japan (longitudinal) (GM - 5) (a) 5% elastic acceleration response spectrum, (b) 5% elastic pseudo velocity response spectrum, (c) 5% elastic displacement response spectrum, (d) Fourier spectrum, (e) acceleration time history, (f) velocity time history, and (g) displacement time history. 94

A.4 10% in 50 years Loma Prieta Corralitos (transverse) (GM - 6) (a) 5% elastic acceleration response spectrum, (b) 5% elastic pseudo velocity response spectrum, (c) 5% elastic displacement response spectrum, (d) Fourier spectrum, (e) acceleration time history, (f) velocity time history, and (g) displacement time history. 95

A.5 10% in 50 years Loma Prieta Gavilan College (transverse) (GM - 7) (a) 5% elastic acceleration response spectrum, (b) 5% elastic pseudo velocity response spectrum, (c) 5% elastic displacement response spectrum, (d) Fourier spectrum, (e) acceleration time history, (f) velocity time history, and (g) displacement time history. 96

A.6 10% in 50 years Tottori, Kofu, Japan (transverse) (GM - 8) (a) 5% elastic acceleration response spectrum, (b) 5% elastic pseudo velocity response spectrum, (c) 5% elastic displacement response spectrum, (d) Fourier spectrum, (e) acceleration time history, (f) velocity time history, and (g) displacement time history 97

A.7 10% in 50 years Loma Prieta Lexington Dam (longitudinal) (GM - 9) (a) 5% elastic acceleration response spectrum, (b) 5% elastic pseudo velocity response spectrum, (c) 5% elastic displacement response spectrum, (d) Fourier spectrum, (e) acceleration time history, (f) velocity time history, and (g) displacement time history. 98

A.8 2% in 50 years Tottori, Kofu, Japan (transverse) (GM - 10) (a) 5% elastic acceleration response spectrum, (b) 5% elastic pseudo velocity response spectrum, (c) 5% elastic displacement response spectrum, (d) Fourier spectrum, (e) acceleration time history, (f) velocity time history and (g) displacement time history. 99

B.1 (a) Mock-laboratory setup of Configuration 1, (b) equipment tested in Configuration 1A, and (c) equipment tested in Configuration 1B. 102

B.2 Instrument layout for mock-laboratory setup Configuration 1 103

B.3 Configuration 1A: Acceleration (upper four rows) and displacement (lower four rows) time histories for 50% in 50 years Morgan Hill Anderson Dam Down (transverse) (GM - 3). 105

B.4 Configuration 1A: Acceleration (upper four rows) and displacement (lower four rows) time histories for 50% in 50 years Morgan Hill Halls Valley (transverse) (GM - 4). 106

B.5 Configuration 1A: Acceleration (upper four rows) and displacement (lower four rows) time histories for 10% in 50 years Kobe, JMA, Japan (longitudinal) (GM - 5). 107
B.6 Configuration 1A: Acceleration (upper four rows) and displacement (lower four rows) time histories for 10% in 50 years Loma Prieta Corralitos (transverse) (GM - 6). 108
B.7 Configuration 1A: Acceleration (upper four rows) and displacement (lower four rows) time histories for 10% in 50 years Loma Prieta Gavilan College (transverse) (GM - 7). 109
B.8 Configuration 1A: Acceleration (upper four rows) and displacement (lower four rows) time histories for 10% in 50 years Tottori, Kofu, Japan (transverse) (GM - 8). 110
B.9 Configuration 1A: Acceleration (upper four rows) and displacement (lower four rows) time histories for 10% in 50 years Loma Prieta Lexington Dam (longitudinal) (GM - 9). 111
B.10 Configuration 1A: Acceleration (upper four rows) and displacement (lower four rows) time histories for 2% in 50 years Tottori, Kofu, Japan (transverse) (GM - 10). 112
B.11 Configuration 1B: Acceleration time histories of 15” monitor, 17” monitor, and 19” monitor where each row represents GM - 3 through GM - 10. 113
B.12 (a) Mock-laboratory setup of Configuration 2, (b) equipment tested in Configuration 2A, and (c) equipment tested in Configuration 2B. 115
B.13 Instrument layout for mock-laboratory setup Configuration 2. 116
B.14 Configuration 2A: Acceleration (upper four rows) and displacement (lower four rows) time histories for 50% in 50 years Morgan Hill Anderson Dam Down (transverse) (GM - 3). 118
B.15 Configuration 2A: Acceleration (upper four rows) and displacement (lower four rows) time histories for 50% in 50 years Morgan Hill Halls Valley (transverse) (GM - 4). 119
B.16 Configuration 2A: Acceleration (upper four rows) and displacement (lower four rows) time histories for 10% in 50 years Kobe, JMA, Japan (longitudinal) (GM - 5). 120
B.17 Configuration 2A: Acceleration (upper four rows) and displacement (lower four rows) time histories for 10% in 50 years Loma Prieta Corralitos (transverse) (GM - 6). 121
B.18 Configuration 2A: Acceleration (upper four rows) and displacement (lower four rows) time histories for 10% in 50 years Loma Prieta Gavilan College (transverse) (GM - 7). 122

B.19 Configuration 2A: Acceleration (upper four rows) and displacement (lower four rows) time histories for 10% in 50 years Tottori, Kofu, Japan (transverse) (GM - 8). 123
B.20 Configuration 2A: Acceleration (upper four rows) and displacement (lower four rows) time histories for 10% in 50 years Loma Prieta Lexington Dam (longitudinal) (GM - 9). 124
B.21 Configuration 2A: Acceleration (upper four rows) and displacement (lower four rows) time histories for 2% in 50 years Tottori, Kofu, Japan (transverse) (GM - 10). 125
B.22 Configuration 2B: Acceleration time histories of SGI CPUs Indy, Octane and Indigo2 along the direction of shaking where each row represents GM - 3 through GM - 10. 126
B.23 (a) Mock-laboratory setup of Configuration 3, (b) equipment tested in Configuration 3A, and (c) equipment tested in Configuration 3B. 128
B.24 Instrument layout for mock-laboratory setup Configuration 3 129
B.25 Configuration 3A: Acceleration (upper four rows) and displacement (lower four rows) time histories for 50% in 50 years Morgan Hill Anderson Dam Down (transverse) (GM - 3). 131
B.26 Configuration 3A: Acceleration (upper four rows) and displacement (lower four rows) time histories for 50% in 50 years Morgan Hill Halls Valley (transverse) (GM - 4). 132
B.27 Configuration 3A: Acceleration (upper four rows) and displacement (lower four rows) time histories for 10% in 50 years Kobe, JMA, Japan (longitudinal) (GM - 5). 133
B.28 Configuration 3A: Acceleration (upper four rows) and displacement (lower four rows) time histories for 10% in 50 years Loma Prieta Corralitos (transverse) (GM - 6). 134
B.29 Configuration 3A: Acceleration (upper four rows) and displacement (lower four rows) time histories for 10% in 50 years Loma Prieta Gavilan College (transverse) (GM - 7). 135
B.30 Configuration 3A: Acceleration (upper four rows) and displacement (lower four rows) time histories for 10% in 50 years Tottori, Kofu, Japan (transverse) (GM - 8). 136
B.31 Configuration 3A: Acceleration (upper four rows) and displacement (lower four rows) time histories for 10% in 50 years Loma Prieta Lexington Dam (longitudinal) (GM - 9). 137
B.32 Configuration 3A: Acceleration (upper four rows) and displacement (lower four rows) time histories for 2% in 50 years Tottori, Kofu, Japan (transverse) (GM - 10). 138

B.33 Configuration 3B: Acceleration time histories of SGI CPU Indigo2 in three directions where each row represents GM - 3 through GM - 10. 139
B.34 (a) Mock-laboratory setup of Configuration 4 and (b) equipment tested in Configuration 4. 141
B.35 Instrument layout for mock-laboratory setup Configuration 4. 142
B.36 Configuration 4: Acceleration (upper four rows) and displacement (lower four rows) time histories for 50% in 50 years Morgan Hill Anderson Dam Down (transverse) (GM - 3). 144
B.37 Configuration 4: Acceleration (upper four rows) and displacement (lower four rows) time histories for 50% in 50 years Morgan Hill Halls Valley (transverse) (GM - 4). 145
B.38 Configuration 4: Acceleration (upper four rows) and displacement (lower four rows) time histories for 10% in 50 years Kobe, JMA, Japan (longitudinal) (GM - 5). 146
B.39 Configuration 4: Acceleration (upper four rows) and displacement (lower four rows) time histories for 10% in 50 years Loma Prieta Corralitos (transverse) (GM - 6). 147
B.40 Configuration 4: Acceleration (upper four rows) and displacement (lower four rows) time histories for 10% in 50 years Loma Prieta Gavilan College (transverse) (GM - 7). 148
B.41 Configuration 4: Acceleration (upper four rows) and displacement (lower four rows) time histories for 10% in 50 years Tottori, Kofu, Japan (transverse) (GM - 8). 149
B.42 Configuration 4: Acceleration (upper four rows) and displacement (lower four rows) time histories for 10% in 50 years Loma Prieta Lexington Dam (longitudinal) (GM - 9). 150
B.43 Configuration 4: Acceleration (upper four rows) and displacement (lower four rows) time histories for 2% in 50 years Tottori, Kofu, Japan (transverse) (GM - 10). 151

LIST OF TABLES

Table Page

3.1 Details of the equipment tested. 14
3.2 Experimentally determined coefficients of static friction μ_s. 22
3.3 Experimentally determined coefficients of kinetic friction μ_k. 22

4.1 Summary of earthquake motions used for base excitation input to the different bench-shelf systems (motions prepared by Sommerville, 2005). 28
4.2 Summary of experimentally derived dynamic characteristics for the different bench-shelf systems. 38

5.1 Summary of vertical components used as shake table inputs for the biaxial study. 46

6.1 Earthquake motions used for ground level input, representing hazard levels of (a) 50% in 50 years, (b) 10% in 50 years, and (c) 2% in 50 years at the UC Lab Building site (Sommerville, 2005). 73
6.2 Equipment categorized by the base resistance. 82
6.3 Coefficients for simplified $PHFA$-DM relation expressed in Equation 6.4. . . 82

B.1 Description of y-axis nomenclature used for the plots of Configuration 1 (Figures B.3– B.10). Refer to Figure B.2 for location of instruments. 104
B.2 Description of y-axis nomenclature used for the plots of Configuration 2 (Figures B.14– B.21). Refer to Figure B.13 for location of instruments. 117
B.3 Description of y-axis nomenclature used for the plots of Configuration 3 (Figures B.25– B.32). Refer to Figure B.24 for location of instruments. 130
B.4 Description of y-axis nomenclature used for the plots of Configuration 4 (Figures B.36– B.43). Refer to Figure B.35 for location of instruments. 143

C.1 Maximum relative sliding displacement of scientific equipment– *Techtonic Autonalyzer* for different shake table trials in case of uniaxial and biaxial bare table tests. 154
C.2 Maximum relative sliding displacement of scientific equipment– *Eppendoff centrifuge* for different shake table trials in case of uniaxial and biaxial bare table tests. 154
C.3 Maximum relative sliding displacement of scientific equipment– *large microscope* for different shake table trials in case of uniaxial and biaxial bare table tests. 155

C.4 Maximum relative sliding displacement of scientific equipment– *small microscope* for different shake table trials in case of uniaxial and biaxial bare table tests. 155
C.5 Maximum relative sliding displacement of SGI CPU– *Indigo* for different shake table trials in case of uniaxial and biaxial bare table tests. 156
C.6 Maximum relative sliding displacement of SGI CPU– *Indy* for different shake table trials in case of uniaxial and biaxial bare table tests. 156
C.7 Maximum relative sliding displacement of SGI CPU– *Octane* for different shake table trials in case of uniaxial and biaxial bare table tests. 157
C.8 Maximum relative sliding displacement of computer monitors– *19″ monitor* for different shake table trials in case of uniaxial and biaxial bare table tests. 157
C.9 Maximum relative sliding displacement of computer monitors– *17″ monitor* for different shake table trials in case of uniaxial and biaxial bare table tests. . . 158
C.10 Maximum relative sliding displacement of computer monitors– *15″ monitor* for different shake table trials in case of uniaxial and biaxial bare table tests. 158

1 Introduction and Background

The overall performance of buildings, bridges, and other civil infrastructure subjected to natural hazards such as earthquakes and wind has dramatically improved over the years due to increased understanding of both component and system behavior. Although the primary structure may perform fairly well, it is now well recognized that extensive nonstructural damage may occur, resulting in potential threat to life safety and in significant economic losses. For equipment and building contents, the primary economic losses may be accrued due to operational failure or repair of the equipment itself and the associated downtime. The recent 2001 Nisqually earthquake in Washington state provided a vivid example of this, where most modern building structures performed well structurally, while significant nonstructural damage was observed (EERI, 2001b). Nonstructural damage and subsequent business disruptions resulted in substantial economic losses for the region with a ripple effect causing loss of wages and employment.

Urban regions in other areas of the United States are equally vulnerable. For example, commercial and industrial building disruptions alone are estimated at approximately $1.3 billion (U.S.) for a potential M7.0 scenario earthquake along the Hayward fault in the San Francisco Bay Area (EERI, 1996). Of particular concern are nonstructural elements within buildings that contain hazardous materials. During post-earthquake response, damage to these elements creates difficulties with assessing the status of the interior of the building structure. For example, during the 1994 Northridge earthquake, 387 hazardous material incidents were identified (EERI, 1995). Nearly 60% of these incidents occurred inside laboratories, resulting in an estimated $1.5 million (U.S.) in clean-up expenses. During this event, these incidents caused subsequent interior building damage before rescue crews could identify hazardous areas within the building. At California State University, Northridge, for example, three separate fires ignited due to hazardous material spills, and subsequently destroyed nine science laboratories. Extensive nonstructural and associated secondary damage were observed as a result of this event.

For critical and potentially hazardous equipment, if a design calculation is desired, several approaches are possible. For small, low-aspect ratio equipment, for example, the potential amount of seismic displacement can be determined. To evaluate the magnitude of this displacement in design, a prescribed lateral force is applied to the equipment and displacement is calculated. The estimation of the magnitude of this force for building components may be

determined through procedures outlined in design documents [e.g. FEMA 356 (2002) or CSA (2001)]. However, this magnitude should be a function of the anticipated seismic hazard at the site, and potential maximum acceleration levels imposed at the level where the equipment is located. The motion of interest must propagate through the building and through the support system; therefore, not only are the characteristics of the building important, but also the characteristics of the support.

1.1 NONSTRUCTURAL SYSTEMS OF INTEREST

There are numerous types of nonstructural systems performing various roles within the interior of building structures. However, the focus of this study is on equipment commonly found in hospitals and/or science research laboratories, and specifically small light equipment critical to the buildings' functions. The interior laboratories within these buildings are critical to the occupants and the primary activities the structure supports. A particularly vulnerable example are science laboratories on university campuses. These campuses contain highly concentrated research facilities; therefore damage to their facilities cripples the productivity of the entire campus. On the University of California, Berkeley (UCB) campus, for example, laboratories occupy 30% of the overall usable space on the campus, resulting in 50% of the research being conducted in seven out of 114 buildings. Even more critical is the research supported by these facilities; for the UCB campus Comerio (2000) noted that 72% of the approximately $400 million in research funding per year is concentrated within the science and engineering disciplines. Laboratory contents within these buildings are estimated at $676 million (21% of the total insured assets for the UCB campus) (Comerio, 2003). For a UCB case study building, Comerio and Stallmeyer (2002) found that 98% of all equipment within the building was valued at $1,500–10,000, while the remaining 2% ranged in value from $10,000–1 million. The value in terms of space is between $200–300 per square ft (typical office space is approximately $25 per square ft). Equipment and contents within these laboratories are not only valuable and important to the researchers, but also they often contain hazardous chemicals, posing operational and life-safety threats.

The specific types of equipment housed in these buildings include scientific instruments such as analyzers, microscopes, centrifuges, monitors, and computer workstations. In general, these equipment are short and rigid; therefore, imposed seismic excitation results in a sliding-dominated, rather than a rocking-dominated response. In science laboratories or hospitals, these equipment are generally placed on the surface of ceramic laboratory benches, which in turn are attached to the structural floor and ceiling systems. Since the sliding of the equipment will be initiated when the acceleration at the top of the supporting element overcomes the resistance due to friction between the two surfaces of contact, considering the acceleration amplification due to a support element (such as a bench or shelf furnishing) is very important. However, there has been little fundamental research focused on defining the dynamic characteristics of the varied supports encountered in the field. An example of the equipment of interest in this

Figure 1.1: Nonstructural equipment of interest: typical laboratory bench-shelf system and mounted equipment in the UC Science building (courtesy of Professor Mary Comerio).

study and the common supporting configuration used in the field are shown in Figure 1.1. This system may be analyzed considering a cascade approach, as schematically depicted in Figure 1.2.

1.2 SCOPE OF THIS REPORT

This report is subdivided into seven chapters and includes three appendices with supplemental data. Previous work and the motivation for sliding response studies are discussed in Chapter 2. In addition, the response variability of equipment due to inherent uncertainties in frictional parameters is studied to motivate successive work. Chapter 3 presents experimental equipment-interface characterization results. Mock-laboratory and bare shake table tests with different pieces of equipment and contents are discussed in this chapter. Experimental characterization of typical bench-shelf systems is discussed in Chapter 4. Using a simple numerical model, the general range of frequencies (first and second) of these systems are provided. Experimental results of the equipment and glassware seismic response are presented in Chapter 5 along with analytical comparisons. Seismic fragility curves are developed in Chapter 6 for various sliding-dominated scientific equipment. In this case, the ground input motion is propagated through a representative building to the floors (as shown in Figure 1.2), then through the supporting

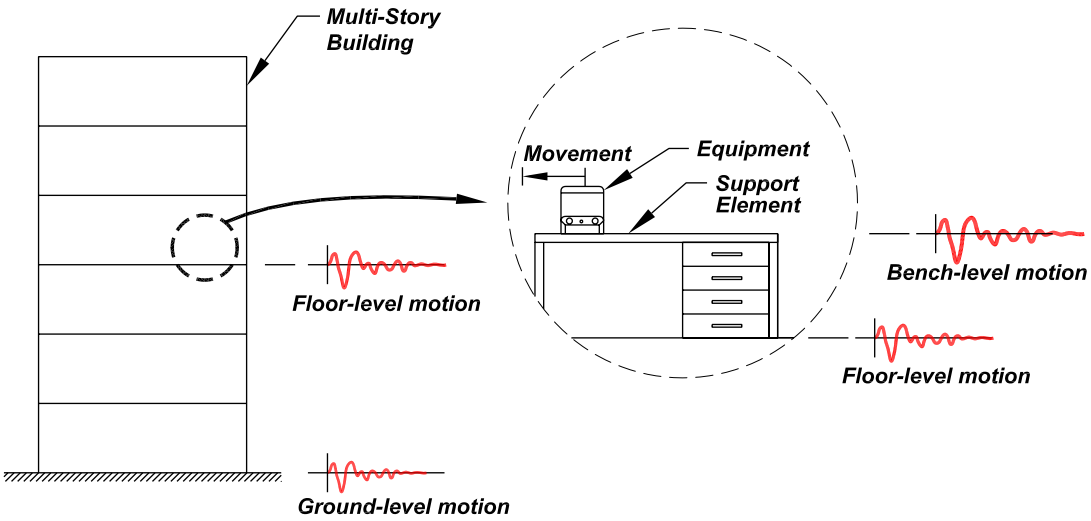

Figure 1.2: Illustration of bench-mounted equipment analysis.

element (in this case, a bench). Finally, estimates of the input motion at the bench-top are obtained and the resulting bench-top motion is used in a sliding friction model to present the sliding response of the bench-mounted equipment. Although, this approach neglects the interaction between the building and bench and also between bench and equipment, considering the low mass of the equipment and bench, relative to the structure, this assumption is reasonable. Finally, conclusions and future work are discussed in Chapter 7. Appendices provide details regarding the ground motions used (Appendix A) and additional shake table experimental results (Appendix B and Appendix C).

2 Previous Work and Motivation for Sliding Response Studies

2.1 INTRODUCTION

The sliding response of rigid bodies depends on the interface parameters, which can be characterized by the coefficients of static and kinetic friction (μ_s and μ_k). The sliding of the equipment will be initiated when the acceleration at the top of the supporting element overcomes the resistance due to friction between the two surfaces of contact. Once the body starts moving, the frictional resistance of the body depends on the coefficient of kinetic friction. This phenomena can be modeled using the concept of Coulomb friction. For the equipment-interface situation of interest in this study, experimental results (which are presented later) indicate that the response of these bench-mounted equipment may vary significantly for a particular ground motion. In addition, a large variation of μ_s and μ_k inherently exists between even similar equipment types. Even with an individual piece of equipment, the coefficient of static friction μ_s, will vary, depending upon the testing technique applied in its determination, for example between an inclined base and pull testing approach. Similar observations were made by Chong and Soong (2000). Therefore, it is very important to study the effect of the uncertainty of frictional parameters on the body's sliding response.

In this chapter, beginning with the governing equations of motion, the sliding response variability for a piece of equipment supported on a bench is studied. The focus of this chapter is placed on understanding the variability of sliding response due to known uncertainty in the coefficients of friction when subjected to an input ground motion.

2.2 LITERATURE REVIEW

The analytical formulation describing the fundamental equations of motion for rigid unattached bodies was presented by Shenton and Jones (1991). In later work, the authors investigate the criteria for sliding and rocking and sliding-rocking of rigid body modes (Shenton, 1996). Shao and Tung (1999) cast the problem into a statistical formulation, studying the mean and standard deviation of sliding relative to a rigid base considering an ensemble of 75 real earthquake motions. This work also considered the probability of overturning and rocking for rigid bodies. Similarly, Choi and Tung (2002) consider the sliding behavior of a freestanding rigid body under the action of base excitation. The objective of this study was to estimate the amount of

sliding when a rigid body is subjected to a real earthquake motion. In this context, the work described in Choi and Tung (2002) applies an extension of Newmark's (1965) sliding block analysis, using absolute base spectral displacement rather than maximum velocity, as was done in Newmark (1965).

Studies have reported the effect of sliding response due to both vertical acceleration and base frictional coefficient (e.g., Taniguchi (2002), Lopez Garcia and Soong (2003)). Taniguchi (2002), for example, investigated the nonlinear seismic response of freestanding rectangular rigid bodies on horizontally and vertically accelerating rigid foundations. The equations of motion and associated boundary conditions corresponding to commencement and termination of liftoff, slip, and liftoff-slip interaction modes are provided. Applying a large number of time histories, this study found that the responses of the body are sensitive to small changes in the friction coefficient and slenderness of the body, and to the wave properties and intensity of ground motions (Taniguchi, 2002). It was also observed that vertical excitation adds irregularities to the behavior, as it excites or dampens the response depending upon the direction. Recent work described in Lopez Garcia and Soong (2003) provide analytically developed seismic sliding fragility curves using design spectrum compatible time histories. Two different damage measures (DMs) are considered for development of the sliding fragility curves in the study of Lopez Garcia and Soong (2003): (i) excessive relative displacement and (ii) excessive absolute acceleration. This study concluded that the sliding response is very sensitive to the coefficient of friction. It was also observed that neglecting vertical acceleration might lead to unconservative estimates of sliding.

2.3 SLIDING MODEL USING COULOMB FRICTION

If one considers a piece of rigid unattached equipment resting on a bench-top and the bench-top is subjected to a horizontal acceleration of $\ddot{x}(t)$, as shown in Figure 2.1, the free body diagram allows an expression of the movement of the equipment as follows.

$$\mid m_e\ddot{x}(t) \mid \geq \mid \mu_s m_e g \mid \tag{2.1}$$

$$m_e(\ddot{x}(t) + \ddot{u}(t)) = -S(\dot{u}(t))\mu_k m_e g \tag{2.2}$$

where $\ddot{u}(t)$ = horizontal acceleration of the equipment relative to the top of the bench, m_e = mass of the equipment, g = acceleration due to gravity, μ_s and μ_k = coefficients of static and kinetic friction, respectively, between the two surfaces and $S = signum$ function (i.e., $S(z) = z/|z|$ for $z \neq 0$ and $S(z) = 0$ for $z = 0$). Equation 2.1 defines the initiation of sliding and Equation 2.2 describes the equation of motion of the equipment during motion (Shenton and Jones, 1991). From these relations it is clear that the dynamic movement of this piece of equipment will be very sensitive to both μ_s and μ_k. It should be noted that vertical motions have been ignored in the above equations.

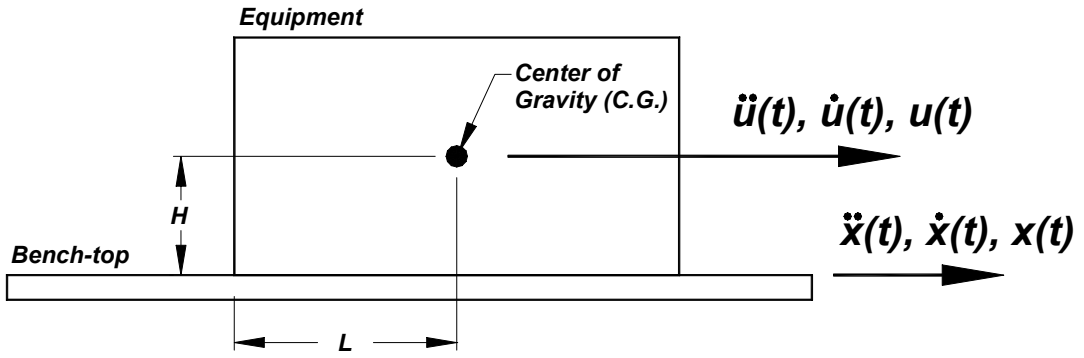

Figure 2.1: Free body diagram of a rigid unattached equipment resting on a bench-top.

2.4 SLIDING RESPONSE VARIABILITY DUE TO UNCERTAIN PARAMETERS (μ_S AND μ_K)

In order to observe the variability of the sliding response due to uncertainty in μ_s and μ_k, only uniaxial seismic excitation is considered herein and a probabilistic approach is used. To account for the uncertainties associated with both the coefficients of static and kinetic friction, μ_s and μ_k are considered as two independent random variables with a uniform distribution. Assuming the uncertainty in μ_s and $\phi(=\frac{\mu_k}{\mu_s})$ is uniformly distributed between their upper and lower limits, UL_{μ_s}, UL_ϕ and LL_{μ_s}, LL_ϕ, respectively, the probability density functions of μ_s and ϕ may be expressed as:

$$p(\alpha) = \frac{1}{UL_\alpha - LL_\alpha} \quad \text{for} \quad LL_\alpha < \alpha < UL_\alpha \tag{2.3}$$
$$= 0, \quad \text{elsewhere}$$

where α may be either μ_s or ϕ. The mean values of μ_s and ϕ can be obtained as $\frac{1}{2}(UL_{\mu_s} + LL_{\mu_s})$ and $\frac{1}{2}(UL_\phi + LL_\phi)$, respectively. Since the coefficients of static and kinetic friction are uncertain, the maximum absolute relative displacement u_{max} and the maximum absolute relative velocity $\dot{u}_{max}$ of the equipment are also uncertain. Therefore, their mean and standard deviation may be determined as follows.

$$m_{u_{max}} = E[U\text{max}] = \int_{-\infty}^{\infty}\int_{-\infty}^{\infty} u\text{max}\, p(\mu_s)p(\phi)\text{d}\mu_s\text{d}\phi \tag{2.4}$$

$$m_{\dot{u}_{max}} = E[\dot{U}\text{max}] = \int_{-\infty}^{\infty}\int_{-\infty}^{\infty} \dot{u}\text{max}\, p(\mu_s)p(\phi)\text{d}\mu_s\text{d}\phi \tag{2.5}$$

$$\sigma_{u\text{max}} = \sqrt{E[U^2_{\text{max}}] - m^2_{u\text{max}}} \tag{2.6}$$

$$\sigma_{\dot{u}\text{max}} = \sqrt{E[\dot{U}^2_{\text{max}}] - m^2_{\dot{u}\text{max}}} \tag{2.7}$$

where

$$E[U^2_{\text{max}}] = \int_{-\infty}^{\infty}\int_{-\infty}^{\infty} u^2_{\text{max}} p(\mu_s)p(\phi)\text{d}\mu_s\text{d}\phi \tag{2.8}$$

$$E[\dot{U}^2_{\text{max}}] = \int_{-\infty}^{\infty}\int_{-\infty}^{\infty} \dot{u}^2_{\text{max}} p(\mu_s)p(\phi)\text{d}\mu_s\text{d}\phi \tag{2.9}$$

2.5 RESULTS AND DISCUSSION

In this study, the effects of different coefficients of static and kinetic frictions and the resulting response variability due to uncertainties in these two parameters is considered. To illustrate the variability of the response, the transverse record from the Erzincan, Turkey, earthquake, scaled to a hazard level of 2% in 50 years is used as the floor level input for the following example. The salient properties of this motion are provided in Chapter 6, Table 6.1. The bench-shelf system is considered as a single degree of freedom (SDOF) for these analyses with a fundamental frequency of f_n = 10 Hz and corresponding damping ratio of ζ_n = 10%. The resulting peak bench-top acceleration of this record is 2.5g. A uniform distribution is considered for both the coefficients of kinetic and static friction. A mean m plus 10% is considered as an upper limit, while the m minus 10% is considered as a lower limit for both the coefficients of static and kinetic friction. Figures 2.2 (a) and (b) show the resulting variability in relative sliding response and relative velocity response of a rigid equipment with a mean μ_s = 0.4 and mean ϕ =50%.

It should be noted that the time scale in Figure 2.2 (b) is bracketed between 0–10 seconds for easier interpretation (where at approximately 10 seconds the body was observed to cease sliding). In both Figures 2.2 (a) and (b), the $m + \sigma$ and $m - \sigma$ response, along with the deterministic response, i.e., assuming μ_s and ϕ to be deterministic parameters with their respective mean values, are shown. During nearly the entire response duration, the deterministic response closely matches the mean response. Only in the velocity response, at approximately 8.5 sec, it is observed that the mean relative velocity is not zero, while its deterministic value is zero. During this time, the ground acceleration could not overcome the force due to friction (for the deterministic case). If the ground acceleration, while expressed in g, is less than the coefficient of static friction but more than 90% of the static friction, the deterministic response is zero, whereas the mean response is not zero. This effect is not observed prominently in the relative displacement response [Figure 2.2(a)]. It is also important to note that the $m + \sigma$ and $m - \sigma$ responses deviate significantly from mean values, when considering residual displacement response.

Considering this same ground motion (Erzincan, Turkey, 2% in 50 years hazard level), Figures 2.3(a) and (b) show the relative displacement and velocity response, respectively, for different values of μ_s and ϕ . To generate the data shown in Figure 2.3, increments of μ_s have been selected at 0.01 intervals. Observing Figure 2.3, as the coefficient of static and kinetic friction increases, the peak displacement and velocity responses generally reduce. However, this reduced response is not linear with μ_s, but rather may be approximated as three piece-wise

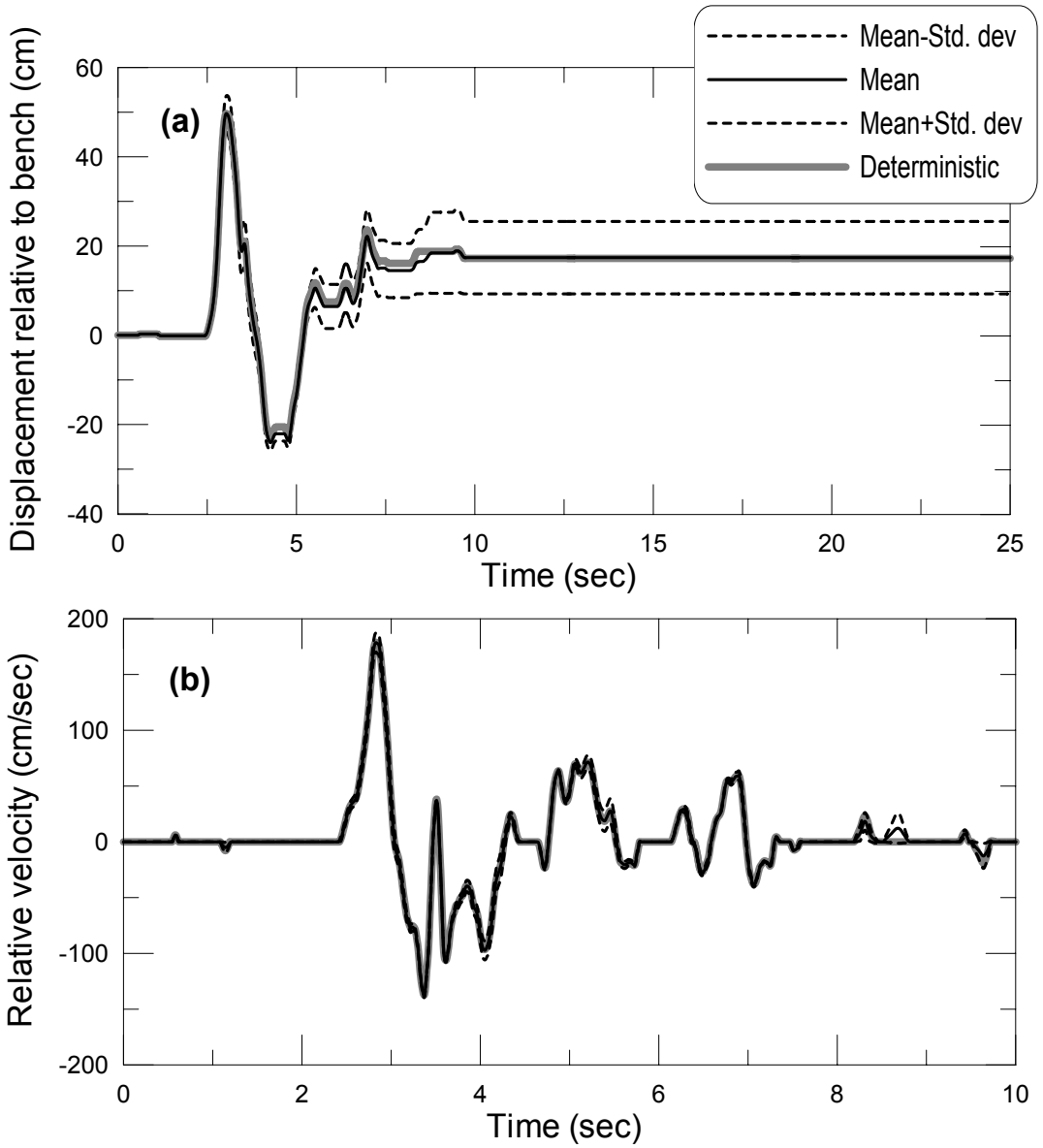

Figure 2.2: Response of rigid unattached equipment with μ_s = 0.4 and ϕ = 50%: (a) relative displacement and (b) relative velocity (Erzincan, Turkey, earthquake, scaled to a hazard level of 2% in 50 years).

linear functions. Figures 2.4(a) and (b) show the absolute value of the percentage deviation for the mean response (displacement and velocity) from the deterministic value, normalized by the mean response. For low values of μ_s this deviation is less, while for higher values of μ_s, the deviation is higher; however, no particular trend is evident.

Figures 2.5(a) and (b) show the coefficient of variation ($COV = \frac{\sigma}{m}$) in percentage for different values of μ_s and ϕ. These plots imply that a 10% variation of μ_s and ϕ on either side of the mean may result in as high as a 45% variation in $m + \sigma$ and $m - \sigma$ relative displacement response and a 27% variation of relative velocity response. The COV is also greater for higher values of μ_s and ϕ for both displacement and velocity. This may be explained by observing that

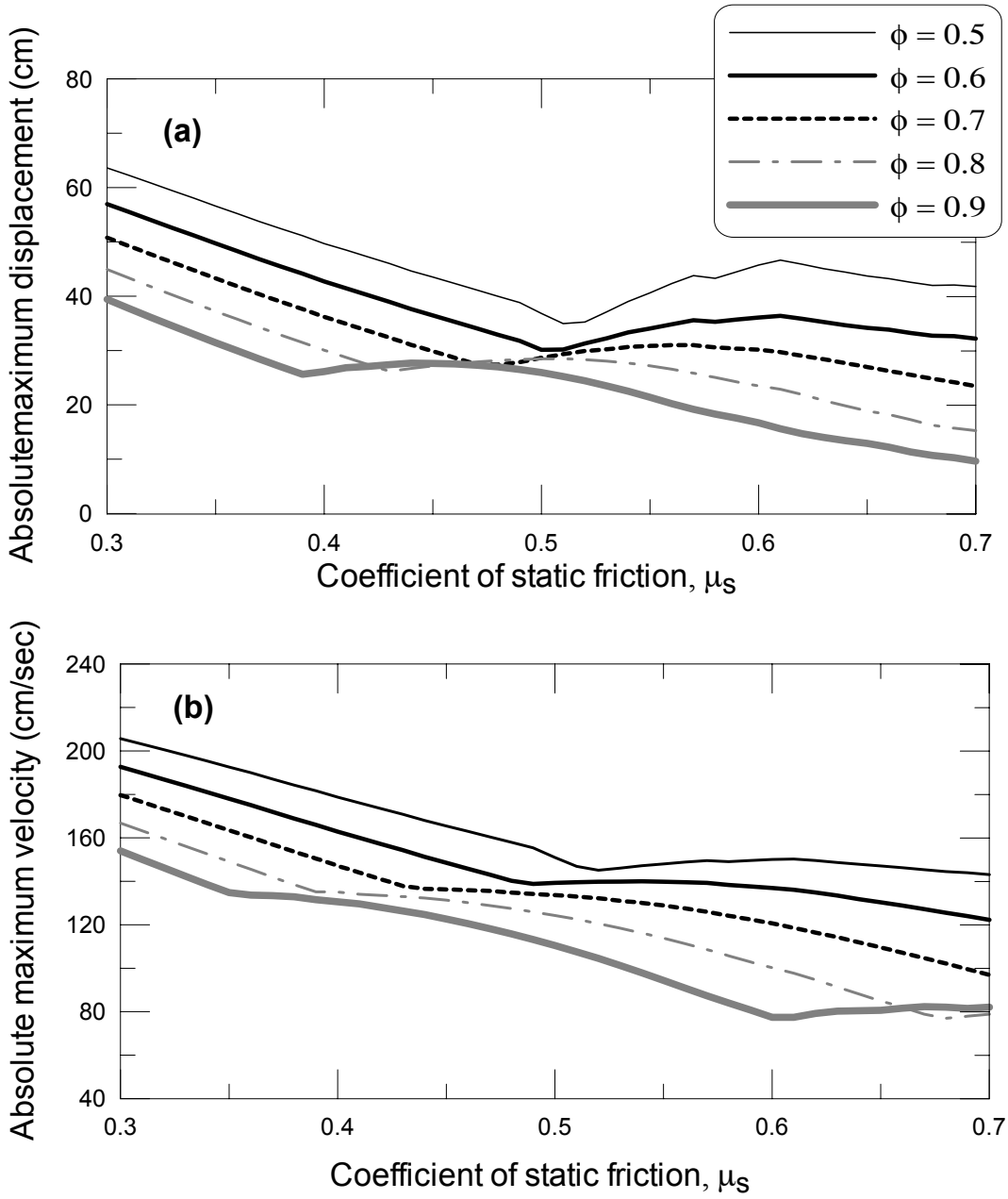

Figure 2.3: Response of rigid unattached equipment subjected to Erzincan, Turkey, earthquake (scaled to a hazard level of 2% in 50 years), in terms of absolute relative (a) maximum displacement and (b) maximum velocity as a function of a range of μ_s and ϕ values.

as μ_s is increasing, the mean m is decreasing at a faster rate than σ. Moreover, the variation is more significant for relative displacement response than relative velocity response, although a similar $\pm 10\%$ uncertainty is taken for both μ_s and μ_k.

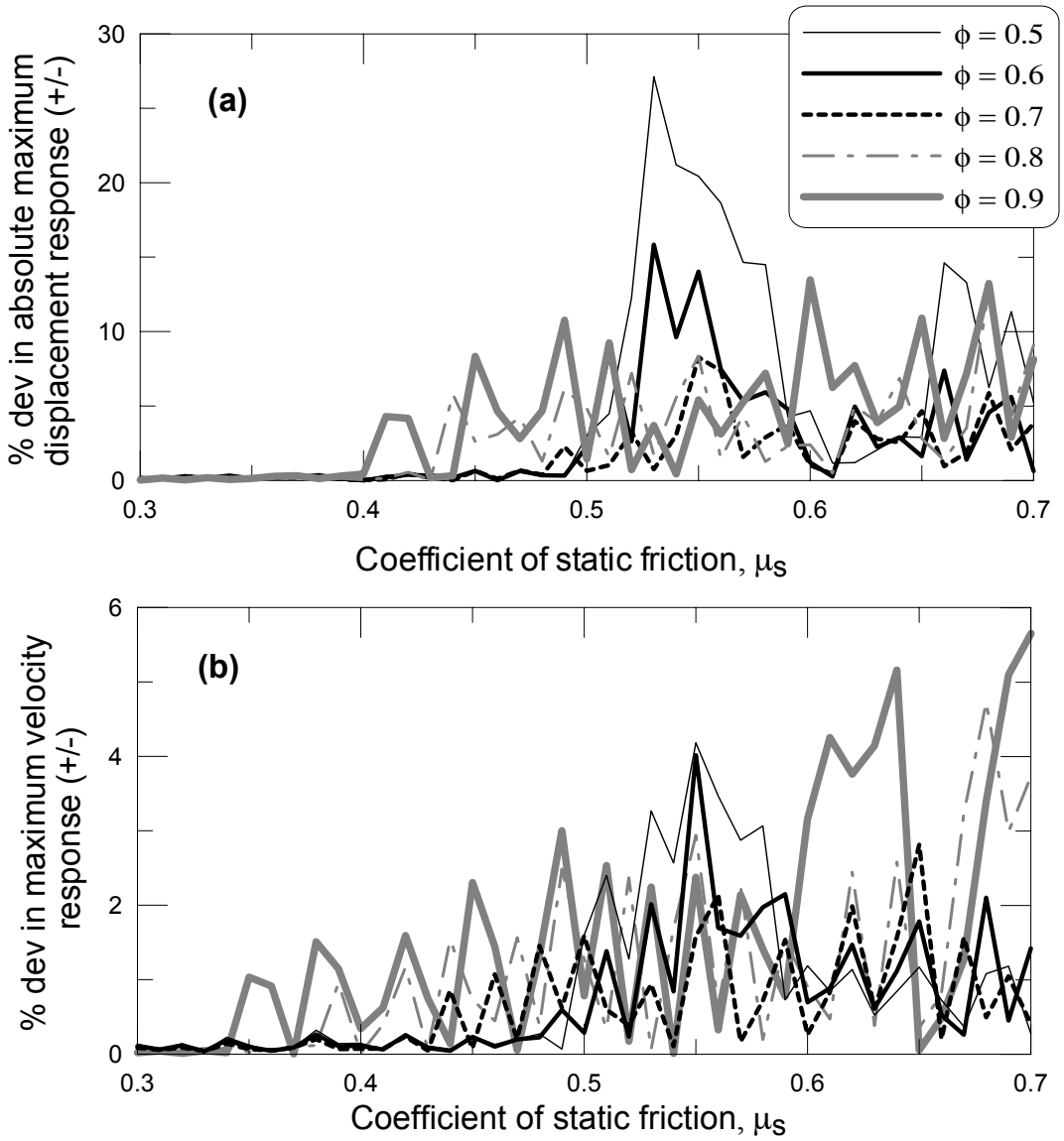

Figure 2.4: Deviation in absolute maximum response of a rigid unattached equipment subjected to Erzincan, Turkey, earthquake (scaled to a hazard level of 2% in 50 years), in terms of relative (a) displacement and (b) velocity, as a function of a range of μ_s and ϕ values.

2.6 SUMMARY REMARKS

In this chapter, the response of a rigid unattached equipment subjected to earthquake excitation is presented using a simple Coulomb sliding friction model and performing nonlinear time history analyses. A range of static and kinetic coefficient of friction values are selected and uncertainty in their estimates is considered. It is observed from these results that the uncertainty in coefficients of static and kinetic friction may lead to significant variation in the maximum and residual sliding response. It will thus be important to experimentally study the interface properties carefully for the different equipment of interest.

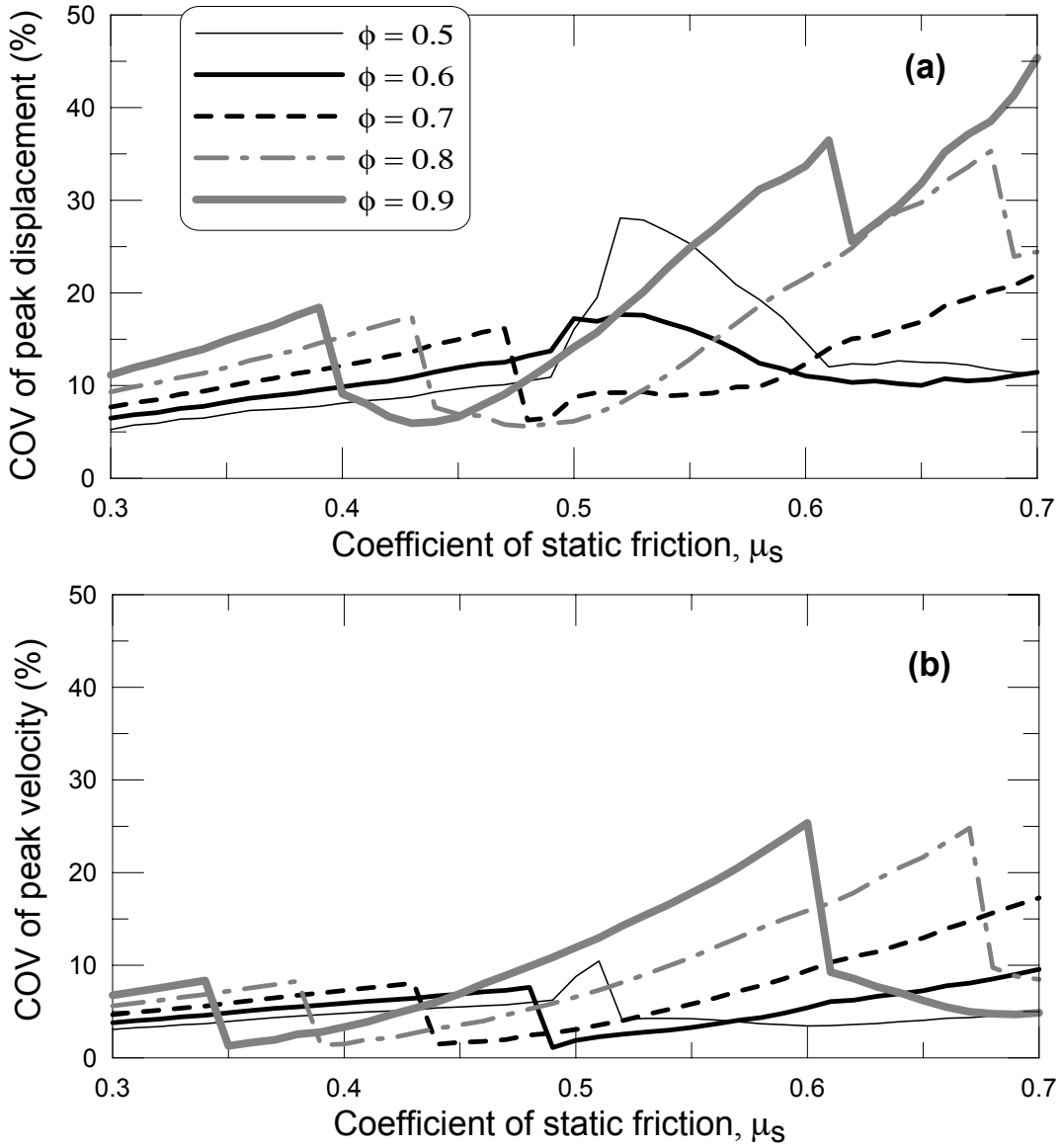

Figure 2.5: Coefficient of variation (COV) in absolute maximum response of a rigid unattached equipment subjected to Erzincan, Turkey, earthquake (scaled to a hazard level of 2% in 50 years), in terms of relative (a) displacement and (b) velocity as a function of a range of μ_s and ϕ values.

3 Equipment Characterization for Seismic Response Prediction

3.1 INTRODUCTION

As mentioned in the previous chapter, careful characterization of interface friction is a fundamentally important aspect of modeling and reasonably capturing the seismic response of a body resting on any surface. In the context of rigid bodies mounted within building structures, the numerous types of elements and interfaces encountered in practice require specific characterization before any modeling assumptions can be undertaken. To this end, in this chapter, the specific problem of characterizing the frictional behavior for a variety of small equipment types typically found in biological and chemical science laboratories is studied using two different methods of testing (an inclined base and a horizontal pull test). Coefficients of static friction μ_s and kinetic friction μ_k are calculated from these experiments and their variability is presented.

3.2 BACKGROUND

Even though it is understood that sliding response of equipment is very sensitive to the coefficients of static and kinetic friction, to the authors' knowledge, no systematic study has been carried out to characterize the behavior for a broad range of equipment types, in particular, light oddly shaped bench-top-mounted equipment. Although the assumption of Coulomb friction is widely accepted, with a variety of generalized functions considered for modeling purposes, the absence of specific testing of these models for different equipment and interface conditions is apparent in the literature. For example, several researchers have developed analytical formulations to represent the stick-slip behavior of dry friction, and their velocity dependence [e.g., Xia (2003); Thomsen and Fidlin (2003); Mostaghel and Davis (1997)]. Experimental studies have also been conducted to observe and measure frictional behavior, with comparisons to analytical models (Ferrero and Barrau, 1997). The behavior commonly studied has typically been of interest to application domains outside of earthquake engineering (e.g., mechanical engineering problems). For example, work by Thomsen and Fidlin (2003) considers the classical "mass-on-moving belt" model for describing friction-induced vibration. The governing law describes friction force that first decreases and then increases smoothly with interface speed.

Friction in the context of seismic response involves limited contact time and random motion. Since almost all the pieces of small equipment considered in this study are fitted with

rubber pads with different properties (geometry, hardness, etc.) at their base, their seismic behavior is not known and warrants evaluation through testing. Moreover, previous studies have indicated that the frictional behavior of rubber is not unique and depends on several factors.

3.3 EXPERIMENTAL STUDY

An experimental study was conducted to investigate the frictional behavior of various types of light unattached oddly shaped equipment and contents commonly found in biological and chemical science laboratories (Ray Chaudhuri and Hutchinson, 2005). Table 3.1 summarizes the equipment and contents tested, which can be divided into three general categories: (i) scientific equipment, (ii) computer monitors, and (iii) Silicon Graphics Inc. (SGI) computer workstations. These equipment were all obtained through donation from an actual science laboratory building on the University of California at Berkeley campus. Pictures of these equipment are provided in Figure 3.1. In general, the equipment and contents tested were less than 40 kg, fairly short, and squat elements, thus dominated in response by their tendency to slide. Two different methods of testing were employed to determine the coefficients of static (μ_s) and kinetic (μ_k) friction, namely, (i) inclined base tests and (ii) horizontal pull tests.

Table 3.1: Details of the equipment tested.

Category	Description	[1]Dimensions (cm)	Mass (kg)
Scientific Equipment	Small Microscope	41.9 x 38.1 x 20.3	10.5
	Large Microscope	45.7 x 55.9 x 39.4	21.7
	Technicon Autoanalyzer	35.6 x 48.3 x 40.5	17.8
	Eppendorf Centrifuge	28.6 x 27.9 x 21.0	5.9
Computer Monitors	38 cm (15” Standard) Diagonal CRT	38.1 x 36.8 x 35.6	14.1
	43 cm (17” Standard) Diagonal CRT	41.9 x 44.5 x 40.6	28.3
	48 cm (19” Standard) Diagonal CRT	44.5 x 58.4 x 45.7	31.1
Silicon Graphics Inc (SGI) Workstations	Indy	7.6 x 40.6 x 34.3	6.8
	Indigo	47.0 x 47.0 x 12.1	18.2
	Octane	29.8 x 40.6 x 27.9	24.5

[1] (depth x width x height)

3.3.1 Inclined Base Tests

In this procedure the coefficient of static and kinetic friction is determined considering two different conditions, (i) a threshold angle and (ii) an angle greater than the threshold angle. For the threshold angle condition, any piece of equipment to be tested is placed on the ceramic bench and the bench is inclined slowly using a hydraulic jack until the element begins moving.

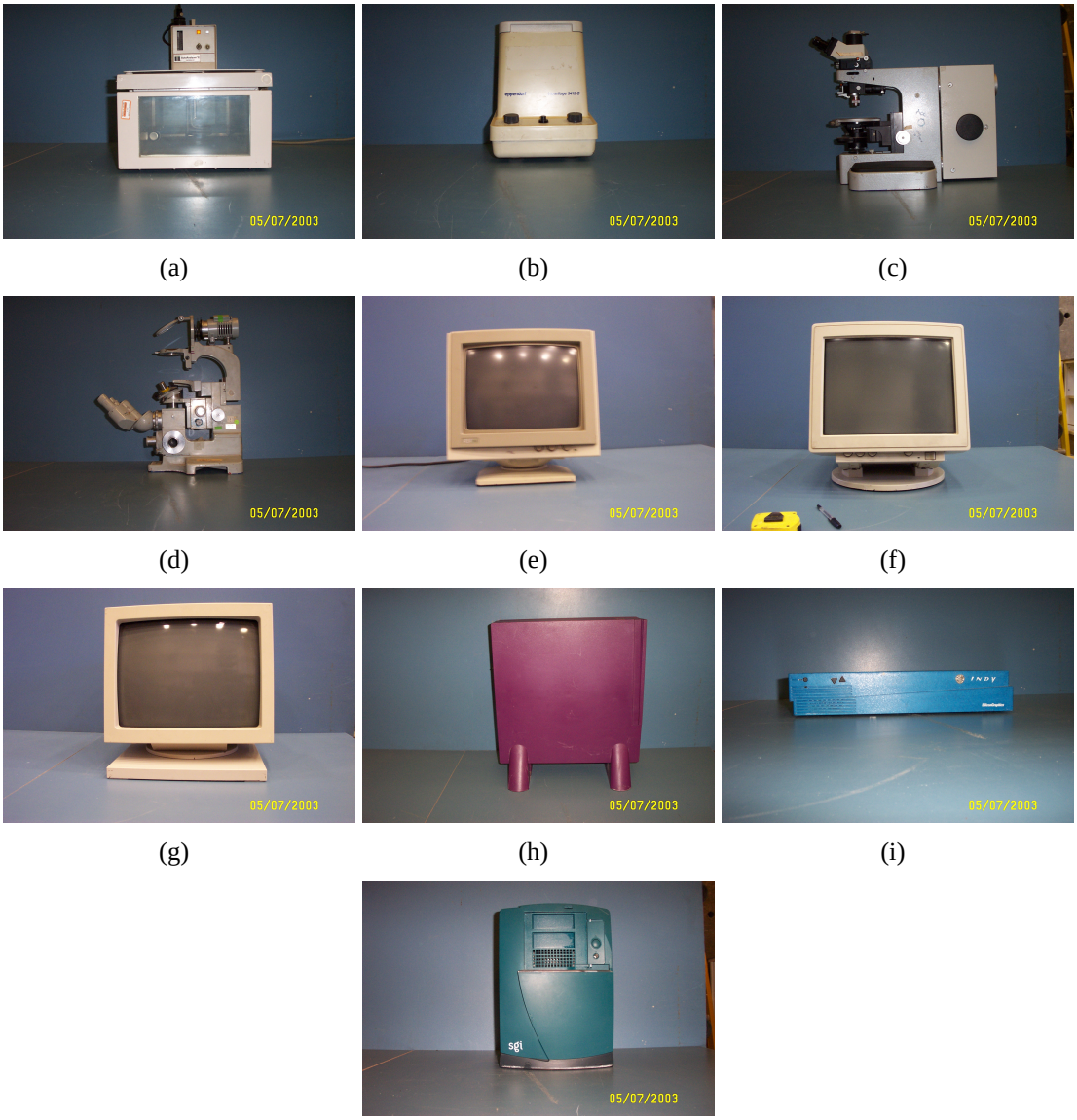

Figure 3.1: Equipment tested for this study: *Scientific equipment*– (a) Technicon autoanalyzer, (b) Eppendoff centrifuge, (c) large microscope, (d) small microscope; *Computer monitors*– (e) 38 cm diagonal (15″ standard) CRT monitor, (f) 43 cm diagonal (17″ standard) CRT monitor, (g) 48 cm diagonal (19″ standard) CRT monitor; and *Silicon Graphics Inc. (SGI) computer workstations*– (h) Indigo, (i) Indy, (j) Octane.

For the greater angle condition, the bench-top is lifted to an angle greater than the observed threshold angle and the equipment is then placed on the bench-top and suddenly released. In this fashion, the movement of the body begins at a velocity greater than in the previous case. Experiments were carried out considering the two cases to study the variability of the coefficient of kinetic friction under different dynamic conditions.

Figure 3.2(a) shows the test setup used for the inclined base test. The movement of the equipment and inclination of bench is measured using a camera (light-based tracking) acqui-

sition system facing the setup. The measurement technique is briefly described in the next section. The advantage of using the light-based tracking system is that it can capture three-dimensional motion of the equipment, in the event the equipment twists, while allowing for multiple measurement points on the object of interest, without cumbersome, potentially conflicting cabling, as typically occurs when using attached transducers. In addition, the equipment is allowed to slide over a length of 140 cm, which would require very long stroke conventional transducers. The inclined experiments were repeated five times for each equipment and for each of the two cases.

Inclined Base Test Measurements

Measurements of the equipment movement with time (in the inclined experiments) were captured using four high-resolution (1024x1024 pixel) charged-couple-device (CCD) cameras mounted on tripods and strategically placed facing the experimental setup. Mounted at the front of each CCD camera was a light-emitting diode (LED) system illuminating the field-of-view (FOV). Special hardware filters were mounted at the aperture of the CCD camera to filter out all light except that reflected from the FOV. C-mount 12.5 mm diameter lenses were used, and the cameras aligned such that each of the four cameras can observe any of the desired points on the specimen at any given time. Retro-reflective (passive) spherical markers discretely located in the FOV are tracked in time in order to obtain positional information. Compared with the mass of the equipment, the mass of the marker elements is negligible. A minimum of four passive markers was placed on each equipment tested (typically in the corners) and four markers were placed on the bench-top to obtain reference positional information. Individual camera data collected are streamed in real-time to a unified break-out box and collectively transferred digitally to a central data station. Data are then transferred via a 10/100 Mbit Ethernet connection to a dedicated 1.8 GHz processing PC. Evaluation of this camera monitoring technique for dynamic seismic movements of a scale steel frame structure is described in Hutchinson and Kuester (2004).

3.3.2 Horizontal Pull Tests

In this procedure, a piece of equipment to be tested is placed over the bench-top, which is kept horizontal. The equipment is then pulled horizontally at approximately its center of gravity (C.G.). Load is applied by placing masses on a load tray connected to a cable, which in turn is attached to the equipment and run through a pulley. A single tension/compression load cell is placed in parallel with the load application - cable assembly to measure the pulling force. Two string potentiometers are used to monitor the movement of the equipment. Details of the experimental setup are shown in Figure 3.2(b). Tests are carried out under two different loading conditions: (i) a threshold load case and (ii) a load greater than the threshold load case. In the first case, the load is increased slowly until it breaks the static frictional resistance between the equipment and bench-top. Once the equipment begins moving, it is allowed to move up to

50 cm, i.e., when the load tray touches the ground. In the second case, a higher load than the previous case is applied suddenly and the body then moves under larger force (and velocity) than the previous case. Five trials are carried out for each case.

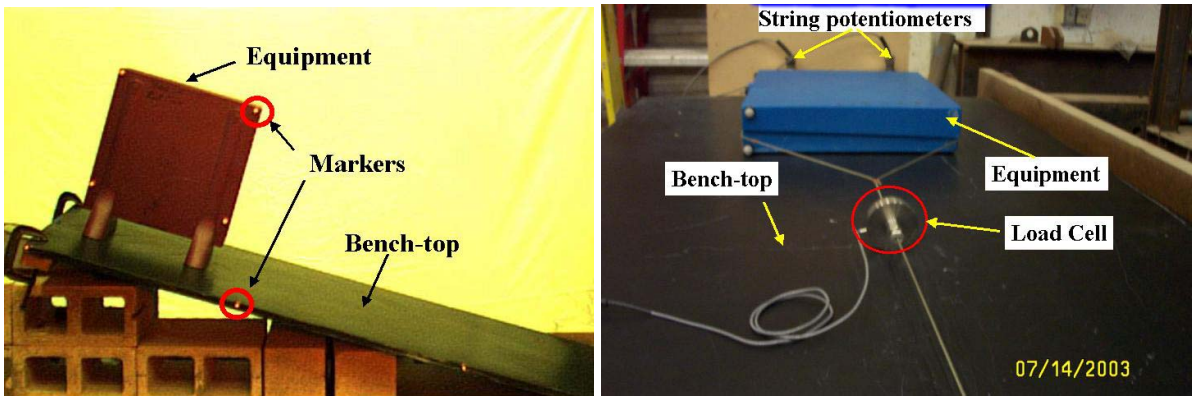

(a) (b)

Figure 3.2: Photographs of the experimental setup for characterizing the frictional resistance of the equipment: (a) inclined base tests and (b) horizontal pull tests.

3.4 DETERMINATION OF μ_S AND μ_K

3.4.1 Inclined Base Test

Considering the coefficient of friction between the equipment and the bench-top surface as a state dependent variable μ, when the equipment is not moving, i.e., under static conditions, $\mu = \mu_s$ and when the equipment is moving, one may state that $\mu = \mu_k$, where μ_k depends on it dynamic condition (e.g., the current velocity, acceleration). The velocity and acceleration, in this case, may be determined from the experimental results. The free body diagram illustrating the loading imposed on the equipment when the bench is in the inclined position, is shown in Figure 3.3(a). The weight of the equipment is $W\ (= m_e g)$, where m_e is the mass of the equipment and g is the acceleration due to gravity, and the bench inclination with respect to horizontal surface is θ. Force equilibrium along the axis perpendicular to the bench-top, results in a normal reaction N that may be expressed as $N = W\cos\theta$. Considering the equation of motion along the direction parallel to the bench, one may write

$$F = F_r + m_e\ddot{x} \tag{3.1}$$

where $\ddot{x}$ = the acceleration of the equipment parallel to the bench-top, in the opposing direction of the frictional force F_r. From Equation 3.1, the coefficient of friction μ may be determined as:

$$\mu = \tan\theta - \frac{\ddot{x}}{g}\sec\theta \tag{3.2}$$

If the angle at which the equipment begins moving is θ, then the coefficient of static friction, μ_s is:

$$\mu_s = \tan\theta \tag{3.3}$$

For all other cases when the body is moving, Equation 3.2 results in the coefficient of kinetic friction μ_k. Therefore, for the threshold angle case, measuring the inclination, one may determine the coefficient of static friction and, from both cases, measuring the angle and acceleration at any time, one may calculate the coefficient of kinetic friction μ_k for that dynamic condition.

3.4.2 Horizontal Pull Tests

Figure 3.3(b) shows the free body diagram of the equipment for the horizontal pull test arrangement. Considering the mass of the equipment as $m_e\,(= W/g)$, and the force by which the equipment is pulled as T, using force equilibrium, the normal reaction may be expressed as $N = W$. Similarly, assuming μ is the state dependent coefficient of friction, the equation of equilibrium along the axis of applied load is:

$$T = F_r + m_e\ddot{x} \tag{3.4}$$

Therefore, the coefficient of friction μ may be expressed as:

$$\mu = \frac{T}{m_e g} - \frac{\ddot{x}}{g} \tag{3.5}$$

where $\ddot{x}$ represents the acceleration of the equipment along the direction of force applied. Therefore, for the first condition considered in the horizontal pull tests, (the threshold load case), the coefficient of static friction μ_s may be determined as:

$$\mu_s = \frac{T}{m_e g} \tag{3.6}$$

The coefficient of kinetic friction for any dynamic state μ_k of any equipment for any load case can be determined from Equation 3.5 by determining the load T and the acceleration $\ddot{x}$.

3.4.3 Results and Discussion

Equipment movement along the bench-top for each run of the inclined base and the horizontal pull tests is plotted with time and observations made regarding their behavior. From these experiments, it is observed that the motion of the equipment is parabolic in nearly all cases. This may be explained by the fact that the opposing frictional force remains the same and the body moves under constant acceleration along the direction parallel to the plane of the bench. In some cases, however, the movement appears to cease (slightly stick) in the middle of the path. This is observed in particular for the inclined base experiments at the critical inclination (i.e., the inclination at which the body begins to move from its rest position). In this situation, a slightly higher inclination is required to instigate the equipment movement again.

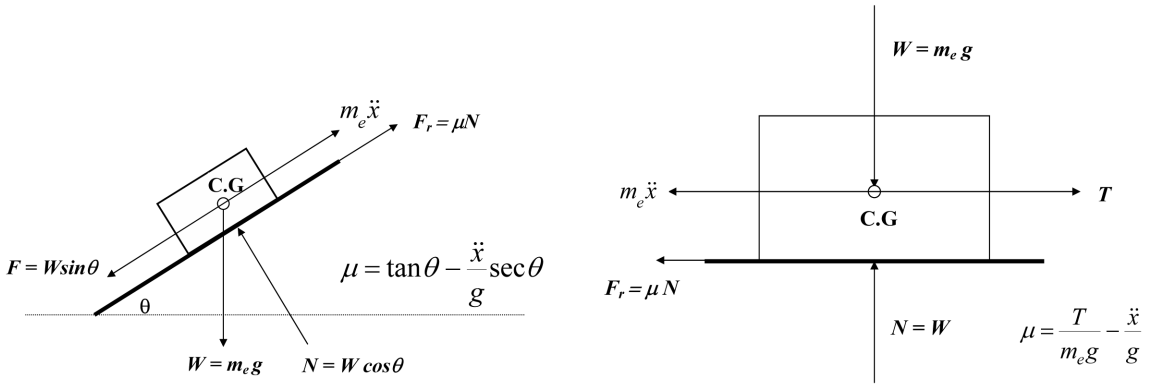

Figure 3.3: Free body diagram for friction experiments performed: (a) inclined base test and (b) horizontal pull tests.

In general, since the observed motion of the equipment is parabolic, the displacement along the axis parallel to the bench-top surface, takes the form:

$$x(t) = \frac{a}{2}(t - t_0)^2 \tag{3.7}$$

where $x(t)$ represents the displacement of the equipment from its original position measured along the axis parallel to bench-top surface (in time), t_0 represents the time instance at which the body begins moving, t is any time instance and a is a coefficient, which may be determined experimentally. Figures 3.4(a) and (b) show the measured and the curve-fitted data, using Equation 3.7 for a typical piece of equipment (Technicon autoanalyzer), for an inclined base experiment. Both the high (part a) and low (part b) velocity cases are shown. For this example, for the high velocity case, the equipment takes approximately 1.6 sec to travel 78 cm, whereas it takes around 3.15 sec to travel approximately the same distance under a low velocity condition.

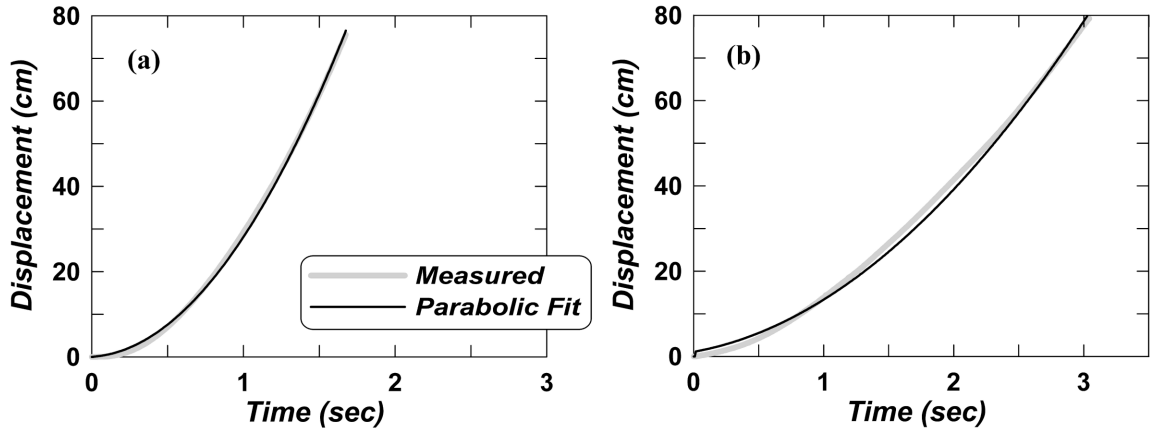

Figure 3.4: Experimental and parabolic fit to equipment displacement (Technicon autoanalyzer): (a) high velocity and (b) low velocity.

It is observed that the parabolic fit curve matches very well with the actual displacement curve describing the motion of the body for this equipment. Therefore, the velocity and acceleration of the equipment can be determined from Equation 3.7, as $a(t - t_0)$ and a, respectively. The coefficient a, represents the constant acceleration of the equipment. This signifies that Coulomb's law of friction holds for this type of equipment. However, this was not always true for all pieces of equipment considered. Among these pieces of equipment, particularly for the large microscope, stick-slip behavior was observed, predominantly for the low velocity cases.

Figures 3.5(a) and (b) show the measured and the curve-fitted displacement, determined using Equation 3.7, for the large microscope. The results are shown for the inclined base method and considering both high (part a) and low (part b) velocity cases. In this case, Figure 3.5(b) illustrates that when the inclination reaches the critical height, the microscope begins moving. However, as it moves, the velocity fluctuates with time. For this example, to travel approximately 130 cm in the low velocity case, the large microscope takes approximately 19 sec. In contrast, for the high velocity case, it takes about 2 sec to travel the same distance. The measured displacement response implies that stick-slip behavior will occur for this piece of equipment when the velocity is comparatively low. The parabolic fit does not hold for this case. In this case, a least-squares fit curve, with the same equation during the duration of movement, may be used to approximate an average a. Moreover, to predict the response for this type of equipment under earthquake excitation, a constant μ_k may not work well when the body moves slowly. To understand the differences in behavior, it is important to observe the base conditions of those equipment. The Autoanalyzer, which exhibited little to no stick-slip behavior, is supported by four, short, stiff thin rubber pads located symmetrically at the base of its rectangular plan, as illustrated in Figure 3.6(a). In contrast, the large microscope is supported by five tall, flexible plastic legs with medium soft rubber at the bottom, placed symmetrically at the four corners of its rectangular plan, as shown in Figure 3.6(b). The taller base pads may create significant variations to sliding response, as they compress and their base area of contact is increased during loading.

The coefficients of static friction determined by the horizontal pull tests and inclined base tests for each of the tested equipment are provided in Table 3.2, including their mean values and percentage of deviation from the mean for both test types. The results indicate that for each piece of equipment the coefficients of static friction evaluated using the inclined base procedure are slightly less than those determined using the horizontal base procedure. In addition, for taller items, such as the microscopes, the difference between the values calculated by either method is greater. This may be because when the equipment is inclined, an overturning moment may cause an uneven pressure distribution at the base, which contributed to an earlier sliding.

After calculating the acceleration using Equation 3.7, the coefficient of kinetic friction is determined by Equations 3.2 and 3.5, for the inclined and pull tests, respectively. Table 3.3 provides the calculated coefficients of kinetic friction for both the inclined base method and the pull test method, and for the two cases mentioned previously. Due to toppling of the equipment

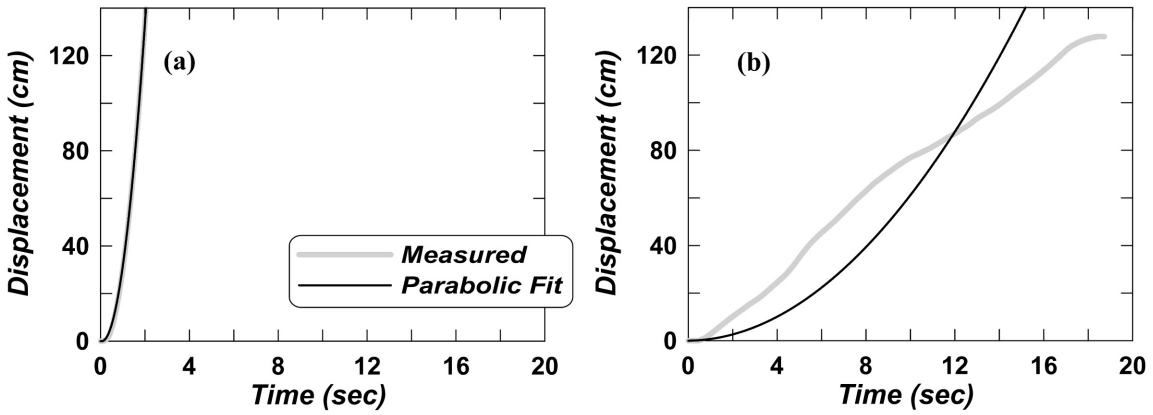

Figure 3.5: Experimental and parabolic fit to equipment displacement– large microscope: (a) high velocity and (b) low velocity.

(a) (b)

Figure 3.6: Photographs of base conditions for select equipment: (a) Technicon autoanalyzer and (b) large microscope.

or load limitation, the coefficient of kinetic friction could not be obtained for select cases. Note that cases I and II denote the high and low velocity cases, respectively.

Representing the coefficient of kinetic friction as some fraction of the coefficient of static friction (i.e., $\mu_k = \phi\mu_s$), Figure 3.7 summarizes the resulting ϕ values as a function of μ_s, for the different tests conducted. Regression lines are calculated through the data values available to illustrate the trends observed. The value of ϕ from these experiments ranges from $1.07 - 0.74$. Theoretically, a value greater than 1.0 (i.e., $\mu_k > \mu_s$) is unrealistic, and these anomalies may be attributed to variability in testing procedures and slight errors in measurement. However, physically for those equipment with a soft rubber base, the compression of the rubber upon instigation of movement may change the contact surface area; this too might be attributed to values of ϕ slightly greater than 1.0.

The regressions shown in Figure 3.7 illustrate that ϕ is always smaller for the inclined base

Table 3.2: Experimentally determined coefficients of static friction μ_s.

Item	μ_S			
	By pulling	By inclined base	Average	% Dev (+/-)
Small Microscope	0.75	0.64	0.70	7.91
Large Microscope	0.37	0.32	0.35	7.25
Technicon Autoanalyzer	0.70	0.62	0.66	6.06
Eppendorf Centrifuge	0.72	0.71	0.72	0.70
38 cm CRT	0.52	0.47	0.50	5.05
43 cm CRT	0.45	0.41	0.43	4.65
48 cm CRT	0.93	0.78	0.86	8.77
Indy	0.37	0.34	0.36	4.23
Indigo	0.68	0.66	0.67	1.49
Octane	0.70	0.61	0.66	6.87

Table 3.3: Experimentally determined coefficients of kinetic friction μ_k.

Item	μ_k			
	By pulling		By inclined base	
	Case I	Case II	Case I	Case II
Small Microscope	0.71	0.63	0.53	0.55
Large Microscope	0.32	0.35	0.26	0.29
Technicon Autoanalyzer	0.64	0.63	0.59	0.60
Eppendorf Centrifuge	0.69	0.71	-	-
38 cm CRT	0.51	0.52	-	-
43 cm CRT	0.44	0.44	-	-
48 cm CRT	0.92	-	-	-
Indy	0.33	0.34	0.29	0.30
Indigo	0.63	0.59	0.58	0.59
Octane	0.68	0.69	0.59	0.60

testing approach, and generally increases with increasing μ_s. However, the friction coefficient ratio ϕ is different for the different base conditions, as well as for different load cases or angles of inclination. As the equipment is subjected to larger loads or higher angles of inclination, beyond the threshold value the value of ϕ increases (case II trend lines are generally higher than for case I). This can be explained by the fact that as the body is subjected to more acceleration, the velocity of the body increases faster, thereby increasing frictional resistance.

Figure 3.7 illustrates that a unique, generalized relation cannot be used to specifically represent this behavior for all pieces of equipment. Although this problem may be cast in a statistical framework, average values may be suitable when analytically evaluating the seismic response for these types of equipment. Such an approach will also simplify the problem.

3.5 SUMMARY REMARKS

In this chapter, the frictional behavior for a variety of small equipment types typically found in biological and chemical science laboratories is studied using two different methods of testing: an inclined base and a horizontal pull test. The coefficients of static μ_s and kinetic friction μ_k are calculated from these experiments and their variability is studied. Testing to determine the coefficient of static friction resulted in a maximum of $\pm 10\%$ deviation from the mean value of μ_s. The coefficient of kinetic friction was found to be dependent on the state of the body and may be as low as 0.74 that of static friction, although it varies depending upon the equipment base type. For higher accelerations, which produce higher velocity, the coefficient of kinetic friction is higher. Although the coefficient of static friction varies by the two methods of testing, and the coefficient of kinetic friction is a state-dependent variable, considering that the mean value may be reasonable for obtaining the seismic response of sliding-dominated equipment. This approach may also simplify the problem of considering time and state-dependent coefficients. However, this needs to be studied and compared with experimental results.

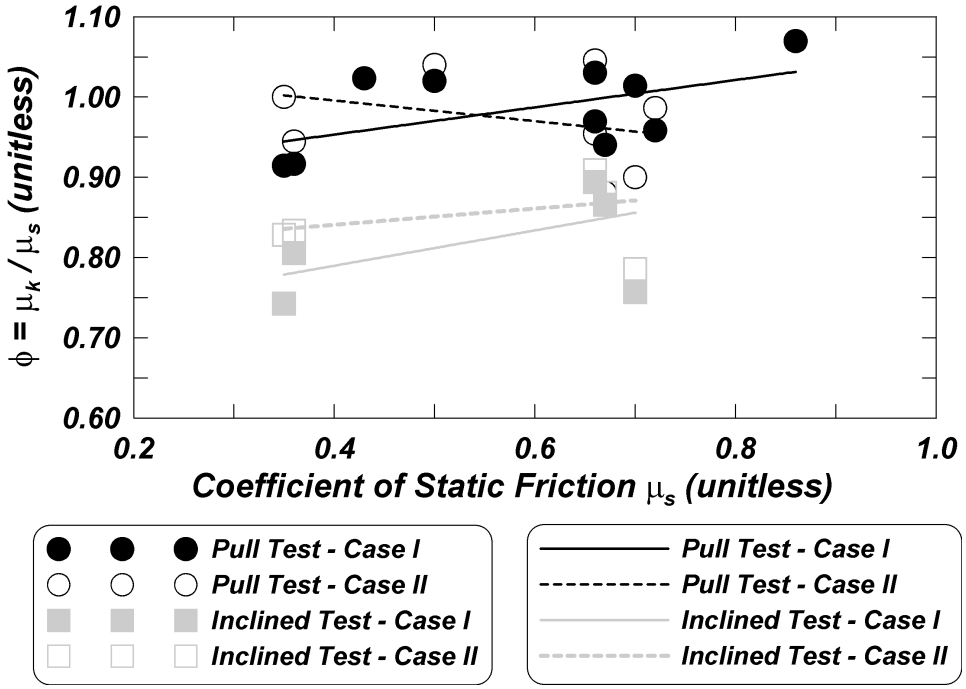

Figure 3.7: Ratio of frictional coefficients $\phi = \frac{\mu_k}{\mu_s}$ versus coefficient of static friction μ_s for the different tests conducted.

4 Dynamic Experiments and Results

4.1 INTRODUCTION

In this chapter, a series of shake table and field experiments are conducted on different bench- and shelf-mounted equipment and contents. The experimental program consisted of both system- and component-level testing. System-level testing involved recreating a mock-laboratory environment within which representative nonstructural systems were tested simultaneously. Component testing involved characterizing the individual components (bench-shelf systems). Transverse and longitudinal bench configurations are considered and a range of light unattached equipment and contents are mounted on these systems. Results from the testing are presented, including measured response for the equipment and contents considered, and summary data from the dynamic characterization of the supporting bench-shelf systems. Testing verifies the importance of determining the potential amplification of motion as imparted through a supporting system, in this case the laboratory bench-shelf system (Hutchinson and Ray Chaudhuri, 2003). Therefore, the investigation of a broader class of systems, with different mass loading and fixity conditions, is conducted using a simple numerical model based on a lumped-mass idealization. Using 22 recorded ground motions applied to these models, maximum acceleration amplification is reported for the parameter space considered.

4.2 SYSTEM-LEVEL SHAKE TABLE TESTS

The experimental setup for the system-level tests consisted of constructing four different integral bench-shelf configurations and assembling them within a mock-laboratory mounted on the shake table. Details for the bench-shelf systems were selected to represent those found in typical biological and chemical laboratories in science buildings (Comerio and Stallmeyer, 2002). Transverse and longitudinal bench configurations, using both single and double (back-to-back) benches were constructed. Unistrut support members were used to connect the bench-shelf system to each other and to a concrete floor and timber ceiling system, with details representative of those used in practice. The plan layout of these four configurations is shown in Figure 4.1. Photographs of two of the configurations considered are shown in Figure 4.2, where (a) shows a single bench aligned in the orthogonal shaking direction and (b) shows a double bench aligned in the longitudinal shaking direction.

Specific details of the framing used to support the benches and shelves are shown in Fig-

ures 4.2(c)–(e). Figure 4.2(c) shows a photograph of the layout of unistrut framing used for support, prior to installation of the bench or shelving system, while Figures 4.2(d) and (e) illustrate the base and middle pinned connections typically used throughout the testing program. At the base of the railing systems the unistruts are seated in a stiff steel-bracket member and anchored into the flooring system [Figure 4.2(d)]. Vertical unistrut rails were placed approximately 0.91 meters apart laterally, and horizontal unistrut rails were placed at 0.81m, 1.67m and 2.2m vertically from the floor, to support the top of the bench and the bottom and top of the shelf system. The connection provided at the lateral railing systems consisted of *U*-shaped brackets and two tightly fitted bolts. These details were designed to match those found in the testbed science building studied by the Pacific Earthquake Engineering Research (PEER) center (Comerio and Stallmeyer, 2002).

4.2.1 Equipment of Interest

Prior to the shake table experiments, different types of light unattached oddly shaped equipment along with other building contents were mounted on the ceramic laboratory bench-top and on the timber shelving systems. Generally two different equipment layouts were considered within any single bench-shelf configuration, and these were differentiated by noting Configuration (number) "A" or "B". The equipment and contents tested in the different configurations are those listed in Table 3.1. Equipment was placed with sufficient edge clearance and was unanchored and free to move on the laboratory bench-top surface. In addition, an array of commonly used chemical glassware was placed on the timber shelving systems, which were fitted with nominal 25 mm tall plexiglas lip. The chemical glassware was tested both empty and filled (with a gelatin substance).

Most of the equipment tested (with the exception of the Indy SGI and the small 38 cm CRT monitor) are heavy at their base, which is typically wide; thus the position of the center of gravity is near to the base of the equipment. The coefficients of static and kinetic friction for each piece of rigid equipment were determined using repeated (horizontal) pull and inclined base experiments (Ray Chaudhuri and Hutchinson, 2005). The results presented in Chapter 3 indicate that μ_s for the equipment considered ranges from 0.35 to 0.86 and ϕ ($= \frac{\mu_k}{\mu_s}$) ranges from 0.74 to 1.06.

4.2.2 Earthquake Input Motions

In terms of earthquake input motions, a total of ten earthquake motions were selected as input motions for the seismic testing. General characteristics of the motions selected are provided in Table 4.1. These motions represent actual ground motions scaled to different seismic hazard levels – representing seismic hazard levels with a probability of 50%, 10% and 2% exceedence over a period of 50 years (Sommerville, 2005). The range of peak ground acceleration (PGA) of these motions is from PGA = 0.13 g to 1.16 g. The maximum peak ground displacement (PGD) of the ten motions is PGD = 19 cm. A few of these motions were measured in the

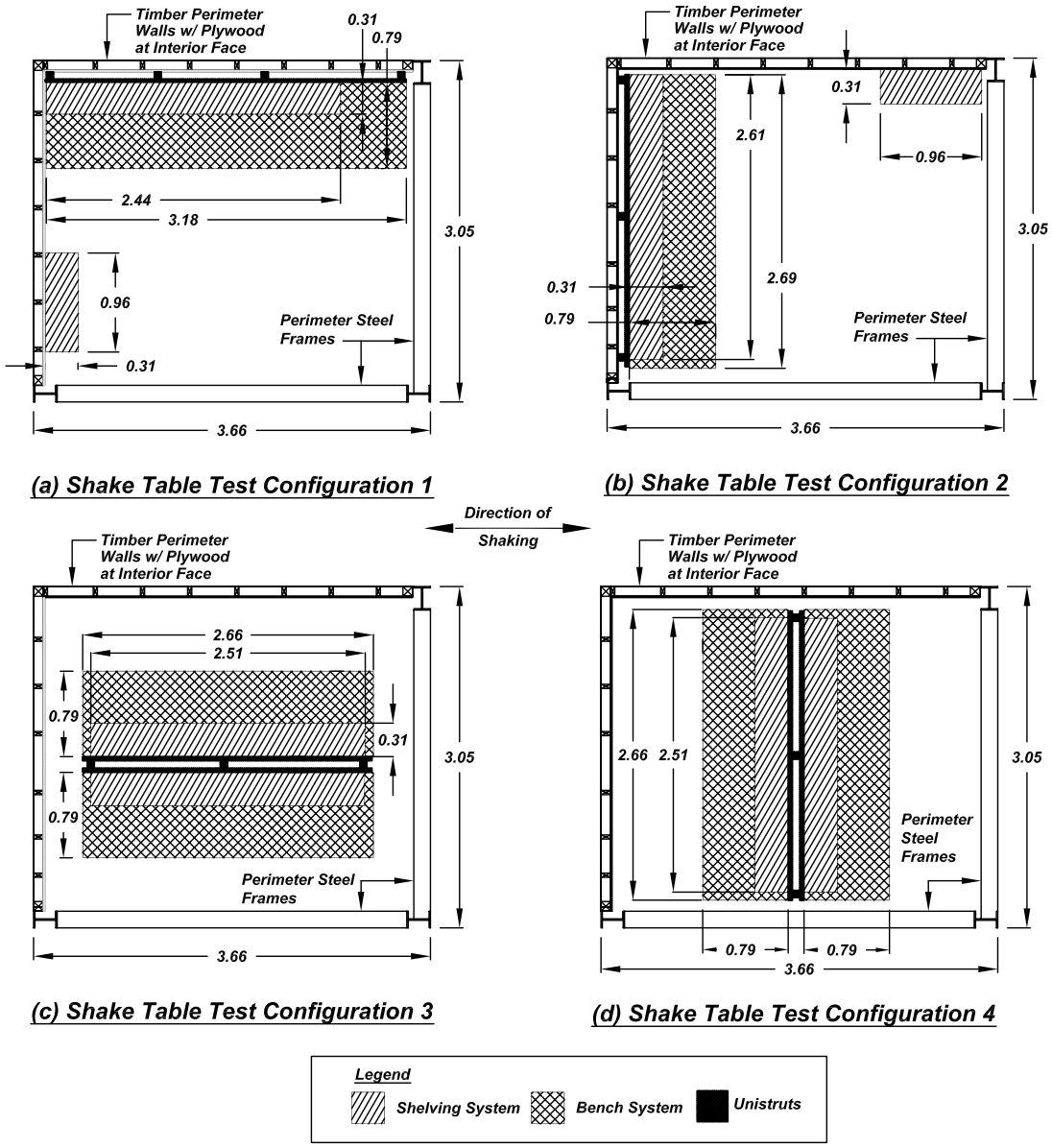

Figure 4.1: Plan layouts of the experimental configurations considered in this study: (a) single bench, longitudinal response, (b) single bench, transverse response, (c) double bench, longitudinal response, and (d) double bench, transverse response (all units in meters).

near-field and thus contain large velocity pulses. Ground motions were selected to envelop the static friction coefficients of the equipment and contents as determined from static bench-top testing. This implies that all of the equipment would slide during the testing. Elastic 5% damped acceleration response spectra for the earthquake input motions considered in this study are shown in Figure 4.3. Summary time histories, Fourier spectra, and response spectra for these motions are provided in Appendix A.

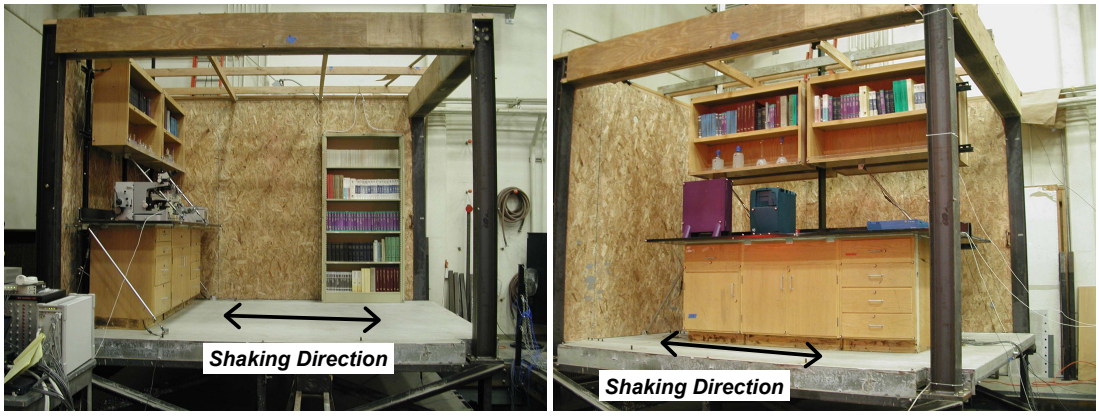

(a) (b)

(c) (d) (e)

Figure 4.2: Photographs of bench-shelf systems on shake table, assembled: (a) single bench, subjected to transverse shaking – Configuration 2A and (b) double bench subjected to longitudinal shaking – Configuration 3A, and connection details: (c) during construction (hanging upper shelves and assembling bench), (d) base attachment condition and (e) connection of unistruts at lateral supports.

Table 4.1: Summary of earthquake motions used for base excitation input to the different bench-shelf systems (motions prepared by Sommerville, 2005).

Input Motion	Earthquake Name and Location of Recording	Date M/D/YY	[1]Station	[2]PGA (g)	[2]PGV (cm/sec)	[2]PGD (cm)
GM-1	Morgan Hill	4/24/1984	Anderson Dam Down (T)	0.13	7	1.7
GM-2	Morgan Hill	4/24/1984	Hall valley (T)	0.18	24	4.8
50% in 50 Year Hazard Level						
GM-3	Morgan Hill	4/24/1984	Anderson Dam Down (T)	0.26	14	3.5
GM-4	Morgan Hill	4/24/1984	Hall valley (T)	0.36	47	9.3
10% in 50 Year Hazard Level						
GM-5	Kobe, Japan	1/17/1995	Kobe JMA (L)	0.44	50	11.0
GM-6	Loma Prieta	10/17/1989	Corralitos (T)	0.53	64	19.0
GM-7	Loma Prieta	10/17/1989	Gavilan College (T)	0.66	63	13.0
GM-8	Tottori, Japan	10/6/2000	Kofu (T)	0.69	33	6.0
GM-9	Loma Prieta	10/17/1989	Lexington Dam (L)	0.84	49	7.3
2% in 50 Year Hazard Level						
GM-10	Tottori, Japan	10/6/2000	Kofu (T)	1.16	55	10

[1] T=Transverse, L=Longitudinal
[2] PGA = peak ground acceleration, PGV = peak ground velocity, PGD = peak ground displacement

4.2.3 Instrumentation

To measure the movement of the equipment, a series of high-speed, high-resolution cameras were used to capture the time-varying displacement of passive retro-reflective markers placed

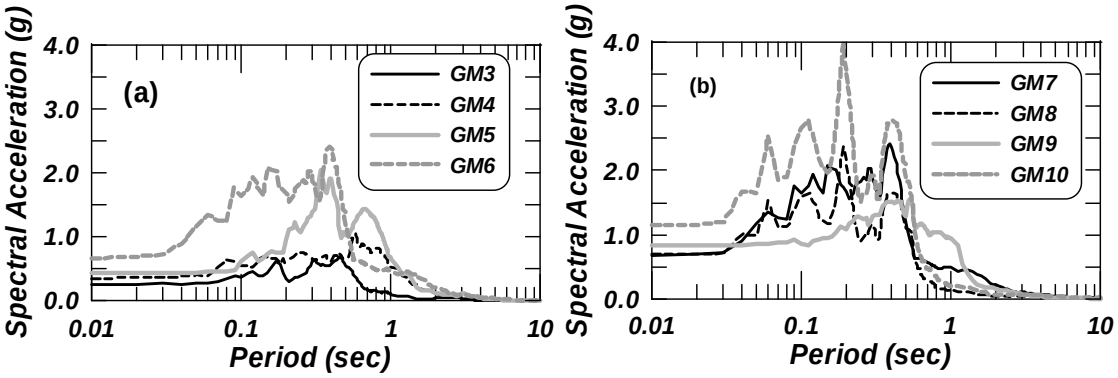

Figure 4.3: Elastic five percent damped acceleration response spectra for the earthquake motions used in this study: (a) GM-3–GM-6 and (b) GM-7–GM-10.

throughout the scene. The method of measurement is similar to that used to capture the inclined base sliding response (Section 3.3.1). In this case, however, a total of six (1024x1024 pixel) charged-couple-device (CCD) cameras, capturing at 120 Hz, were mounted on tripods and strategically placed facing the experimental setup. The passive markers used in the scene are 12.5 mm diameter Styrofoam spheres wrapped in retro-reflective tape. In addition to the camera measurement data, uniaxial and triaxial accelerometers were placed at various locations (on the floor, bench, shelf, and equipment) to measure dynamic accelerations. Inter-story displacement between the floor and bench and between the bench and shelf was also measured using linear variable displacement transducers (LVDTs) placed within a spring-loaded rod assembly. Slip between the bench and concrete floor system was measured using small amplitude linear potentiometers. In total, approximately 32 analog channels were used, typically 7 seismic accelerometers (uniaxial and biaxial) and 15 displacement transducers per experiment, each recorded using a high-speed data acquisition system, sampled at 200 Hz. Instrument layouts for each configuration are shown in Appendix B.

4.3 SHAKE TABLE RESULTS AND DISCUSSION

Shake table results are presented in terms of measured equipment and contents response and bench-shelf system response. General observations made during testing regarding the nonstructural system performance are also discussed. Although very little noise is observed, experimental accelerations are generally processed using a 4^{th} order bandpass butterworth filter, with low and high cut-off frequencies of 0.4 Hz to 15 Hz, respectively. For camera captured data, only minimal processing was required (zero offset and data organization). Additional shake table results are presented in Appendix B.

4.3.1 Observations during Shake Table Tests

During simulated seismic loading, the equipment considered were predominantly observed to slide laterally in the direction of input motion, as shown in Figure 4.4(a). Select equipment, such as the microscopes and centrifuge, due to their unsymmetric mass, were observed to slide and rotate about their supports, in plan, as shown in Figure 4.4(b). One piece of equipment was susceptible to toppling, as shown in Figure 4.4(c). In general, testing began with equipment placed far enough from the bench-top edge to prevent falling from the surface. This was done to assure that the equipment would be useful for subsequent testing, as well as to assure that demands could be measured directly.

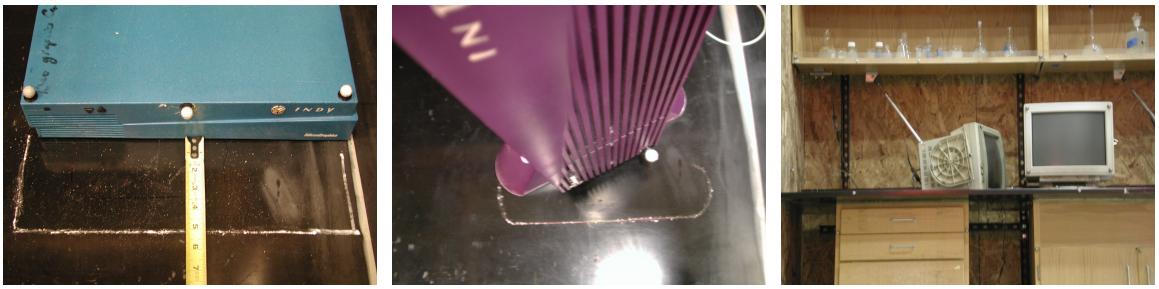

(a) (b) (c)

Figure 4.4: Photographs of final position of a piece of equipment due to simulated seismic loading: (a) pure translation for symmetric equipment, (b) translation and rotation of an unsymmetric equipment, and (c) only observed toppling failure of computer monitor.

4.3.2 Equipment and Contents Measured Response

Of particular importance in these experiments is the maximum sliding displacement experienced by the equipment relative to the bench-top surface. A sample of the measured movement for one of the scientific equipment is shown in Figure 4.5. Part (a) of Figure 4.5 shows the locations of three discrete marker elements placed on a small bifocal microscope and part (b) shows measured response of these three locations, as well as the response at the bench-top surface. The instigation of sliding is clearly observed at time t = 12 seconds. Observation of the movement of these three locations reveal residual (which are also maximum) displacements of varying amounts ($\Delta_{x(res)}$ = 21.5, 23.7, and 26.5 cm, for locations two, three and one, respectively), indicating that the element is rotating in the plane of the bench surface. All other response data for these equipment are provided in Appendix B.

Summary analyses of the measured response of the different scientific equipment considered in this study are shown in Figures 4.6(a)–(f). These results show the maximum displacement of the equipment (relative to the bench surface) versus the maximum acceleration, taken at either the bench surface or the floor surface. Parts (a) through (c) are shown against the peak horizontal bench acceleration ($PHBA$), whereas parts (d) through (f) are shown against

the peak horizontal floor acceleration ($PHFA$). The differences observed in $PHBA$ (a–c) and $PHFA$ (d–f) illustrate the acceleration amplification provided by the bench-shelf system. As anticipated, for these sliding-dominated, acceleration-sensitive equipment, increasing maximum relative displacement is observed with increasing input acceleration. Although there is some scatter in the data, generally below a $PHFA$ of 0.8g, the equipment resting in these three general configurations observed maximum relative sliding of less than 10 cm. In excess of 20 cm maximum relative sliding was observed for $PHFA$ greater than one-g. It is interesting to note, that for a given $PHFA$, the maximum relative displacement experienced by the equipment is not the same as between the different bench-system configurations, illustrating the sensitivity of response to the supporting system.

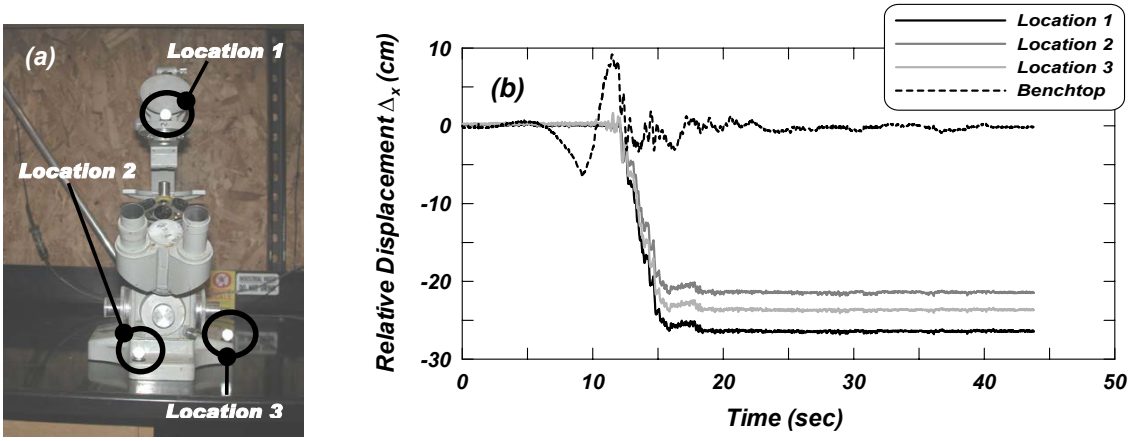

Figure 4.5: Response of a small microscope subjected to GM - 10 in Configuration 1: (a) photograph of equipment and location of passive markers and (b) displacement of bench and relative x-direction displacement time history of the three passive markers placed on the microscope.

4.3.3 Input Motion Amplification

The laboratory benches being considered are typically attached using unistrut railing systems as shown in Figure 4.2, resulting in approximately a pinned support at the floor and ceiling to anchor the bench, thereby creating a system with some flexibility. The result may be that the natural frequency of the laboratory bench lies within the acceleration sensitive zone of the input floor response spectrum, thereby resulting in acceleration amplification. To illustrate the input motion amplification through the bench-shelf system, Figure 4.7 shows the displacement and acceleration response of the floor, bench, and shelf levels. Parts (a) and (c) of this figure show the entire duration of input excitation, while parts (b) and (d) provide a zoomed-in window of time (from t = 2 – 5 seconds) for this same experiment, within which the maximum accelerations were measured. From these figures, it is observed that the bench-shelf system displaces laterally with the floor system as a unit (displacements shown on Figure 4.7(a) and (c) are perfectly overlaid). However, more importantly, it is observed that the acceleration is amplified,

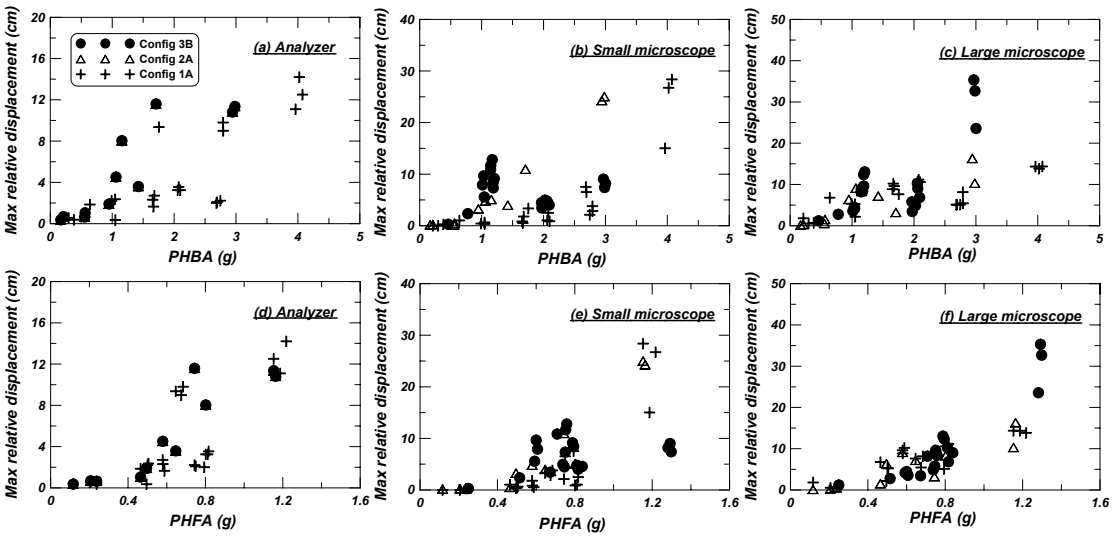

Figure 4.6: Maximum equipment movement (relative to bench surface) versus peak horizontal *bench* acceleration (PHBA) for the (a) analyzer, (b) small microscope, and (c) large microscope, and maximum equipment movement (relative to bench surface) versus peak horizontal *floor* acceleration (PHFA) for the (d) analyzer, (e) small microscope, and (f) large microscope.

from an input acceleration at the floor level of $PHFA$ = 0.69g, to a bench-level acceleration of 1.16g (1.7 times) and to a shelf-level acceleration of 1.39g (2.0 times). It is also noted that the frequency content at the various levels of the bench and shelf becomes narrow banded as the waveform passes through the bench.

4.3.4 Other Observations from Shake Table Experiments

Measurements of bench slip, bench-top and shelf acceleration, bench-shelf drift, and acceleration of equipment are summarized in Appendix B. Observation of the additional data yields the following:

1. The maximum slip between the bottom of the bench cabinet and the floor was approximately 1.3 cm (0.5 inch).

2. The maximum bench level acceleration was approximately 5.0 g and the shelf level acceleration was approximately 5.0 g.

3. The freestanding steel shelf was very unstable when subjected to motion along its short direction. Note that it was removed after GM - 6, Configuration 1A.

4. Although an elevated diaphragm was used as shown in the photographs of Figure 4.2(a), the final floor motion was almost the same as the shake table motion, suggesting that the floor system was stiff.

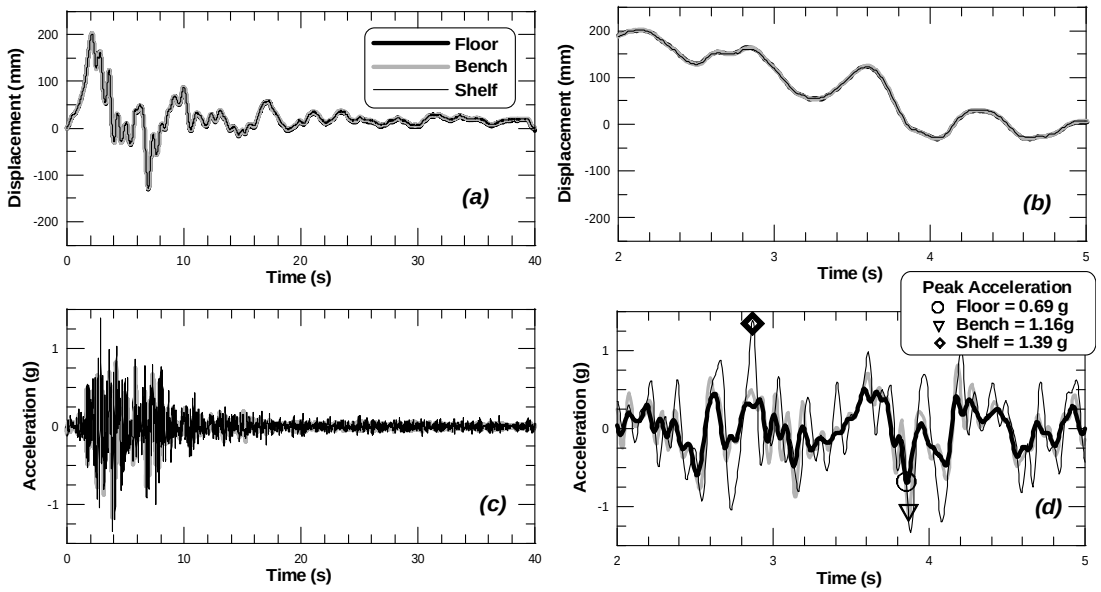

Figure 4.7: Measured time history response at floor (input), bench surface, and shelf within Configuration 4, for base excitation GM - 6: (a) absolute displacement (full duration), (b) absolute displacement (from t = 2 – 5 seconds), (c) absolute acceleration (full duration), and (d) absolute acceleration (from t = 2 – 5 seconds).

5. The small computer monitor was observed to rock significantly and topple twice during the testing, whereas all other equipment response was generally sliding dominated.

6. The primary mode of glassware response was sliding. The glassware generally did not topple, and little rocking was observed.

4.4 COMPONENT-LEVEL BENCH-SHELF DYNAMIC CHARACTERIZATION

The sliding response of equipment and contents resting on bench and shelf surfaces is nonlinear due to their nonlinear frictional behavior. Therefore, their response can not be obtained using the floor acceleration time history and then scaling the sliding response to take into account the acceleration amplification due to the bench and shelf system. Similar conclusions have also been presented by other researchers [e.g., Shao and Tung (1999); Lopez Garcia and Soong (2003)]. Therefore, to determine the sliding response of equipment mounted on furnishings, it is important to consider the dynamic characteristics of the entire system (building, bench, nonlinear equipment-interface). The focus of this section is therefore the dynamic characterization of the bench-shelf system.

In these experiments, low-amplitude, impulse-type (tap) experiments were used to evaluate the dynamic characteristics (frequency, damping, transmissibility) of the various bench-shelf systems constructed in the mock-laboratory environment. In addition, shake table experiments were conducted using (i) low-amplitude, band-limited white noise (base excitation) and (ii) earthquake ground motion (base excitation) to identify the modal parameters. These experi-

ments were carried out on the representative configurations schematically shown in Figure 4.1. In addition, a number of low-amplitude, impulse-type (tap) experiments were conducted in the field on installed bench-shelf systems to supplement the database of characterization results.

4.4.1 Impulse (Tap) Excitation

The concept of modal analysis involves setting the structure into vibration (either via a transient source or using an impulse loading) and measuring the response (displacement, velocity, or acceleration) at one or more points on the structure. In these experiments, fixed response impulse (tap) methods and transient response methods are used. Low-amplitude impulse (tap) testing involves using a force-calibrated hammer and discretely located mobility measurement devices (accelerometers or velocimeters). These types of tests, typically termed "hammer" modal experiments, are appealing, since they provide data rapidly and are nondestructive to the system. The fixed response impulse method involves using an impact hammer over a number of points along the surface of the structure and measuring the system response using an accelerometer. A piezoelectric transducer is placed at the end of the hammer and measures the force imposed under compression during impact. Using an impact hammer, it is difficult to ensure similarity between impacts (position, magnitude, and orientation normal to the surface). For this reason, multiple impact experiments were conducted.

In this study, several strategic points at the bench and shelf levels were first identified. It should be noted that these points may be identified as degrees of freedom (DOFs) corresponding to a lumped-mass idealization of the physical structure. For example, for one of the bench-shelf systems in the field, nine points were identified as potential degrees of freedom. Of these, three were at the bench-top level and six were at the shelf level. A hammer with a mounted force transducer and an accelerometer was connected to the input channels of a digital signal analyzer. The frequency output range was set from 0.125 to 25 Hz. Accelerometers are sequentially placed at all nine points and impact using the hammer was imposed at the same location. This was conducted for two orthogonal directions (transverse and longitudinal). At each point, 25 frequency-response-functions (FRF's) were calculated and an average of them reported. In addition, the coherence was recorded to assure the quality of the data. It was observed that the coherence was very good (greater than 99%), with the exception of the lower frequency range (approximately 0–2.5 Hz).

The recorded FRFs for all the points and directions for a bench-shelf system were then analyzed using the ME Scope software (ME scopeVES, 2001). Overlaying all recorded FRFs and using global polynomial curve fitting, the frequencies, damping ratios, and residues corresponding to each mode were obtained. A wire-frame model of the bench-shelf system was constructed. By observing animated mode shapes, the first mode was identified along the longitudinal direction and the second mode along the transverse direction, and the third mode was a torsional response of the system. Snapshots of the first two mode shapes obtained are shown in Figures 4.8(a) and (b).

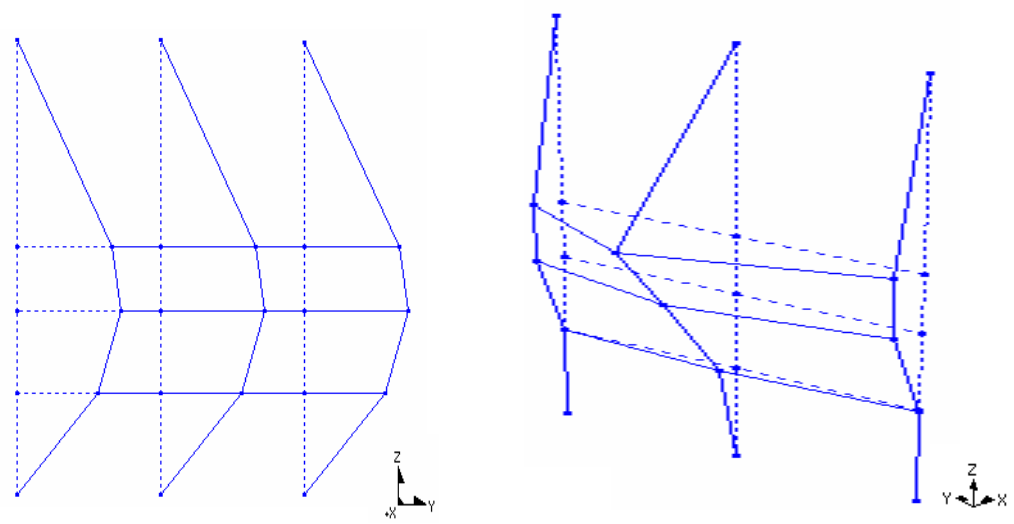

(a) (b)

Figure 4.8: Sample mode shapes for a nine-point hammer impact test on a typical bench-shelf system: (a) 1^{st} mode (longitudinal) and (b) 2^{nd} mode (transverse).

A sample of the obtained FRF curves, representing the FRF when the accelerometer was placed at the middle of the bench-top and the hammer hit was at one edge of the bench-top for Configuration 3 of the mock-laboratory, is shown in Figure 4.9. These tests were conducted before and after several base excitation (earthquake) input motions, and by the similarity of the results, it may be noted that the system remained linear with little or no change in fundamental frequency. From these curves, although a low frequency is identified at approximately f = 7 Hz, the dominant peaks are clearly seen at f_n = 11.8 to 12.8 Hz for the longitudinal and transverse directions, respectively.

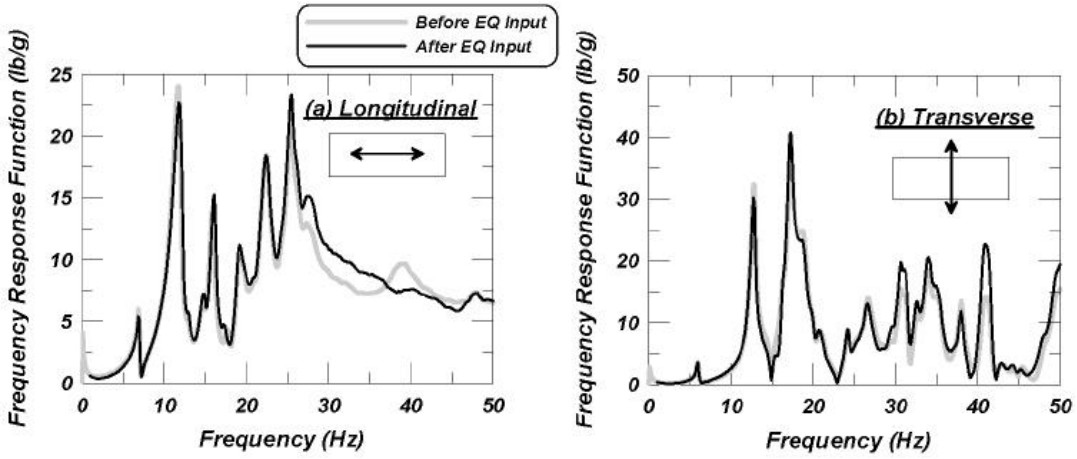

Figure 4.9: Low-amplitude hammer FRFs for Configuration 3, where impact is provided along the (a) longitudinal and (b) transverse directions.

4.4.2 White Noise Excitation

Using band-limited white-noise base excitation input through the shake table, the acceleration transfer function of the bench-shelf system was determined. The frequency band of the generated motion were selected as 0–50 Hz with maximum displacement of the shake table in the horizontal direction of 0.25 inch. Typical duration of the motions was 2 minutes. It may be noted that the long duration motion used here later chopped off in several small durations to calculate average transfer function. This method eliminates the effect of transient vibration. An example of the transfer function for Configurations 3 and 4 is shown in Figures 4.10(a) and (b), respectively. These figures show the ratio of bench-top acceleration to input acceleration (at floor level) in the frequency domain. Figure 4.10(a) illustrates two dominant frequencies, namely, f_n = 5.4–5.6 and 9.4–10 Hz, with resulting base (input) acceleration amplification of approximately 4.4 and 3.2–3.4 at these respective frequencies.

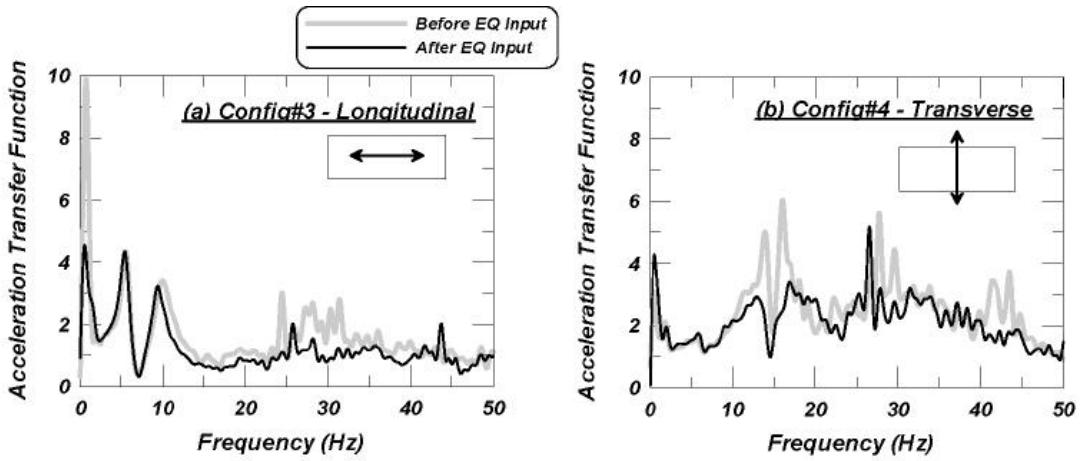

Figure 4.10: Acceleration transfer functions generated from low-amplitude white noise (base excitation) for (a) Configuration 3 (shaking along longitudinal direction) and (b) Configuration 4 (shaking along transverse direction).

4.4.3 Earthquake Excitation

Assuming that the bench-shelf system may be idealized as a multi-degree-of-freedom (MDOF) system and if the first n modes of this system dominate the response, then by using the modal superposition rule, the acceleration response of the system may be expressed as:

$$\ddot{x}_i(t) = \sum_{r=1}^{n} \Phi_i^r \ddot{u}^r(t) \tag{4.1}$$

where $\ddot{x}_i(t)$ is the response of the i$^{\text{th}}$ DOF, Φ_i^r is the mode shape of i$^{\text{th}}$ DOF for r$^{\text{th}}$ mode, and $\ddot{u}^r(t)$ is the modal acceleration response of r$^{\text{th}}$ mode. If one considers that there is negligible cross correlation between two adjacent modes and only the first mode approximately represents

the total response of the bench system, the transfer function relating the bench-top acceleration to the floor acceleration in the frequency domain may be expressed as:

$$|H(\omega)| = \left|\frac{\ddot{x}(\omega)}{\ddot{y}(\omega)}\right| = \alpha \frac{\omega_n^4 + 4\omega_n^2\omega^2\zeta_n^2}{\left(\omega_n^2 - \omega^2\right)^2 + 4\omega_n^2\omega^2\zeta_n^2} \tag{4.2}$$

where α is a constant introduced for the mode shape factor, ω_n is the first natural frequency of the bench system, ζ_n is the damping ratio associated with the first mode, and ω is the frequency. The values of α, ω_n, and ω may be determined from the experimental results by fitting the above equation. Figures 4.11(a) and (b) show the resulting acceleration transfer functions, considering the SDOF-fit (Equation 4.2) applied to the earthquake input frequency response spectrum, for GM - 3 for Configurations 3 and 4, respectively.

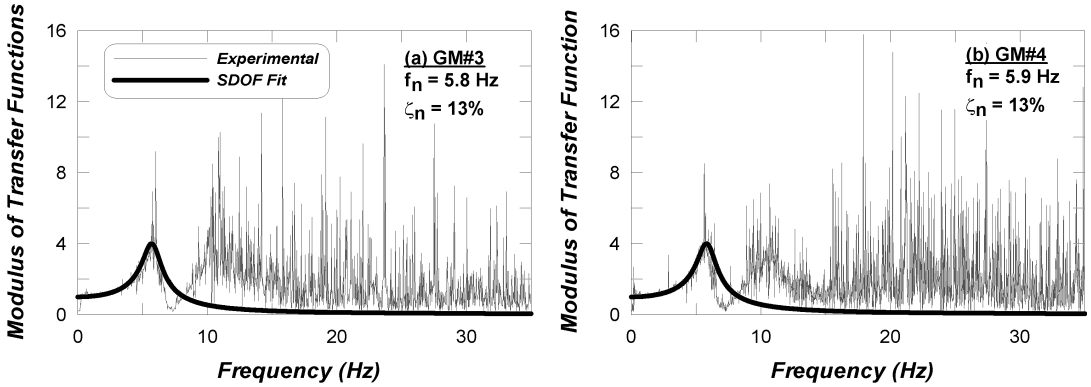

Figure 4.11: SDOF-fit analysis to earthquake input motion (GM - 3) to generate transfer functions: (a) Configuration 3 and (b) Configuration 4.

4.4.4 Summary of Dynamic Characterization Results

A summary of the dynamic characteristics of the various configurations, considering the different testing techniques used is provided in Table 4.2. The table is subdivided into the field and laboratory results and both white noise and hammer testing techniques. Boundary conditions and mass loading conditions observed are noted. Although six plausible mass loading conditions are noted in the footnote, only three were observed in these tests. Additional mass loading conditions are investigated in the numerical modeling in the following section. Note that field experiment (in-situ) data are also included in this table (Table 4.2). Photographs of configurations tested in the field are shown in Figure 4.12.

Summary results illustrate that the fundamental frequency of bench-shelf systems is generally between 10–16 Hz when the shelf is not loaded (case 1 mass loading). Mass loading on the lower shelf results in an approximate reduction of 50% in the first and second fundamental frequencies. The results also indicate that relatively high levels of damping may be obtained at these frequencies, where ζ_n, for these systems varied between 2–12%. Due to the larger

amplitude white noise excitation, friction develops at the connections within the system, resulting in damping levels generally above 5%. In contrast, damping levels determined from the low-amplitude hammer tests are generally below 5%, with a few exceptions.

Table 4.2: Summary of experimentally derived dynamic characteristics for the different bench-shelf systems.

Name[1]	Observed[2] B.C.	Mass Loading[3]	f_1 (Hz)	ζ_1 (%)	f_2 (Hz)	ζ_2 (%)	Comments
Mock Laboratory Experiments: Hammer Tests							
M-DL-3	C-C	2	11.8	3	-	-	Similar Lengths
M-DL-4	C-C	2	14.5	3	-	-	
M-ST-2	C-C	1	16.0	12			
M-DT-3	C-C	2	12.8	3	-	-	
M-DT-4	C-C	2	12.5	3	-	-	
Mock Laboratory Experiments: White Noise Excitation							
M-DL-3-B	C-C	4	5.6	9	10.0	8	Similar Lengths
M-DL-3-A	C-C	4	5.4	9	9.4	8	
M-ST-2	C-C	4	4.8	12	10.2	10	
M-DT-4	C-C	1	13.9	7	16.0	3	
M-DT-4	C-C	1	12.9	5	16.7	9	
Field Experiments: Hammer Tests							
F-DL-1	C-F	1	10.8	8	19.4	5	Varied Lengths
F-DL-2	C-F	1	13.8	10	-	-	
F-DL-3	C-F	1	10.5	3	15.2	5	
F-DL-4	C-F	1	10.2	3	14.7	5	
F-DT-1	C-F	1	13.3	5	-	-	
F-DT-3	C-F	1	9.6	3	13.0	5	
F-DT-4	C-F	1	8.9	2	11.3	4	

[1]Nomenclature defined as follows:
"*Location-general configuration - setup number-* (*sequence* - optional)"
Location: F = Field, M = Mock Laboratory
General configuration: SL = Single Longitudinal, DL = Double Longitudinal, ST = Single Transverse, DT = Double Transverse
[2]Boundary Conditions: C – C = bottom and top both connected, C – F = bottom connected and top free
[3]Mass loading (arranged according to increasing mass of the system), defined as:
1 = bench & shelves empty, 2 = only equipment, 3 = book on lower shelves, 4 = equipment + book on lower shelves, 5 = book on both shelves and 6 = equipment + book on both shelves

4.5 NUMERICAL MODELING AND RESULTS

Numerical models of the single and double bench-shelf systems were developed and compared with the dynamic results from the experiments. Models were based upon a lumped-mass idealization and constructed within the OpenSees platform (OpenSees, 2003). Figure 4.13 provides a general schematic of the lumped-mass model constructed, in this case for a fixed-fixed boundary condition. Note the larger mass contributions for the center elements. In the background, the general configuration of the shelving and bench units are shown. Elastic beam-column elements were used to model the horizontal and vertical unistrut members with representative

Figure 4.12: Photograph of a typical field laboratory environment.

sectional properties (4.1 cm square vertical members and 4.1 cm by 2.1 cm horizontal members, with back-to-back vertical elements used for the double bench-shelf systems).

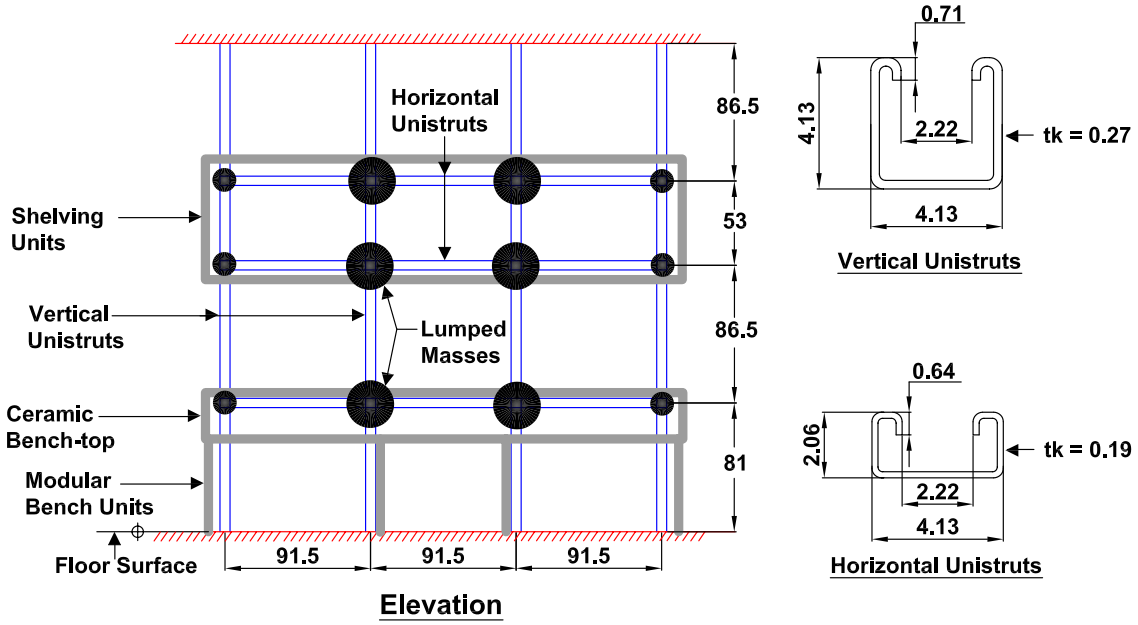

Figure 4.13: Idealized lumped-mass model of a fixed-fixed bench-shelf system (all units in cm).

For these analyses, two variables, which may be considered to have great uncertainty in practice, were investigated, namely, (i) mass and (ii) boundary conditions. Under realistic conditions, both the bench and shelf systems may be loaded fully or partially, with books, equipment, or other contents. Partial loading of the shelf systems is common, as glassware is kept on the lower shelving units. Clearly, this will change the systems' dynamic properties. Therefore, six plausible mass scenarios are considered in the numerical model. Ordered in increasing total system mass, these include: (i) bench and shelf not loaded, (ii) bench loaded and shelf not loaded, (iii) bench not loaded and shelf half loaded, (iv) bench loaded and shelf half loaded, (v) bench not loaded and shelf loaded, and (vi) bench loaded and shelf loaded. Although the first case has the lowest possible occurrence in the field, it is useful for defining the lower-bound mass conditions. The magnitude of mass for these systems was estimated using plausible equipment and book scenarios for the bench and shelf systems, respectively.

Varying boundary conditions are considered at the top and the bottom connections for the structure. In view of the connection details commonly adopted in the field (e.g. Figure 4.2(d)), an approximate pinned-pinned condition could be envisioned. However, exceedingly tight bolts can provide for moderate fixity. In contrast, lightly tightened bolts (due to improper workmanship), or loosening of bolts, which may occur during seismic excitation can provide additional freedom at the top or bottom connections. Therefore, a number of plausible boundary conditions are considered in the numerical model, including: (i) fixed-fixed, (ii) fixed-pinned, (iii) pinned-pinned, (iv) pinned-free.

4.5.1 Eigenvalue Analysis

Figures 4.14(a)-(f) provide a summary of the numerical model eigenvalue analysis presented in terms of normalized frequencies versus normalized mass, considering the above parameter space. First and second fundamental frequencies (f_1 and f_2) are presented and normalized by the maximum corresponding frequencies ($(f_1)_{max}$ or $(f_2)_{max}$) for the case under consideration. Note that the maximum frequencies are provided, therefore, the first or second fundamental frequencies can easily be obtained from the plot. Masses have been normalized by the maximum total system mass for each configuration (single or double). A schematic illustration of the results presented in each plot (single or double configuration *and* longitudinal or transverse directions) is provided in the upper portion of each figure. Note that the longitudinal direction double bench-shelf systems have double the mass and stiffness of the single systems, thus the frequencies will be identical.

Experimental frequencies corresponding to the different cases are overlaid with the numerical results. Open circles denote the hammer test results, whereas solid circles denote the white noise excitation. From these results, it can be seen that the hammer tests generally result in the higher frequency estimates (stiffest case, approaching fixed-fixed boundary conditions). In contrast, in general, the white noise excitation results approach the lower frequencies, typically resembling the pinned-pinned condition. However, the condition of the double unistrut sys-

tem, in the transverse direction does not follow this trend. This can be explained by reviewing Figure 4.10(b). Due to the physical separation of the two side-by-side benches, during base excitation, two closely located modes are observed, which is not captured in the numerical model, where perfect attachment between the separated benches is assumed. This is confirmed by noting that the peaks are greatly reduced and more separated in Figure 4.10(b), after numerous runs of earthquake input excitation. However, if one considers the next dominant mode as the second mode (f_2 = 26 Hz), the ratio of $\frac{f_2}{(f_2)_{max}}$ = 0.70, more closely approaching the pinned-pinned condition, and confirming the higher frequency estimates.

4.5.2 Acceleration Amplification

To provide insight into the amplified response of these systems under real earthquake excitations, 22 ground motions (Sommerville, 2005) are selected and used as floor level (top and bottom) input motions to the numerical models of a subset of the bench-shelf configurations. This assumes negligible differential movement between the top and bottom supports. Analysis results are presented for the pinned-pinned and fixed-fixed conditions, considering the mass loading case (iv), where the bench is loaded and the shelf is half loaded. This was observed as the most common practical situation in the field. For each time history analysis, the maximum acceleration amplification Ω (=$\frac{\text{output acceleration}}{\text{input acceleration}}$) is calculated at both the bench and lower shelf levels and plotted against the ratio of the predominant ground motion period T_p with the fundamental period of the system T_n [Figure 4.15(a)-(f)]. In this case, T_p is taken as the dominant period from the Fourier spectrum of each individual ground motion.

Figure 4.15 illustrates that Ω is always greater than 1.0, indicating that the motion is always amplified, with slightly higher Ω values observed for the pinned-pinned condition. These data also indicate that there is little difference in the general trend between the different configurations. Intuitively, as the ratio $\frac{T_P}{T_n}$ approaches 1.0, Ω increases more rapidly, while for $\frac{T_P}{T_n} \geq$ 10.0, both the amplitude and dispersion in Ω are significantly reduced. Note that only small differences are observed between the magnitude of shelf and bench amplification. This is confirmed by reviewing nonlinear regression trendlines overlaid with the numerical results, as summarized in parts (e) and (f) of Figure 4.15. This view of the data illustrates that there is significant scatter in the analysis results due to the ground motion characteristics. Considering the nonlinear regression, the acceleration amplification for a fixed-fixed system ranges from Ω = 2.6 to 1.4, over the period range considered. Note also that for the pinned-pinned systems, Ω is quite large, ranging from 4.3 to 1.6, with a maximum value of 7.0, where $\frac{T_p}{T_n}$ = 1.22.

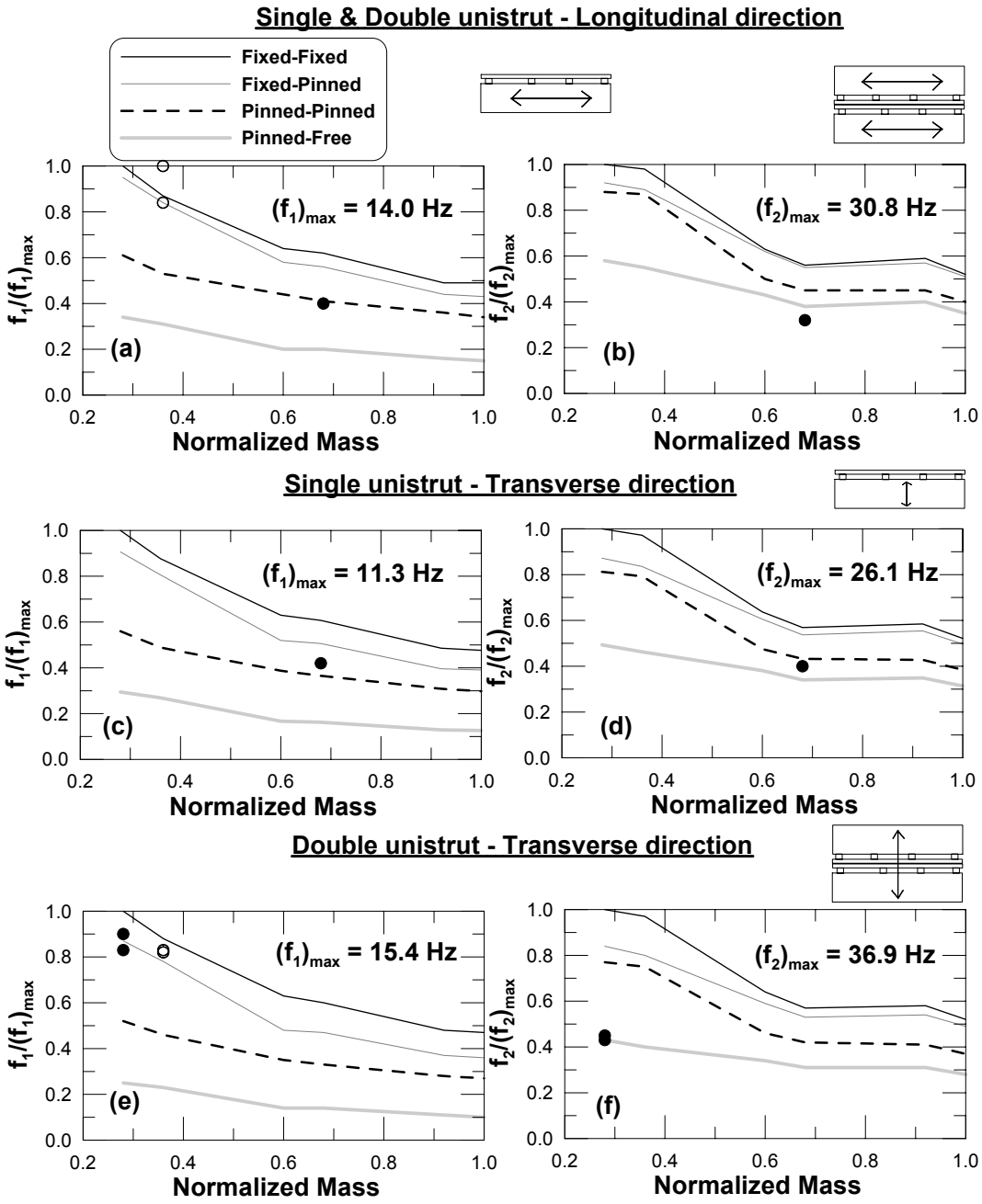

Figure 4.14: (a) First and (b) second fundamental frequencies, for the single and double bench-shelf systems in the *longitudinal* direction; (c) first and (d) second fundamental frequencies, for the single bench-shelf systems in the *transverse* direction; and (e) first and (f) second fundamental frequencies, for the double bench-shelf systems in the *transverse* direction.

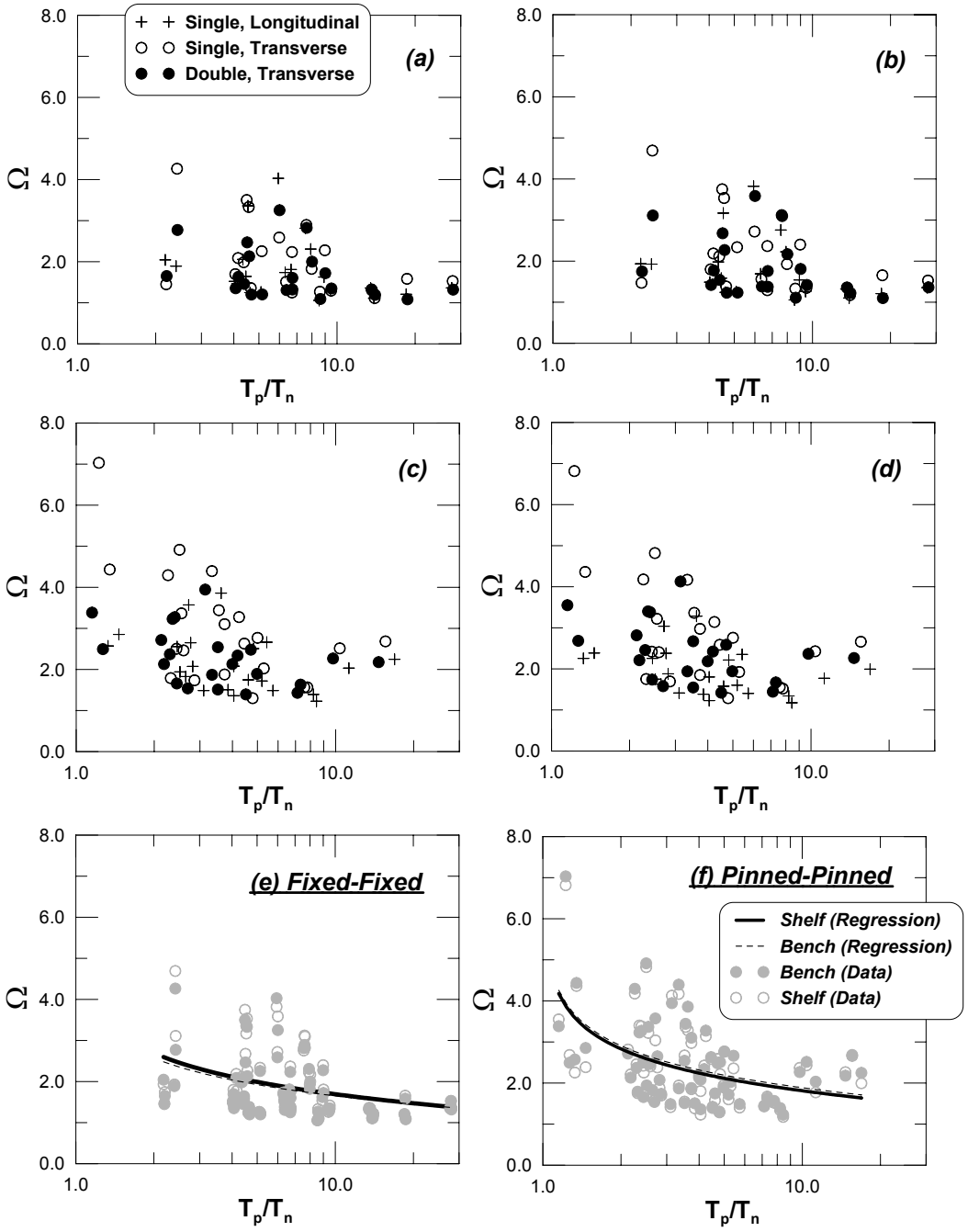

Figure 4.15: Maximum acceleration amplification Ω for the fixed-fixed case: (a) bench level and (b) shelf level, and pinned-pinned case: (c) bench level and (d) shelf level (mass loading case (iv): bench loaded and shelf half loaded) and summary regression analyses for (e) fixed-fixed and (f) pinned-pinned cases.

4.6 SUMMARY REMARKS

This chapter presents an experimental and numerical investigation of the dynamic characteristics of bench-shelf supporting structures, for the purposes of defining the amplification and seismic input motion, which may be imparted on equipment of interest. Among the vast types of nonstructural equipment and contents, the important aspect of dynamic amplification due to supporting structures, in particular, has received little attention in the past. In this study, four different integral bench-shelf configurations with details representative of typical biological and chemical laboratories in science buildings were mounted on a large shake table and subjected to a range of dynamic excitations. Transverse and longitudinal bench configurations, using both single and double (back-to-back) benches were considered. In addition, field experiments were conducted to evaluate the in-place, low-amplitude dynamic characteristics of the bench-shelf system. In addition, the movement of various equipment mounted on a bench-shelf system was also studied. Numerical models of four typical bench-shelf systems are developed and the eigenvalue solution of these models are overlaid with experimentally obtained results. It is found that the experimental results are in good agreement with the analytical calculations. Using 22 ground motions, the amplification of floor acceleration at the bench and shelf levels is presented. For typical pinned-pinned bench-shelf systems, under the mass loading conditions analyzed, the acceleration amplification is observed to be as high as 7.0. Thus, this bench-shelf system amplification is expected to play a significant role in the sliding response of equipment and the contents they support.

5 Bare Shake Table Experiments

5.1 INTRODUCTION

The shake table testing of different mock-laboratory configurations (Chapter 4), illustrated that the floor acceleration may amplify at the bench-top or shelf-level due to the flexibility of the bench-shelf system. This amplification may lead to larger response of the equipment and contents. It was also observed that the equipment movement is not unique and depends on uncertainty in frictional behavior as well as the ground motion characteristics. The use of the mock-laboratory system allowed dynamic testing considering only the horizontal component of ground motion. To broaden the equipment and glassware response study, more detailed tests were performed using a bare shake table scenario, where only a ceramic bench-top and shelf surface as shown in Figures 5.1(a) and (b) were used. In this case, the input motion at the bench or the shelf surface may be expected to be the same as the input motion to the table. Although it is expected that these motions would be filtered by the building and bench-shelf system, the ground level motions were used to allow comparison with previous experiments. These data can then be used for modeling the seismic response of the equipment and the glassware under a broader range of input motions.

Given the general lightweight nature of these equipment, it is well recognized that vertical input motion may have an effect on the sliding behavior of the body, particularly if the vertical component is in phase with significant horizontal excitation. To investigate these effects, both the horizontal and vertical component of ground motion excitation was considered in the bare shake table scenario. In this chapter the experimental setup and results for the equipment and glassware tested using the bare table scenario and considering uniaxial input (horizontal motion only) and biaxial input (both horizontal and vertical motions) are presented. All ten pieces of equipment are tested on the shake table using the exact ceramic bench interface. Six pieces of glassware, two each of three typical glassware (500 ml conical flask, 1000 ml conical flask, and 1000 ml bottle) are tested with empty and full conditions using the exact shelf interface. Experimental results and analytical comparisons with experiments using the Coulomb friction model are also presented. Eight ground motions (GM - 3 through GM - 10) as described in Chapter 4, are used in these tests. Table 5.1 shows the peak vertical parameters (PVGA, PVGV and PVGD) as well as the ratio of peak vertical to horizontal ground acceleration of the target shake table inputs. It may be mentioned here that for the stroke limitation of the shake table,

the vertical component of GM - 9 is amplitude scaled down by half and used as the shake table vertical input.

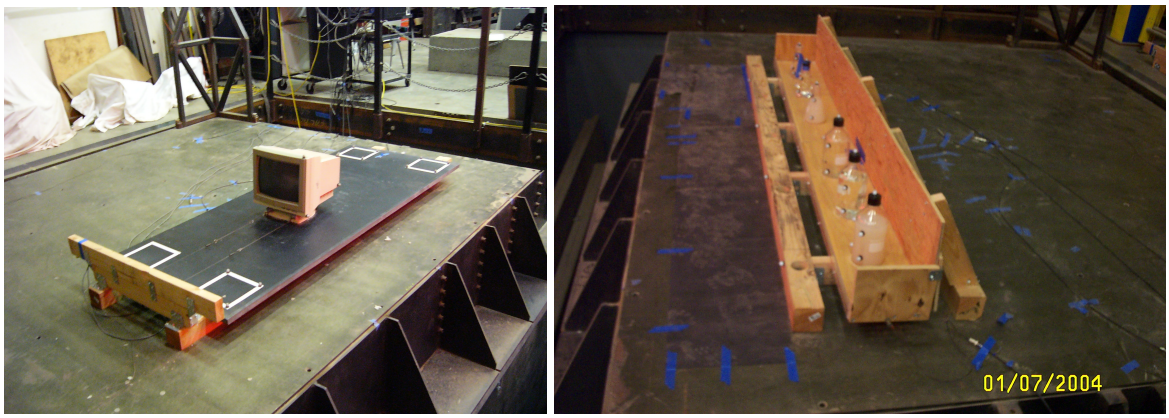

(a) (b)

Figure 5.1: Photographs of the bare shake table experiments (uniaxial as noted and biaxial-including vertical component): (a) equipment on bench-top surface and (b) glass-ware on shelf surface.

Table 5.1: Summary of vertical components used as shake table inputs for the biaxial study.

Input Motion	PVGA (g)	PVGA/PHGA	PVGV (cm/s)	PVGD (cm)
GM-3	0.14	0.53	6.60	1.22
GM-4	0.15	0.42	16.65	1.70
GM-5	0.31	0.71	36.28	8.62
GM-6	0.63	1.20	24.63	9.91
GM-7	0.40	0.60	25.20	12.03
GM-8	0.43	0.62	11.18	3.67
GM-9	0.13	0.16	19.63	6.63
GM-10	0.72	0.62	18.85	6.19

5.2 EQUIPMENT TESTING: EXPERIMENTAL SETUP AND INSTRUMENTATION

For the testing of the ten pieces of equipment, the bench-top is attached to the shake table as shown in Figure 5.1(a). Equipment are placed one at a time on the bench-top during the testing. Six accelerometers are used to capture the shake table and bench horizontal and vertical motions. Four displacement transducer channels are also used to capture shake table horizontal and vertical motions. Two accelerometers are used for each equipment tested to record horizontal and vertical equipment accelerations. Two string potentiometers are also used to record the horizonal sliding of the equipment. Figure 5.2 shows the picture of some of the analog sensors used in bare table tests. Apart from these analog instruments, four cameras are also used to capture the motion of the shake table and equipment as shown in Figure 5.3(a). Twelve

passive markers are used to measure the movement of the bench-top and typically four passive markers are used to capture the three-dimensional movement of equipment (Figure 5.3(b)).

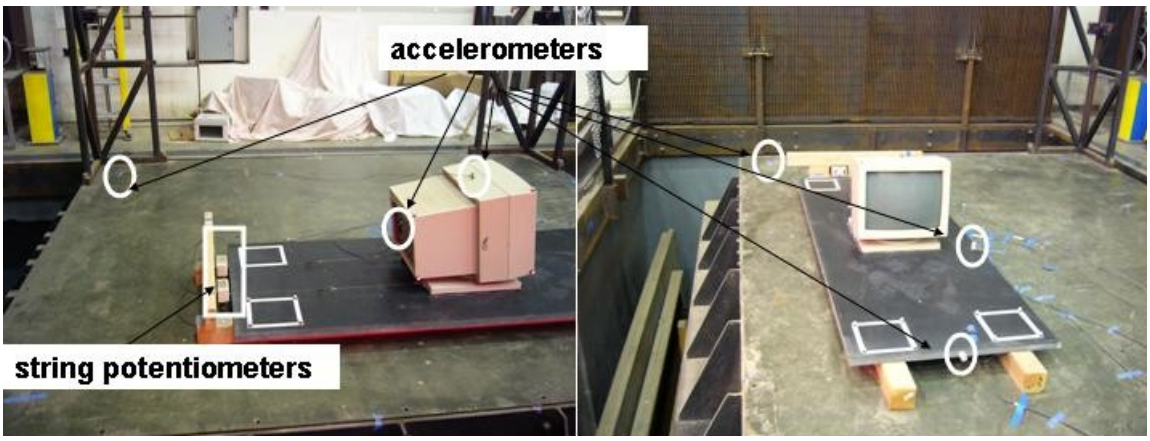

Figure 5.2: Photograph of sensors used in bare shake table experiments.

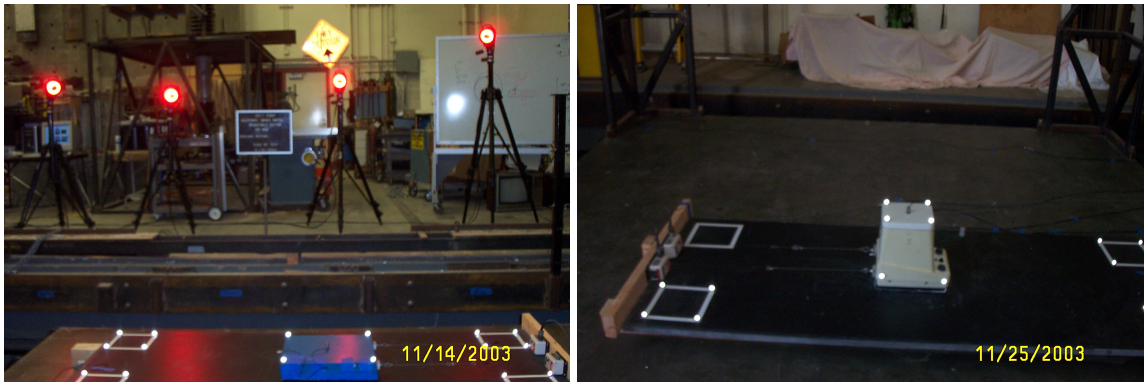

(a) (b)

Figure 5.3: Photograph of digital measurement system used in bare shake table experiments: (a) camera layout surrounding experiments and (b) passive marker layout for typical equipment.

5.3 EQUIPMENT RESPONSE: UNIAXIAL AND BIAXIAL TESTS

By using the same ten ground motions listed in Table 4.1, the response of the equipment was obtained when the shake table was subjected to horizontal only and horizontal and vertical biaxial shaking (Table 5.1). Typically three trials per ground motion input are performed (for higher amplitude motions, where first equipment movement are observed). Figures 5.4– 5.6 show the sliding response of the scientific equipment (Techtonic Autoanalyzer, Eppendoff centrifuge, small microscope, and large microscope), the SGI CPUs (Indy, Indigo, and Octane) and computer monitors (19″, 17″, and 15″ monitors), respectively, plotted against peak horizontal

table acceleration. Summary of measured equipment response is provided in Appendix C. In each sub-figure of Figures 5.4 to 5.6, a vertical line is also shown to point out the measured average coefficient of static friction, μ_s for equipment. It should be noted that observations during testing indicate that the response of the equipment is mainly sliding dominated though equipment such as the monitors, small microscope, and SGI Indigo did show some rocking behavior, which can be attributed to their tall, top heavy, small-base configurations.

From Figure 5.4, it may be observed that out of these four scientific equipment, the response of the large microscope (which has the lowest μ_s) is greatest (36 cm, approximately), while the Eppendoff centrifuge (which has the highest μ_s) moves only GM - 10. The behavior of the centrifuge is governed by the suction cup mechanism at its base, which minimizes any rocking. The Techtonic Autoanalyzer and large microscope are observed to move only when the PHTA (when expressed in g) exceeds the average μ_s value, where as the small microscope moves before PHTA (in g) exceeding μ_s, which may be due to its rocking behavior. From Figure 5.5, it may be observed that the SGI Indigo shows the largest response of the three SGI equipment, even though its μ_s value is greater than that of the SGI Indy and almost the same as that of the SGI Octane. In addition, the SGI Indigo begins moving before the PHTA (in g) exceeds the value of μ_s. This may be due to the slight rocking behavior of this equipment. The contribution of the vertical component may clearly be observed from GM - 6 (PHTA = 0.55 g approximately) trials of SGI Octane, where the equipment moves only when the motion is biaxial.

Figure 5.6 provides the maximum relative displacement of the monitors. It is observed from this figure that the behavior of the small monitor is most random and less repeatability of the response is observed for the same trial. It should be mentioned that the small monitor showed the maximum rocking and in-plane rotation of all ten equipment. It may be concluded from these tests that, in general, reasonable repeatability of response may be expected and that less rocking attributed to better repeatability of response for the same trial. In addition, vertical motion does play a role in the equipment response.

5.4 EQUIPMENT RESPONSE: ANALYTICAL-EXPERIMENTAL COMPARISON AND DISCUSSION

To illustrate a comparison between the analytical and experimental (bare shake table) results, a detailed study for the SGI Indy equipment is presented. In the numerical calculations, the mean values of the coefficients of static and kinetic friction provided in Tables 3.2 and 3.3 are considered, i.e., $\mu_s = 0.36$ and $\mu_k = 0.315$. Figure 5.7(a) shows the comparison of the analytical and experimental results for the SGI Indy, subjected to the biaxial input motion GM - 9 (Lexington Dam, 1989 Loma Prieta motion, scaled to a hazard level of 10% exceedance in 50 years). The results illustrate that at the commencement of motion, the peak and residual relative displacement of the equipment match very well with the experimental results. However, the analytical curve is observed to deviate slightly from the experimental curve in some places. This may be due to uncertainty in the frictional behavior of the underlying Coulomb friction

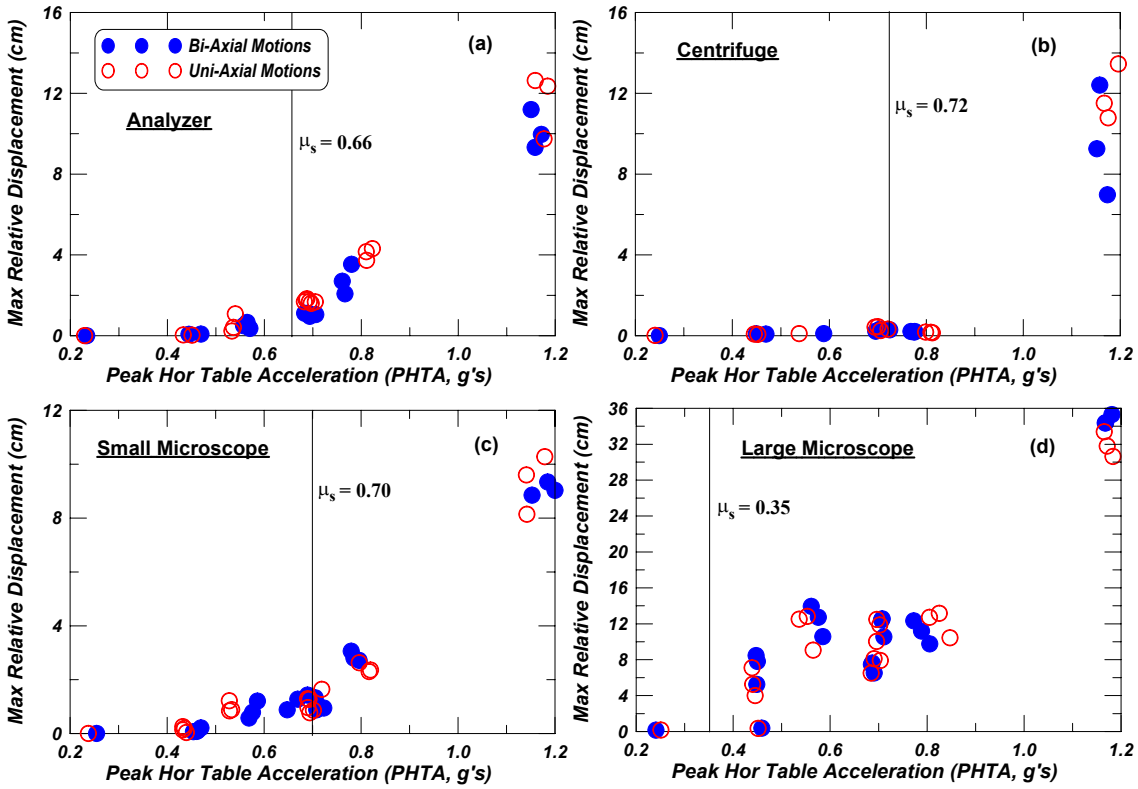

Figure 5.4: Maximum relative sliding displacement of *scientific equipment*: (a) Techtonic autoanalyzer, (b) Eppendoff centrifuge, (c) small microscope, and (d) large microscope, for uniaxial and biaxial bare shake table tests.

model or slight numerical errors. For this example, it is important to note that the total sliding distance of the equipment is predominantly a result of a single sliding incident. Considering the biaxial case of GM - 10 (Kofu, 2000 Tottori, Japan motion, scaled to a hazard level of 2% exceedance in 50 years) the body moves in several steps as shown in Figure 5.8. The motion has significant high-frequency content, with several strong acceleration peaks, leading to sliding at several instances. This is illustrated by observing Figures 5.9(a) and (b), which illustrate the measured horizontal and vertical acceleration time histories taken during testing for GM - 9 and GM - 10, respectively.

Observing Figure 5.8, the body is predicted to stop and start at approximately the same times as those measured in the experiments. However, the amplitude of sliding in the experimental and analytical cases for each new instigation of sliding is different. For this example, the analytical solution tended to under-predict the response. This may be due to several factors. First, the coefficient of kinetic friction may not be constant during the movement as mentioned before. This is due to the multiple sliding incidences, each with lower maximum velocities. If one considers that the resistance transitions from static friction-dominated to kinetic friction-dominated, when the body begins moving, and it takes some time to reach μ_k from μ_s, the over-prediction can be interpreted as a low estimate of μ_k used in the analytical solution. Since

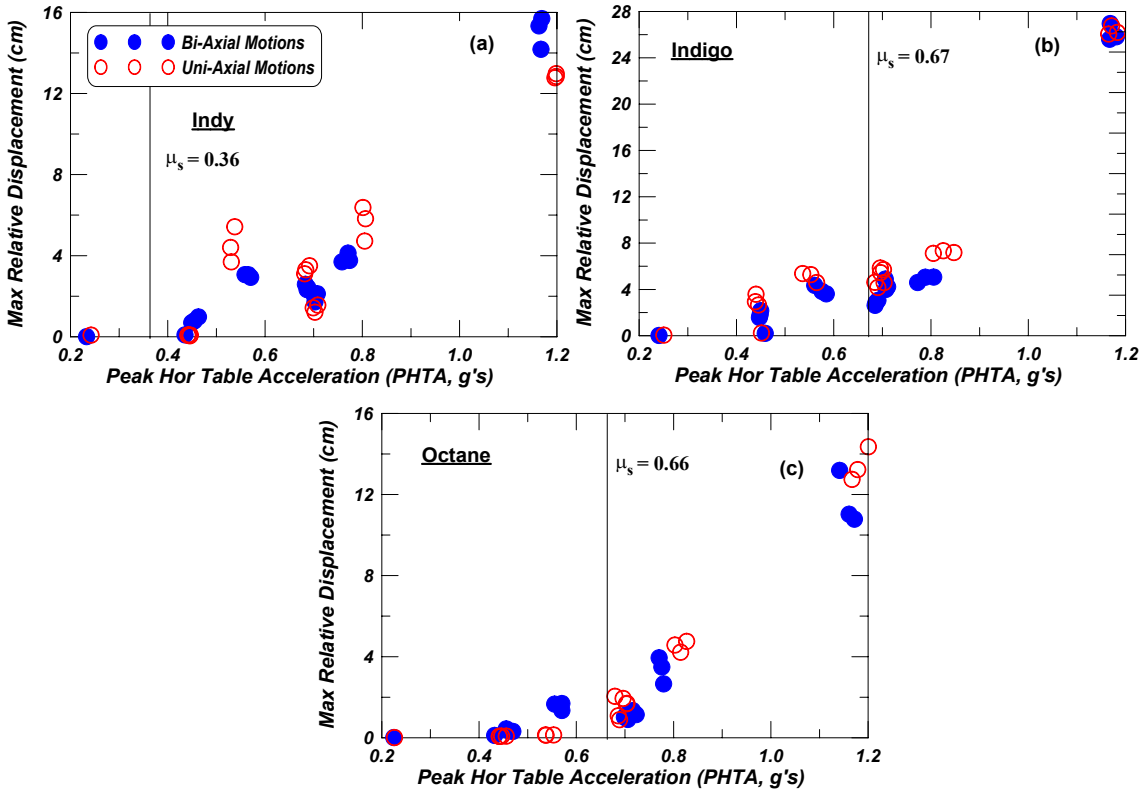

Figure 5.5: Maximum relative sliding displacement of *SGI CPUs*: (a) Indy, (b) Indigo, and (c) Octane for uniaxial and biaxial bare shake table tests.

the uncertainty in the coefficient of kinetic friction is also observed during the pull tests and the inclined base tests it is reasonable to conclude that μ_k may be a function of velocity, contact time, and other factors.

A sensitivity study is performed for this equipment, considering the uncertainty in μ_k and its affect on the response. In this case, the same motion GM - 10 is considered, with three cases of μ_k used in the solution. Given the range of uncertainty obtained in the pull and inclined base experiments, a high estimate of $\mu_k = 1.1\times$ the mean μ_k (=0.315), and a low estimate of $\mu_k = .9\times$ the mean μ_k are taken. The response of this equipment is illustrated in Figure 5.10. Even small uncertainties in μ_k are observed to play a major role in predicting the sliding response. These examples illustrate a consistently observed trend from this study. Specifically, when considering other analysis cases, the analytical predictions are observed to be very close to the experimental responses, when the body moves predominantly by one pulse. Alternatively, if the body moves due to high-frequency vibration, experimental-analytical matching becomes less accurate.

Figure 5.11(a) provides measured sliding displacement for the SGI Indy equipment for all significant ground motion shake table trials and both the biaxial and uniaxial conditions. Motions for which the equipment did not move significantly, are omitted from this plot. In this case, ground motions GM - 6 through GM - 10 are considered, as they produce noticeable

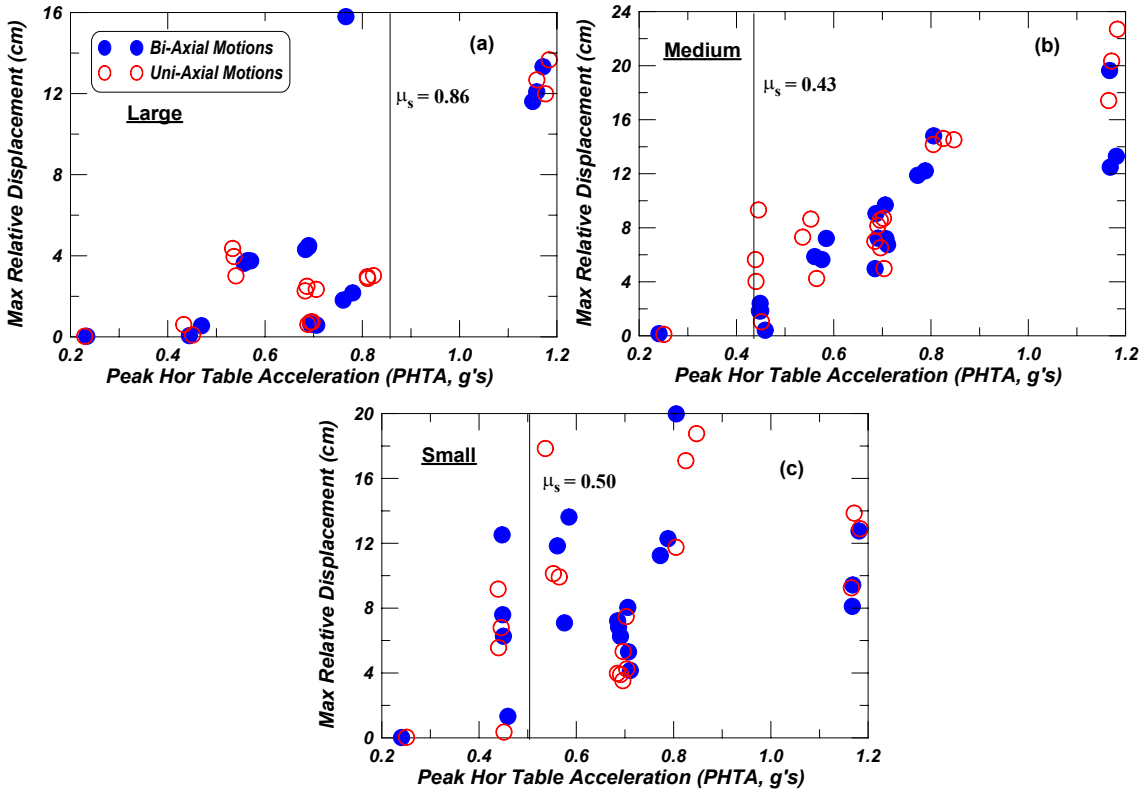

Figure 5.6: Maximum relative sliding displacement of *computer monitors*: (a) large monitors (19″), (b) medium monitors (17″), and (c) small monitors (15″) for uniaxial and biaxial bare shake table tests.

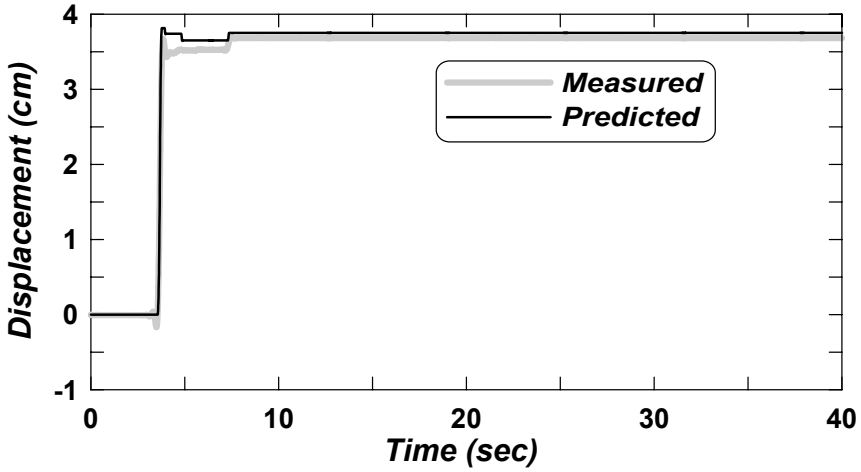

Figure 5.7: Comparison of experimental and analytical equipment displacement – SGI Indy subjected to GM - 9.

sliding. For each motion, three trials are carried out and reported. The solid points represent the biaxial cases, where the equipment is excited with horizontal motion along with the vertical motion, while for the uniaxial cases, the body is excited with only a horizontal component.

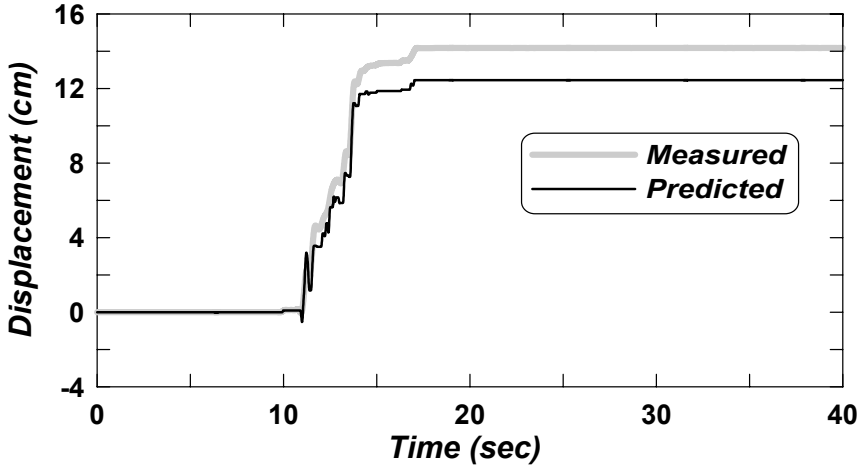

Figure 5.8: Comparison of experimental and analytical equipment displacement – SGI Indy subjected to GM - 10.

Figure 5.11(b) shows the percentage deviation of measured displacement for each of the three trials for a given ground motion when compared with the mean (of three trials) measured values for that ground motion. Figures 5.11(a) and (b) illustrate that the sliding is not unique for all trials of a given input motion. This reinforces the uncertainty in frictional behavior for different cases. A slightly different ground motion generated during the shake table testing may change the behavior of the equipment. The maximum deviation observed for any trials is approximately 20% for this equipment. To get an idea of the deviation of each data point from its corresponding mean and for all trials, the relative L_2 norm of deviation is determined. For this case, relative L_2 norm deviation is expressed as:

$$(L_2)_{\text{dev}} = \sum_{j=1}^{n} \sum_{i=1}^{3} \left(d_{ij} - \bar{d}_j\right)^2 / (3 \sum_{j=1}^{n} \bar{d}_j^2) \tag{5.1}$$

where d_{ij} is the measured sliding displacement of the ith trial for the jth ground motion; $\bar{d}_j$ is the mean measured displacement for jth ground motion and n is the total number of ground motions. For uniaxial trials, the value of $(L_2)_{\text{dev}}$ is found to be 0.04, while for the biaxial case, this value is found to be 0.01. Therefore, it may be concluded that for each of the three trials, experimental sliding is approximately same. It may also be mentioned that the uniaxial cases produce more variability of sliding response, while for the biaxial case repeatability is more readily observed.

Figure 5.11(c) shows the percentage error between the experimentally measured and analytically obtained displacement with respect to the measured case, for ground motions GM - 6 through GM - 10. Mean μ_s and μ_k values are used for the analytical cases. Although an input vertical motion was not used in the purely uniaxial case, any small vertical oscillations were measured and used in the computation to account for any component of vertical motion induced on the body. It may be observed from Figure 5.11(c) that with the exception of only

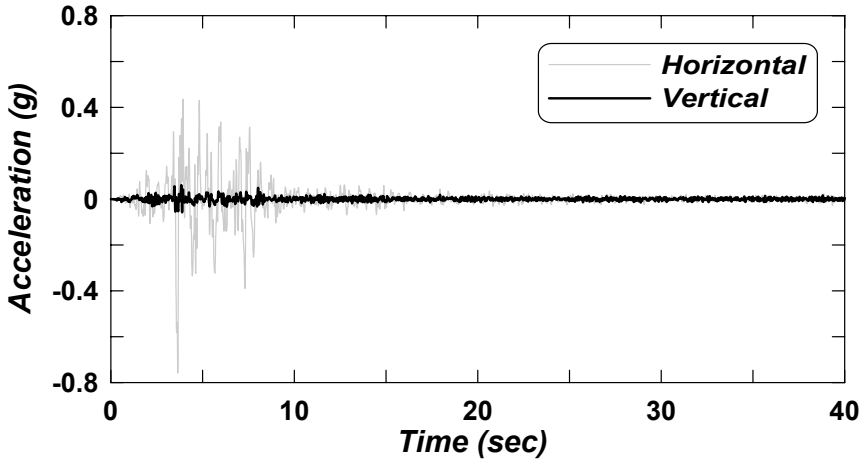

(a)

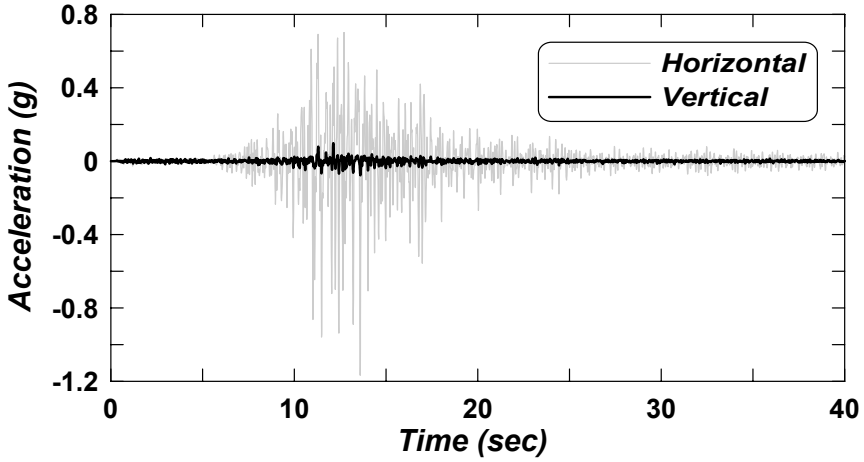

(b)

Figure 5.9: Measured bench-top acceleration time histories for (a) GM - 9 and (b) GM - 10.

a few cases, using the frictional characteristics obtained in the pull and inclined experiments coupled with the sliding model generally resulted in unconservative response predictions. It may also be observed that the error in predicted response is not higher even when the sliding distance is large. Maximum unconservative predictions were 57% and 30% below experimental observations, for the uniaxial and biaxial cases, respectively. This unconservative estimate may be a result of considering higher μ_k, values which are obtained by averaging the high and low velocity measurements cases. For low sliding distance, the body moves with low velocity, and thus considering a lower μ_k than the average value would have resulted in less error. To show the error in the predicted response compared to the corresponding measured values and considering all cases, the relative L_2 norm error is presented. In this case, the relative L_2 norm is obtained by the following expression:

$$(L_2)\text{error} = \sum_{j=1}^{n}\sum_{i=1}^{3}\left(d_{ij} - \hat{d}_{ij}\right)^2 \Big/ \left(\sum_{j=1}^{n}\sum_{i=1}^{3} d_{ij}^2\right) \tag{5.2}$$

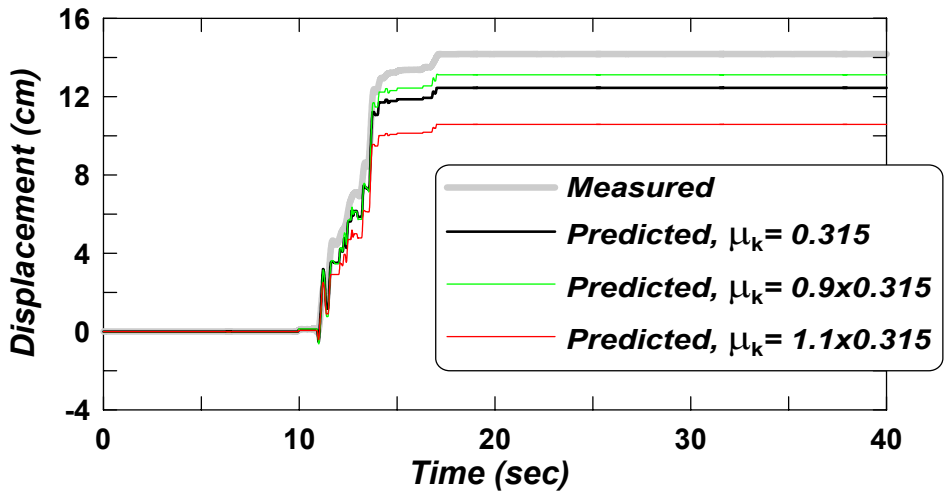

Figure 5.10: Comparison of experimental and analytical equipment sliding displacement subjected to GM - 10 (for $\mu_k = 1.1 \times 0.315$, $\mu_k = 0.315$ (mean), and $\mu_k = .9 \times 0.315$.

where $\hat{d}_{ij}$ is the predicted sliding displacement of the ith trial for the jth ground motion. The value of $(L_2)_{\text{error}}$ is found to be 0.31 for the uniaxial cases, while for the biaxial case, this value is found to be 0.22. Therefore, it may be concluded that by using the determined coefficients of friction, the seismic response can be predicted with fairly reasonable accuracy, depending, of course, upon the desired level of accuracy. To better predict the response of these pieces of equipment, efforts may be given to understand and modify models for the frictional behavior, accounting for velocity-dependent frictional characteristics and contact time. However, considering the complexity of possible mathematical solutions for the broad variety of types of interface conditions encountered in practice, such a refined analysis may not be justified. Alternatively, the problem may be cast in a probabilistic framework, considering a reasonable variation in μ_k and μ_s, to assist with bounding the response and assigning a confidence level to these bounds.

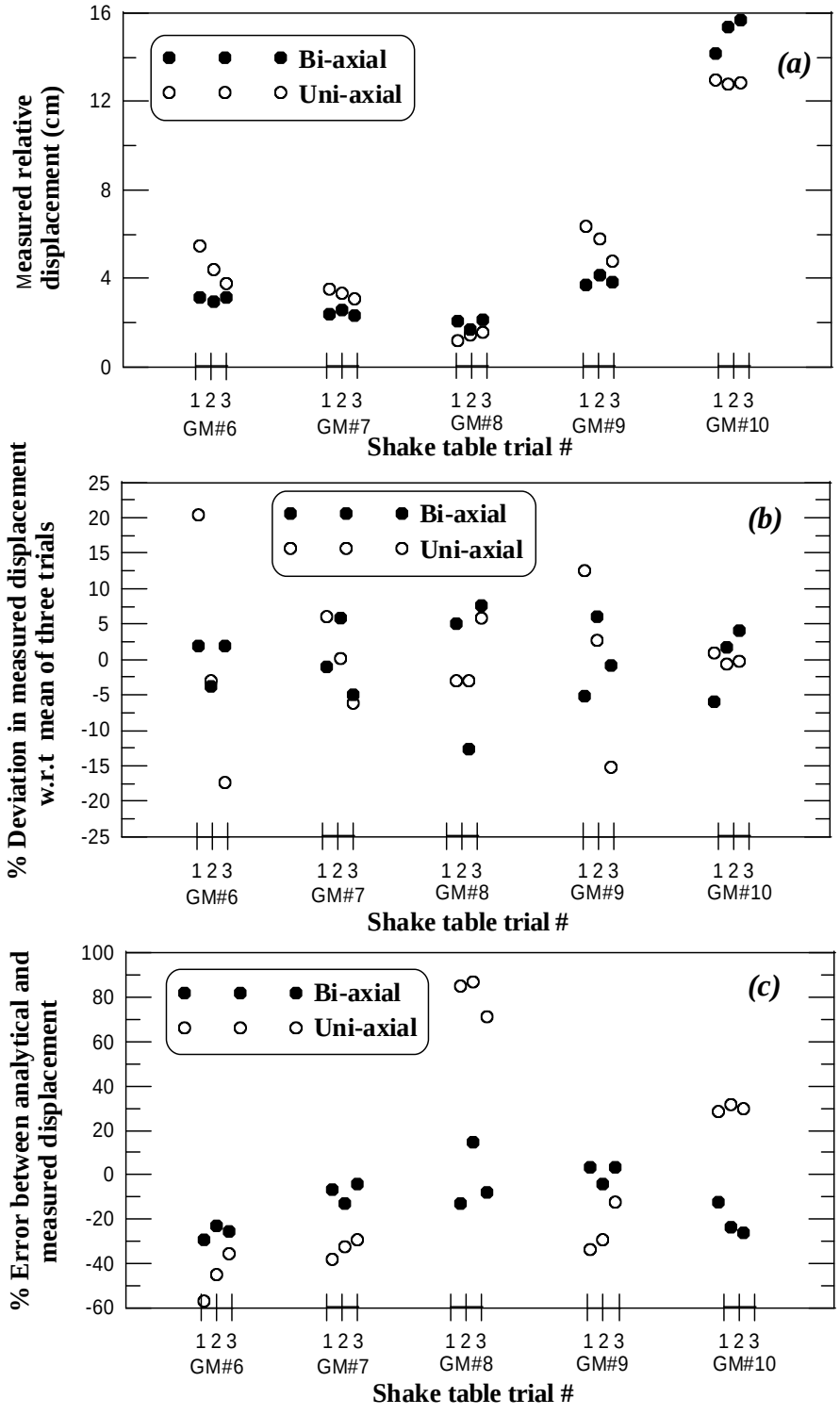

Figure 5.11: Shake table experimental results and analytical predictions of maximum relative displacement for the SGI Indy equipment: (a) measured relative displacement, (b) percentage deviation in measured relative displacement w.r.t. corresponding mean measured values for each ground motion, and (c) percentage error in predicted relative displacement w.r.t. measured relative displacement.

5.5 CHEMICAL GLASSWARE TESTING: EXPERIMENTAL SETUP AND INSTRUMENTATION

Experiments were conducted on representative samples of chemical glassware, also obtained from the UC Science building and science laboratories on UC Irvine's campus. The shelf surface is attached to the shake table for the glassware testing as shown in Figure 5.12. Biaxial and uniaxial shake table experiments were performed, considering different (i) bottle types, (ii) empty and filled bottles, and (iii) input motions. Different bottle types tested included: (a) 500 mL conical flasks, (b) 1000 mL conical flasks, and (c) 1000 mL bottles. Photographs of these glassware are shown in Figures 5.13(a)–(c).

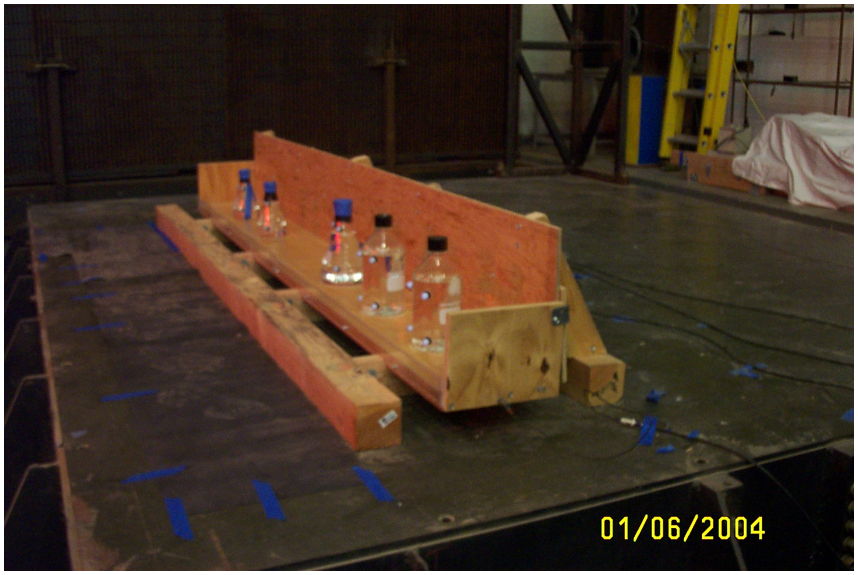

(a)

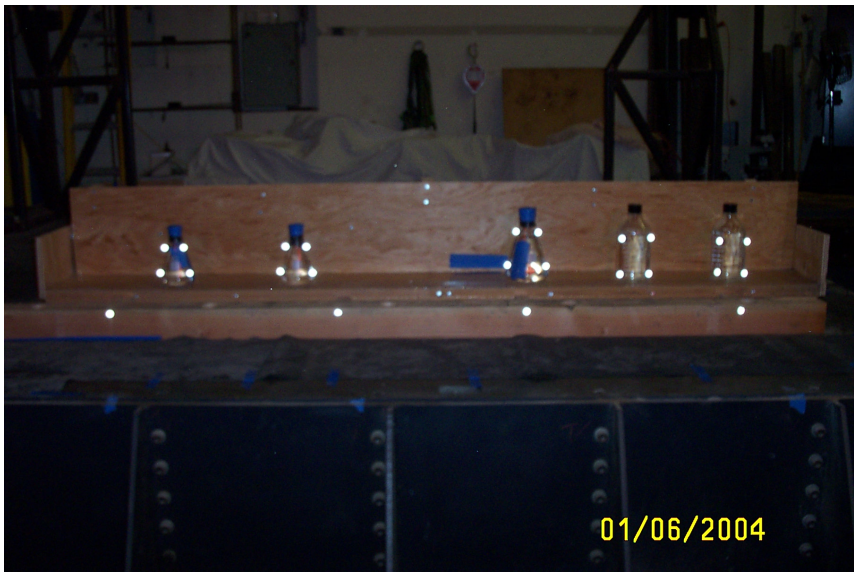

(b)

Figure 5.12: Photographs of glassware tests using mock-shelf: (a) front view and (b) side view of assembly.

(a) (b) (c)

Figure 5.13: Photographs of glassware tested: (a) 500 mL flask, (b) 1000 mL flask, and (c) 1000 mL bottle.

For the testing of the glassware, three conditions were adopted as shown in Figure 5.14. First, all empty glassware were placed on the shelf surface and tested. Second, all glassware were filled with water and tested on the shelf surface. Finally in the third case, a mix of glassware conditions (empty, filled with water, and filled gelatine conditions) were tested simultaneously. For the first and the second cases, two 500 mL conical flasks, one 1000 mL conical flask, and two 1000 mL bottle samples were tested. For the third case, two bottles of each type were tested at the same time. Each ground motion was repeated three times for each of the three cases.

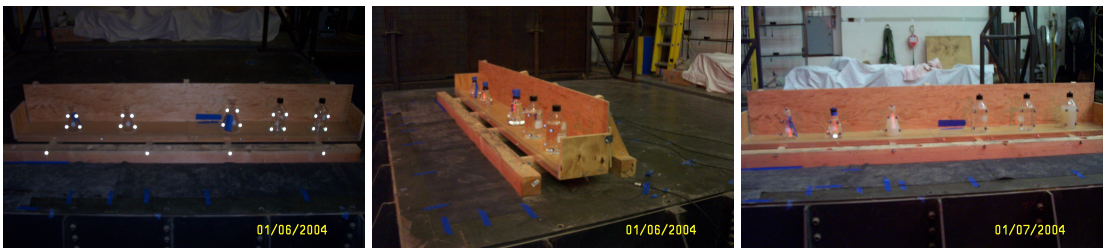

(a) (b) (c)

Figure 5.14: Photographs of the bare shake table testing of glassware using shelf surface (uniaxial and biaxial): (a) all empty glassware (b) all water-filled glassware (c) mixed glassware (empty, filled with water and filled with gelatine conditions).

Six accelerometers and four displacement transducers were used to measure the shake table and the shelf motion. Measurements of glassware movement were taken using the same four camera array used for the equipment testing. Typically, four passive markers were placed on the bottle to track the translation, rotation, and vertical motions of the glassware, as shown in Figure 5.12(b). The shelf and the table movements were also captured using four passive markers.

5.5.1 Seismic Response of Chemical Glassware: Results and Discussion

Figures 5.15(a) and (b) demonstrate the effect of empty and full bottle conditions on the sliding response of 500 mL conical flasks and 1000 mL bottles, respectively, for a trial of GM - 10. It may be observed that different conditions have a different impact on the two glassware. The 500 mL conical flask attains its maximum movement under the empty condition, whereas the 1000 mL bottle attains its maximum movement when filled with water.

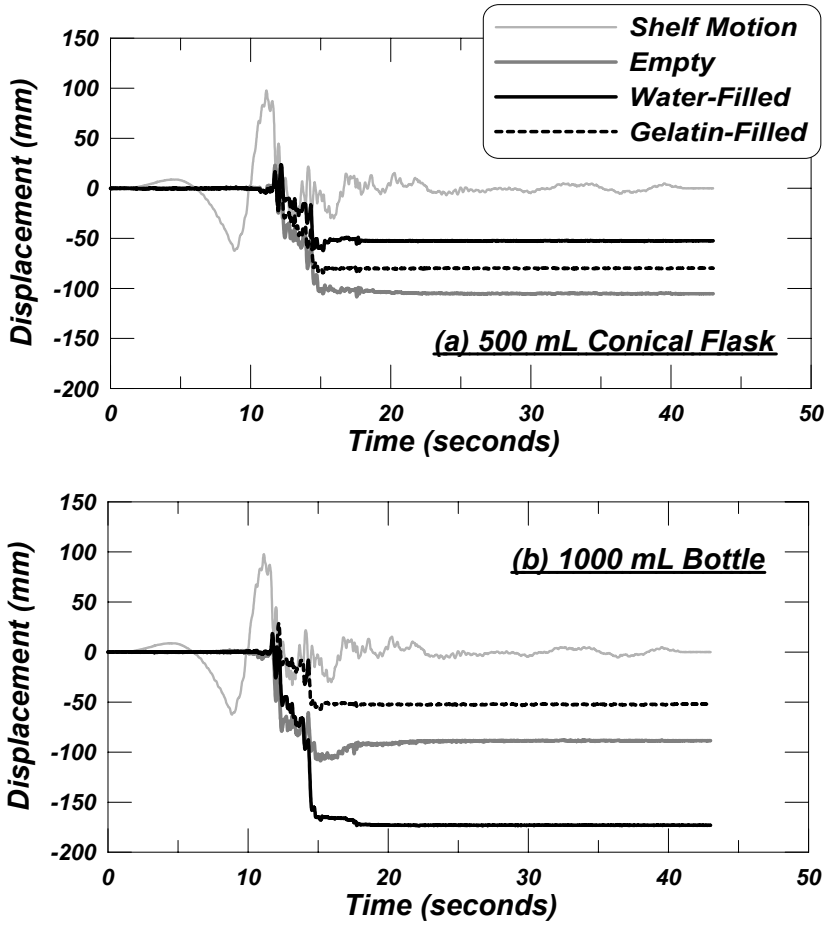

Figure 5.15: Displacement response of glassware samples to GM - 10 (Tottori, Kofu 2% in 50 year) record: (a) 500 mL conical flask and (b) 1000 mL bottle.

Figures 5.16–5.18, 5.19–5.21, and 5.22–5.24 show the sliding response, rocking response, and in-plane rotational response of 500 mL conical flasks, 1000 mL conical flasks, and 1000 mL bottles, respectively, under empty and water-filled conditions. These results are separated into uniaxial and biaxial input conditions. It may be observed from these figures that rocking is minimal (less than 2 degrees) for all glassware. However, significant in-plane rotational response is observed (maximum 70 degrees). It may be noted here that the coefficients of static friction for all the glassware are approximately equal to 0.20. Other observations are listed below.

1. In general, with increasing $PHTA$ maximum relative displacement is increasing.

2. Biaxial motion tended to increase maximum relative displacement with the exception of the 1000 mL bottles.

3. Conical flasks (500 mL and 1000 mL) were more dominated by sliding (lower rocking) due to their lower center of gravity.

4. Rotation about the vertical axis was insensitive to horizontal acceleration input. This might be attributed to the random sloshing effect, which is instigated even before any sliding begins.

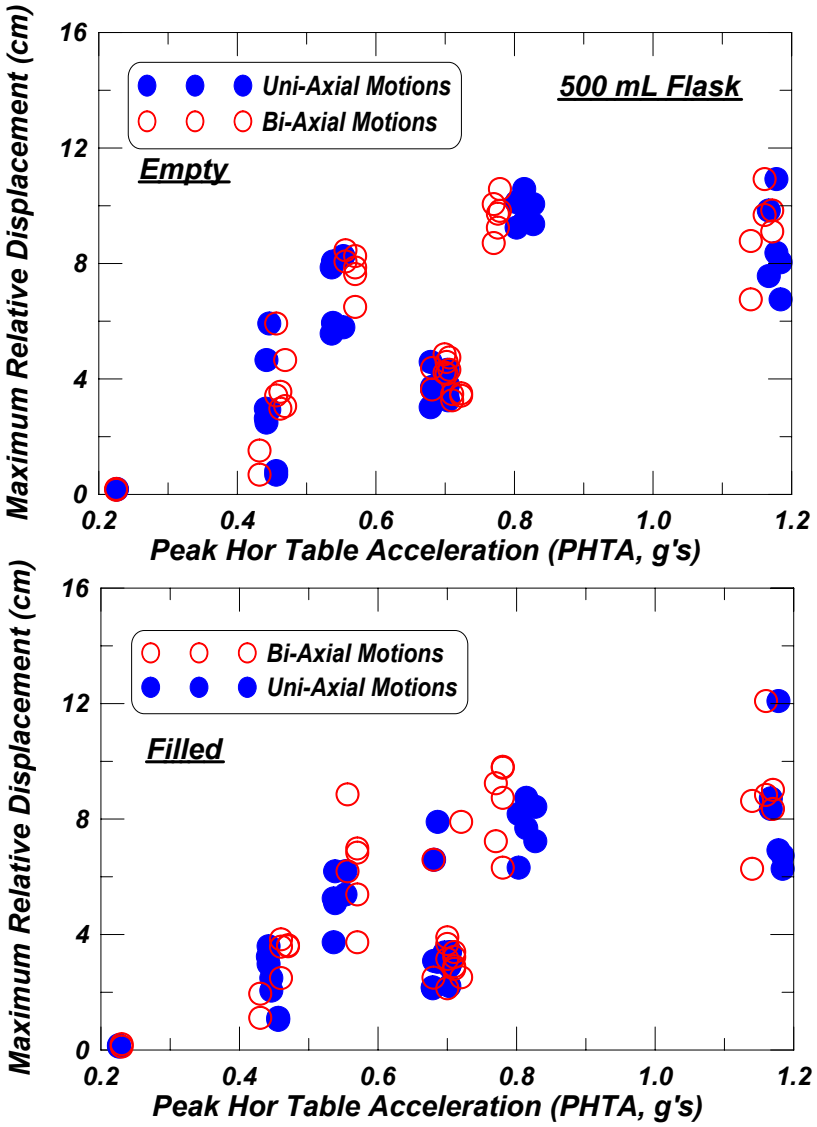

Figure 5.16: Summary glassware maximum relative displacement response – *500 mL flask*: (a) empty and (b) water-filled condition.

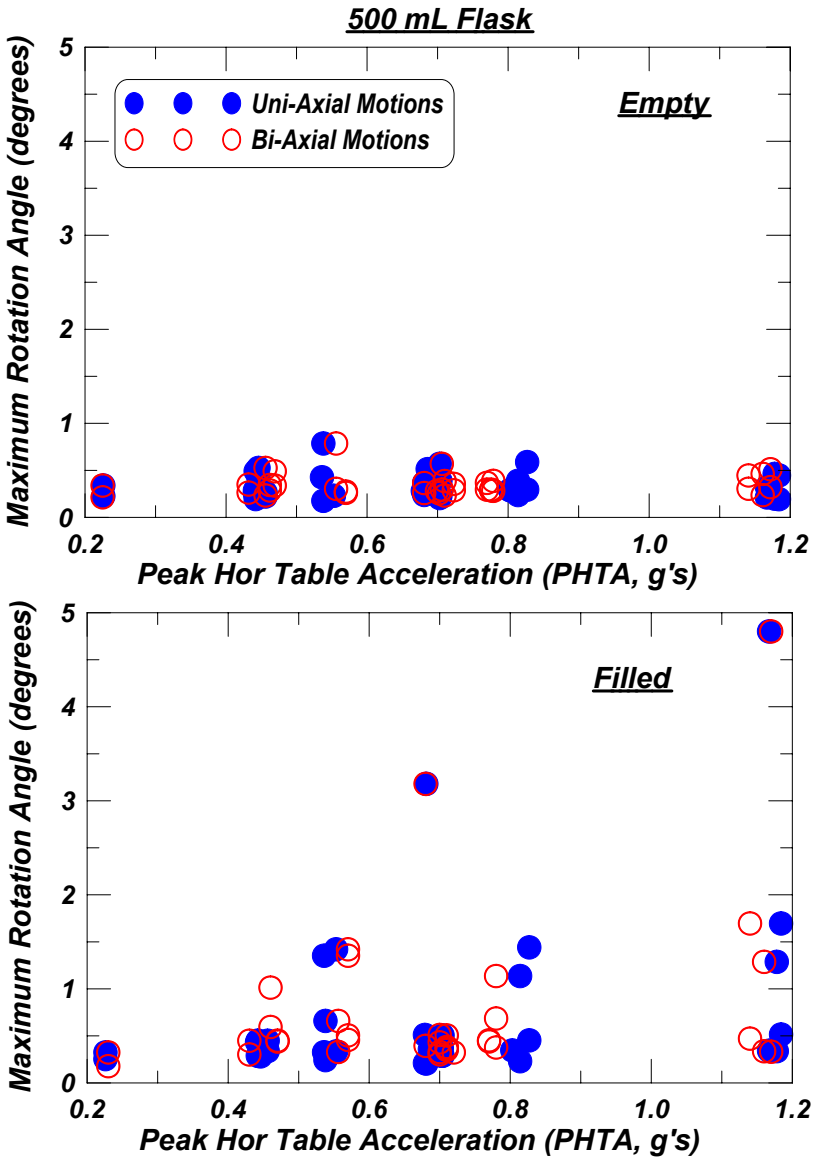

Figure 5.17: Summary glassware maximum rocking rotation (rotation about y-axis) response – *500 mL flask*: (a) empty and (b) water-filled condition.

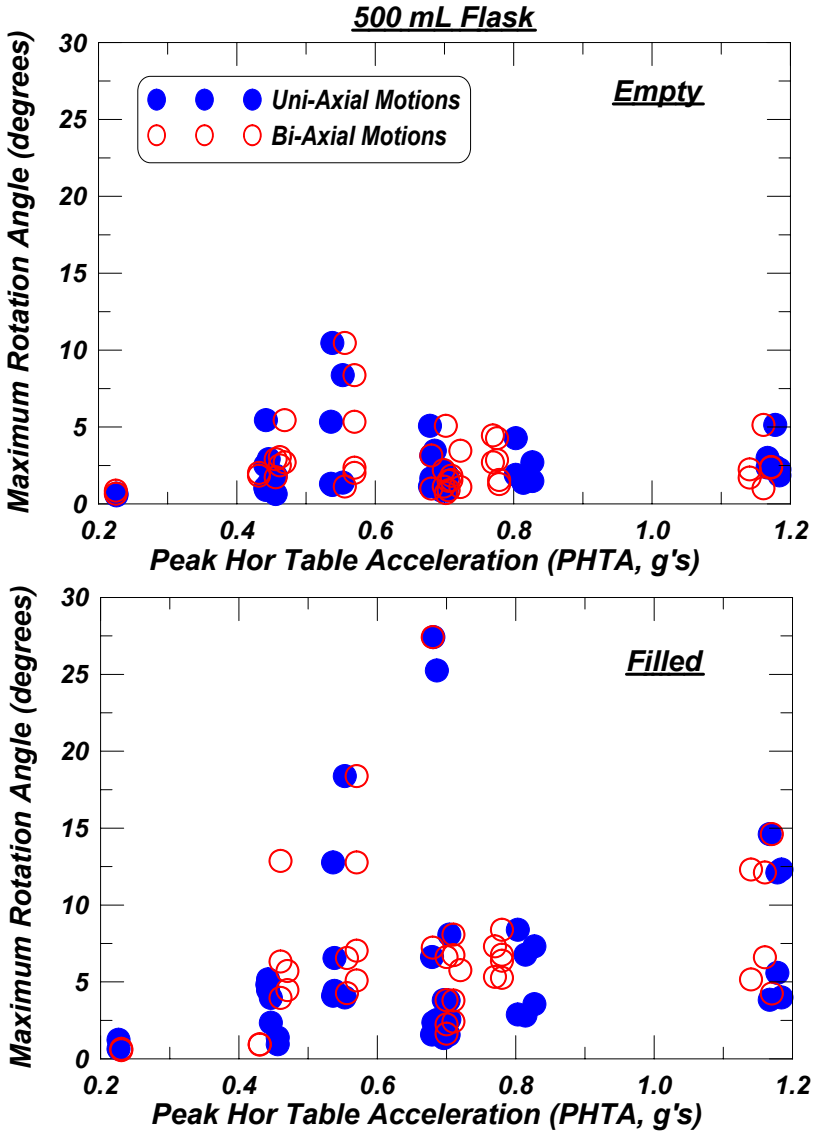

Figure 5.18: Summary glassware maximum in-plan rotation (rotation about z-axis) response – *500 mL flask*: (a) empty and (b) water-filled condition.

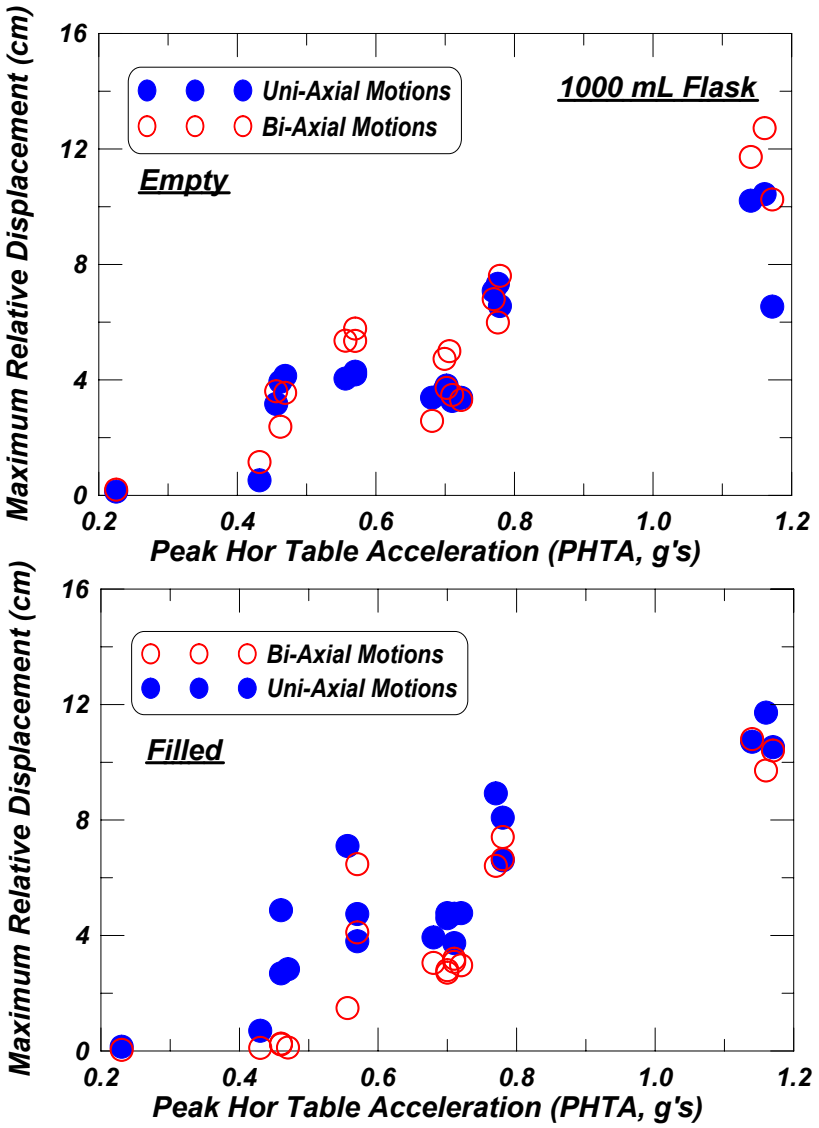

Figure 5.19: Summary glassware maximum relative displacement response – *1000 mL flask*: (a) empty and (b) water-filled condition.

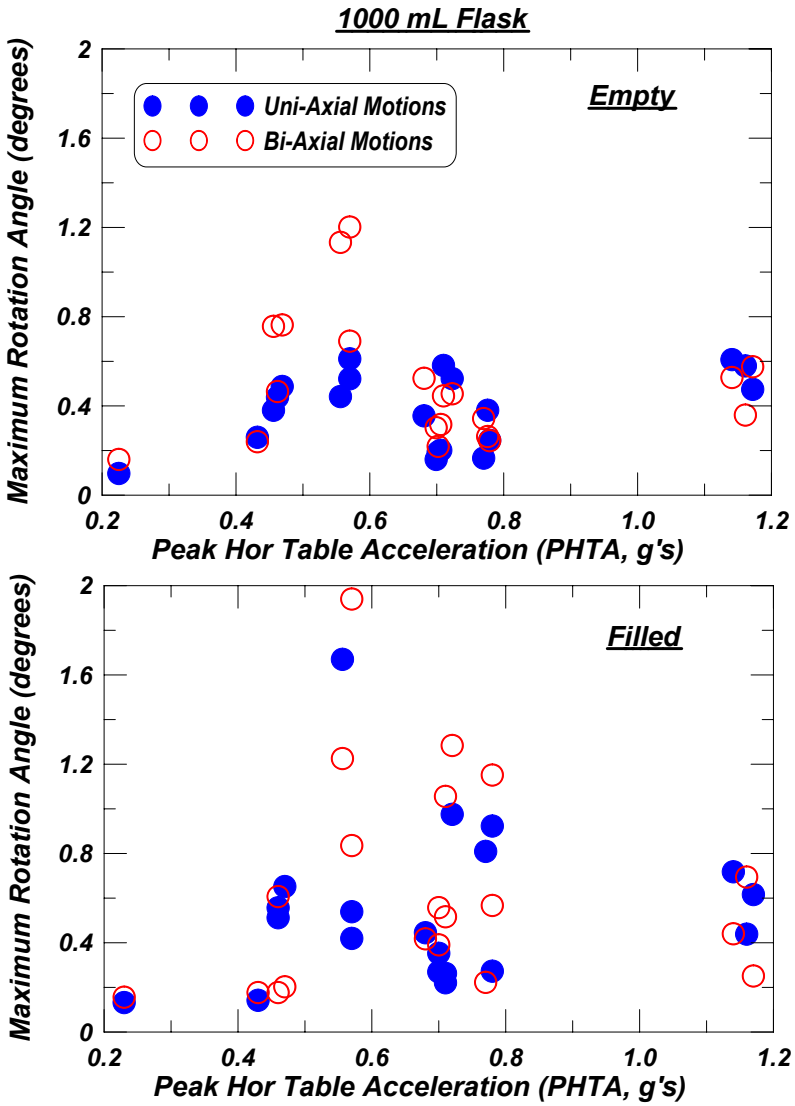

Figure 5.20: Summary glassware maximum rocking rotation (rotation about y-axis) response – *1000 mL flask*: (a) empty and (b) water-filled condition.

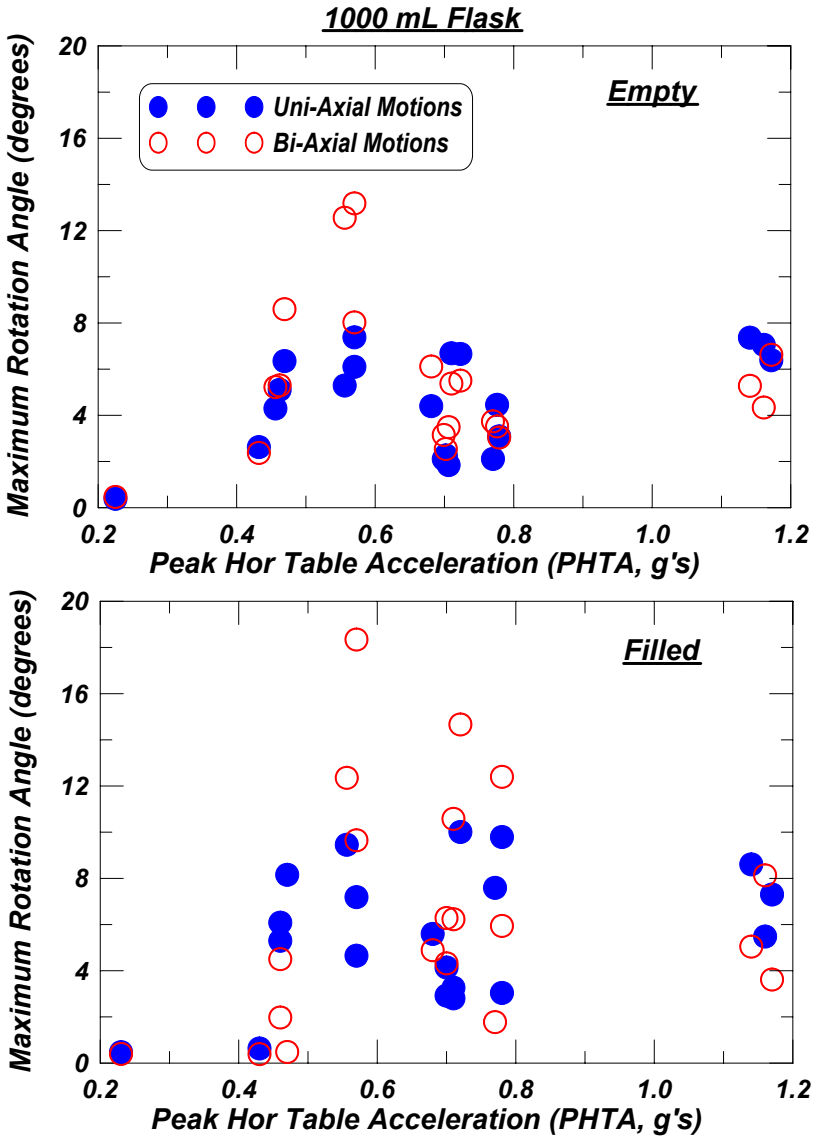

Figure 5.21: Summary glassware maximum in-plan rotation (rotation about z-axis) response – *1000 mL flask*: (a) empty and (b) water-filled condition.

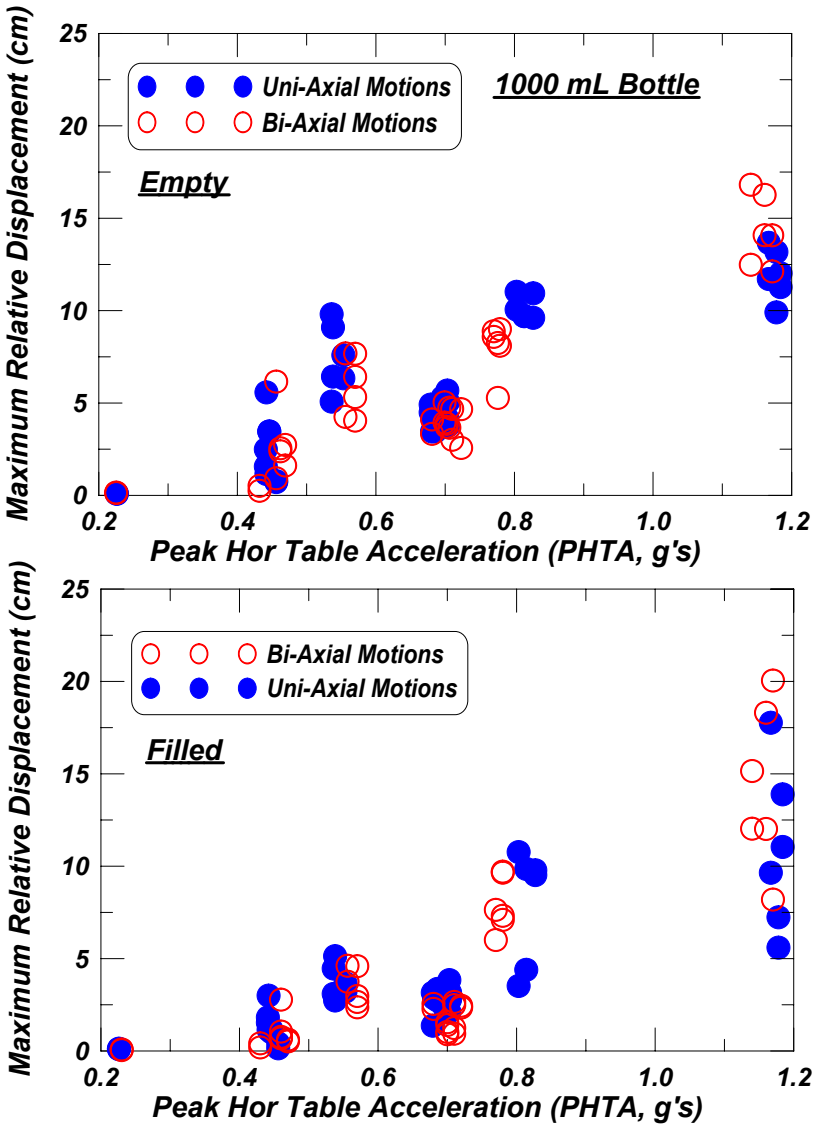

Figure 5.22: Summary glassware maximum relative displacement response – *1000 mL bottle*: (a) empty and (b) water-filled condition.

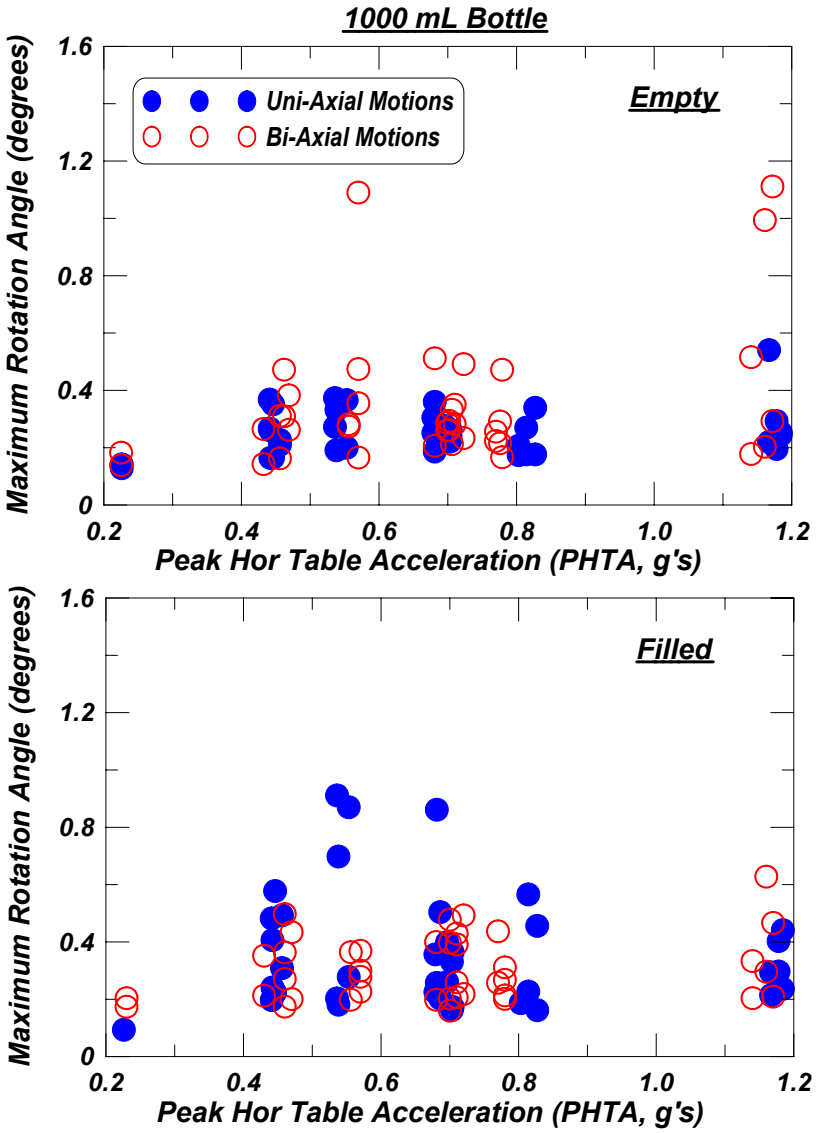

Figure 5.23: Summary glassware maximum rocking rotation (rotation about y-axis) response – *1000 mL bottle*: (a) empty and (b) water-filled condition.

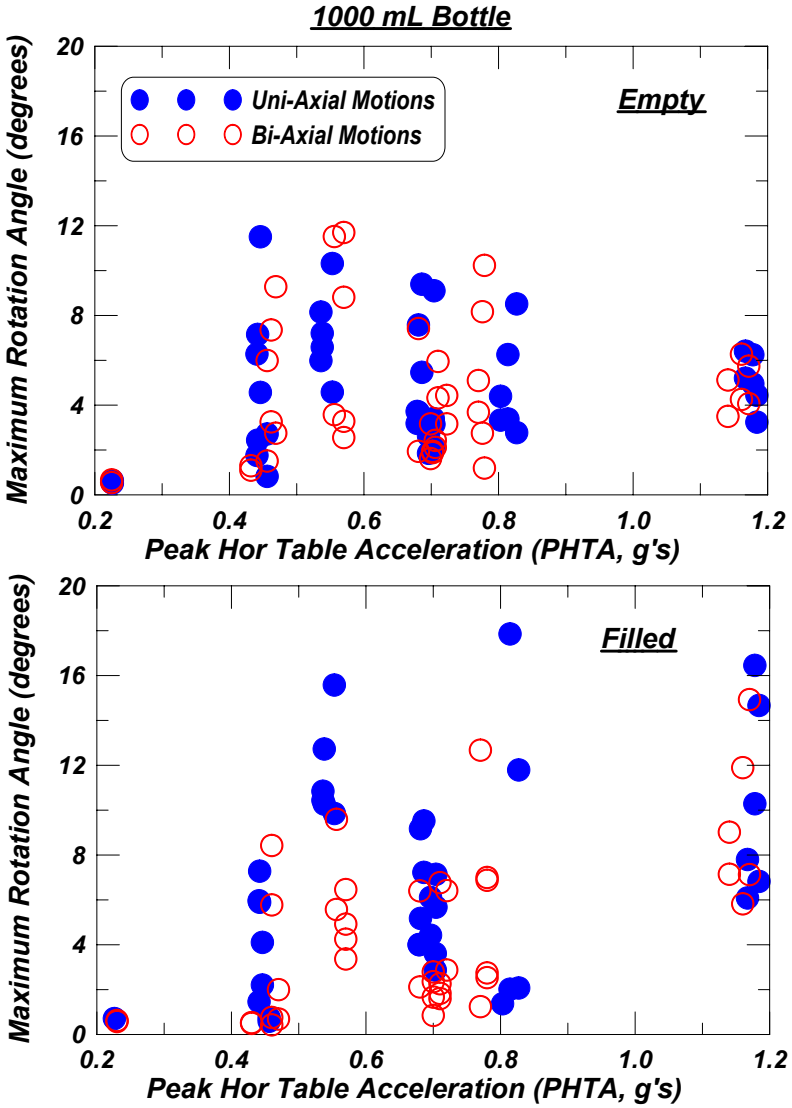

Figure 5.24: Summary glassware maximum in-plan rotation (rotation about z-axis) response – *1000 mL bottle*: (a) empty and (b) water-filled condition.

Figure 5.25 shows the relative sliding response of the 1000 mL bottles and the 500 mL conical flasks under uniaxial and biaxial motion for the mixed testing case (third case). It may be observed that, in general, the response of the empty glassware is larger when compared with the gelatine and water-filled conditions. This may be due to energy dispassion by liquid sloshing. In addition, for a given $PHFA$, the response of the taller 1000 mL is generally greater than that of the 500 mL flasks. Figure 5.26 demonstrates the effect of vertical input. It may be observed here that there is no discernible trend in the difference of response between the uniaxial and biaxial input cases.

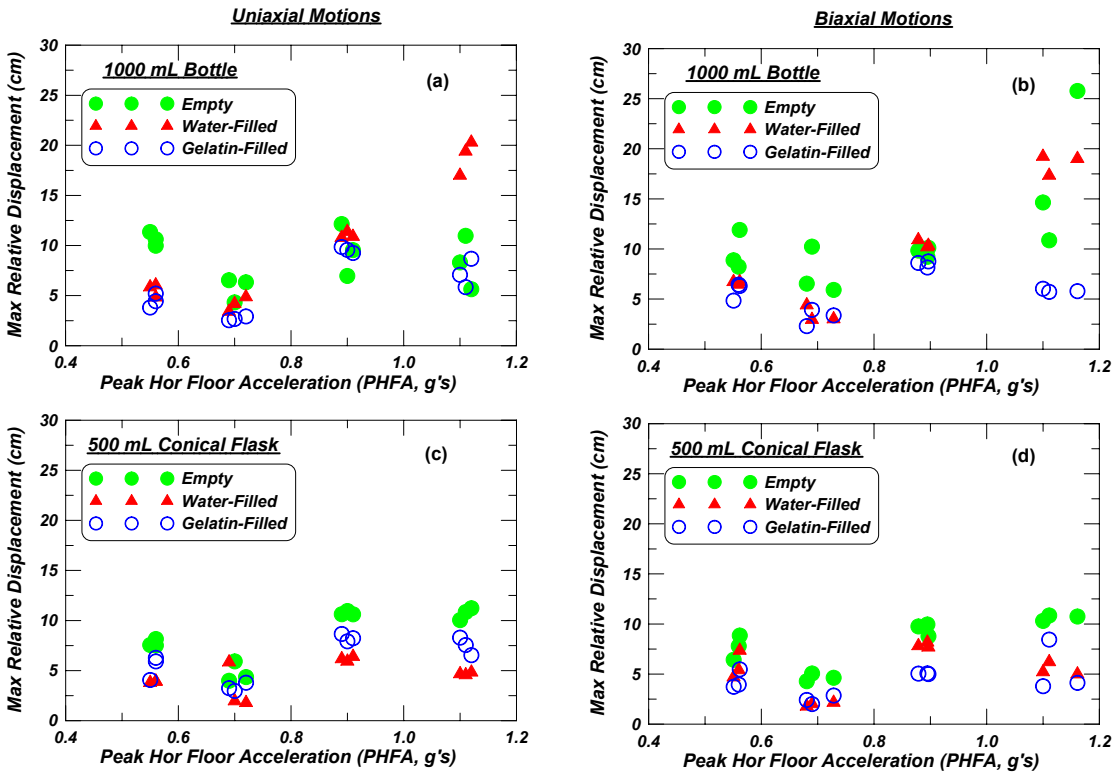

Figure 5.25: Summary glassware maximum relative displacement response. Glassware are empty, filled with water and filled with gelatine conditions: (a) 1000 mL bottle subjected to uniaxial input, (b) 1000 mL bottle subjected to biaxial input, (c) 500 mL flask subjected to uniaxial input, and (d) 500 mL flask subjected to biaxial input.

5.6 SUMMARY REMARKS

In this chapter, results are presented from shake table testing of equipment and glassware using a bare shake table scenario where only bench and shelf interfaces are considered. The experiments show that the response of equipment is predominantly sliding, although some equipment are observed to be sensitive to rocking behavior. It is also observed that the response of equipment is in good agreement with analytical predictions when the measured bench-top

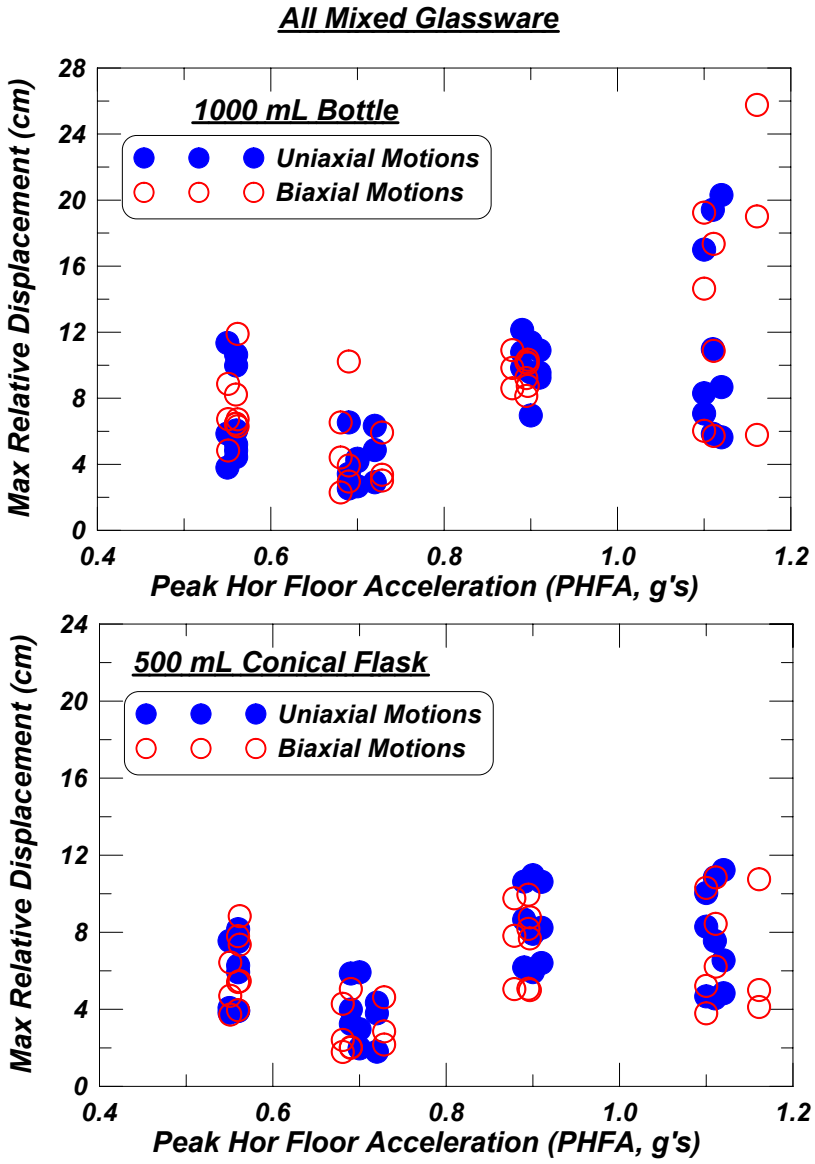

Figure 5.26: Summary glassware maximum relative displacement response – *uniaxial and biaxial input condition*: (a) 1000 mL bottle and (b) 500 mL flask.

acceleration is considered and using average coefficients of friction. It is also observed that, the response magnitude is very sensitive to the coefficient of kinetic friction.

Shake table testing of glassware in three different setups also shows that the response of glassware is sliding dominated. The rocking is not observed to be significant for these glassware. It is found that glassware rotates significantly about its vertical axis while sliding. Therefore, it may be expected that in a real scenario glassware may fail due to sliding and impacting with a shelf or plexiglass barrier.

6 Development of Seismic Fragility Curves

6.1 INTRODUCTION

A seismic fragility curve associates the probability of exceedance of a defined limit state (a damage measure, DM) with an engineering demand parameter (EDP). An EDP may be considered an input parameter to the fragility curve, e.g., maximum floor acceleration or maximum inter-story drift, whereas a DM may be considered an output parameter, e.g., excessive amount of sliding or impact. Seismic fragility curves are useful in the context of performance-based earthquake engineering, as they are cast in a probabilistic form and can be formulated to account for uncertainties in the problem of interest. Such fragility curves are also useful for loss-estimation studies (Comerio and Stallmeyer, 2002; Comerio, 2003).

In this chapter, analytically developed fragility curves for bench-mounted equipment subjected to seismic excitation are presented. It is assumed that the equipment response is dominated by unidirectional sliding behavior, and vertical seismic motion is not considered in the formulation. Fragility curves are developed for bench-mounted rigid equipment considering different: (i) types and magnitudes of damage measures (DM) (displacement and velocity), (ii) coefficients of static and kinetic friction, and (iii) supporting bench characteristics. In addition, the overall uncertainty due to the range of excitations (provided by the structure and at the ground level) is considered. The importance of maximum relative displacement as a damage measure can be appreciated by considering the possibility of the bench-mounted equipment moving beyond the clear distance from the center of the equipment to the edge of the bench, which may cause the equipment to fall from the bench-top and become damaged. Alternatively, due to impact with a neighboring object, loss of functionality may occur. In the latter case, the displacement threshold is dependent upon the distance to neighboring objects. Given such potential damage to the equipment, a reasonable damage measure can be expressed as the maximum value of the absolute relative sliding exceeding some threshold value of sliding. The threshold distance may be the minimum of either the minimum distance between two neighboring pieces of equipment or the minimum edge distance from the center of gravity of the equipment. A velocity DM may be important considering the impact between two pieces of equipment. In this study, a simplified design expression is presented relating the input EDP to the DM of maximum relative displacement.

6.2 SYSTEM AND PARAMETERS CONSIDERED

Twenty-two measured ground motions are scaled to different hazard levels of 50, 10, and 2% in 50 years, resulting in a total of 32 input motions (Sommerville, 2005). It is important to note that the scaled ground motions considered for this study are generated from actual ground motions obtained from different sites comparing their magnitude and distance from the fault plane to the location of the building. Therefore, these ground motions are representative of actual motions that may occur at the selected site. These motions are subsequently used as base input for a numerical model of a representative seven-story science building (Lee and Mosalem, 2005), generating a total of 224 (base and floor level) motions, which are used for development of the fragility curves.

The cascade approach (as illustrated Chapter 1, Figure 1.2) is adopted, where component level characterization involves considering the frequency response function (FRF), dominant natural frequency f_n and associated damping ratio ζ_n for the support structure, and using the static and kinetic coefficients of friction for the equipment of interest. System-level characterization involves correlating the floor-level motions generated by a numerical model to the response of the components at the floor levels. This correlation is framed in the context of fragility curves. The ground motions selected, and the building model and framework used are described in the following sections.

6.2.1 Ground Motions Selected

The list of the ground motions used along with their different peak parameters is provided in Table 6.1. These motions represent records from the West Coast of the U.S., and from Japan and Turkey. The resulting range of peak ground accelerations (PGA) encompasses the coefficient of friction for the equipment of interest, with PGA = 0.26–2.5g. The range of peak ground velocity (PGV) for these motions is PGV = 14–260.5 cm/sec, and the range of peak ground displacements (PGD) for these motions is PGD = 1.2–141.2 cm. It may be noted here that the distance of the recording station from the epicenter is between 0–10 km for these records.

6.2.2 Numerical Model of a Representative Science Building

For this study, a numerical model of a representative science building where such equipment would be found is constructed by Lee and Mosalem (2005). The building is a seven-story reinforced concrete structure with a lateral load-resisting system consisting of coupled shear walls in the transverse direction and perforated shear walls in the longitudinal direction. The floors consist of a waffle slab system with solid portions providing an integral beam between the columns. A numerical model was developed in OpenSees (OpenSees, 2003) for this structure, using a representative 2D section of the building along the transverse direction (Lee and Mosalem, 2005). The building has a reasonable amount of nonlinearity contributed through coupling beams connected to elastic, rigid shear walls. The building is supported by a mat

Table 6.1: Earthquake motions used for ground level input, representing hazard levels of (a) 50% in 50 years, (b) 10% in 50 years, and (c) 2% in 50 years at the UC Lab Building site (Sommerville, 2005).

(a) 50% in 50 year hazard level at UC Lab Building

Earthquake	Mw	Station	Distance	Site	Scale	PGA (g)	PGV (cm/s)	PGD (cm)
Coyote Lake, 1979/6/8	5.7	Coyote Lake Dam abutment (T)	4.0	C	1.395	0.39	29.8	3.6
		Gilroy # 6 (T)	1.2	C	0.999	0.47	49.6	7.1
Parkfield, 1966/6/27	6.0	Temblor (T)	4.4	C	1.143	0.64	44.3	5.0
		Array # 5 (T)	3.7	D	0.978	0.36	47.0	9.3
		Array # 8 (T)	8.0	D	2.302	0.56	25.6	8.2
Livermore, 1980/1/27	5.5	Fagundes Ranch (T)	4.1	D	1.644	0.39	23.9	5.1
		Morgan Territory Park (T)	8.1	C	2.958	0.39	23.8	5.6
Morgan Hill, 1984/4/24	6.2	Coyote Lake Dam abutment (T)	0.1	C	0.673	0.75	40.5	3.2
		Anderson Dam Downstream (T)	4.5	C	0.572	0.26	14.0	3.5
		Halls Valley (T)	2.5	C	1.362	0.39	20.2	1.2

(b) 10% in 50 year hazard level at UC Lab Building

Earthquake	Mw	Station	Distance	Site	Scale	PGA (g)	PGV (cm/s)	PGD (cm)
Loma Prieta, 1989/10/17	7.0	Los Gatos Presentation Center (T)	3.5	C	1.016	0.74	92.5	16.6
		Saratoga Aloha Ave (T)	8.3	C	2.653	0.65	94.1	30.3
		Corralitos (T)	3.4	C	1.394	0.53	64.1	19.4
		Gavilan College (T)	9.5	C	2.097	0.66	63.2	12.9
		Gilroy historic		C	2.319	0.67	88.0	24.1
		Lexington Dam abutment (T)	6.3	C	1.925	0.87	209.0	42.6
Kobe, Japan, 1995/1/17	6.9	Kobe JMA (T)	0.5	C	0.912	1.48	154.5	41.6
		Kobe JMA (L)	0.5	C	0.912	0.78	94.6	22.1
Tottori, Japan, 2000/10/6	6.6	Kofu (T)	10.0	C	1.039	0.78	94.6	22.1
		Hino (T)	1.0	C	0.827	0.85	145.9	83.7
Erzincan, Turkey, 1992/3/13	6.7	Erzincan (T)	1.8	C*	2.455	0.69	32.6	6.2

(c) 2% in 50 year hazard level at UC Lab Building

Earthquake	Mw	Station	Distance	Site	Scale	PGA (g)	PGV (cm/s)	PGD (cm)
Loma Prieta, 1989/10/17	7.0	Los Gatos Presentation Center (T)	3.5	C	1.713	1.25	155.9	28.0
		Saratoga Aloha Ave (T)	8.3	C	4.473	1.09	158.6	51.1
		Corralitos (T)	3.4	C	2.350	0.89	108.0	32.7
		Gavilan College (T)	9.5	C	3.535	1.12	106.5	21.8
		Gilroy historic		C	3.910	1.14	148.4	40.6
		Lexington Dam abutment (T)	6.3	C	3.245	1.48	352.4	71.9
		Lexington Dam abutment (L)	6.3	C	3.245	1.41	83.0	12.3
Kobe, Japan, 1995/1/17	6.9	Kobe JMA (T)	0.5	C	1.537	2.50	260.5	70.1
Tottori, Japan, 2000/10/6	6.6	Kofu (T)	10.0	C	1.751	1.31	159.4	37.3
		Hino (T)	1.0	C	1.395	1.44	246.0	141.2
Erzincan, Turkey, 1992/3/13	6.7	Erzincan (T)	1.8	C*	4.139	1.16	55.0	10.4

foundation, which is represented with a nominal base flexibility through a series of elastic-no-tension elements. A lumped mass model is considered and nodal masses are directly computed from the dead load including the superimposed dead load. The first and second modal periods of the numerical model are 0.28 and 0.64 seconds, respectively. Five percent Rayleigh damping is applied to both of these vibration modes. Nonlinear time history analyses using this

numerical model are performed using a modified Newton-Raphson solution strategy.

6.3 PROBABILISTIC FORMULATION

The approach adopted uses the 224 ground- and floor-level acceleration time histories, excluding the roof-level motions, to generate the fragility curves. The bench-top acceleration is determined using the experimental values of bench dynamic behavior (f_n and ζ_n) provided in Chapter 4. Bench-top accelerations are then considered as input into the Coulomb sliding model described in Chapter 2 and, for the different pieces of equipment, with their uncertainty in μ_s and μ_k, the absolute maximum displacement and velocity relative to the bench is determined. Engineering judgment must then be applied in the selection of limit states for the DMs considered. Upon analysis of the results, if the limit state is exceeded, then the probability of exceeding that limit state for that particular result is unity, and if the limit state is not exceeded, then the probability is zero. This process is continued for each of the EDP values. In this work, the peak horizontal floor acceleration ($PHFA$) is selected as the EDP in fragility construction, given the trends observed during testing (Section 4.3.2). To develop the fragility curves, the framework of probability theory is applied, with the underlying assumption that the probability of exceeding a particular limit state is a lognormal distribution. The probability of exceeding a particular limit state is therefore given by:

$$F(a_i) = \Phi\left(\frac{\ln(a_i/\tilde{m})}{\tilde{\sigma}}\right) \tag{6.1}$$

where $F(a_i)$ = probability of exceeding a particular limit state for a given $PHFA$ taken as a_i, and $\tilde{m}$ and $\tilde{\sigma}$ = the median and log-standard deviation of the lognormal distribution, respectively. $\Phi(x)$ = the value of the standard normal for the variable x. Provided that the median and log-standard deviation of the lognormal distribution are evaluated, for each a_i one may determine the probability that a particular limit state has been exceeded. To determine $\tilde{m}$ and $\tilde{\sigma}$, the maximum likelihood theory is used (Shinozuka *et al.*, 2000). Considering, for any case with the peak horizontal floor acceleration a_i, the probability of exceeding a limit state is provided by $F(a_i)$, and for any case in which the limit state is not exceeded, the probability of exceeding that limit state is then provided by $(1 - F(a_i))$. The likelihood function $L(\tilde{m}, \tilde{\sigma})$ may then be expressed as:

$$L(\tilde{m}, \tilde{\sigma}) = \left(\prod_{i=1}^{q} F(a_i)\right)\left(\prod_{j=1}^{n-q} (1 - F(a_j))\right) \tag{6.2}$$

where n = the total number of data points, q = number of cases in which the limit state is exceeded; therefore, $(n - q)$ = number of cases in which the limit state is not exceeded. To obtain the maximum values of $L(\tilde{m}, \tilde{\sigma})$, the following two conditions must be satisfied:

$$\frac{\partial \ln L(\tilde{m}, \tilde{\sigma})}{\partial \tilde{m}} = 0 \qquad \text{and} \qquad \frac{\partial \ln L(\tilde{m}, \tilde{\sigma})}{\partial \tilde{\sigma}} = 0 \tag{6.3}$$

Solving the above two-dimensional optimization problem numerically, m and σ may be determined. After obtaining $\tilde{m}$ and $\tilde{\sigma}$, the probability of exceeding a limit state for which $\tilde{m}$ and

$\tilde{\sigma}$ are determined and for any peak horizontal floor acceleration a_i may be determined using Equation 6.1.

6.4 RESULTS AND DISCUSSION

Five different mean values of μ_s for the different equipment of interest are considered (μ_s = 0.3, 0.4, 0.5, 0.6 and 0.7). The static coefficient of friction A lower and upper limit of these values is assumed as the mean $\pm$10% of the mean, based on the general range of uncertainty observed during static testing. Mean values of μ_k are assumed as 50%, 60%, 70%, 80% and 90% of the coefficient of static friction, i.e., ϕ is assumed as 0.5, 0.6, 0.7, 0.8 and 0.9. Similarly, upper and lower limits of the mean (as $\pm$10% of the mean) are considered for each ϕ. The coefficients of static and kinetic friction are assumed as independent random variables. For the generation of the fragility curves, two values of the mean sliding displacement limit states are considered, namely DM = 5 cm and DM = 10 cm. These values were selected based on review of the general layout of typical laboratories and by engineering judgment. The underlying assumption is that if the piece of equipment moves beyond these selected DM values, the piece equipment will fall from the bench-top and will be damaged. Fragility curves are also generated for DM as equipment relative sliding velocity of 30 cm/s and 50 cm/s. These values were selected assuming equipment may be damaged from a free fall from the bench-top onto the floor system. Considering a limiting drop height of 5 and 10 cm from the bench surface, an ultimate velocity of 100 and 140 cm/s will occur just prior to impact. A reduction of approximately one third was selected to provide two lower-bound relative velocity thresholds. The selection of displacement and velocity limits was consistent with values measured during shake table experiments.

Figure 6.1 shows a sample of the analytical fragility curves for a mean sliding displacement of 5 cm for mean μ_s = 0.3, 0.4, 0.5, 0.6, and 0.7 respectively, with different mean ϕ values. In this case, the bench dynamic properties are taken as f_n = 10 Hz and ζ_n = 10%. For these fragility curves, the peak horizontal floor acceleration is considered as the engineering demand parameter (EDP). It is observed that the fragility curves are sensitive to both the coefficient of static and kinetic friction. From the figures, it is also noted that for a particular mean sliding limit state, as the coefficient of kinetic friction or coefficient of static friction increases, the median value (i.e., 50% of probability of exceedance) of the peak floor acceleration increases. This can be more clearly seen by observing Figure 6.2(a), where high and low bounds of μ_s (= 0.3 and 0.7) and ϕ (= 0.5 and 0.9) are shown and also damage measures of (a) DM = 5cm and (b) DM = 10cm. Comparing (a) to (b), as the value of the mean sliding limit increases, the fragility curve becomes flatter, i.e., both the median and variance of the probability of exceedance increase. It may also be noted that for higher μ_s values, the spread between high and low ϕ (= 0.5 and 0.9) is larger. In Figure 6.2(b), large changes in peak horizontal floor acceleration are required to increase the probability of exceedance only moderately, at the largest resistance parameters (μ_s = 0.7 and ϕ = 0.9); i.e., the curve is very flat in comparison with other curves. Figure 6.2 implies that when other parameters remain the same, the magnitude

of sliding displacement is less for equipment with higher μ_s and μ_k values.

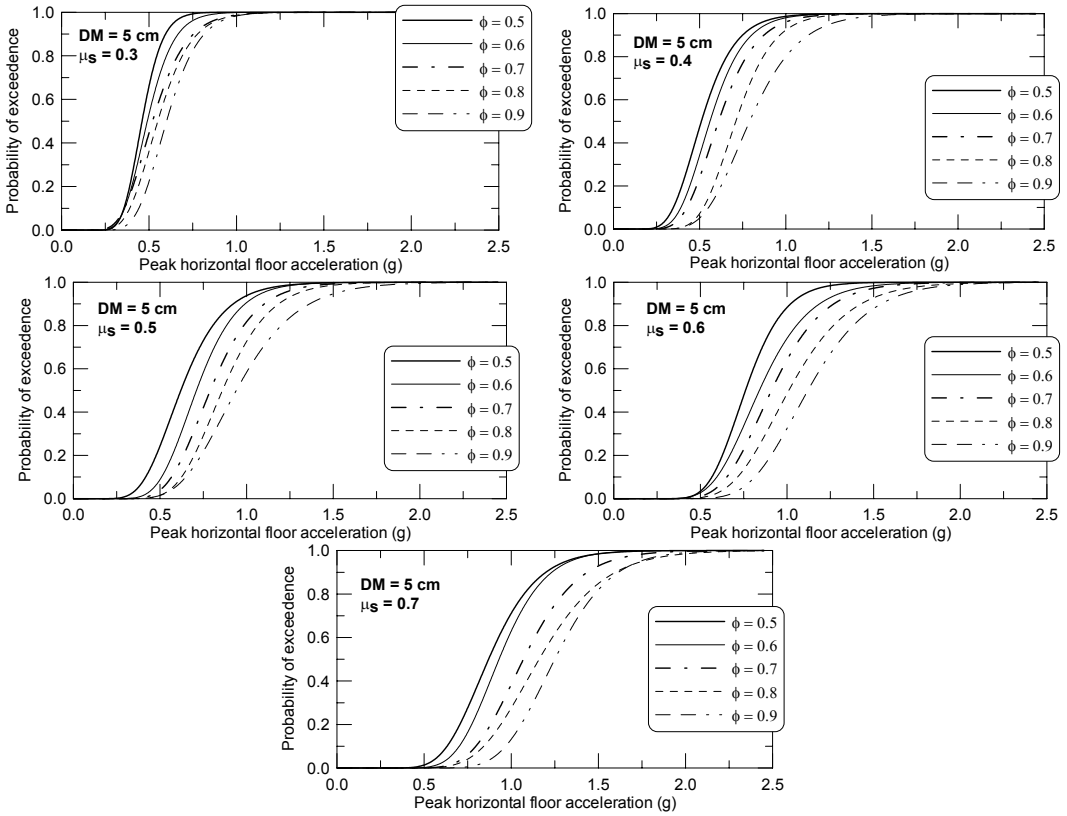

Figure 6.1: Example seismic fragility curves for damage measure DM = 5 cm and range of μ_s and ϕ values.

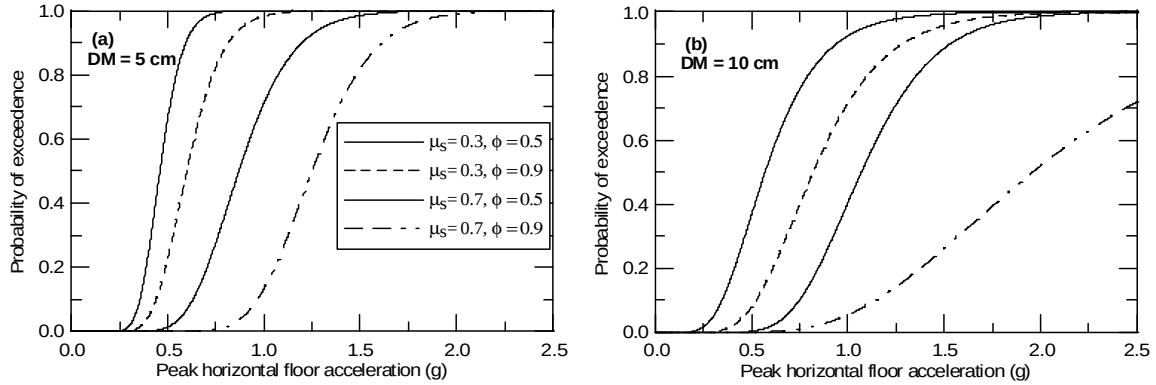

Figure 6.2: Effect of μ_s and ϕ on seismic fragility curves, considering different DMs: (a) 5 cm and (b) 10 cm.

Comparing fragility curves developed by Lopez Garcia and Soong (2003) to those presented herein, it is observed that (for a compatible level of sliding, e.g., at 5 cm, and considering

only horizontal motion) curves by Lopez Garcia and Soong (2003) are unconservative. This is largely due to the bench contributions, which amplify the base level (input) motions. In addition, motions used in the study by Lopez Garcia and Soong (2003) were design spectrum compatible (synthetically generated) ground motions, whereas motions used in this study were field measured and scaled to different representative hazard levels. It is also important to note that the building properties considered in this study contribute to the final properties of the fragility curves.

Figure 6.3 shows a sample of the analytical fragility curves for a mean relative sliding velocity of 50 cm/sec for mean μ_s = 0.3, 0.4, 0.5, 0.6, and 0.7, with different mean ϕ values. Similar to Figure 6.2, the bench dynamic properties are taken as f_n = 10 Hz and ζ_n = 10% for these curves. Similar trends are observed in these (velocity-based) fragility curves. Figures 6.4(a) and (b) provide a comparison plot of the curves for the upper- and lower-bound mean μ_s (= 0.3 and 0.7) and mean ϕ (= 0.5 and 0.9) and damage measures of (a) DM = 30cm/sec and (b) DM = 50cm/sec. Similar to the displacement damage measure curves, comparing Figures 6.4(a) to (b), as the value of the mean sliding velocity increases, the fragility curve becomes flatter, i.e., both the median and log-standard deviation of the probability of exceedance increase.

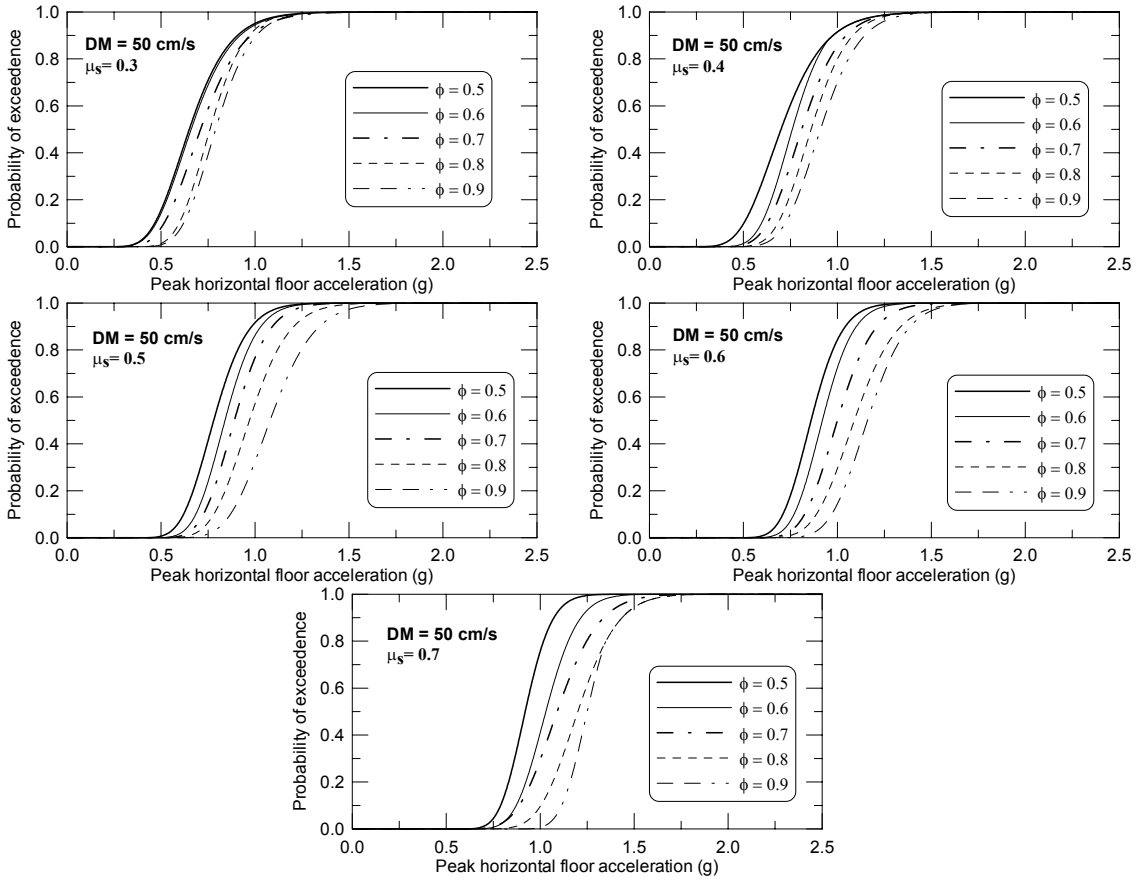

Figure 6.3: Sample seismic fragility curves for damage measure = 50 cm/sec and range of μ_s and ϕ values.

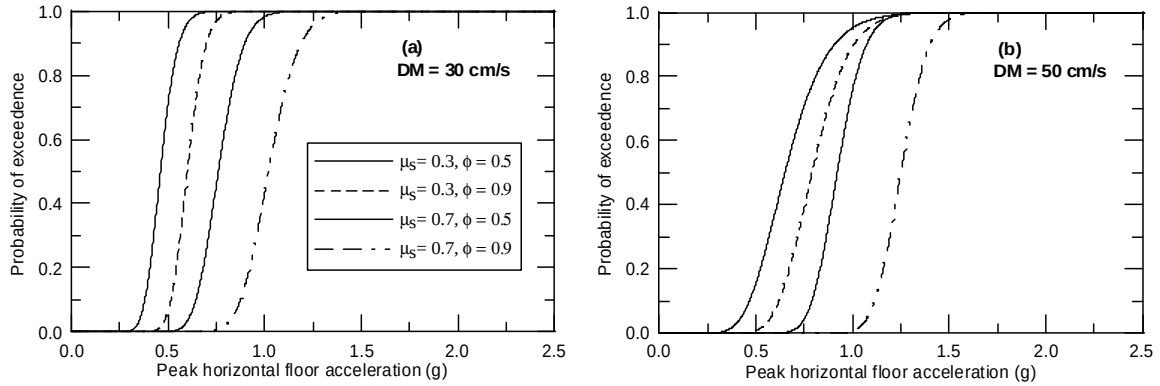

Figure 6.4: Effect of μ_s and ϕ on seismic fragility curves (high and low bounds study), considering different maximum relative velocity DMs where: (a) DM = 30 cm/s and (b) DM = 50 cm/s.

To observe the effect of uncertainties in the coefficients of static and kinetic friction, fragility curves are generated considering the mean, mean $+\,\sigma$, and mean $-\,\sigma$ and then compared with curves generated considering a deterministic value (i.e., no uncertainties considered and the mean values of the coefficients of static and kinetic friction are deterministic). Figure 6.5 shows these curves developed for the upper- and lower-bound mean μ_s (= 0.3 and 0.7) and mean ϕ (= 0.5 and 0.9), and a damage measure of mean relative displacement, DM = 5 cm. For all cases considered in this study, the deterministic curves follow very closely to the mean curves. In addition, the deviation of the mean, with the $m + \sigma$ and $m - \sigma$ fragility curve, increases when the value of the coefficient of static and kinetic friction is increased. Comparing these curves with higher limit states (DM = 10 cm), it is also noted that the deviation between the $m + \sigma$ and $m - \sigma$ increases. It is also observed that this variation is less than $\pm 10\%$ (when the median is considered), even considering the higher limit state of 10 cm.

6.4.1 Effect of Variability of Support Structure

To study the effect of the dynamic behavior of the supporting bench on the fragility of the equipment, Figures 6.6 and 6.7 consider a range of natural frequencies f_n (= 10 and 15 Hz) and damping levels, ζ_n (= 10 and 15%), for mean relative sliding limit states of 5 cm and 10 cm. Figures 6.6 (a) and (b) illustrate that as the supporting bench becomes stiffer, the median value of the fragility curve increases. In other words, as the bench becomes stiffer, the dynamic amplification of the system reduces, thus leading to less sliding. It may also be noted from Figures 6.6(a) and (b) that higher values result in greater sensitivity to f_n. For example, for the ϕ = 0.9 curves, the variation between f_n = 10 and 15 Hz for a given μ_s and DM is larger than those of the ϕ = 0.5. Observing Figure 15(b), for higher DM values, the dispersion between the curves (for the f_n values) increases with increasing probability of exceedance. Figure 6.7 illustrates that as the damping ratio is increased from ζ_n = 10 to 15%, the value of the peak horizontal acceleration at the median value increases. It is also noted that the fragility curve is

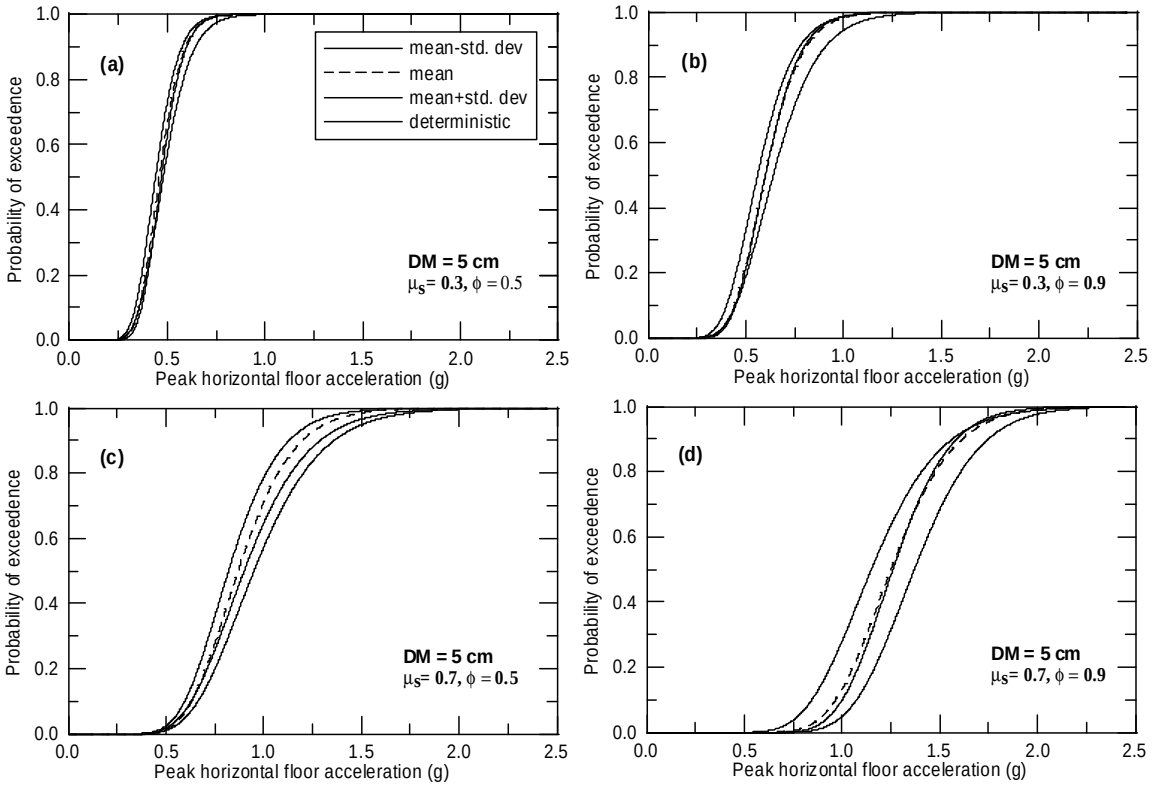

Figure 6.5: Fragility curves for DM = 5cm, uncertain μ_s and ϕ, considering m , $m+\sigma$, $m-\sigma$, and deterministic approach (no uncertainties in μ_s and ϕ).

more sensitive to damping for larger ϕ values (e.g., for ϕ = 0.9 the dispersion of a given curve for ζ_n = 10 and 15% is greater than those curves for ϕ = 0.5). These examples illustrate the sensitivity of the maximum sliding response to the dynamic properties of the support structure (bench), which may be characterized by f_n and ζ_n.

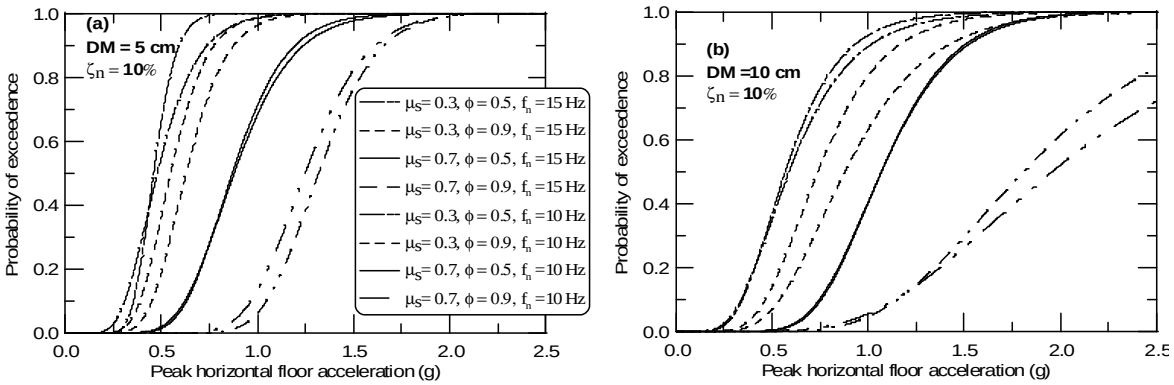

Figure 6.6: Effect of f_n on the fragility curves for a range of μ_s and ϕ values and considering different maximum relative displacement DMs where: (a) DM = 5 cm and (b) DM = 10 cm.

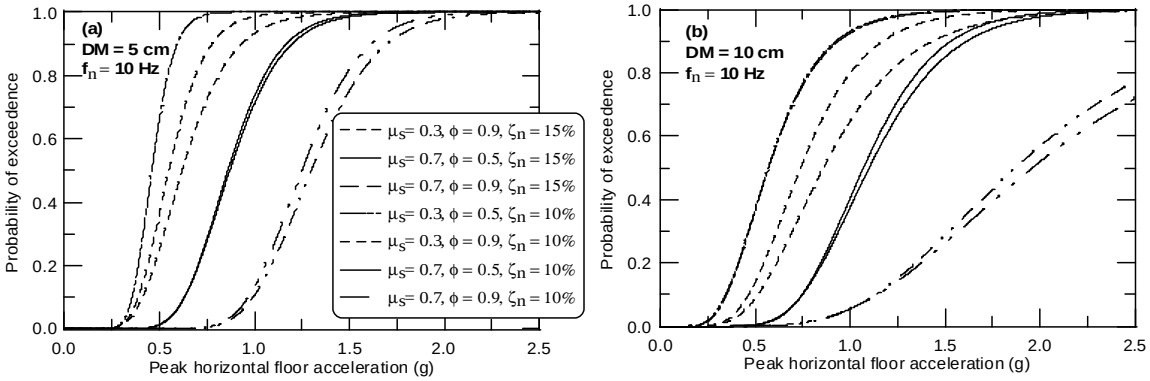

Figure 6.7: Effect of ζ_n on the fragility curves for a range of μ_s and ϕ values and considering different maximum relative displacement DMs where: (a) DM = 5 cm and (b) DM = 10 cm.

6.5 DEVELOPMENT OF SIMPLIFIED FRAGILITY CURVES

Although the fragility curves may be developed on a per-equipment basis, the equipment may be categorized by their frictional behavior into five broad categories. Moreover, an unknown threshold of sliding may be desirable. Table 1 shows the classification selected for the bench-mounted science equipment of interest in this study. Therefore, a useful presentation of these fragility curves from a loss estimation (and designers) perspective is to represent the median and log-standard deviation values as a function of the different DMs and the equipment categories noted in Table 6.2. Figure 6.8 shows the parameters for the lognormal distribution of all five categories of equipment given in Table 6.2, with changing displacement level, where (a) to (e) show the median $\tilde{m}$, and (f) to (i) show the coefficient of variation ($COV = \frac{\tilde{\sigma}}{\tilde{m}}$). These parameters are determined for both the mean and mean+sigma response (considering a similar $\pm$ 10% variation in μ_s and μ_k). These curves are generated by calculating the response at an incremental DM of 0.5 cm. It is observed that as the value of the damage measure increases, $\tilde{m}$ increases; however, there is no clear trend observed in the COV. In general, the COV is observed to become constant at higher damage measures. It is interesting to note that although a $\pm$10% variability in μ_s and μ_k is considered, it is observed that as the DM increases, the percentage deviation of median between mean and mean+standard deviation decreases. These plots in Figure 6.8 therefore represent a generalized fragility curves.

It may be observed from Figure 6.8 that for a damage measure of 3cm or more, the lognormal parameters ($\tilde{m}$ and COV) follow a straight-line trend. Therefore, both of these parameters can be simplified to fit a straight line in a least-square sense or in a conservative manner (i.e., considering the lower bounds). The median $\tilde{m}$ can be simplified as a straight line of the form $\tilde{m} = b_1 DM + c_1$, and the COV can be assumed as a straight line parallel to abscissa (i.e., $COV = c_2$). Using the simplified expression for $\tilde{m}$ and COV, and re-arranging the terms of Equation 6.1, and neglecting smaller terms, the $PHFA$ (which is the EDP for this case) can

Table 6.2: Equipment categorized by the base resistance.

Category	**Items**	**Average** μ_s	**Average** ϕ
1	Large Microscope Indy	0.35	0.90
2	38 cm CRT 43 cm CRT	0.45	0.90
3	Technicon Autoanalyzer Indigo Octane	0.65	0.95
4	Eppendorf Centrifuge	0.70	0.90
5	48 cm CRT	0.85	0.95

be expressed in terms of the DM for a given probability of exceedence as:

$$PHFA = \bar{c}_1 + \bar{c}_2 DM + \bar{c}_3 DM^2 \tag{6.4}$$

where $PHFA$ is expressed in g, DM is the damage measure in cm, and $\bar{c}_1$, $\bar{c}_2$ and $\bar{c}_3$ are constants depending upon the equipment category and the probability of exceedence. For example, for a piece of equipment with Category 1, the coefficients become $\bar{c}_1$= 0.35, $\bar{c}_2$ = 0.037, and $\bar{c}_3$ = -0.0017 for 5% probability of exceedence. It may be noted that for a piece of equipment with $\mu_s = 0.35$, $PHFA$ increases beginning with 0.35g at a DM = 0 cm. Table 6.3 gives the values of these coefficients for different scientific equipment categories.

Table 6.3: Coefficients for simplified $PHFA$-DM relation expressed in Equation 6.4.

Probability of Exceedence	Equipment Category	$\bar{c}_1$	$\bar{c}_2$	$\bar{c}_3$
5%	1	0.35	0.037	-0.0017
	2	0.44	0.046	-0.0017
	3	0.55	0.058	-0.0017
	4	0.56	0.064	-0.0019
	5	0.65	0.117	-0.0037
10%	1	0.35	0.056	-0.0016
	2	0.45	0.057	-0.0016
	3	0.57	0.069	-0.0016
	4	0.58	0.076	-0.0018
	5	0.66	0.137	-0.0036

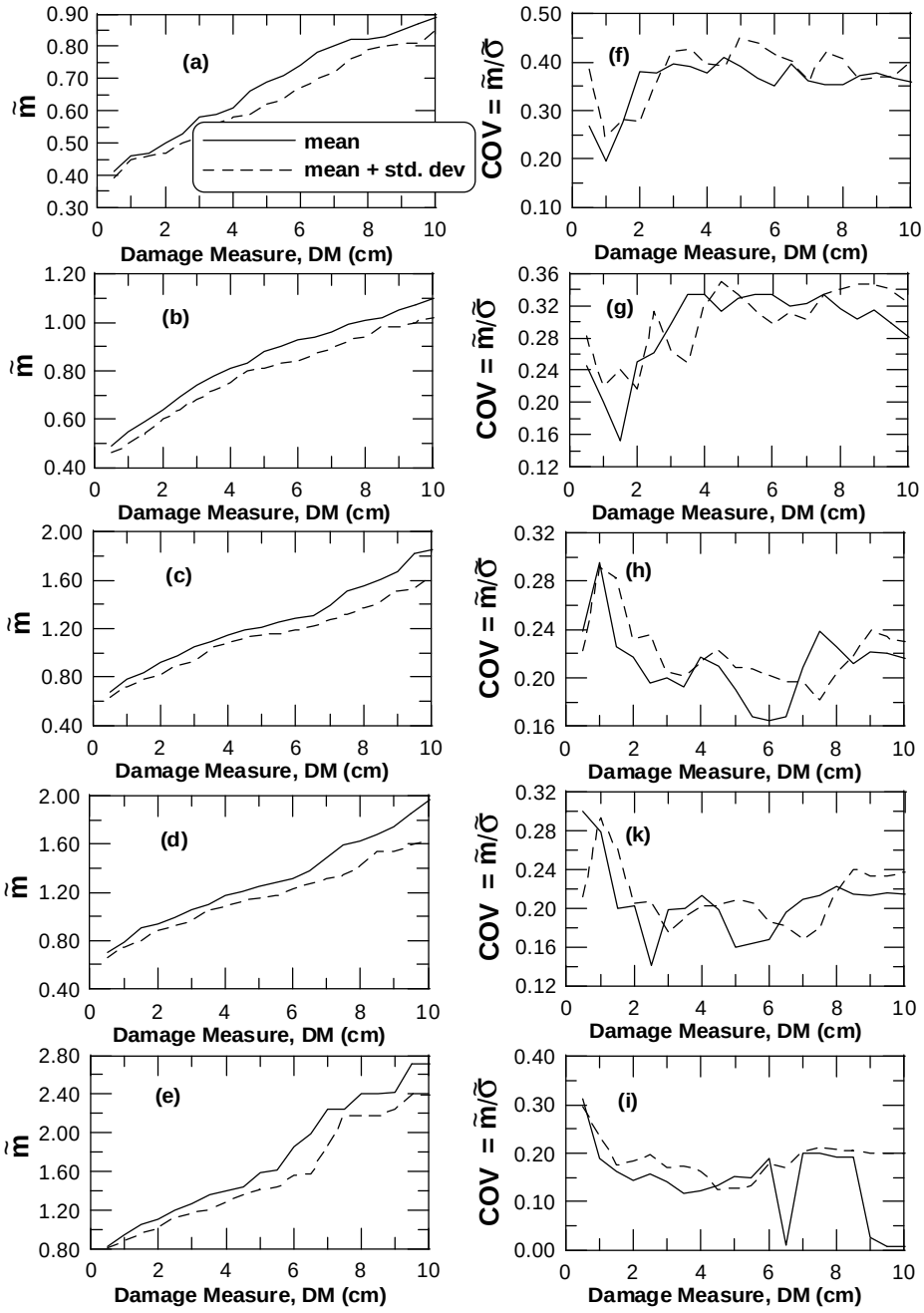

Figure 6.8: Parameters of the lognormal distribution, for varying relative maximum displacement magnitudes: (a)–(e) represent median $\tilde{m}$ and (f)–(i) represent coefficient of variation COV respectively for Categories 1–5, considering the mean and mean + standard deviation response.

6.6 SUMMARY REMARKS

In this chapter, seismic fragility curves associating the probability of exceedence of a defined limit state (damage measure, DM) with an engineering demand parameter (EDP) are developed for a range of rigid sliding-dominated equipment mounted on bench surfaces. For this study, only uniaxial seismic excitation is considered to provide insight into the contributions

and sensitivity of the fragility curves to different uncertain parameters. Uncertain parameters considered in this study include: (i) static and kinetic coefficients of friction (μ_s and μ_k, respectively) and (ii) supporting (bench) characteristics. It is observed that the fragility curve is highly sensitive to both the static and kinetic coefficients of friction. However, considering the variation in μ_s and μ_k of $\pm 10\%$, the variability of the seismic fragility curves, particularly at the median values, is comparable with the assumed uncertainty ($\pm 10\%$). It is also concluded that the shape and distribution of the fragility curve for higher coefficients of kinetic friction are less sensitive to the supporting bench dynamic characteristics. A set of simplified fragility curves are then presented for various scientific equipment categories. These curves may be useful for design purposes. To use these curves, (i) an equipments static and kinetic friction must be estimated, (ii) depending upon the value of the coefficient of static and kinetic friction, an equipment category may be assumed (iii) the desired probability of exceedence is selected for the design, and (iv) assuming a target damage measure, the limiting $PHFA$ demand may be obtained using Equation 6.4.

7 Conclusions and Future Work

7.1 CONCLUSIVE FINDINGS

Damage to the nonstructural components has gained significant importance following recent earthquakes. It is now well recognized that extensive nonstructural damage may occur, resulting in significant economic losses and potential threat to life safety. For equipment and building contents, the primary economic losses may be accrued due to operational failure or repair of the equipment and the associated downtime.

In this study, the behavior of a variety of small equipment, glassware and contents typically resting on laboratory benches within biological and chemical science buildings, is studied using experimental and analytical methods. In the analytical study, it is observed that the uncertainty in the coefficients of static and kinetic friction may lead to significant variation in the sliding response of equipment and contents. Therefore, the frictional behavior of all equipment and glassware considered in this work is studied using two different methods of testing (an inclined base and a horizontal pull test). The coefficients of static μ_s and kinetic friction μ_k are calculated from these experiments and their variability is reported. Testing to determine the coefficient of static friction resulted in a maximum of a $\pm 10\%$ deviation from the mean value of μ_s. The coefficient of kinetic friction was found to be dependent on the state of the body, and may be as low as 0.74 that of the coefficient of static friction, though it varies depending upon the equipment base type. For higher accelerations, which produce higher velocities, the coefficient of kinetic friction is higher.

Shake table testing of four different integral bench-shelf configurations, with details representative of typical biological and chemical laboratories in science buildings, shows that the floor motion is amplified at the bench and shelf level, due to the flexibility of the bench-shelf system. Low-amplitude hammer testing, broad-band and narrow-band shake table testing, and field testing of existing bench-shelf systems show that the natural frequency of the bench-system may vary between approximately 5 to 16 Hz, and damping at the fundamental mode varies between 2% to 12%. Analyses of numerical models of the four typical bench-shelf systems indicate good agreement with the experimental results in terms of the first and second mode frequencies. For typical pinned-pinned bench-shelf systems under the loading conditions analyzed, the acceleration amplification is observed to be as high as 7.0.

From the shake table testing of equipment and glassware it was observed that the response

of equipment and glassware is predominantly sliding. It is also observed that the response of equipment can be predicted with reasonable accuracy using determined average coefficients of friction even though the response magnitude is very sensitive to the coefficient of kinetic friction. Rocking of the glassware is not observed to be significant because the frequency related parameters for the glassware are well above the frequency content of the selected ground motions. However, it is observed that the glassware rotates significantly about the vertical axis while sliding. Therefore, it may be expected that in a real scenario, glassware is vulnerable to sliding and impact with a shelf or plexiglass barrier.

Seismic fragility curves associating the probability of exceedance of a defined limit state (damage measure, DM) with an engineering demand parameter (EDP), are also developed for a range of rigid sliding-dominated equipment mounted on bench surfaces. Only uniaxial seismic excitation is considered in order to provide insight into the contributions and sensitivity of the fragility curves to different uncertain parameters. It is observed that the fragility curve is sensitive to both the static and kinetic coefficients of friction, and particularly at the median values, the variation of fragility curves is comparable with the assumed uncertainty in μ_s and μ_k. It is also found that the shape and distribution of the fragility curve for higher coefficients of kinetic friction are less sensitive to the supporting bench dynamic characteristics. Finally, after classifying the equipment according to their frictional resistance, a set of simplified fragility curves are presented for various scientific equipment which may be useful for design purposes.

7.2 RECOMMENDATIONS FOR FUTURE WORK

Future studies are needed in the following areas:

1. For estimating the vulnerability of equipment and contents, simplified fragility curves should be developed for different buildings, and a relationship should be established with the building period and simplified fragility parameters for design purposes.

2. Since the behavior of equipment and glassware is sliding dominated, any retrofitting strategy employed should keep this behavior in mind.

3. The types of equipment and contents in buildings is very broad, and test data are critical to understanding their behavior during seismic shaking. Additional testing on a variety of types of equipment and contents is needed, particularly on those that may be toppling sensitive.

4. Similarly, there is a broad type of furnishing supports in buildings, which will have a variety of effects on equipment and contents. Additional study into the types of systems and their behavior under seismic shaking is needed.

5. This study only considered unattached equipment and contents. The dynamic behavior of restrained elements should also be investigated experimentally and analytically.

REFERENCES

Andreus, U. and Casini, P. (1999). Dynamics of three-block assemblies with unilateral deformable contacts. part 1: Contacts modelling. *Earthquake Engineering and Structural Dynamics* 28: 1621–1636.

Choi, D. and Tung, C. C. (2002). Estimating sliding displacement of an unanchored body subjected to earthquake excitation. *Earthquake Spectra* 18(4): 601–613.

Chong, W. H. and Soong, T. T. (2000). *Sliding fragility of unrestrained equipment in critical facilities*. Report No. MCEER-00-0005, Multidisciplinary Center for Earthquake Engineering Research, State University of New York, Buffalo. 125 pp.

Comerio, M. C. (2000). *The economic benefits of a disaster resistant university: Earthquake loss estimation for UC Berkeley*. Report No. WP-2000-02, Institute of Urban and Regional Development, University of California, Berkeley. 47 pp., URL `http://www-iurd.ced.berkeley.edu/pub/abstract_wp200002.htm`.

Comerio, M. C. (2003). *Seismic protection of laboratory contents: The UC Berkeley science building case study*. Report No. WP-2003-02, Institute of Urban and Regional Development, University of California, Berkeley. 157 pp., URL `http://www-iurd.ced.berkeley.edu/pub/abstract_wp200302.htm`.

Comerio, M. C. and Stallmeyer, J. C. (2002). *Nonstructural loss estimation: The UC Berkeley case study*. Report No. PEER-2002/01, Pacific Earthquake Engineering Research (PEER) Center, University of California, Berkeley. 174 pp.

CSA (2001). *Guideline for seismic risk reduction of operational and functional components (OFCs) of buildings*. Canadian Standards Association.

CUREE (1998). *Proceedings of the NEHRP conference and workshop on research on the Northridge, California Earthquake of January 17, 1994*. Consortium of Universities for Research in Earthquake Engineering. Sponsored by the National Earthquake Hazards Reduction Program (NEHRP).

EERI (1995). Northridge Earthquake reconnaissance report Vol. 1. Supplement C to Volume 11, Publication 95-03, Ed.: Hall, J. F., *Earthquake Spectra*, pp. 523.

EERI (1996). *Scenario for a magnitude 7.0 earthquake on the Hayward fault*. Publication no. HF-96, Earthquake Engineering and Research Institute (EERI), 109 pp.

EERI (2001a). 1999 Chi-Chi, Taiwan Earthquake reconnaissance report. Supplement A to Volume 17. Publication 2001-02, Eds.: Uzarski, J. and Arnold, C., *Earthquake Spectra*, pp. 183.

EERI (2001b). *The Nisqually, Washington earthquake of February 28 2001 - Preliminary reconnaissance report*. EERI Learning from Earthquakes Project, Nisqually Earthquake Clearinghouse Group, University of Washington, Earthquake Engineering and Research Institute (EERI), 26 pp.

FEMA 356 (2002). *Prestandard and commentary for the seismic rehabilitation of buildings*. Federal Emergency Management Agency.

Ferrero, J. F. and Barrau, J. F. (1997). Study of dry frictional under small displacements and near zero sliding velocity. *Wear* 209: 322–327.

Hutchinson, T. C. and Kuester, F. (2004). Monitoring global earthquake-induced demands using vision based sensors. *IEEE Transactions on Instrumentation and Measurement* 35(1): 31–36.

Hutchinson, T. C. and Ray Chaudhuri, S. (2003). Bench- and shelf-mounted equipment and contents: Shake table experiments. In *Seminar on Seismic Design, Performance, and Retrofit of Nonstructural Components in Critical Facilities*, ATC-29-2, Applied Technology Council. Newport Beach, CA, pp. 485–499.

Lee, T. H. and Mosalem, K. (2005). *PEER testbed study on a laboratory building: Exercising seismic performance assessment*. Ch. 4. Ed.: Comerio, M. C. Report No. PEER-2005/xx, Pacific Earthquake Engineering Research (PEER) Center, University of California, Berkeley, 140 pp. (Forthcoming).

Lopez Garcia, D. and Soong, T. T. (2003). Sliding fragility of block-type non-structural components. Part 1: unrestrained components. *Earthquake Engineering and Structural Dynamics* 32: 111–129.

ME scopeVES (2001). Operating Manual (Version 3.0). Vibrant Technology, Inc., Jamestown, California. URL `http://www.vibetech.com/MEscope.htm`.

Mostaghel, N. and Davis, T. (1997). Representation of coulomb friction for dynamic analysis. *Earthquake Engineering and Structural Dynamics* 26: 541–548.

Newmark, N. M. (1965). Effects of earthquakes on dams and embankments. *Geotechnique* XV(2): 139–159.

OpenSees (2003). OpenSees: Open System for Earthquake Engineering Simulation. Pacific Earthquake Engineering Research (PEER) Center, University of California, Berkeley. URL `http://opensees.berkeley.edu`.

Ray Chaudhuri, S. and Hutchinson, T. C. (2005). Characterizing frictional behavior for use in predicting seismic response of unattached equipment. *Soil Dynamic and Earthquake Engineering* 25: 591–604.

Shao, Y. and Tung, C. C. (1999). Seismic response of unanchored bodies. *Earthquake Spectra* 15(3): 523–536.

Shenton, H. W. I. (1996). Criteria for initiation of slide, rock, and slide-rock rigid-body modes. *Journal of Engineering Mechanics, ASCE* 122(7): 690–693.

Shenton, H. W. I. and Jones, N. P. (1991). Base excitation of rigid bodies. I: formulation. *Journal of Engineering Mechanics, ASCE* 117: 2286–2306.

Shinozuka, M., Feng, M. Q., Kim, H. K., and Kim, H. S. (2000). Nonlinear static procedure for fragility curve development. *Journal of Engineering Mechanics, ASCE* 126(12): 1287–1295.

Sommerville, P. (2005). *PEER Testbed Study on a Laboratory Building: Exercising Seismic Performance Assessment*. Ch. 3. Ed.: Comerio, M. C. Report No. PEER-2005/xx, University of California, Berkeley, 140 pp. (Forthcoming).

Taniguchi, T. (2002). Non-linear response analyses of rectangular rigid bodies subjected to horizontal and vertical ground motion. *Earthquake Engineering and Structural Dynamics* 31: 1481–1500.

Thomsen, J. P. and Fidlin, A. (2003). Analytical approximations for stick-slip vibration amplitudes. *International Journal of Non-Linear Mechanics* 38: 389–403.

Xia, F. (2003). Modelling of a two-dimensional coulomb friction oscillator. *Journal of Sound and Vibration* 265: 1063–1074.

Appendix A: Ground Motions Used For Mock-Laboratory Shake Table Tests

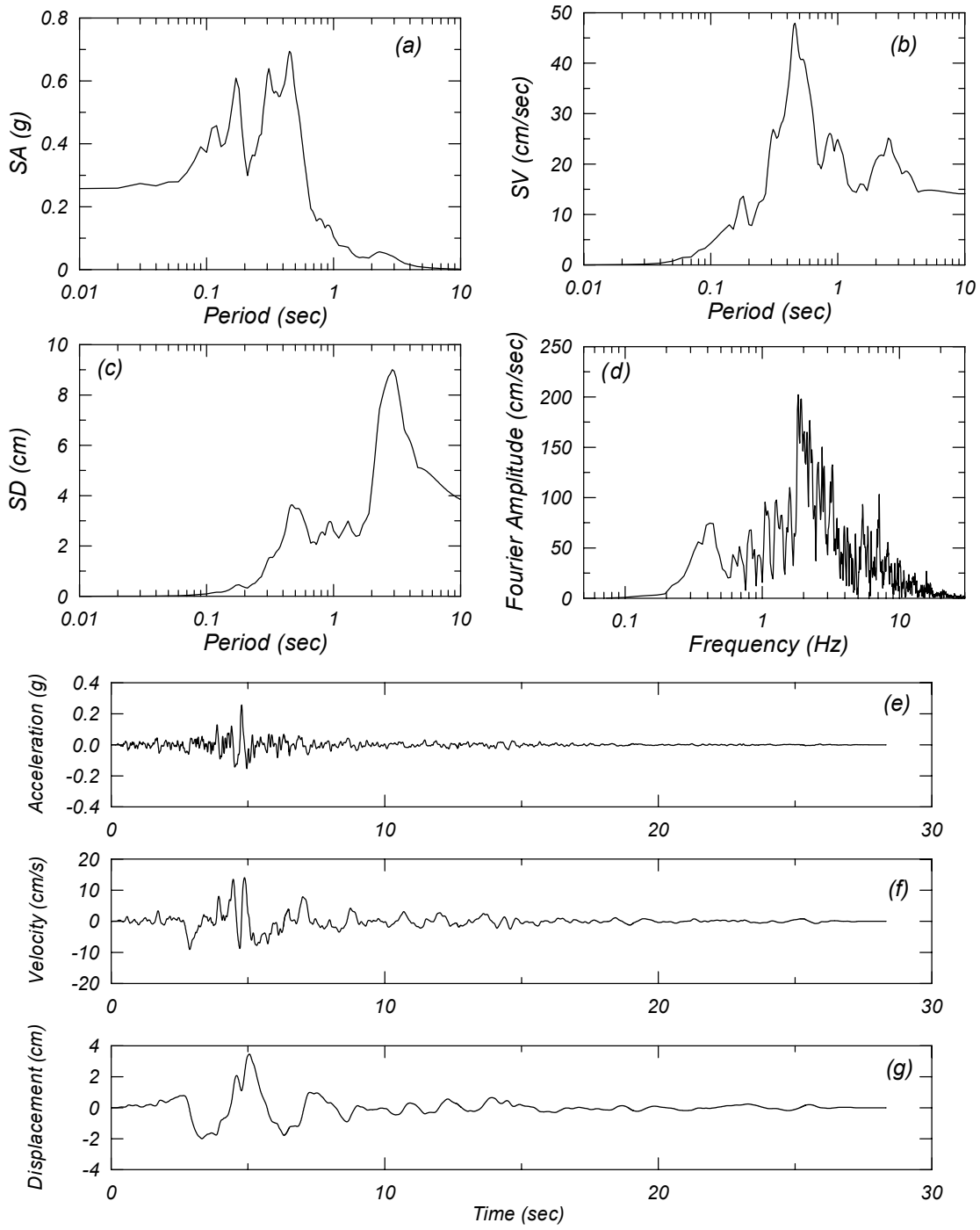

Figure A.1: 50% in 50 years Morgan Hill Anderson Dam Down (transverse) (GM - 3) (a) 5% elastic acceleration response spectrum, (b) 5% elastic pseudo velocity response spectrum, (c) 5% elastic displacement response spectrum, (d) Fourier spectrum, (e) acceleration time history, (f) velocity time history, and (g) displacement time history.

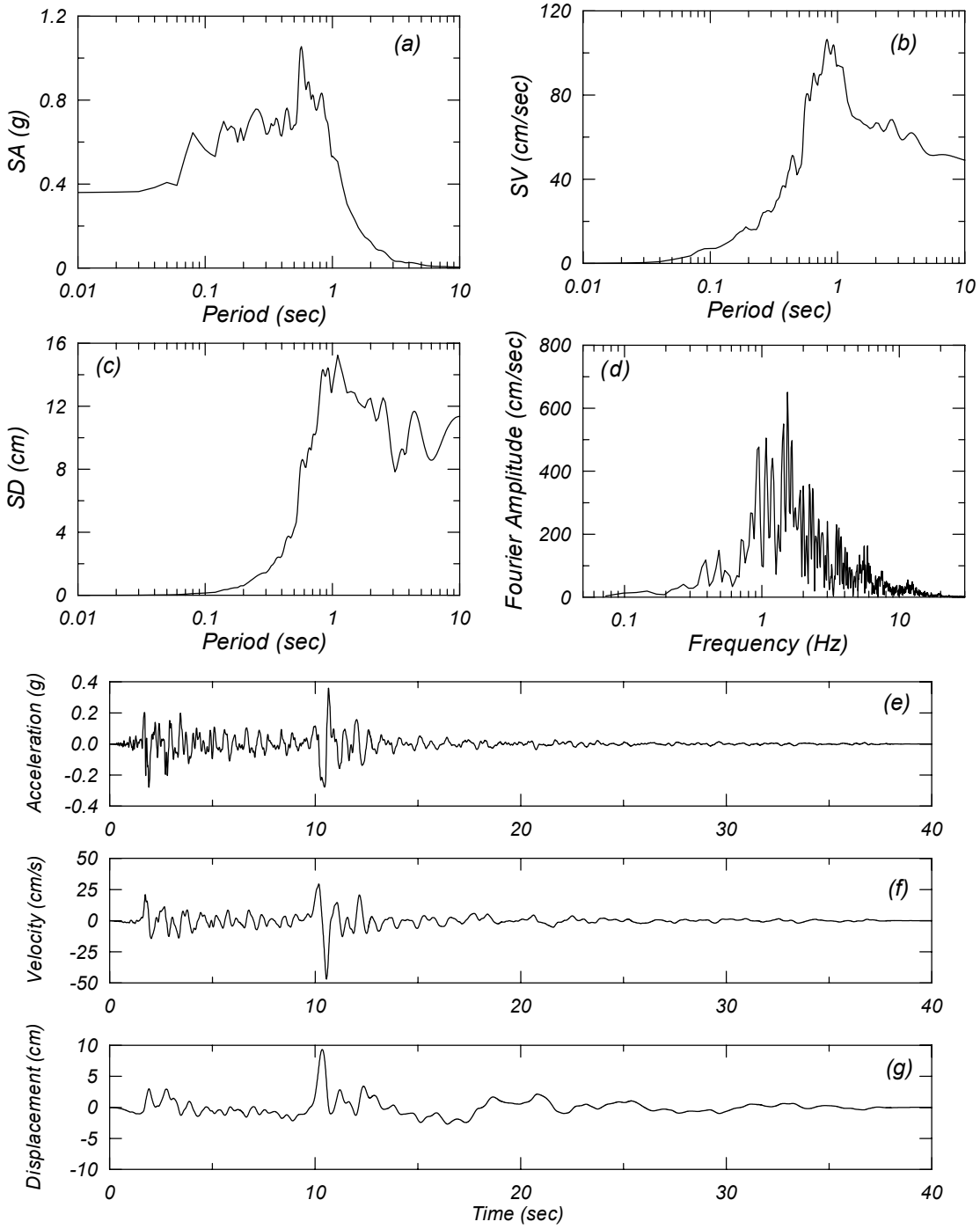

Figure A.2: 50% in 50 years Morgan Hill Halls Valley (transverse) (GM - 4) (a) 5% elastic acceleration response spectrum, (b) 5% elastic pseudo velocity response spectrum, (c) 5% elastic displacement response spectrum, (d) Fourier spectrum, (e) acceleration time history, (f) velocity time history, and (g) displacement time history.

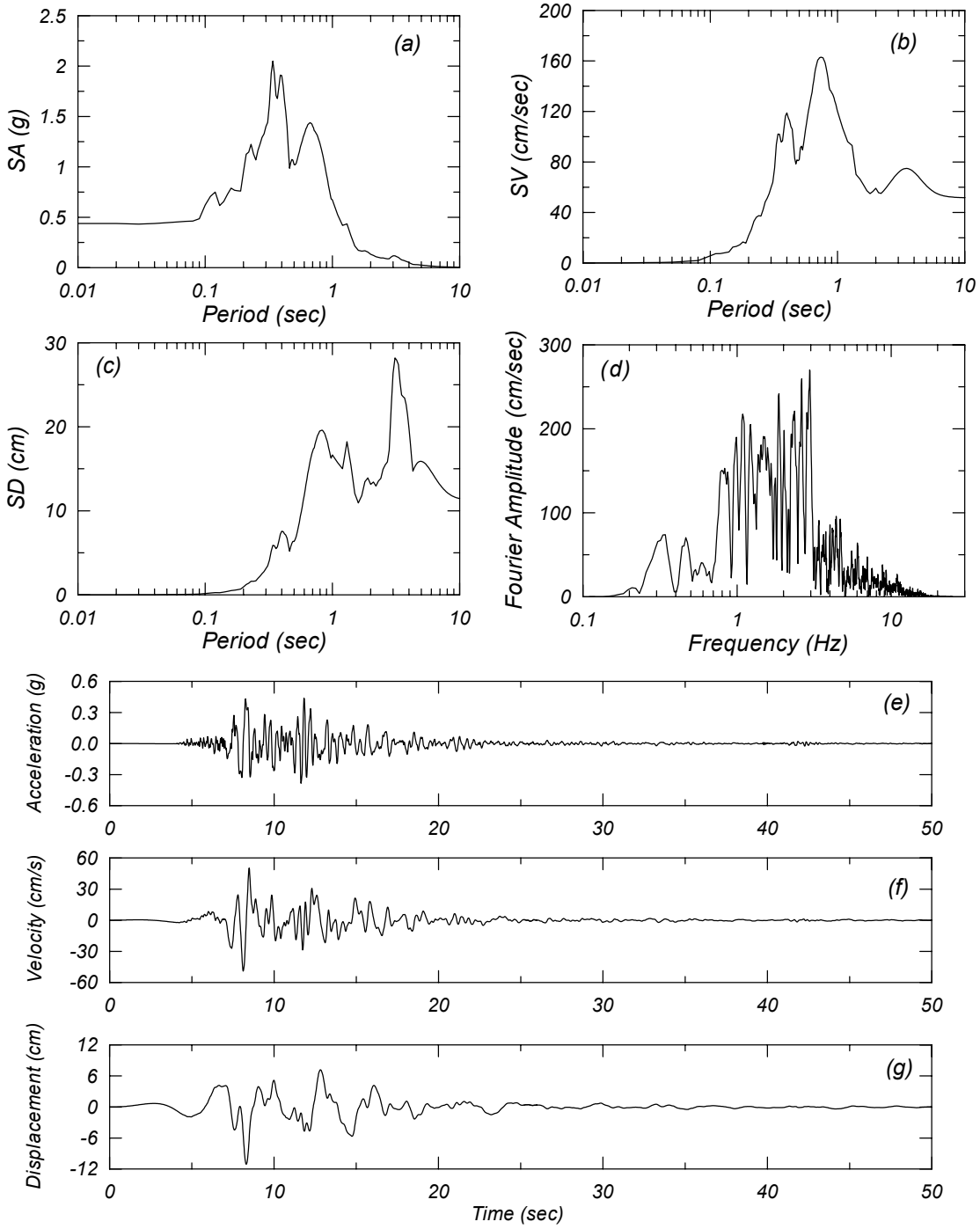

Figure A.3: 10% in 50 years Kobe, JMA, Japan (longitudinal) (GM - 5) (a) 5% elastic acceleration response spectrum, (b) 5% elastic pseudo velocity response spectrum, (c) 5% elastic displacement response spectrum, (d) Fourier spectrum, (e) acceleration time history, (f) velocity time history, and (g) displacement time history.

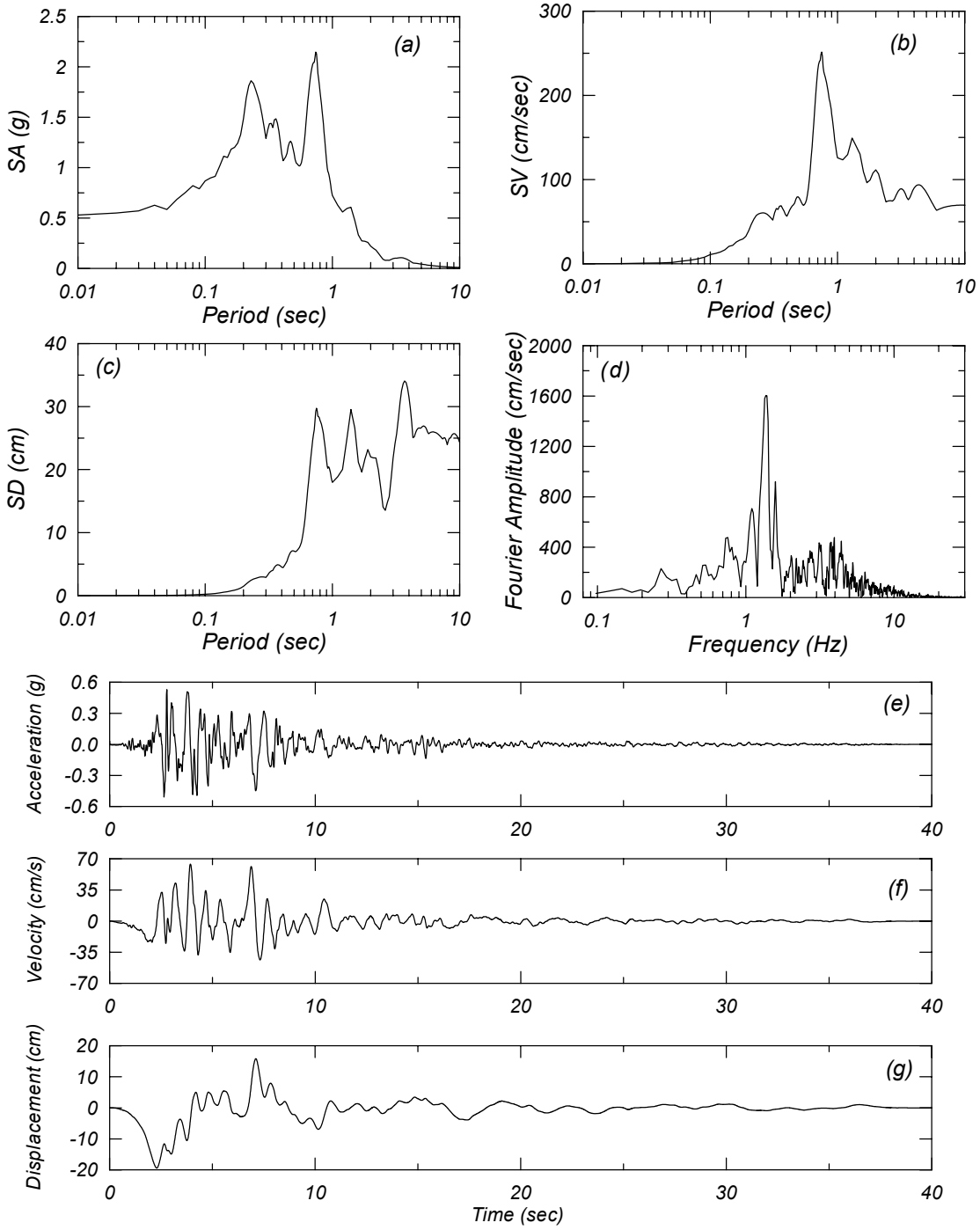

Figure A.4: 10% in 50 years Loma Prieta Corralitos (transverse) (GM - 6) (a) 5% elastic acceleration response spectrum, (b) 5% elastic pseudo velocity response spectrum, (c) 5% elastic displacement response spectrum, (d) Fourier spectrum, (e) acceleration time history, (f) velocity time history, and (g) displacement time history.

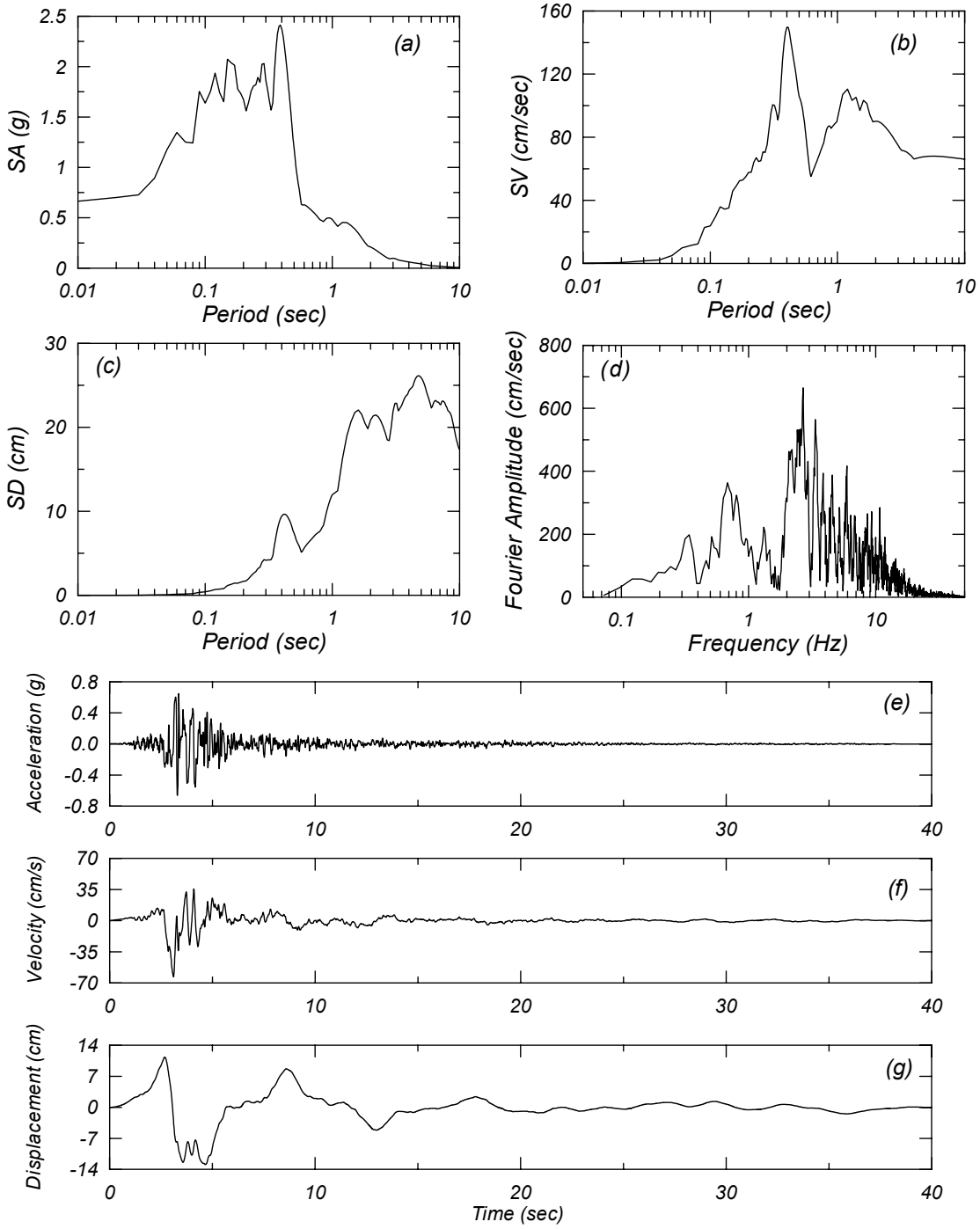

Figure A.5: 10% in 50 years Loma Prieta Gavilan College (transverse) (GM - 7) (a) 5% elastic acceleration response spectrum, (b) 5% elastic pseudo velocity response spectrum, (c) 5% elastic displacement response spectrum, (d) Fourier spectrum, (e) acceleration time history, (f) velocity time history, and (g) displacement time history.

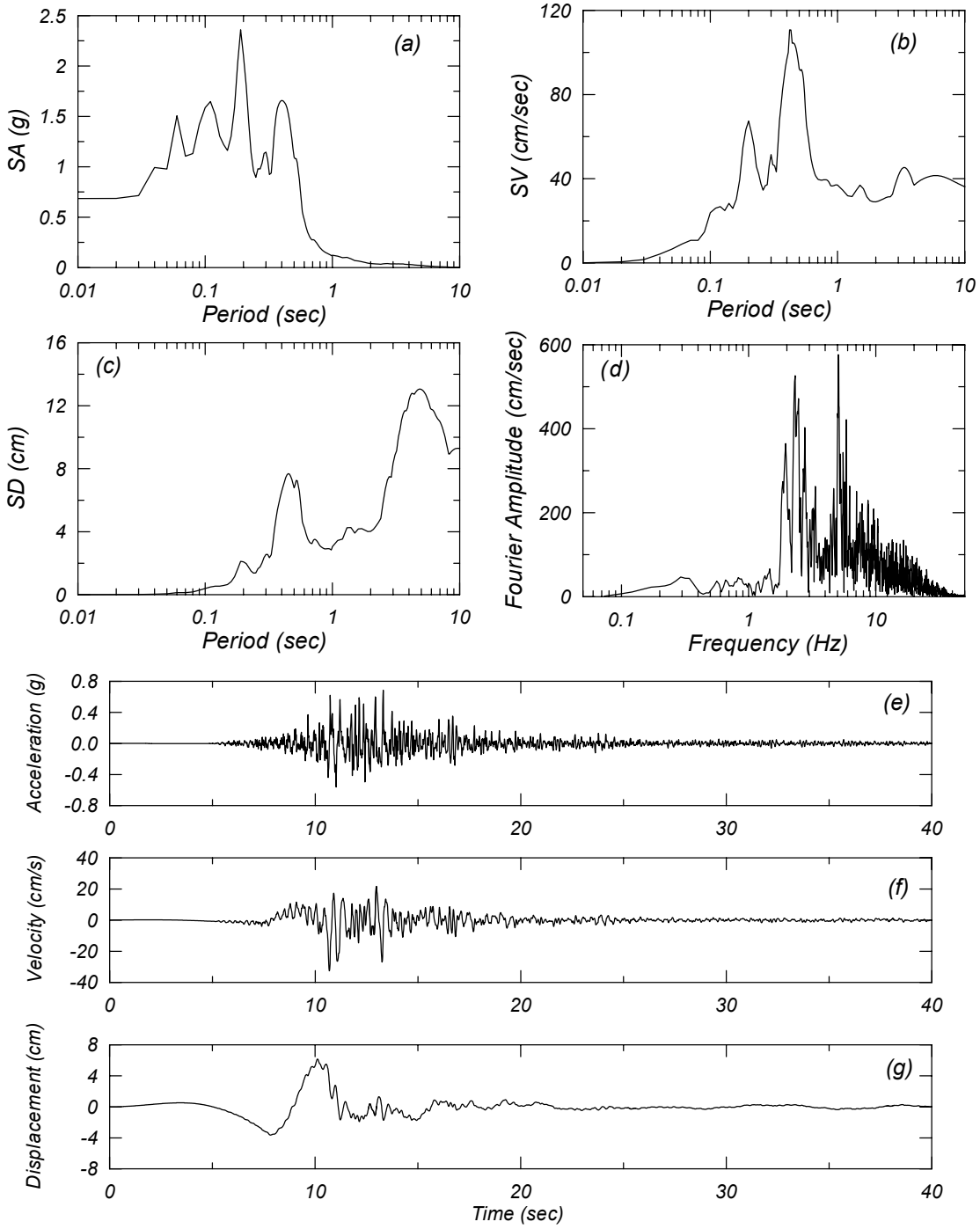

Figure A.6: 10% in 50 years Tottori, Kofu, Japan (transverse) (GM - 8) (a) 5% elastic acceleration response spectrum, (b) 5% elastic pseudo velocity response spectrum, (c) 5% elastic displacement response spectrum, (d) Fourier spectrum, (e) acceleration time history, (f) velocity time history, and (g) displacement time history

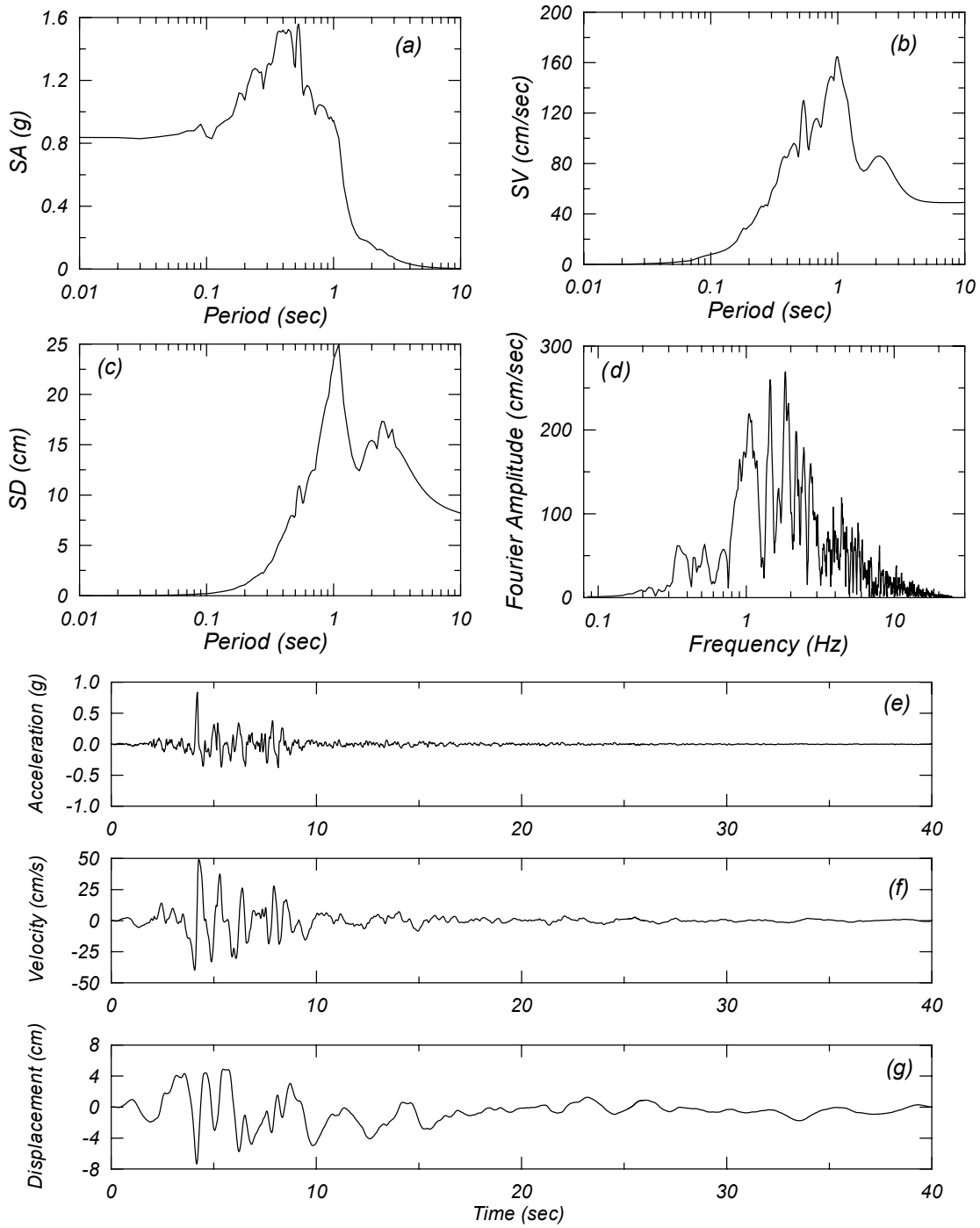

Figure A.7: 10% in 50 years Loma Prieta Lexington Dam (longitudinal) (GM - 9) (a) 5% elastic acceleration response spectrum, (b) 5% elastic pseudo velocity response spectrum, (c) 5% elastic displacement response spectrum, (d) Fourier spectrum, (e) acceleration time history, (f) velocity time history, and (g) displacement time history.

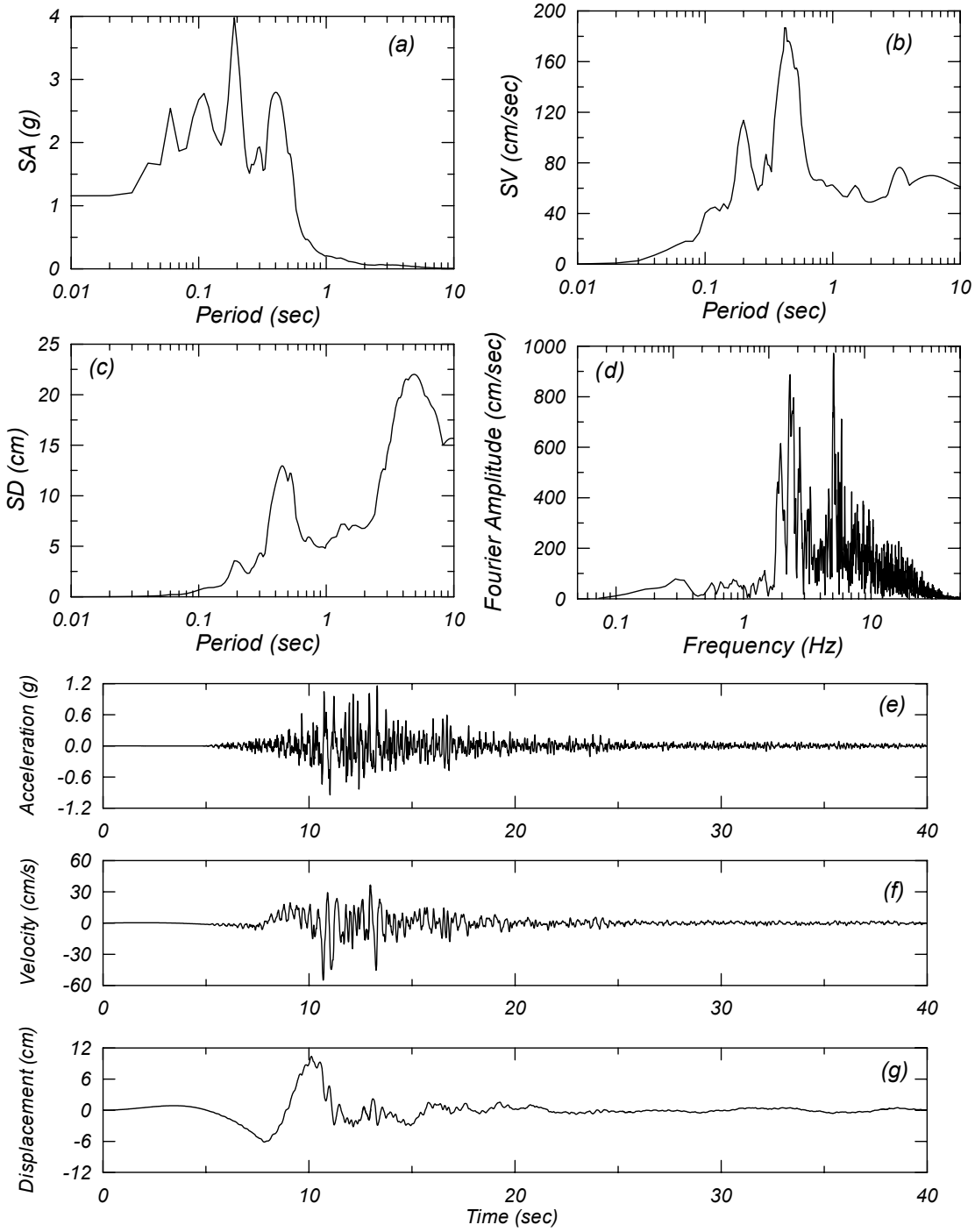

Figure A.8: 2% in 50 years Tottori, Kofu, Japan (transverse) (GM - 10) (a) 5% elastic acceleration response spectrum, (b) 5% elastic pseudo velocity response spectrum, (c) 5% elastic displacement response spectrum, (d) Fourier spectrum, (e) acceleration time history, (f) velocity time history and (g) displacement time history.

Appendix B: Experimental Results

This appendix provides plots of experimental data from mock laboratory shake table testing. The results are subdivided into four sections, based on the mock-laboratory configurations described in Chapter 4.

B.1 CONFIGURATION 1

This configuration is a single bench-shelf placed along the wood shear wall of the mock laboratory, as shown in Figure B.1(a). The direction of shaking, i.e., (x axis as used in the following figures) is along the longitudinal direction of the bench. Two sets of equipment were tested in this setup, and the corresponding configurations are named 1A and 1B. The equipment tested in Configuration 1A are a small microscope, Technicon autoanalyzer, and a large microscope, respectively, from left to right in Figure B.1(b). Also, a steel shelf full of books was tested in this configuration. The equipment tested in Configuration 1B are a 15″ monitor (small), a 17″ monitor (medium), a 19″ monitor (large), and an Eppendoff centrifuge, respectively, from left to right in Figure B.1(c). Figure B.2 shows the general analog instrument layout of the accelerometers and displacement transducers. Figures B.3–B.10 give the acceleration and displacement time histories for analog transducers. The y-axis label description (nomenclature) for these figures is given in Table B.1.

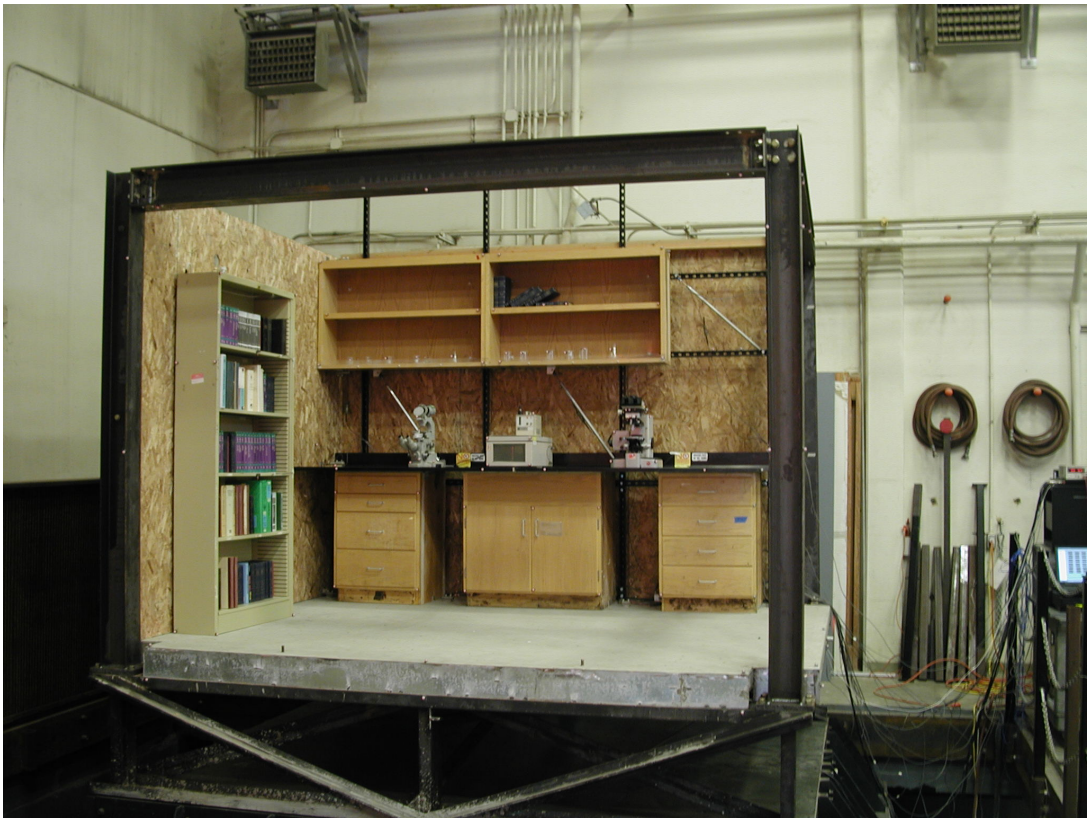

(a)

(b)

(c)

Figure B.1: (a) Mock-laboratory setup of Configuration 1, (b) equipment tested in Configuration 1A, and (c) equipment tested in Configuration 1B.

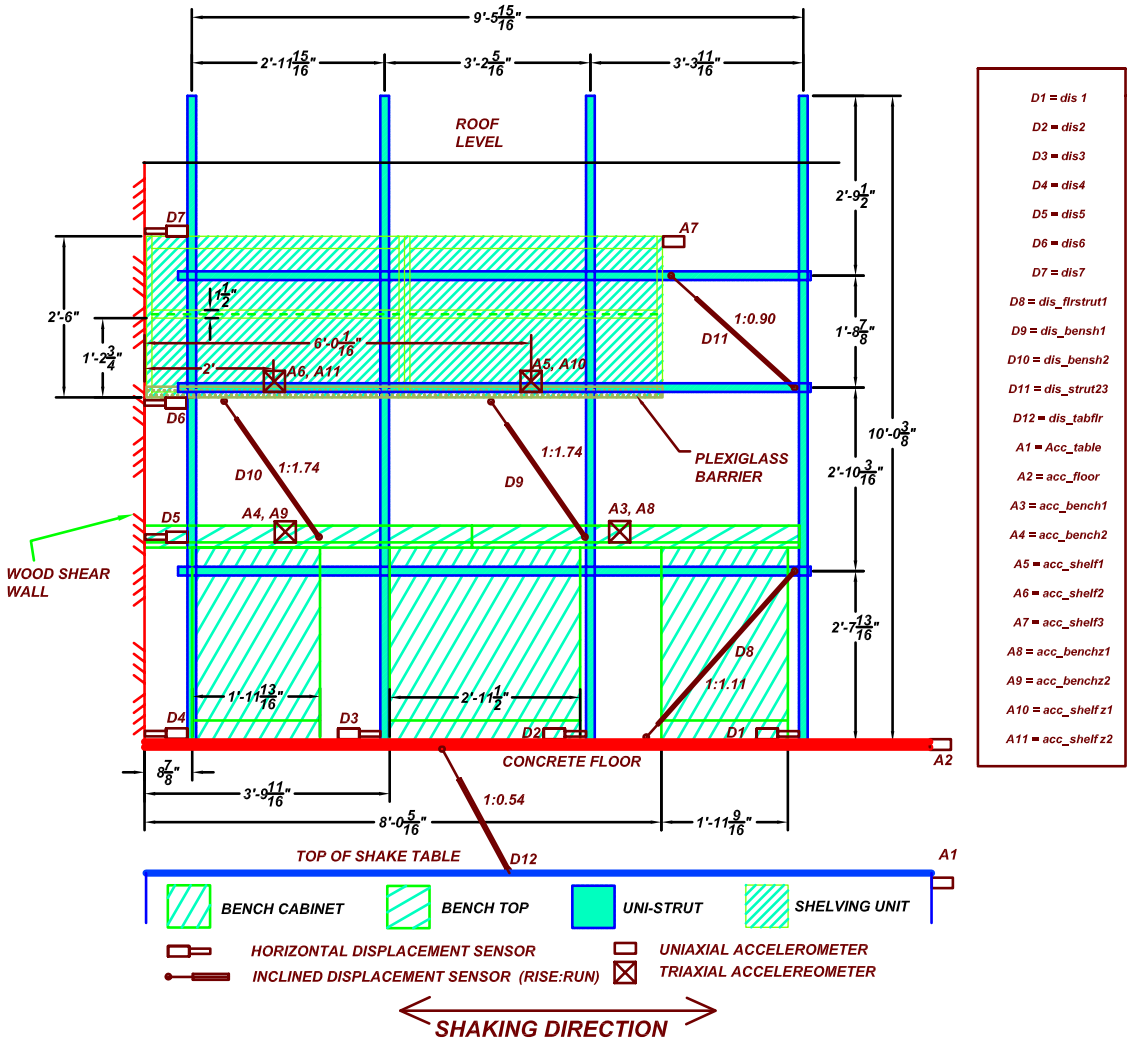

Figure B.2: Instrument layout for mock-laboratory setup Configuration 1

Table B.1: Description of y-axis nomenclature used for the plots of Configuration 1 (Figures B.3– B.10). Refer to Figure B.2 for location of instruments.

Y axis title	Description
Acc_table	Shake table acceleration
acc_floor	Acceleration of concrete floor
acc_bench1	Acceleration of bench
acc_bench2	Acceleration of bench
acc_shelf1	Acceleration of shelf
acc_shelf2	Acceleration of shelf
acc_shelf3	Acceleration of shelf
acc_benchz1	Acceleration of bench
acc_benchz2	Acceleration of bench
acc_shelfz1	Acceleration of shelf
acc_shelfz2	Acceleration of shelf
acc_analyzer	Acceleration of Tecnicon analyzer
dis1	Displacement of bench cabinet 1 w.r.t floor
dis2	Displacement of bench cabinet 2 w.r.t floor
dis3	Displacement of bench cabinet 3 w.r.t floor
dis4	Displacement of wood shear wall w.r.t floor
dis5	Displacement of bench w.r.t wood shear wall
dis6	Displacement of shelf-bottom w.r.t wood shear wall
dis7	Displacement of shelf-top w.r.t wood shear wall
dis_flrstrut1	Displacement of bottom strut w.r.t floor
dis_bensh1	Displacement of bench top w.r.t shelf bottom
dis_bensh2	Displacement of bench top w.r.t shelf bottom
dis_strut23	Displacement of middle strut w.r.t top strut
dis_tabflr	Displacement of floor w.r.t shake table

Unless otherwise mentioned, all the measurements are in the direction of shaking

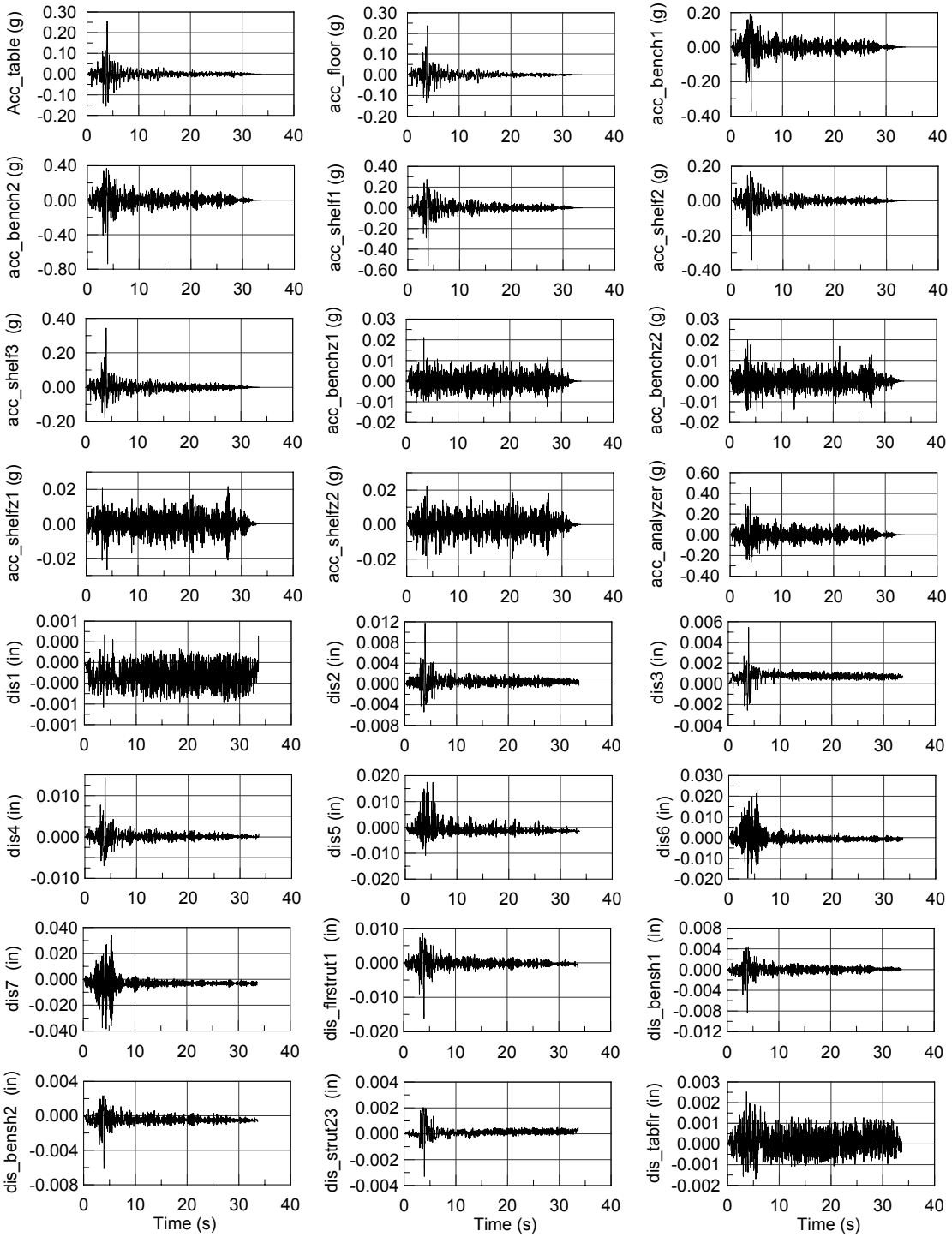

Figure B.3: Configuration 1A: Acceleration (upper four rows) and displacement (lower four rows) time histories for 50% in 50 years Morgan Hill Anderson Dam Down (transverse) (GM - 3).

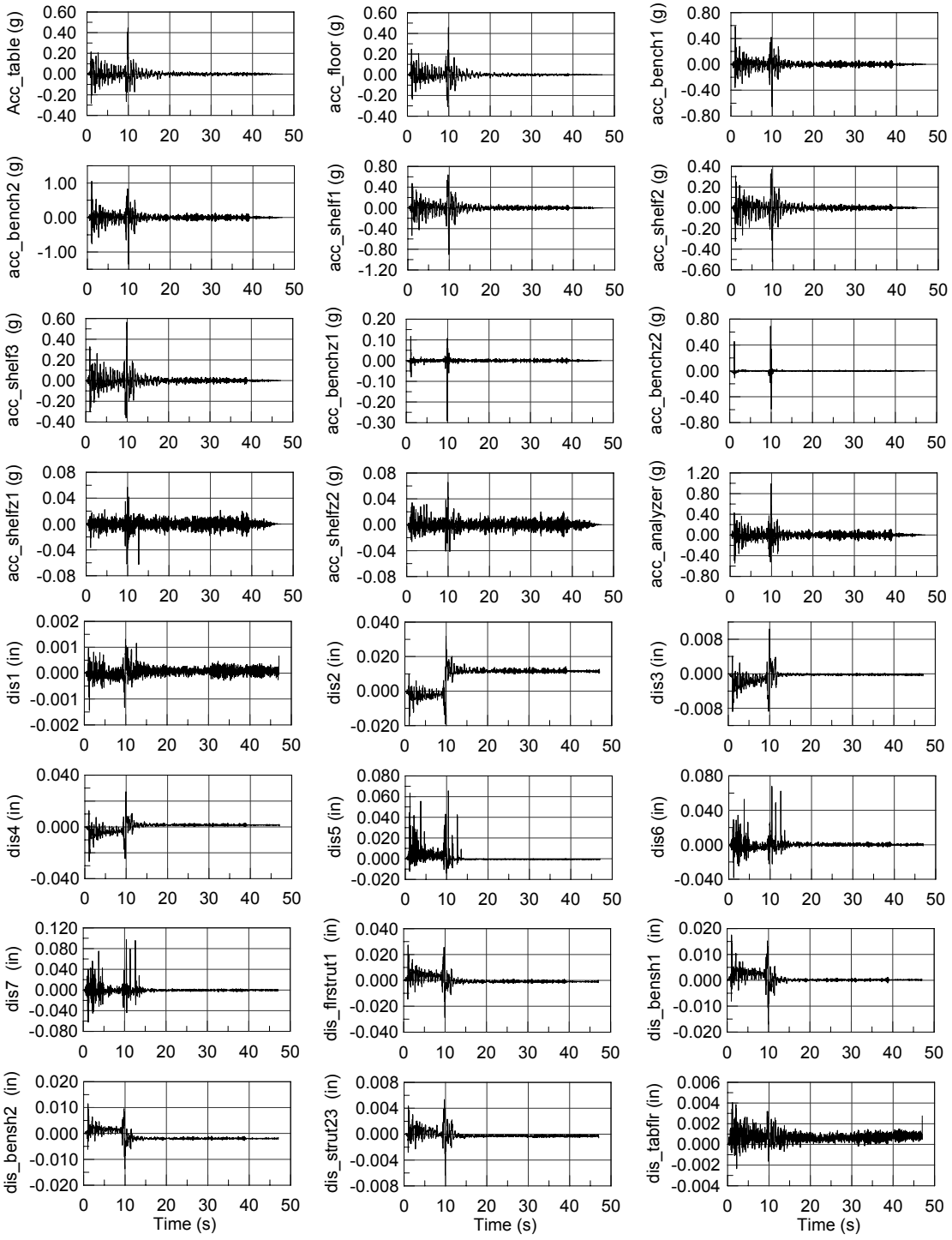

Figure B.4: Configuration 1A: Acceleration (upper four rows) and displacement (lower four rows) time histories for 50% in 50 years Morgan Hill Halls Valley (transverse) (GM - 4).

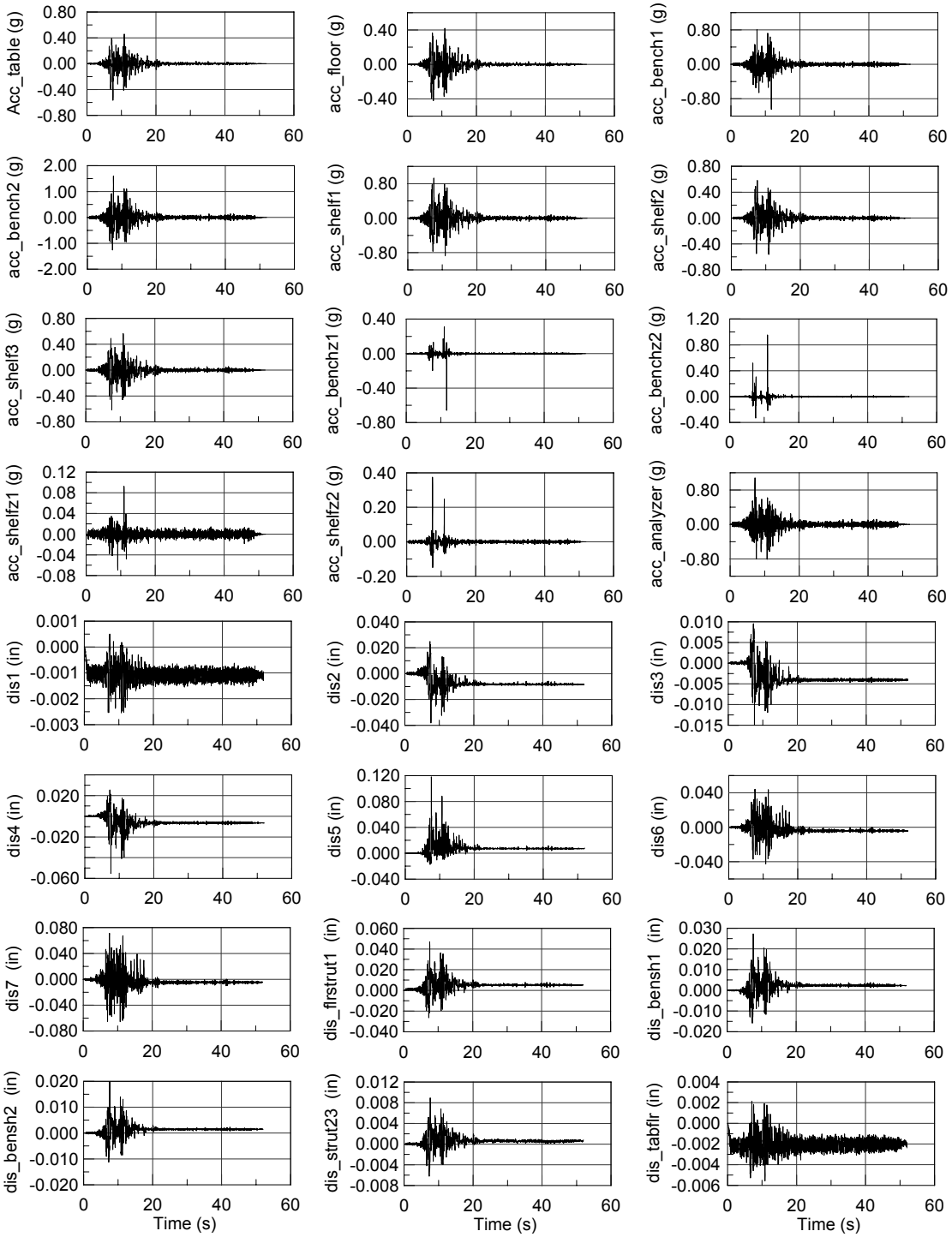

Figure B.5: Configuration 1A: Acceleration (upper four rows) and displacement (lower four rows) time histories for 10% in 50 years Kobe, JMA, Japan (longitudinal) (GM - 5).

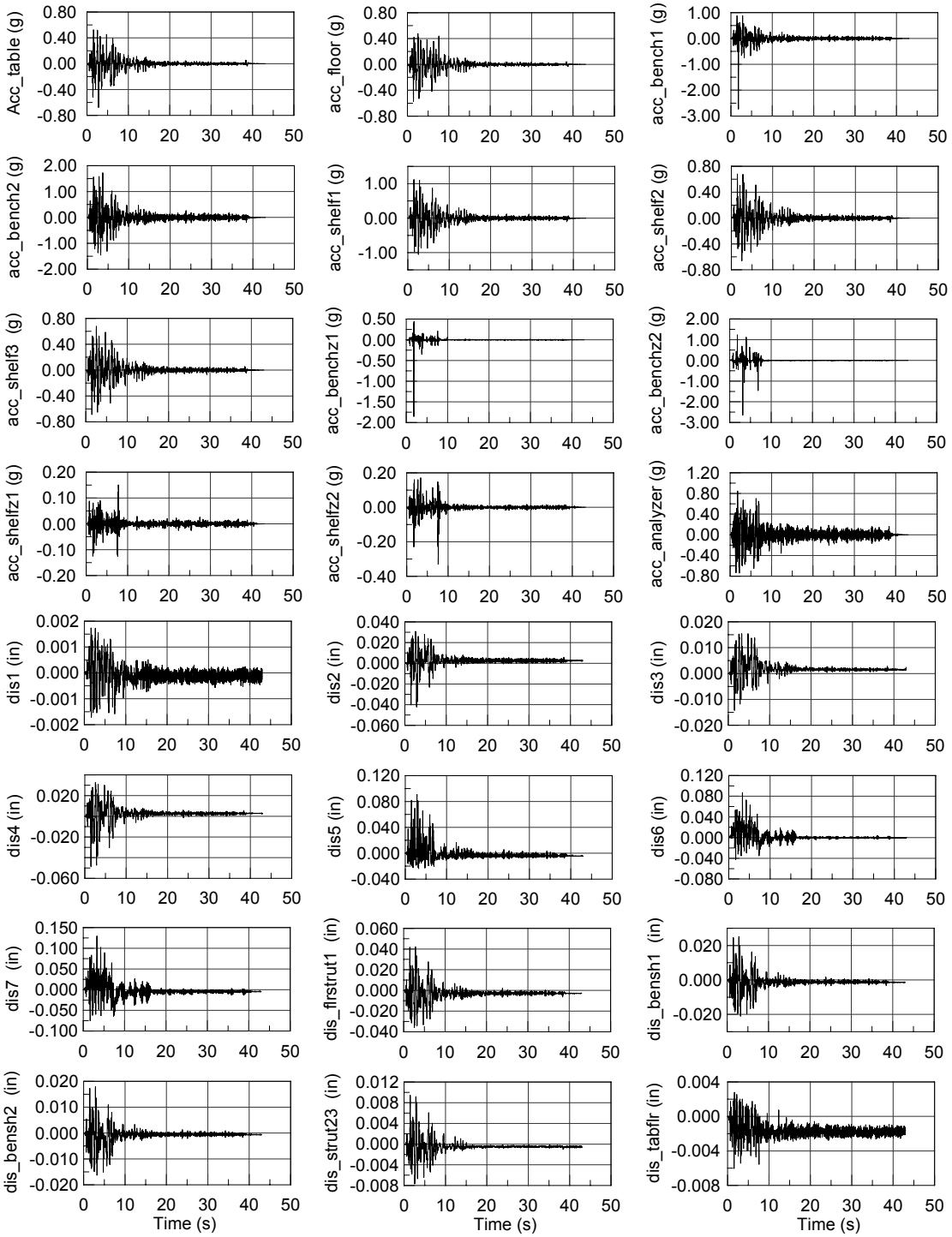

Figure B.6: Configuration 1A: Acceleration (upper four rows) and displacement (lower four rows) time histories for 10% in 50 years Loma Prieta Corralitos (transverse) (GM - 6).

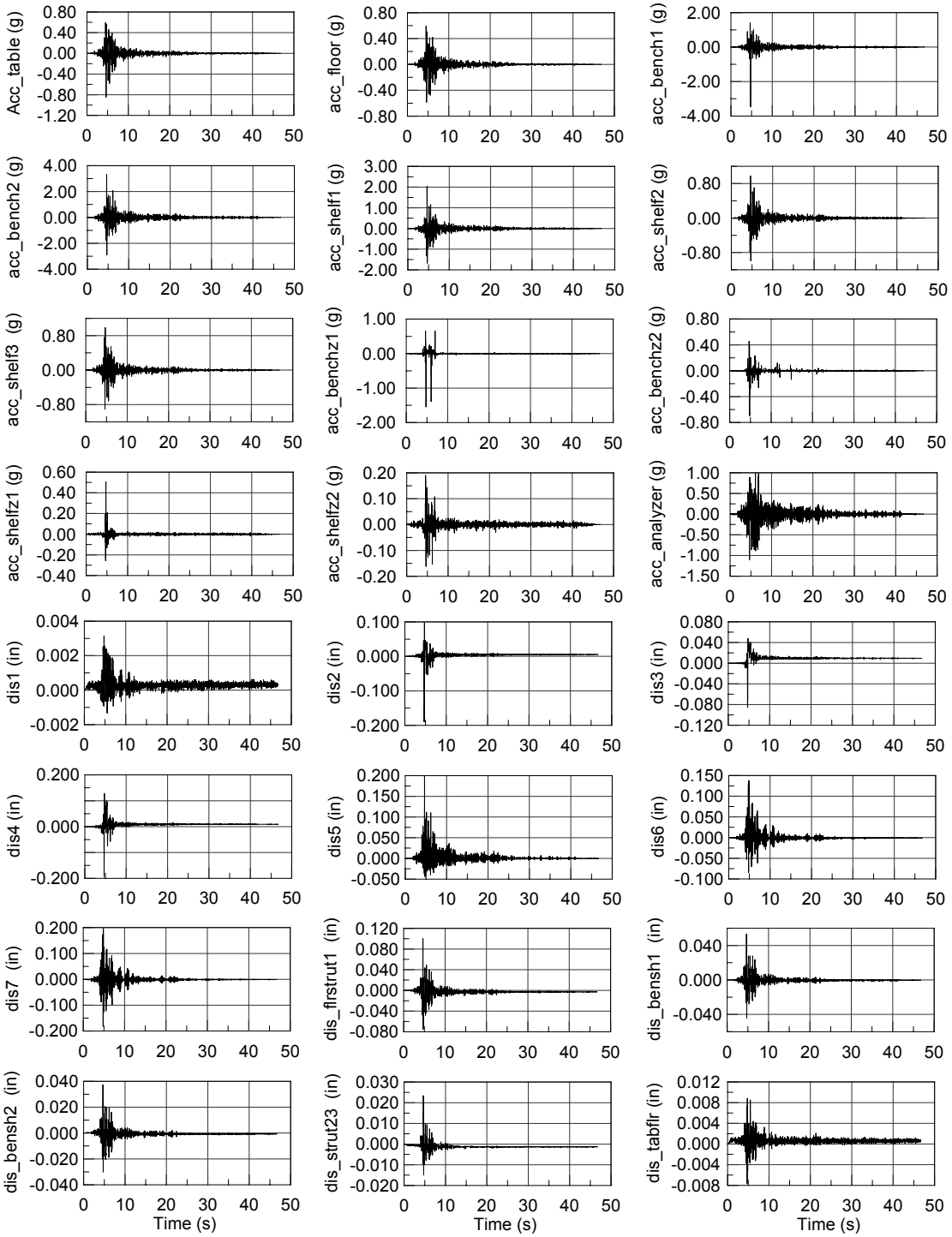

Figure B.7: Configuration 1A: Acceleration (upper four rows) and displacement (lower four rows) time histories for 10% in 50 years Loma Prieta Gavilan College (transverse) (GM - 7).

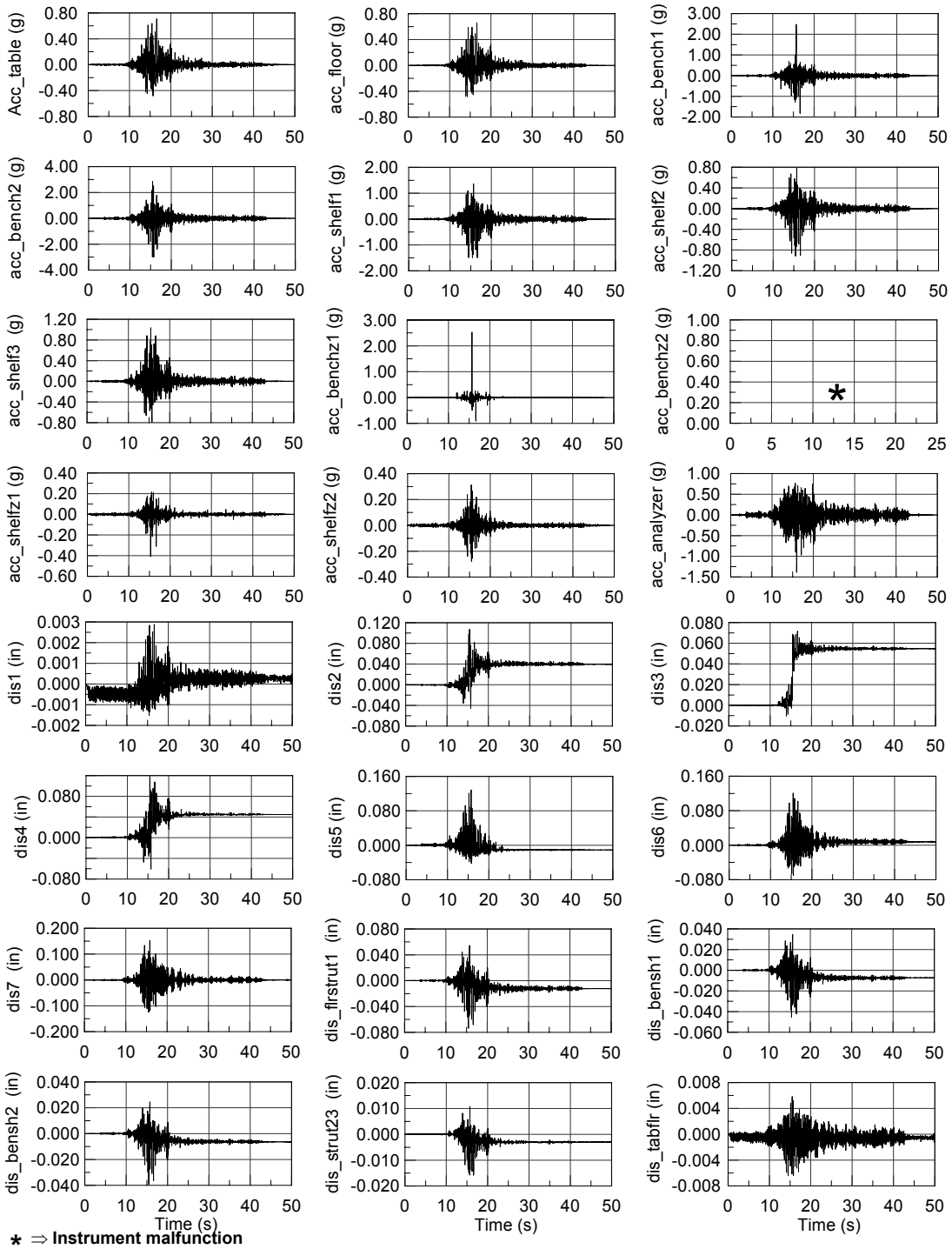

Figure B.8: Configuration 1A: Acceleration (upper four rows) and displacement (lower four rows) time histories for 10% in 50 years Tottori, Kofu, Japan (transverse) (GM - 8).

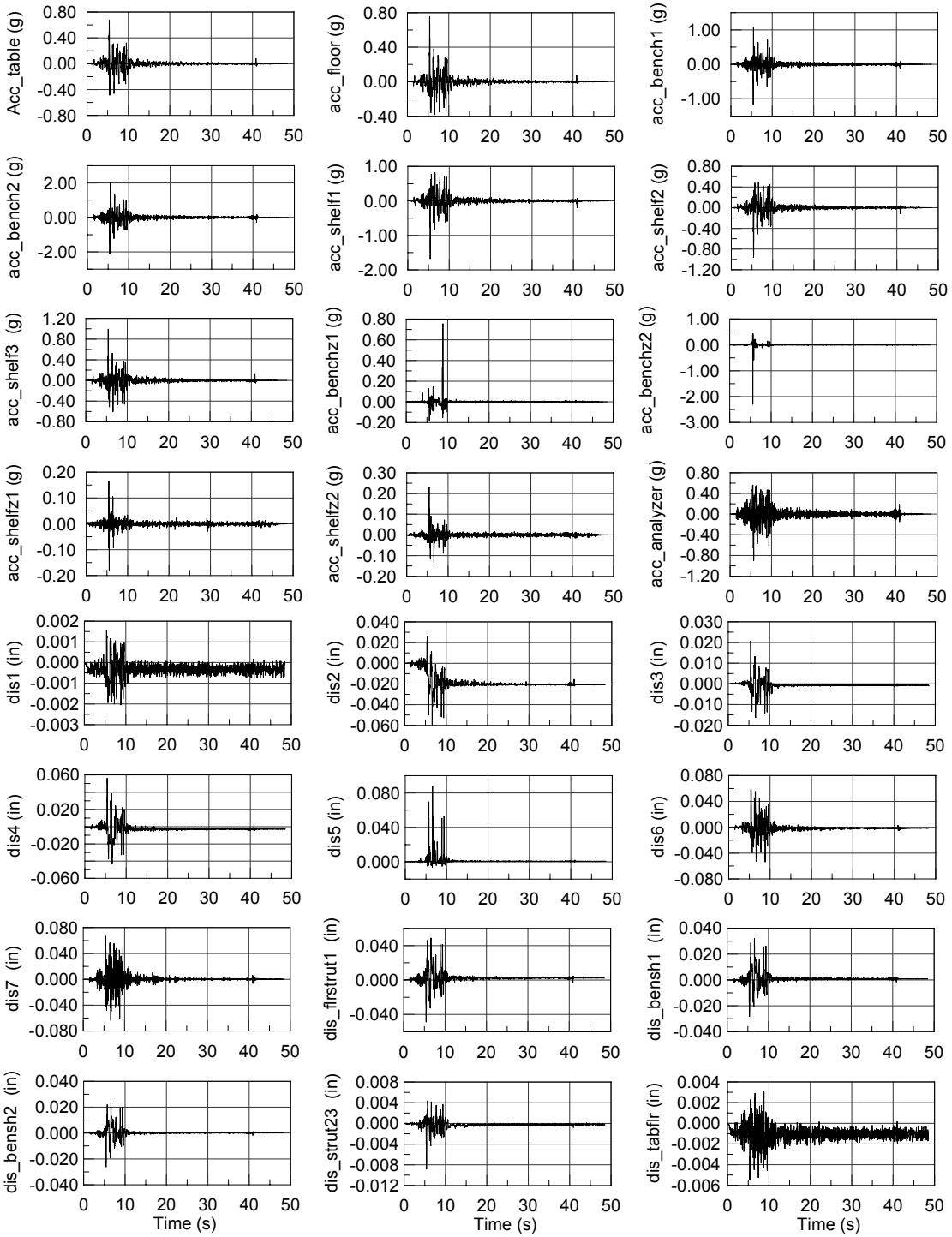

Figure B.9: Configuration 1A: Acceleration (upper four rows) and displacement (lower four rows) time histories for 10% in 50 years Loma Prieta Lexington Dam (longitudinal) (GM - 9).

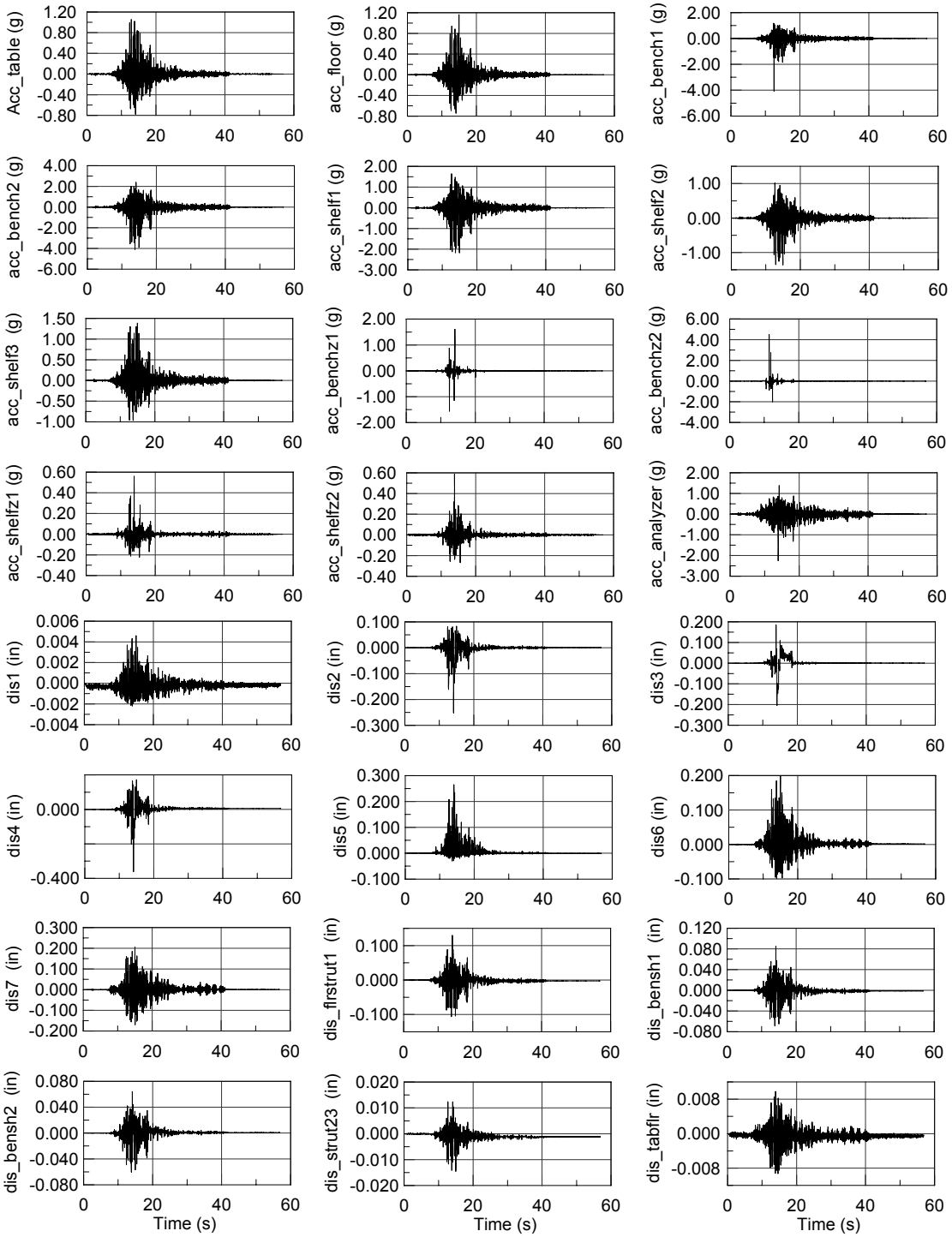

Figure B.10: Configuration 1A: Acceleration (upper four rows) and displacement (lower four rows) time histories for 2% in 50 years Tottori, Kofu, Japan (transverse) (GM - 10).

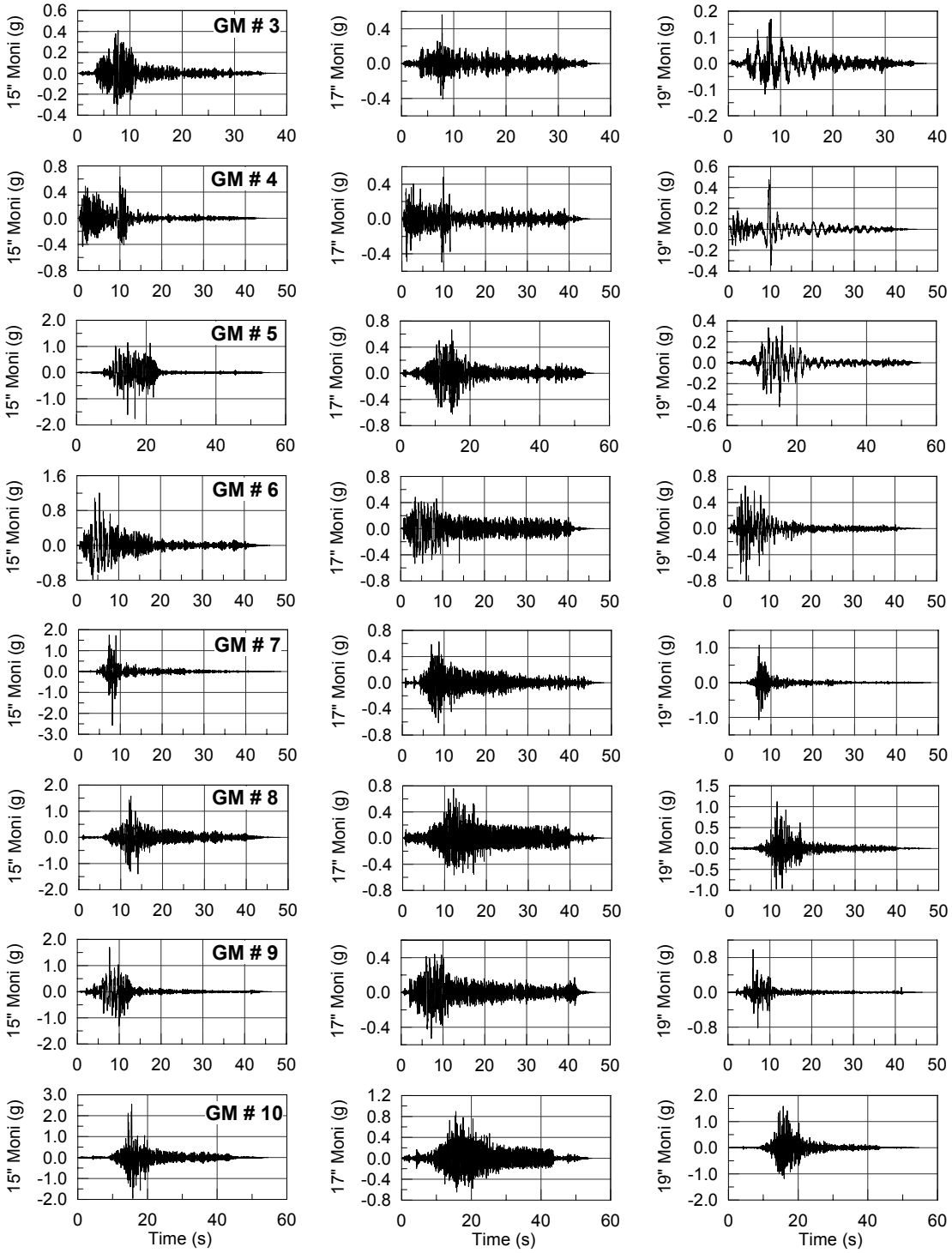

Figure B.11: Configuration 1B: Acceleration time histories of 15” monitor, 17” monitor, and 19” monitor where each row represents GM - 3 through GM - 10.

B.2 CONFIGURATION 2

This configuration is a single bench-shelf placed along the wood shear wall of the mock laboratory perpendicular to Configuration 1, as shown in Figure B.12(a). Therefore, the direction of shaking, i.e., (x axis as used in the following figures) is along the transverse direction of the bench. Two sets of equipment were tested in this setup, and the corresponding configurations are named 2A and 2B. The equipment tested in Configuration 2A are a large microscope, Eppendoff centrifuge, small microscope, and Technicon autoanalyzer, respectively, from left to right in Figure B.12(b). Also, a steel shelf full of books was tested in this configuration and kept near the other wood shear wall. The equipment tested in Configuration 2B are SGI CPUs Octane (green), Indy (blue), and Indigo2 (purple), respectively, from left to right in Figure B.12(c). Figure B.13 shows the general analog instrument layout of the accelerometers and displacement transducers. Figures B.14–B.21 give the acceleration and displacement time histories for analog transducers. The y-axis label description (nomenclature) for these figures are given in Table B.2.

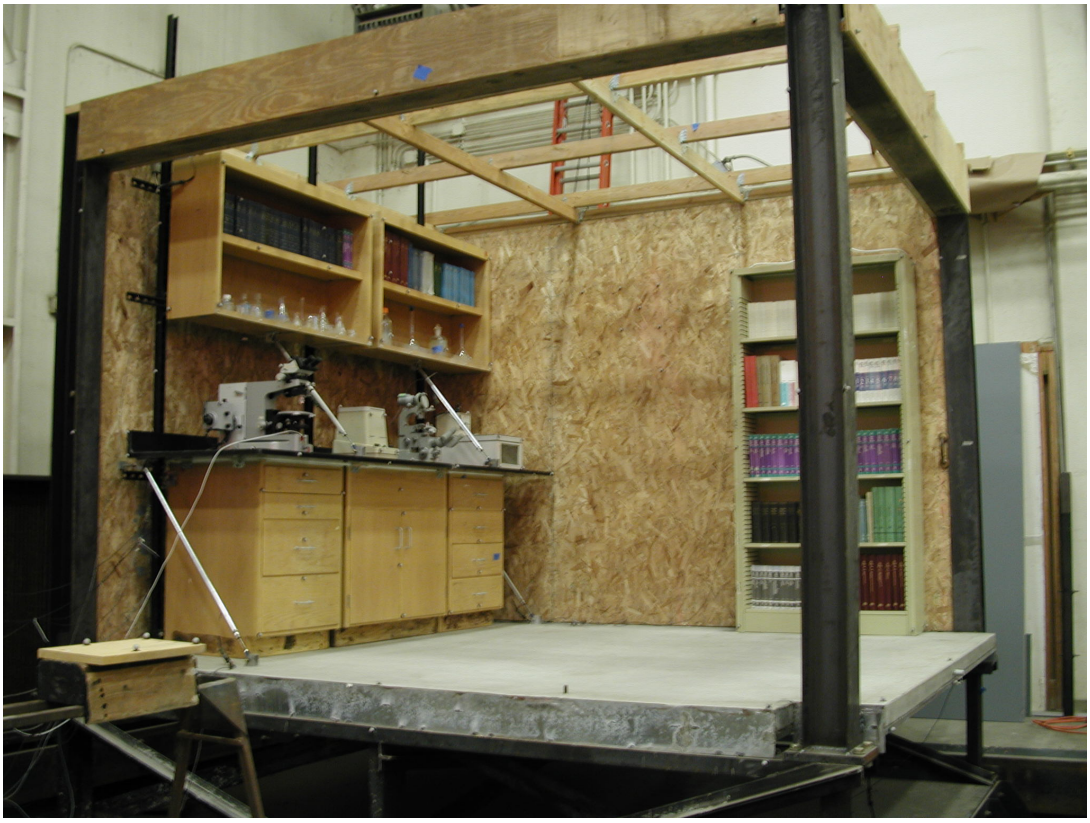

(a)

(b)

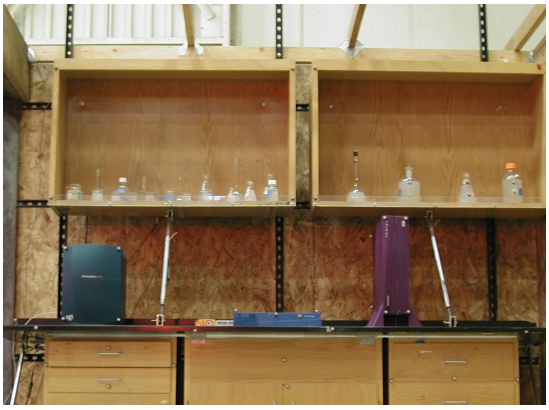

(c)

Figure B.12: (a) Mock-laboratory setup of Configuration 2, (b) equipment tested in Configuration 2A, and (c) equipment tested in Configuration 2B.

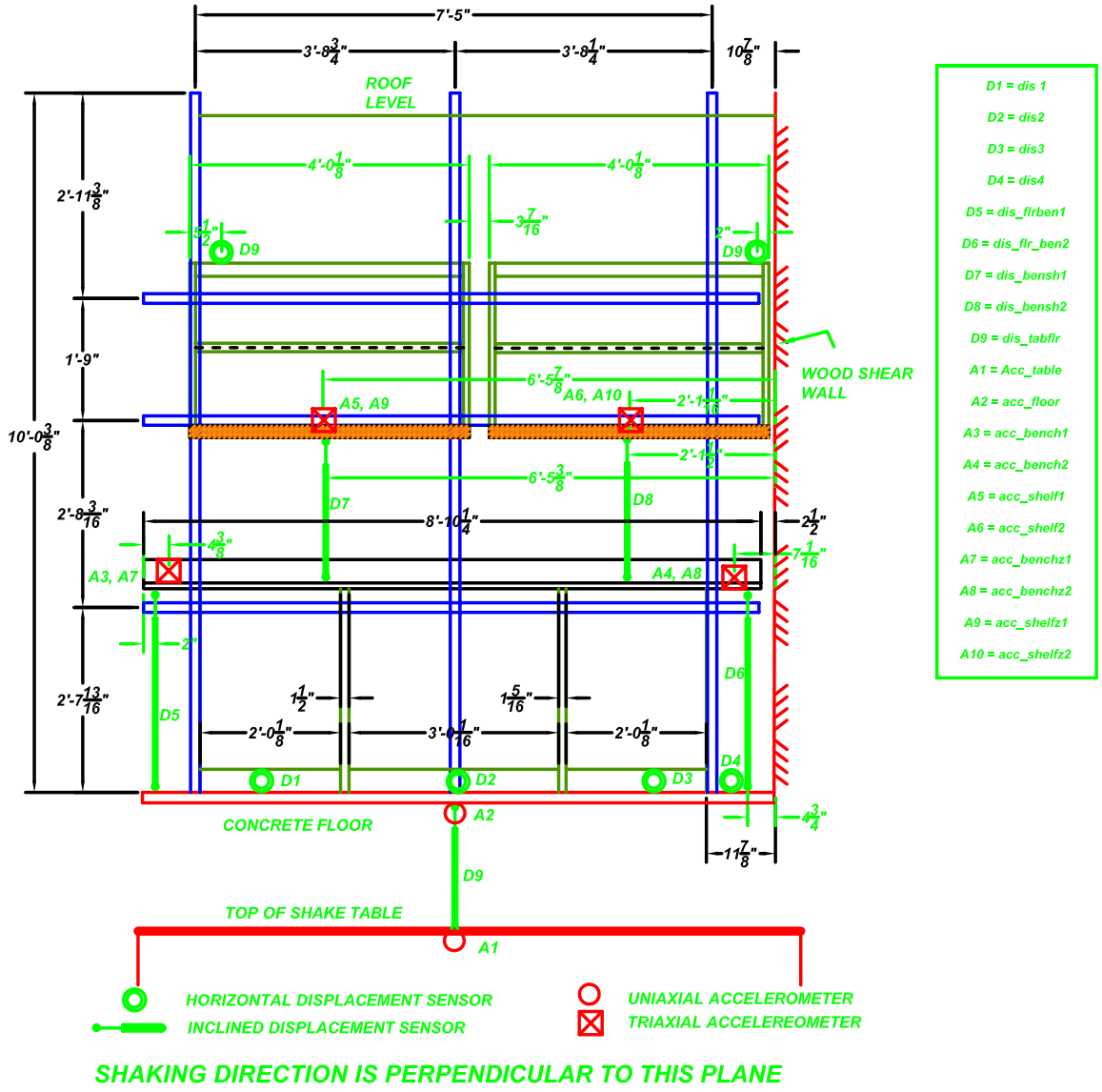

Figure B.13: Instrument layout for mock-laboratory setup Configuration 2.

Table B.2: Description of y-axis nomenclature used for the plots of Configuration 2 (Figures B.14– B.21). Refer to Figure B.13 for location of instruments.

Y axis title	Description
Acc_table	Shake table acceleration in
acc_floor	Acceleration of concrete floor
acc_bench1	Acceleration of bench
acc_bench2	Acceleration of bench
acc_shelf1	Acceleration of shelf
acc_shelf2	Acceleration of shelf
acc_benchz1	Acceleration of bench
acc_benchz2	Acceleration of bench
acc_stshelfm	Acceleration of middle of steel shelf
acc_stshelft	Acceleration of top of steel shelf
acc_smicro	Acceleration of small microscope
acc_lmicro	Acceleration of large microscope
dis1	Displacement of bench cabinet 1 w.r.t floor
dis2	Displacement of bench cabinet 2 w.r.t floor
dis3	Displacement of bench cabinet 3 w.r.t floor
dis4	Displacement of wood shear wall w.r.t floor
dis_flrben1	Displacement of bench top w.r.t floor
dis_flrben2	Displacement of bench top w.r.t floor
dis_bensh1	Displacement of bench top w.r.t shelf bottom
dis_bensh2	Displacement of bench top w.r.t shelf bottom
dis_tabflr	Displacement of floor w.r.t shake table
dis_tablex	Displacement shake table
dis_tablez1	Displacement of shake table (middle of north-side) in vertical direction
dis_tablez1	Displacement of shake table (south-east corner) in vertical direction

Unless otherwise mentioned, all the measurements are in the direction of shaking

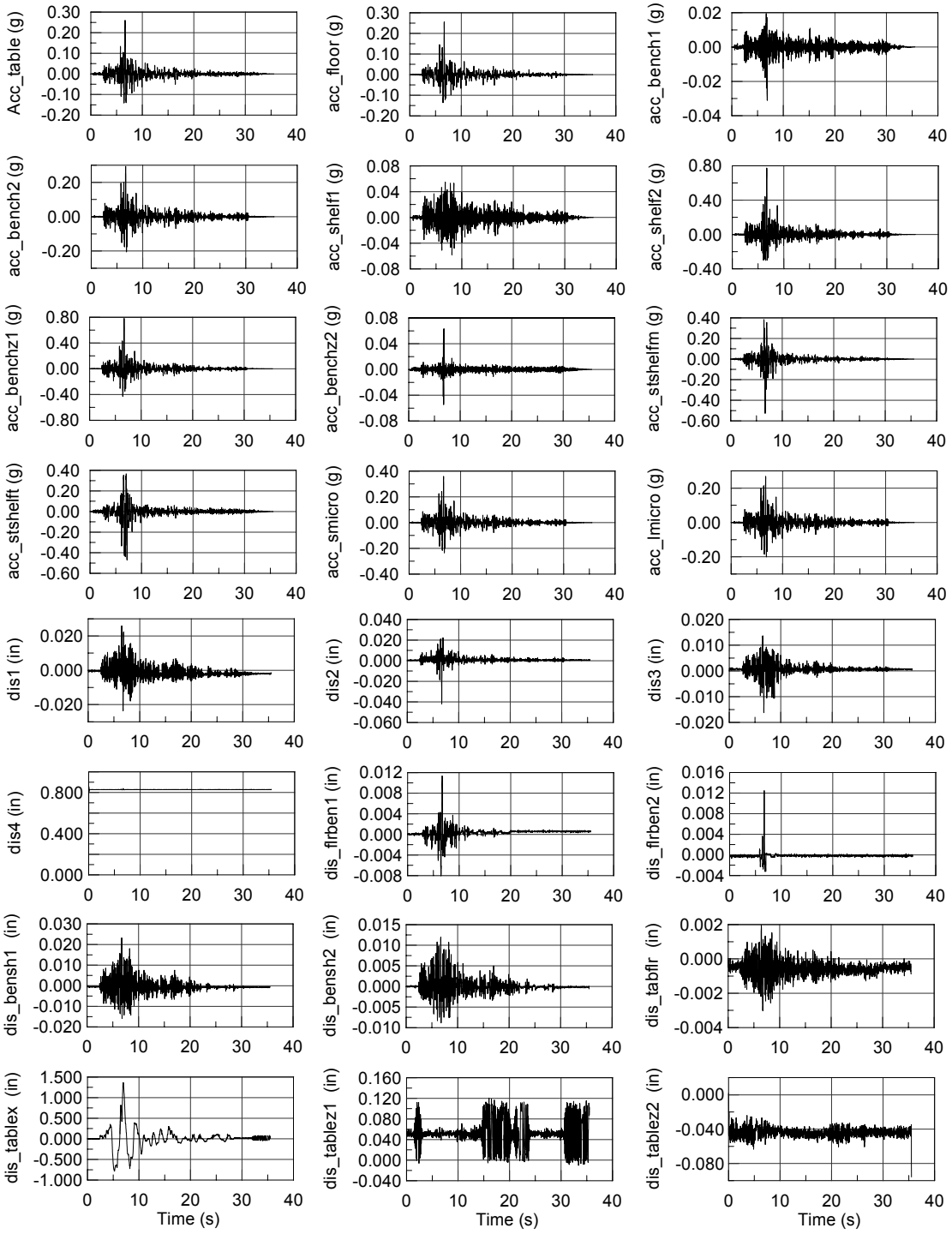

Figure B.14: Configuration 2A: Acceleration (upper four rows) and displacement (lower four rows) time histories for 50% in 50 years Morgan Hill Anderson Dam Down (transverse) (GM - 3).

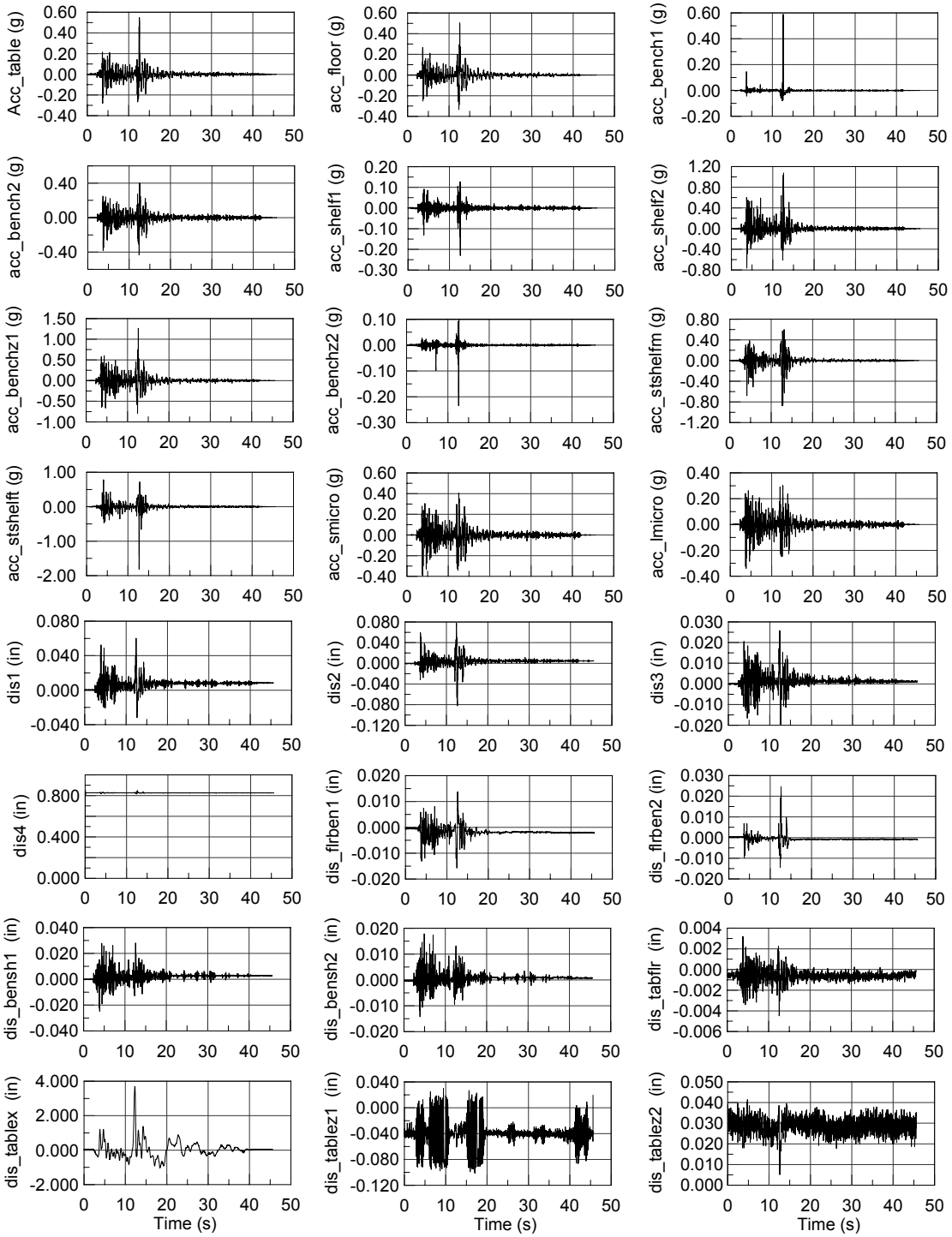

Figure B.15: Configuration 2A: Acceleration (upper four rows) and displacement (lower four rows) time histories for 50% in 50 years Morgan Hill Halls Valley (transverse) (GM - 4).

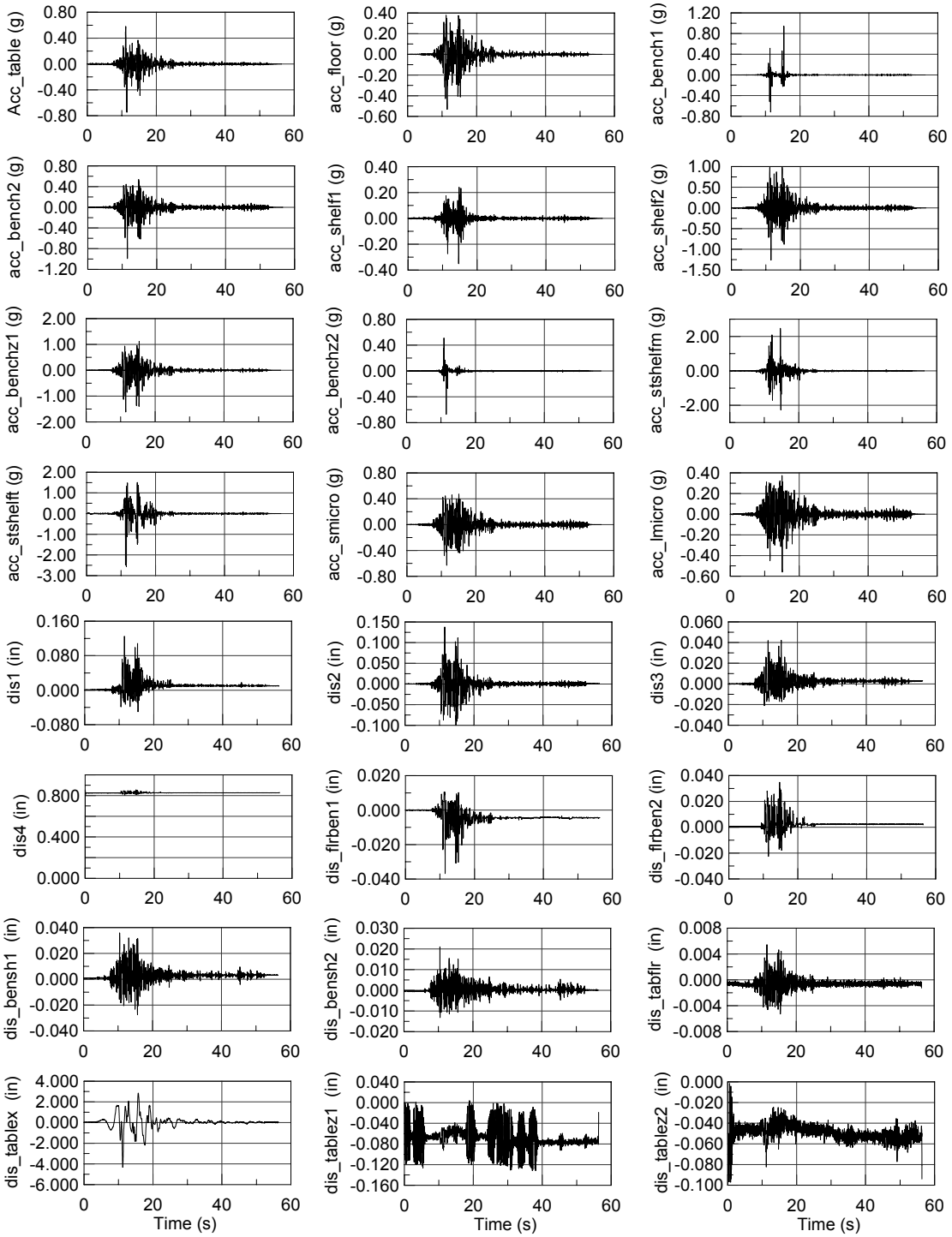

Figure B.16: Configuration 2A: Acceleration (upper four rows) and displacement (lower four rows) time histories for 10% in 50 years Kobe, JMA, Japan (longitudinal) (GM - 5).

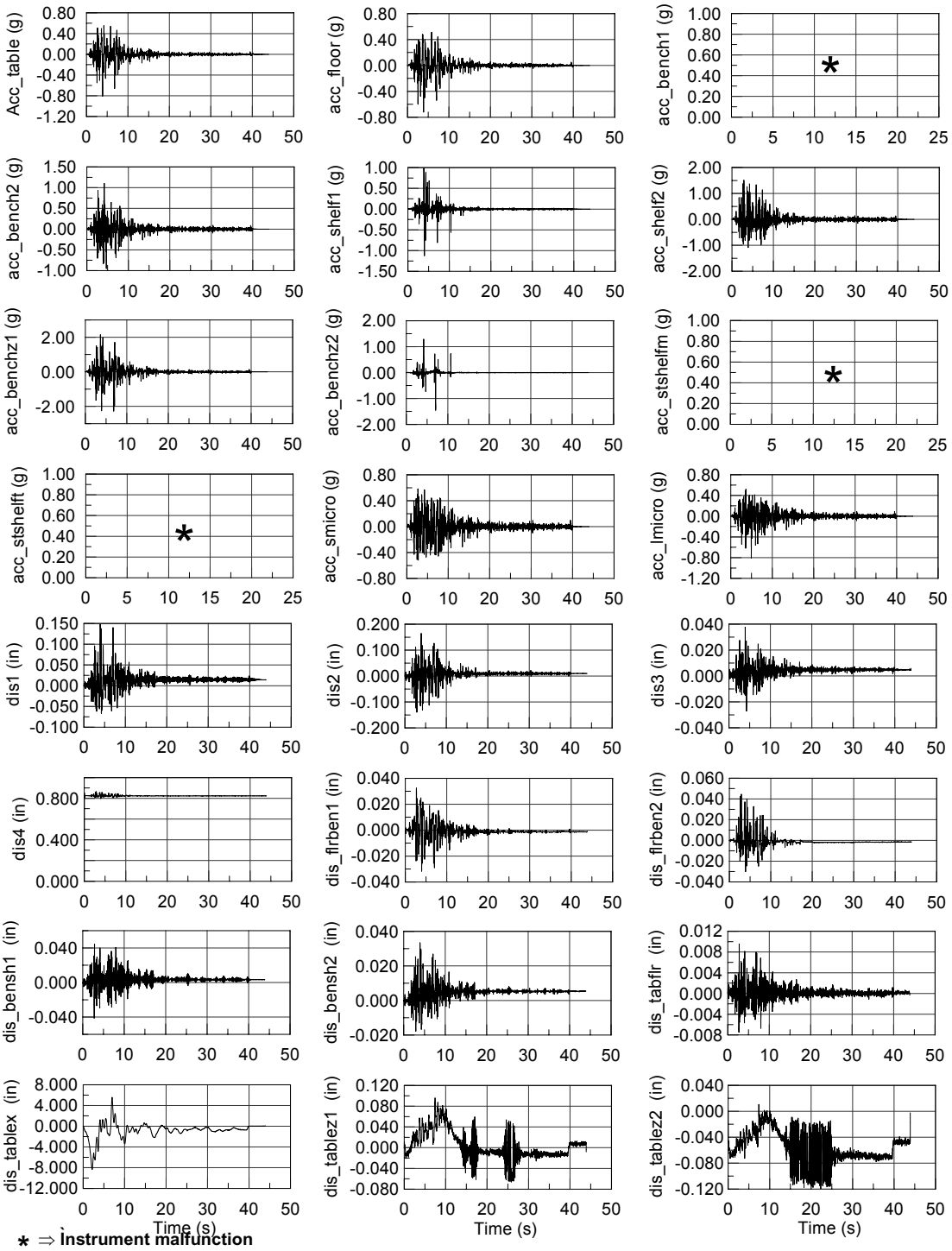

Figure B.17: Configuration 2A: Acceleration (upper four rows) and displacement (lower four rows) time histories for 10% in 50 years Loma Prieta Corralitos (transverse) (GM - 6).

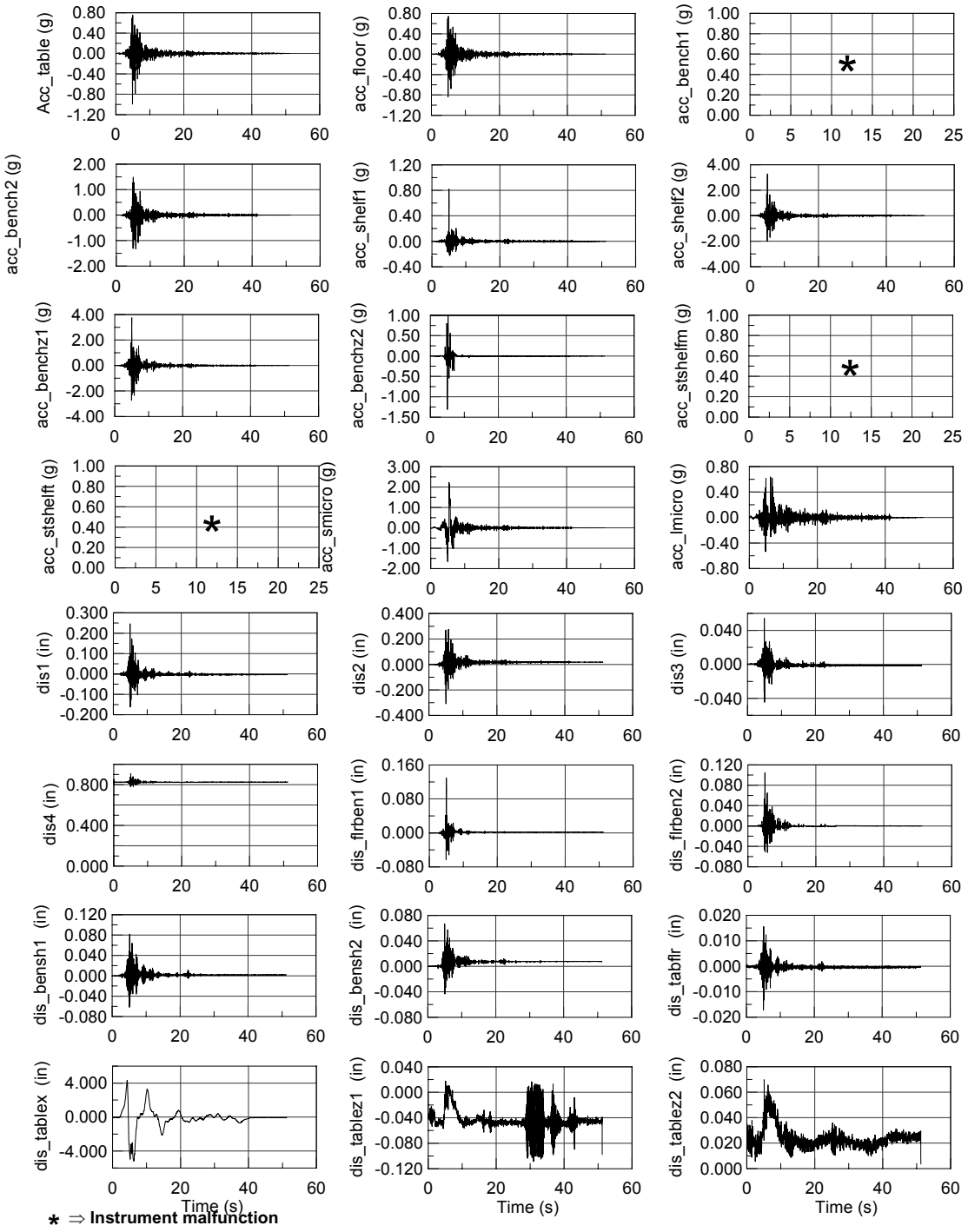

Figure B.18: Configuration 2A: Acceleration (upper four rows) and displacement (lower four rows) time histories for 10% in 50 years Loma Prieta Gavilan College (transverse) (GM - 7).

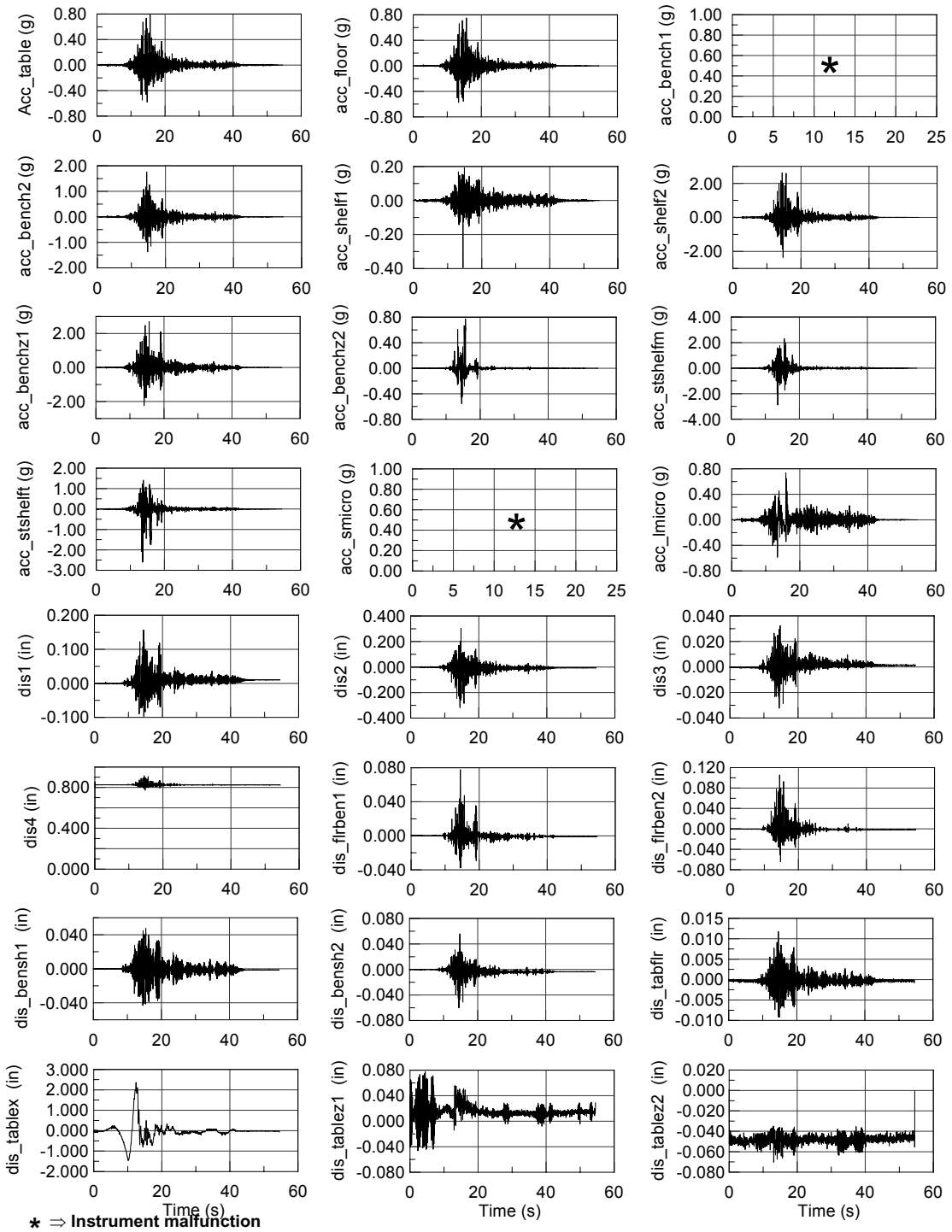

Figure B.19: Configuration 2A: Acceleration (upper four rows) and displacement (lower four rows) time histories for 10% in 50 years Tottori, Kofu, Japan (transverse) (GM - 8).

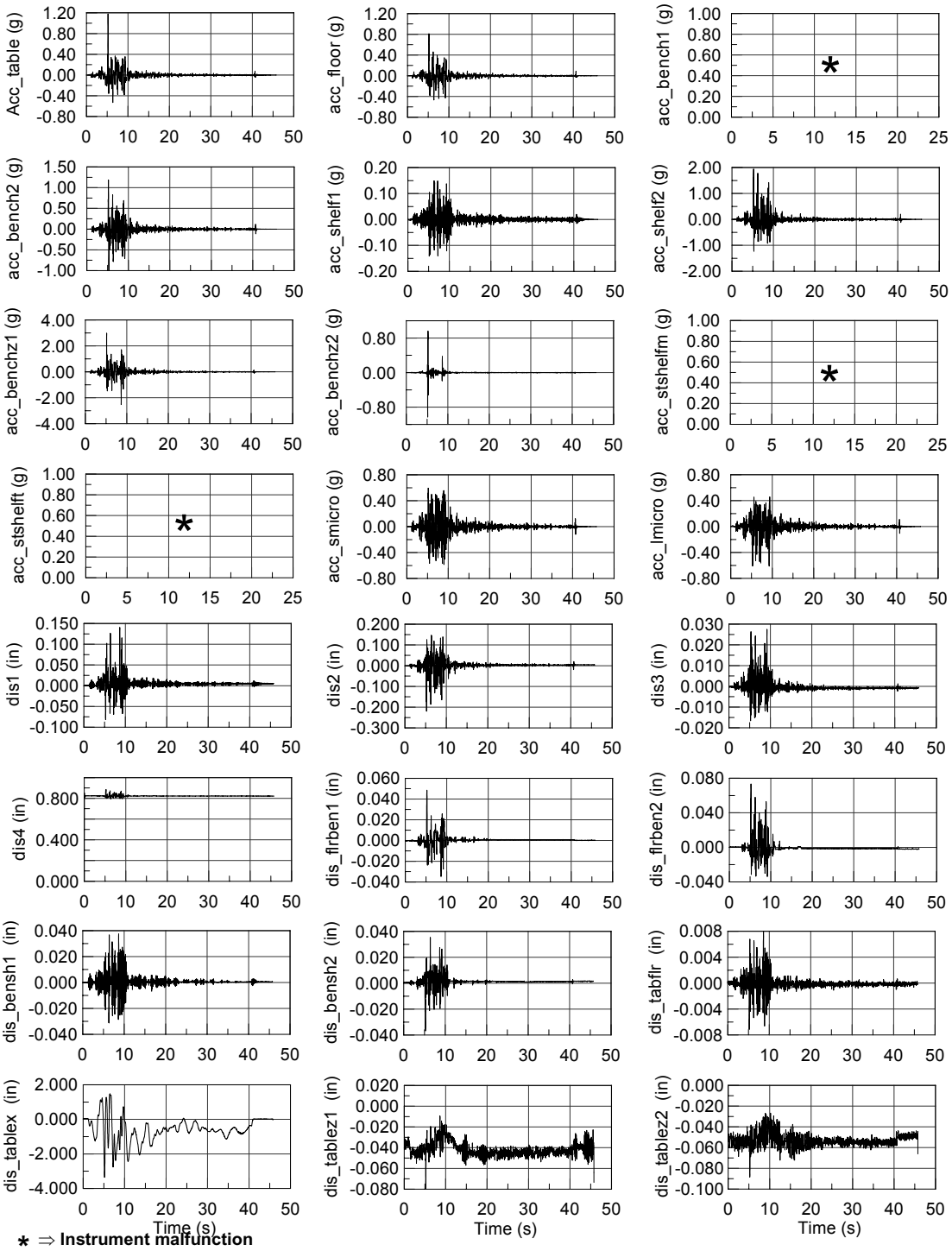

Figure B.20: Configuration 2A: Acceleration (upper four rows) and displacement (lower four rows) time histories for 10% in 50 years Loma Prieta Lexington Dam (longitudinal) (GM - 9).

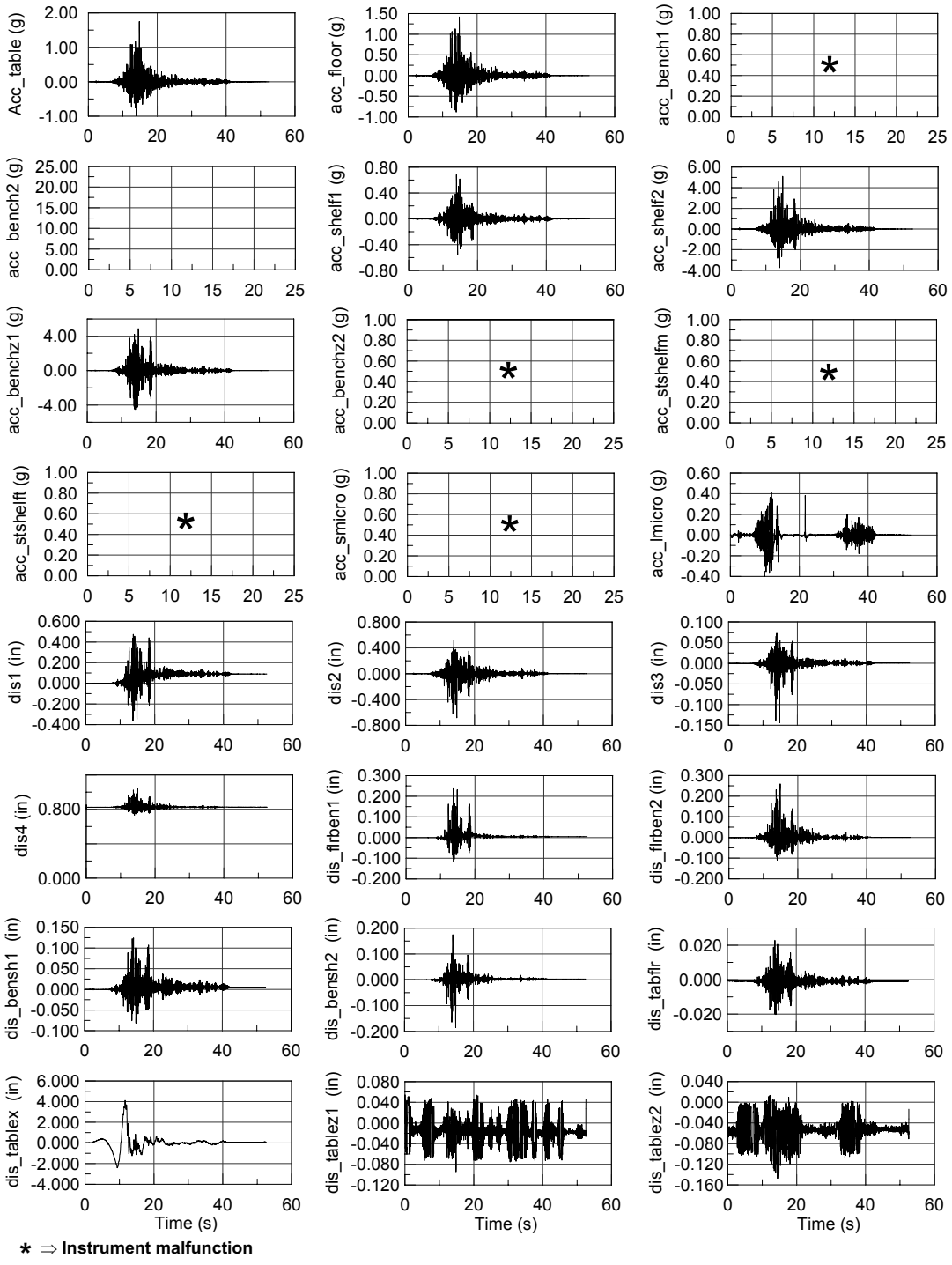

Figure B.21: Configuration 2A: Acceleration (upper four rows) and displacement (lower four rows) time histories for 2% in 50 years Tottori, Kofu, Japan (transverse) (GM - 10).

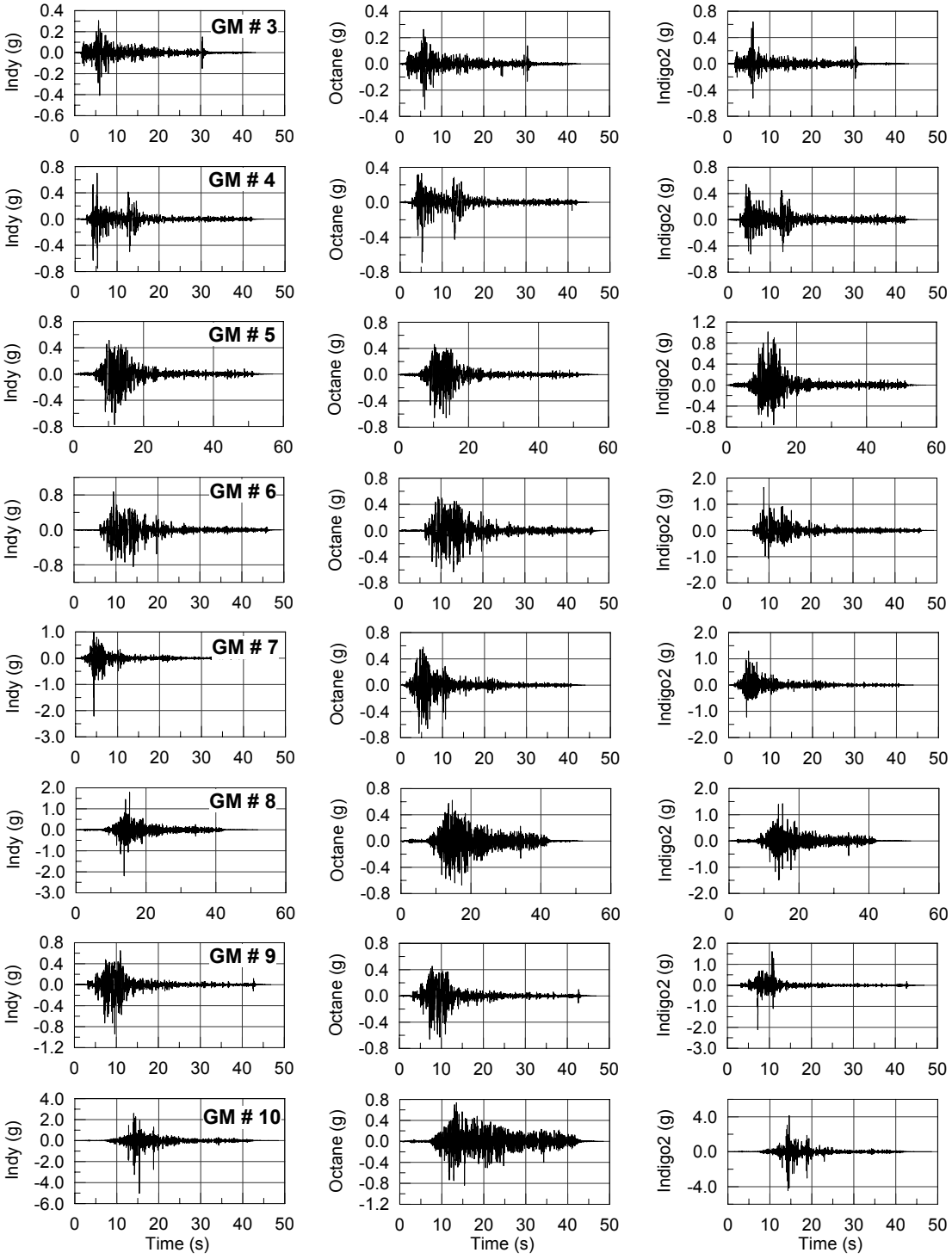

Figure B.22: Configuration 2B: Acceleration time histories of SGI CPUs Indy, Octane and Indigo2 along the direction of shaking where each row represents GM - 3 through GM - 10.

B.3 CONFIGURATION 3

This configuration is a back to back double bench-shelf placed in the middle of the mock laboratory, as shown in Figure B.23(a). The direction of shaking, i.e., (x axis as used in the following figures) is along the longitudinal direction of the bench. Two sets of equipment were tested in this setup, and the corresponding configurations are named 3A and 3B. The equipment tested in Configuration 3A are SGI CPUs, Indigo2 (purple), Octane (green), and Indy (blue), respectively, from left to right in Figure B.23(b). The equipment tested in Configuration 3B are a small microscope, SGI CPU Indigo2 (purple), a large microscope, and a Technicon autoanalyzer, respectively, from left to right in Figure B.23(c). Figure B.24 shows the general analog instrument layout of the accelerometers and displacement transducers. Figures B.25–B.32 give the acceleration and displacement time histories for analog transducers. The y-axis label description (nomenclature) for these figures is given in Table B.3.

(a)

(b)

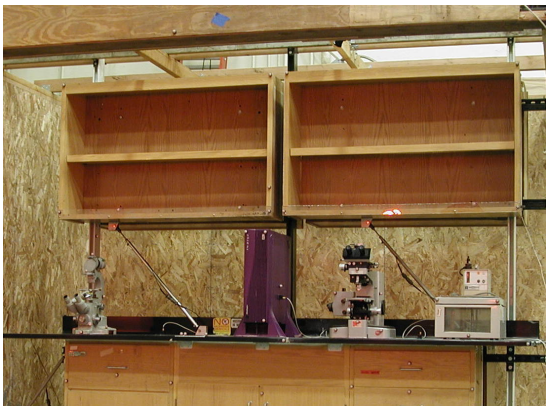

(c)

Figure B.23: (a) Mock-laboratory setup of Configuration 3, (b) equipment tested in Configuration 3A, and (c) equipment tested in Configuration 3B.

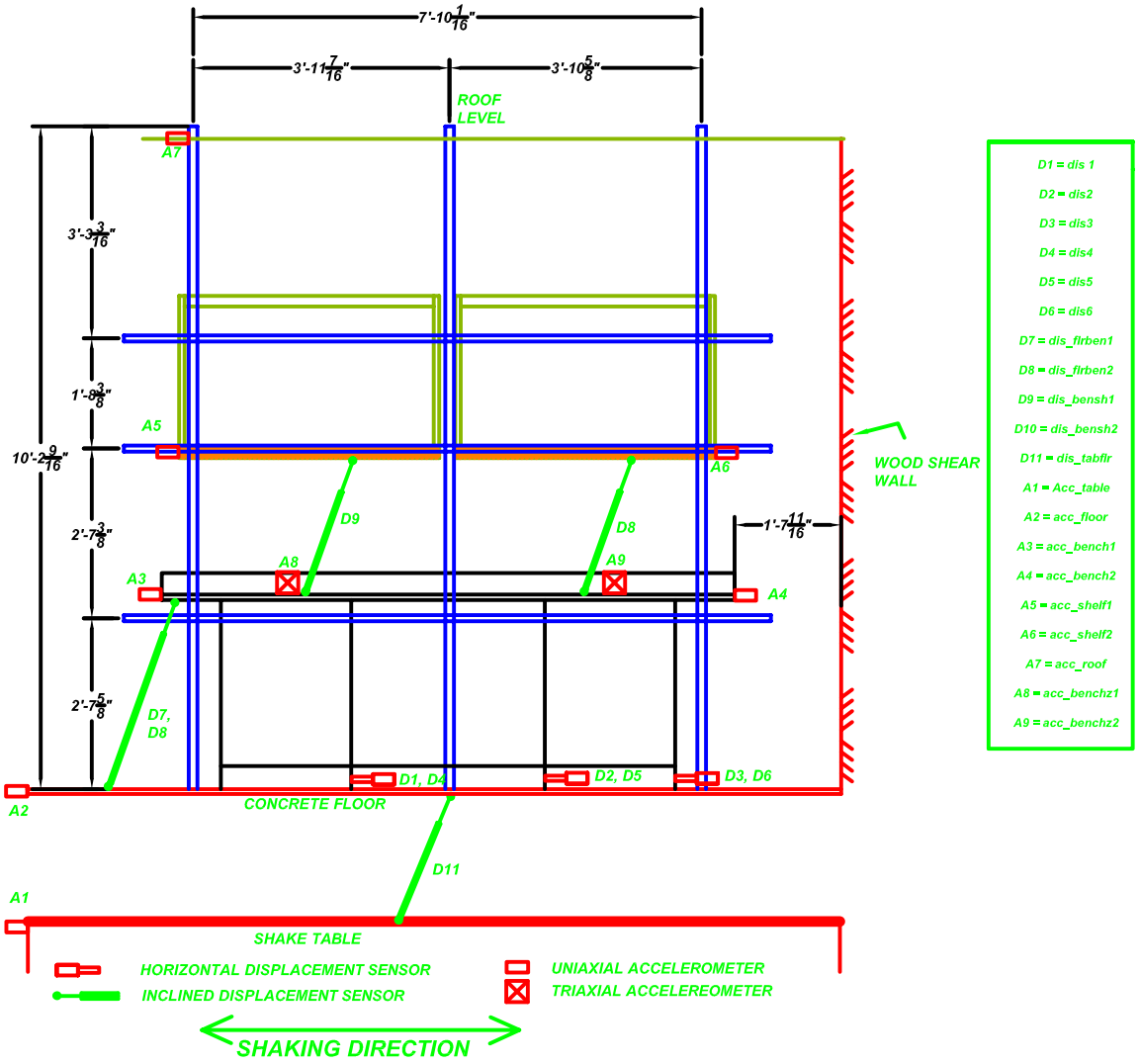

Figure B.24: Instrument layout for mock-laboratory setup Configuration 3

Table B.3: Description of y-axis nomenclature used for the plots of Configuration 3 (Figures B.25– B.32). Refer to Figure B.24 for location of instruments.

Y axis title	Description
Acc_table	Shake table acceleration
acc_floor	Acceleration of concrete floor
acc_bench1	Acceleration of bench
acc_bench2	Acceleration of bench
acc_bench3	Acceleration of bench
acc_roof	Acceleration of beam at roof level
Acc_shelf	Acceleration of shelf
acc_benchz1	Acceleration of bench in the vertical direction
acc_benchz2	Acceleration of bench in the vertical direction
acc_CPU x	Acceleration of SGI Octane CPU in the direction of shaking
acc_CPU y	Acceleration of SGI Octane CPU in the direction perpendicular to shaking
acc_CPU z	Acceleration of SGI Octane CPU in the vertical direction
dis1	Displacement of bench cabinet 1 w.r.t floor
dis2	Displacement of bench cabinet 2 w.r.t floor
dis3	Displacement of bench cabinet 3 w.r.t floor
dis4	Displacement of bench cabinet 4 (opposite to cabinet 1) w.r.t floor
dis5	Displacement of bench cabinet 5 (opposite to cabinet 2) w.r.t floor
dis6	Displacement of bench cabinet 6 (opposite to cabinet 3) w.r.t floor
dis_bensh1	Displacement of bench top w.r.t shelf bottom
dis_bensh2	Displacement of bench top w.r.t shelf bottom
dis_flrben1	Displacement of bench top w.r.t floor
dis_flrben2	Displacement of bench top w.r.t floor
dis_tabflr	Displacement of shake table w.r.t floor of the mock laboratory
dis_table	Shake table displacement

Unless otherwise mentioned, all the measurements are in the direction of shaking

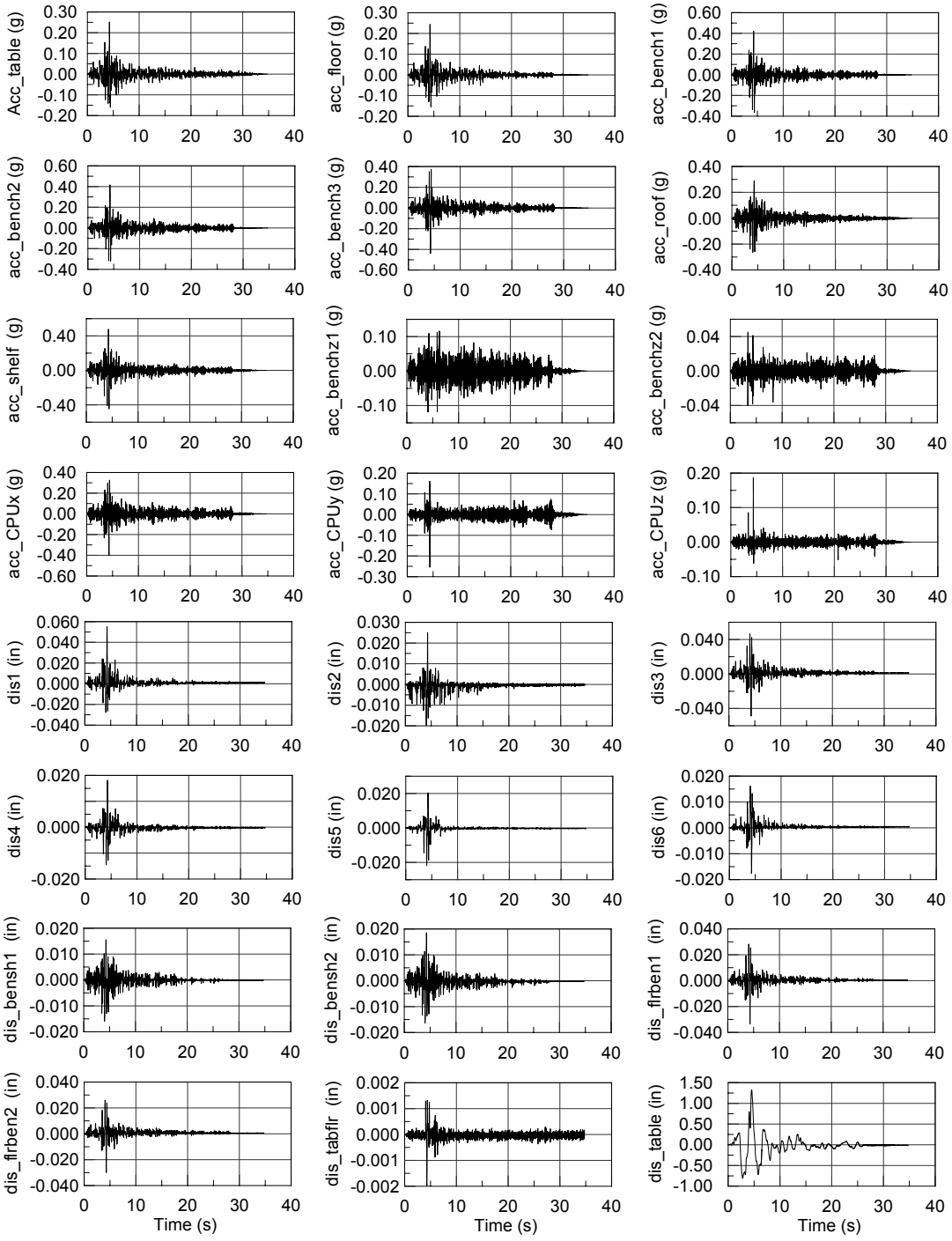

Figure B.25: Configuration 3A: Acceleration (upper four rows) and displacement (lower four rows) time histories for 50% in 50 years Morgan Hill Anderson Dam Down (transverse) (GM - 3).

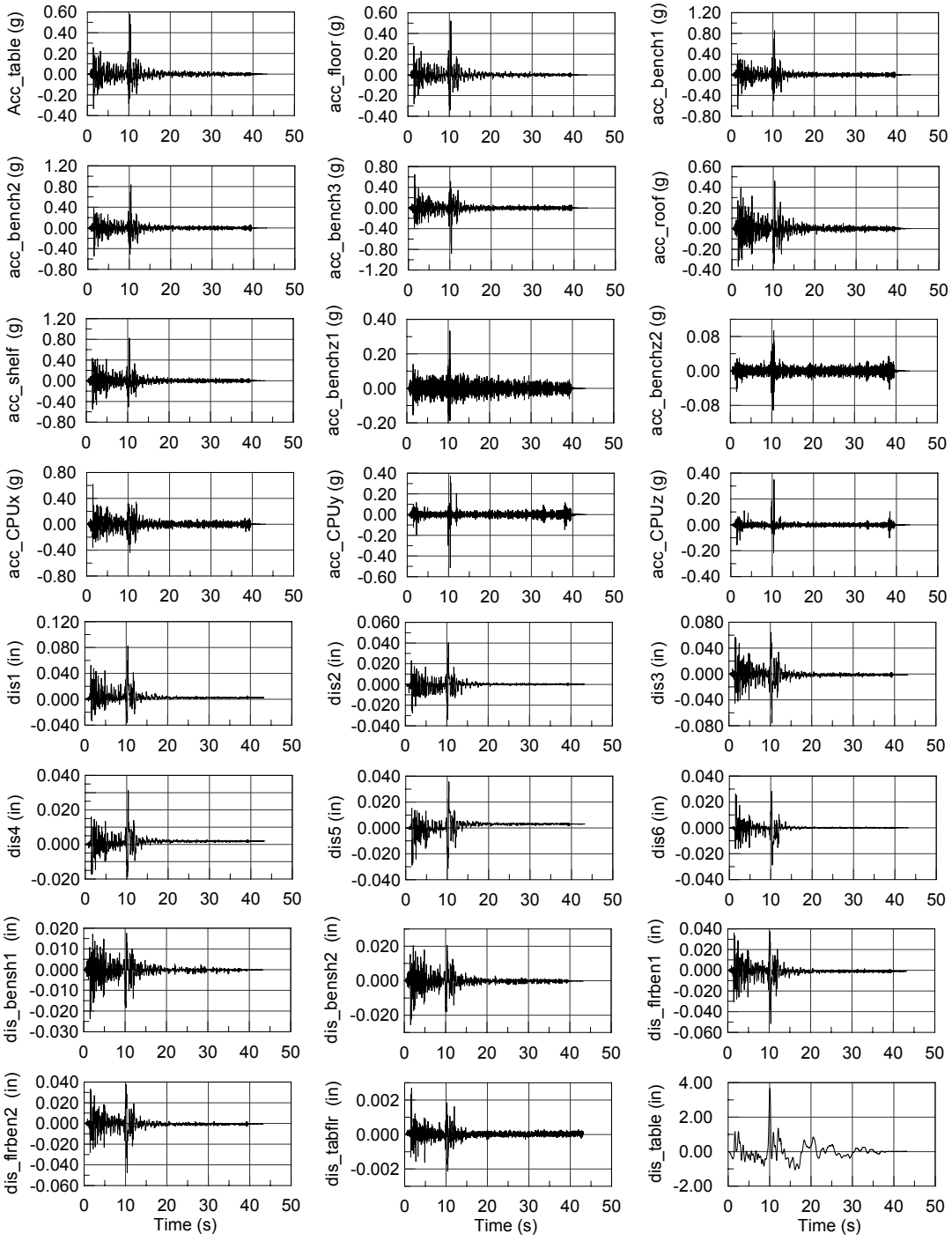

Figure B.26: Configuration 3A: Acceleration (upper four rows) and displacement (lower four rows) time histories for 50% in 50 years Morgan Hill Halls Valley (transverse) (GM - 4).

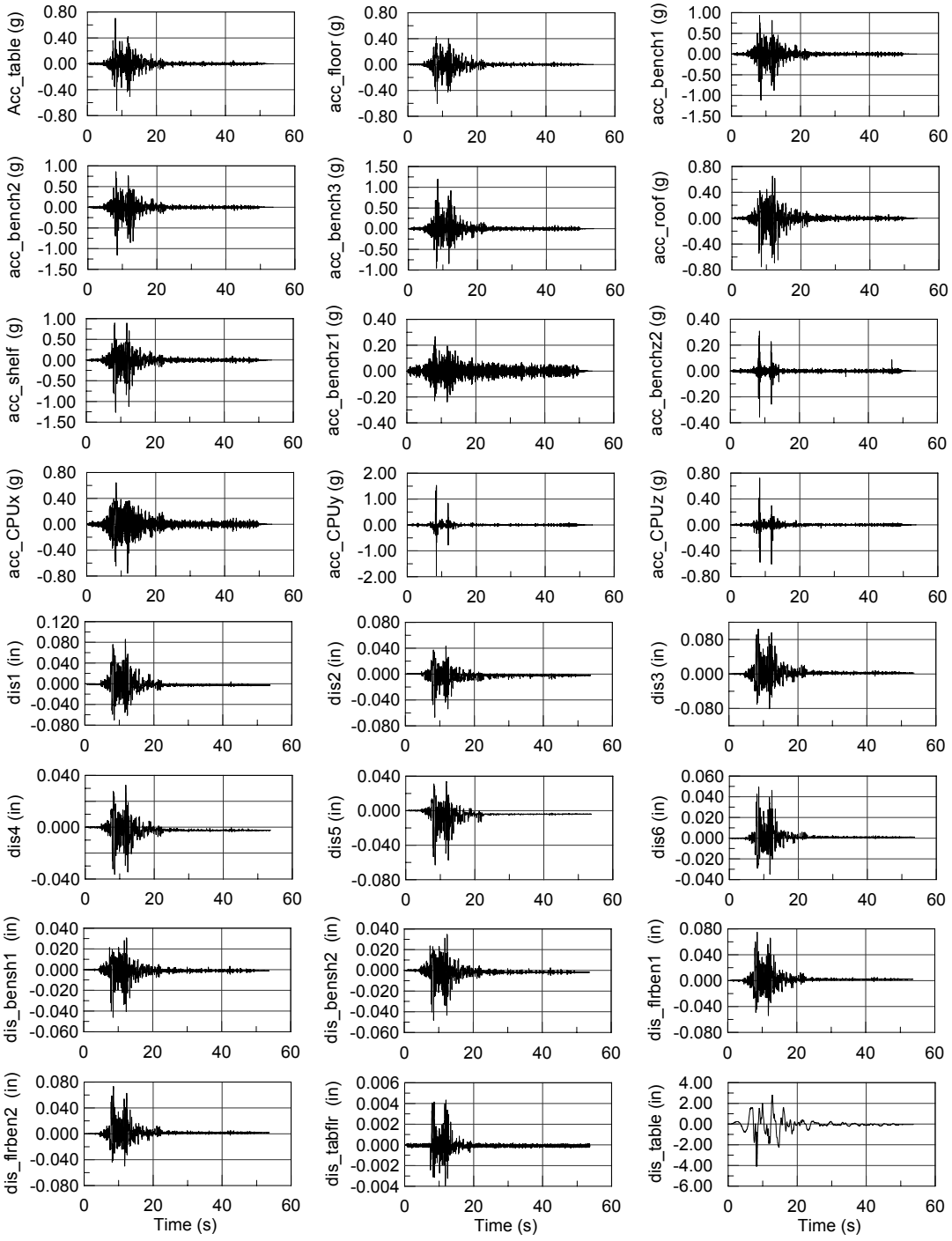

Figure B.27: Configuration 3A: Acceleration (upper four rows) and displacement (lower four rows) time histories for 10% in 50 years Kobe, JMA, Japan (longitudinal) (GM - 5).

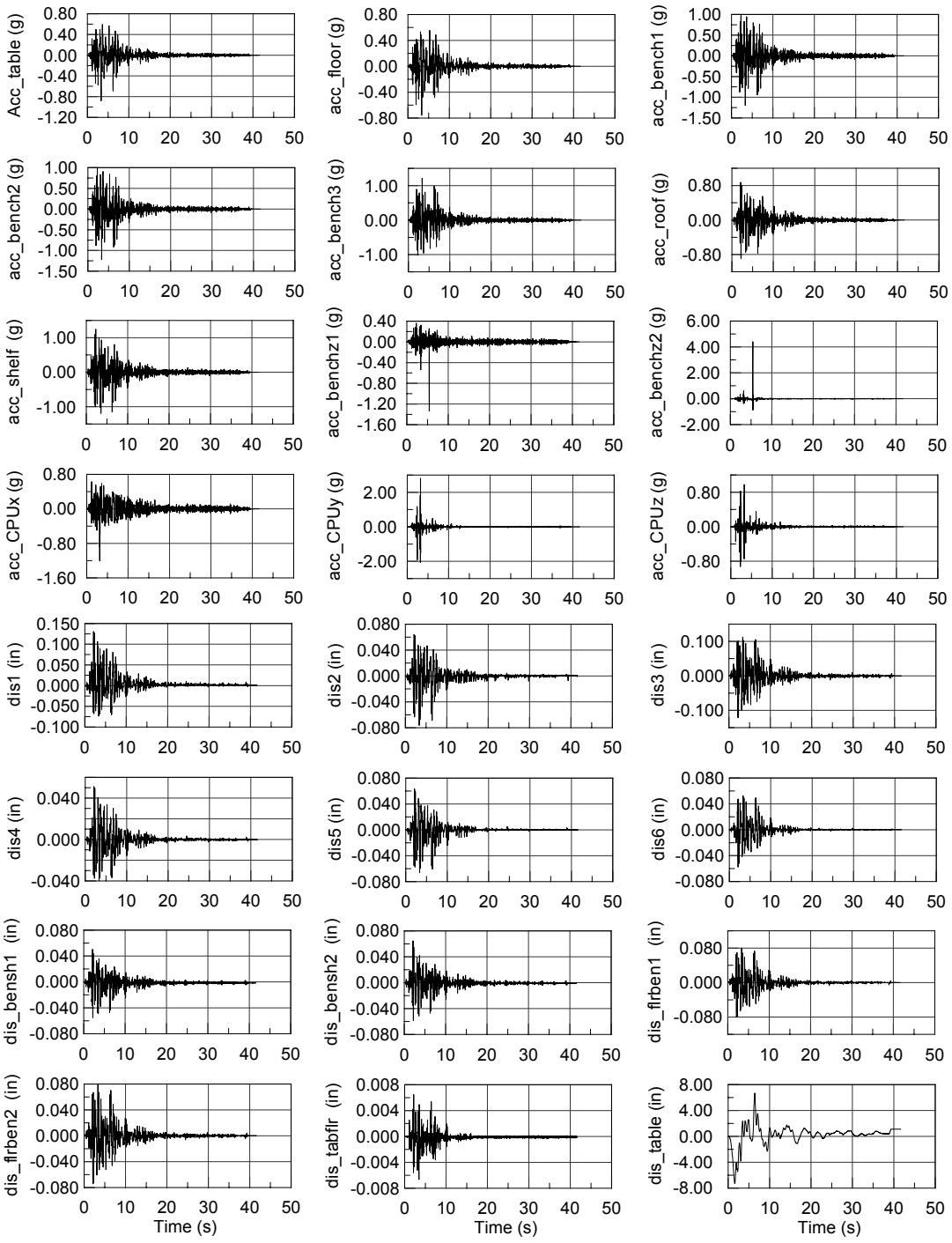

Figure B.28: Configuration 3A: Acceleration (upper four rows) and displacement (lower four rows) time histories for 10% in 50 years Loma Prieta Corralitos (transverse) (GM - 6).

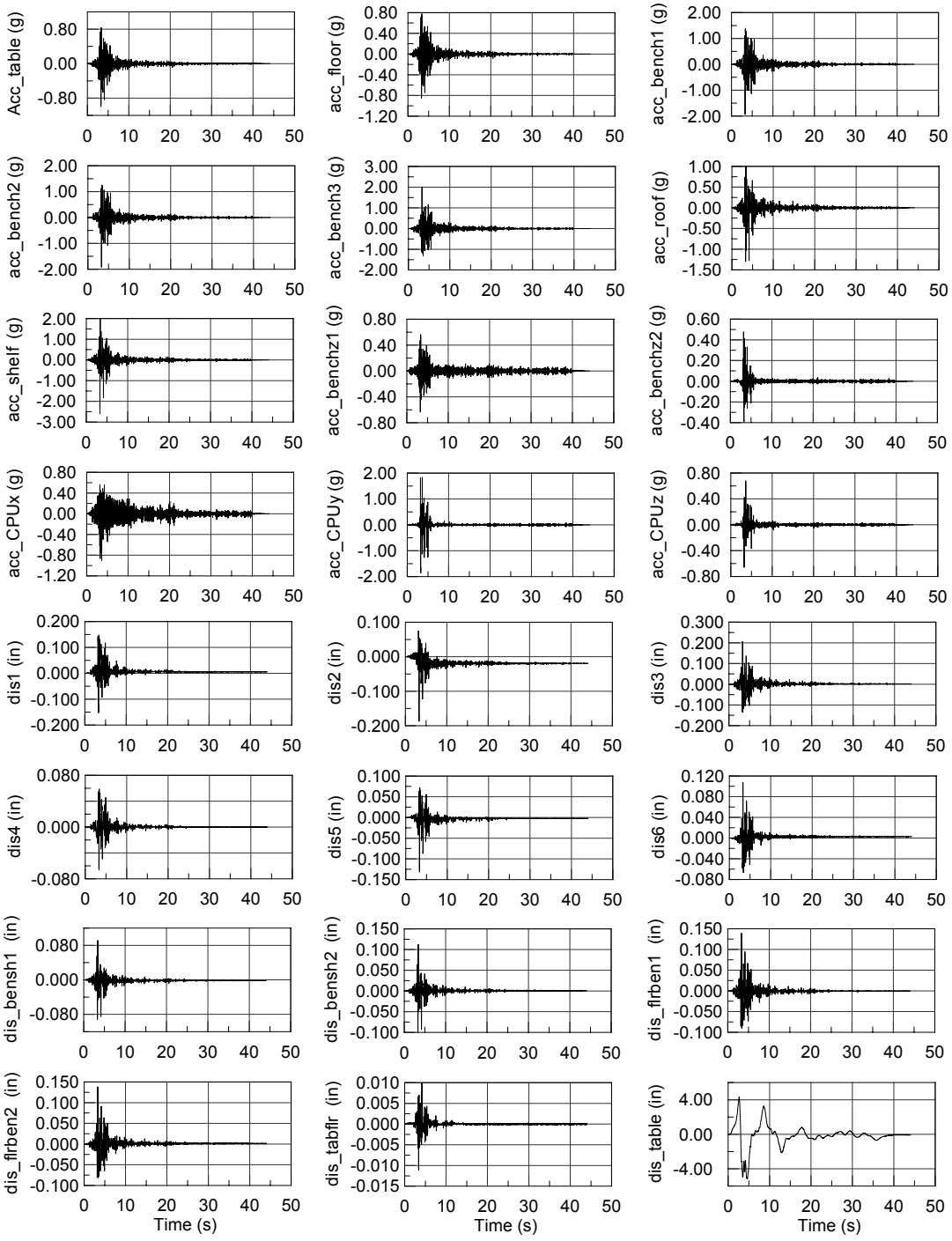

Figure B.29: Configuration 3A: Acceleration (upper four rows) and displacement (lower four rows) time histories for 10% in 50 years Loma Prieta Gavilan College (transverse) (GM - 7).

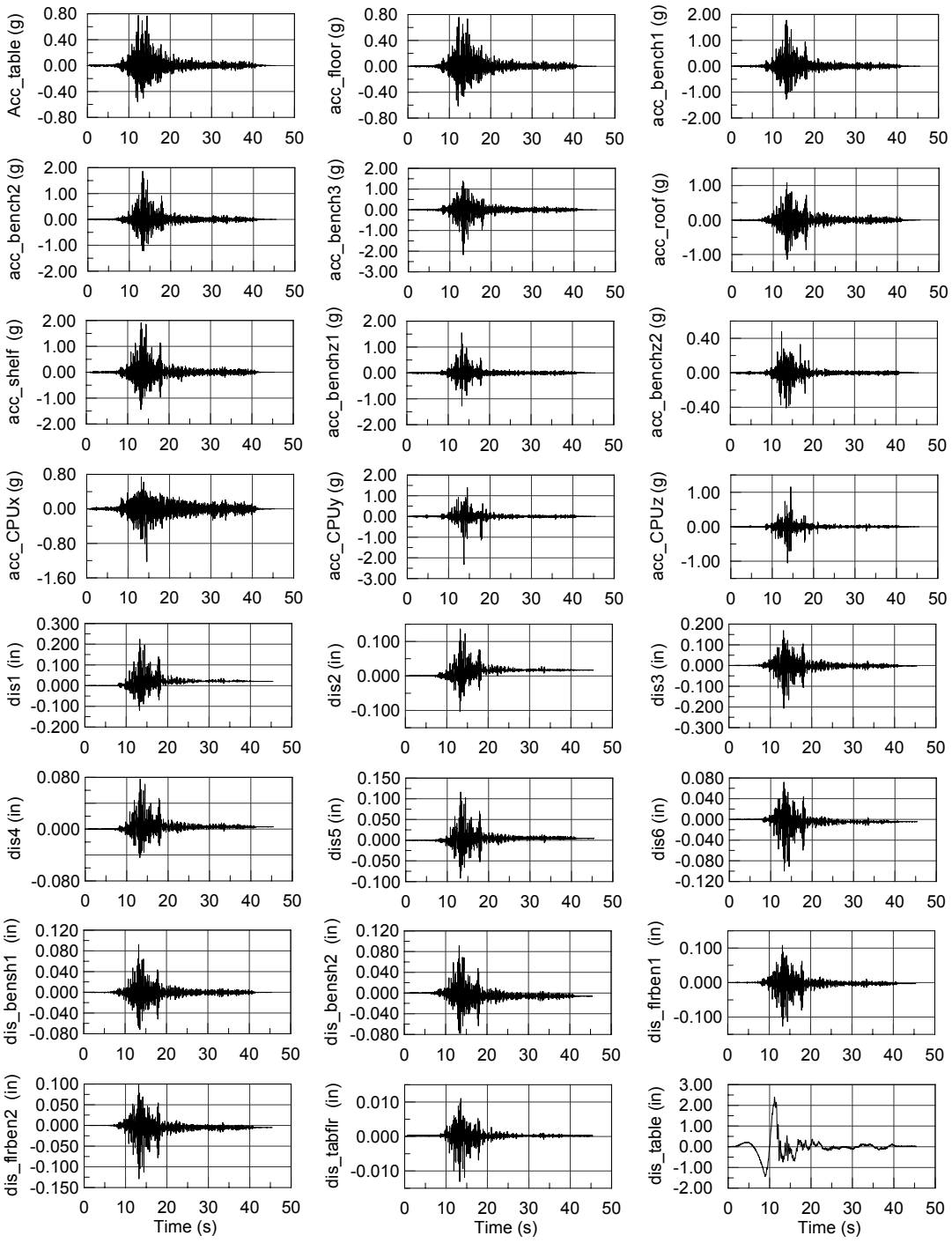

Figure B.30: Configuration 3A: Acceleration (upper four rows) and displacement (lower four rows) time histories for 10% in 50 years Tottori, Kofu, Japan (transverse) (GM - 8).

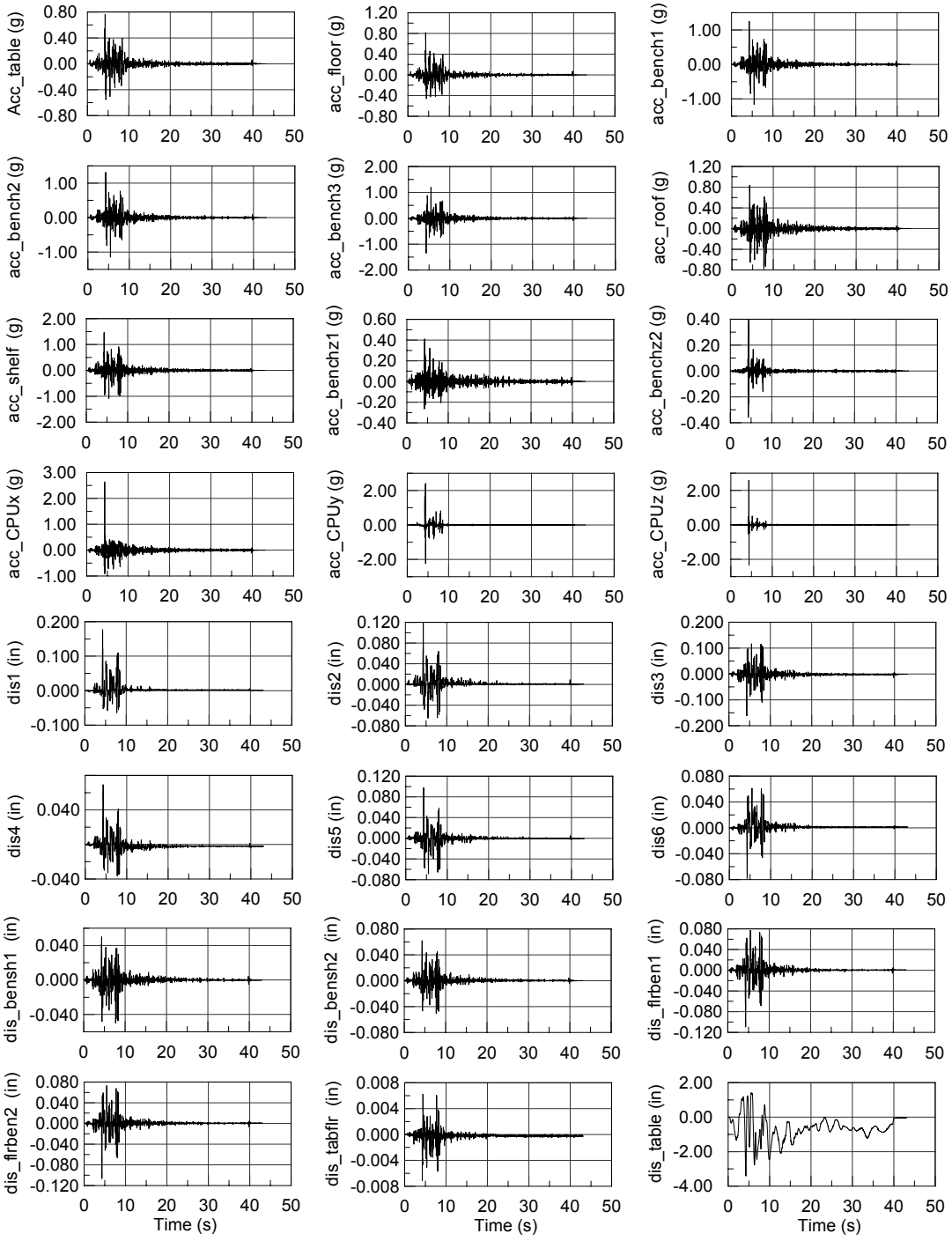

Figure B.31: Configuration 3A: Acceleration (upper four rows) and displacement (lower four rows) time histories for 10% in 50 years Loma Prieta Lexington Dam (longitudinal) (GM - 9).

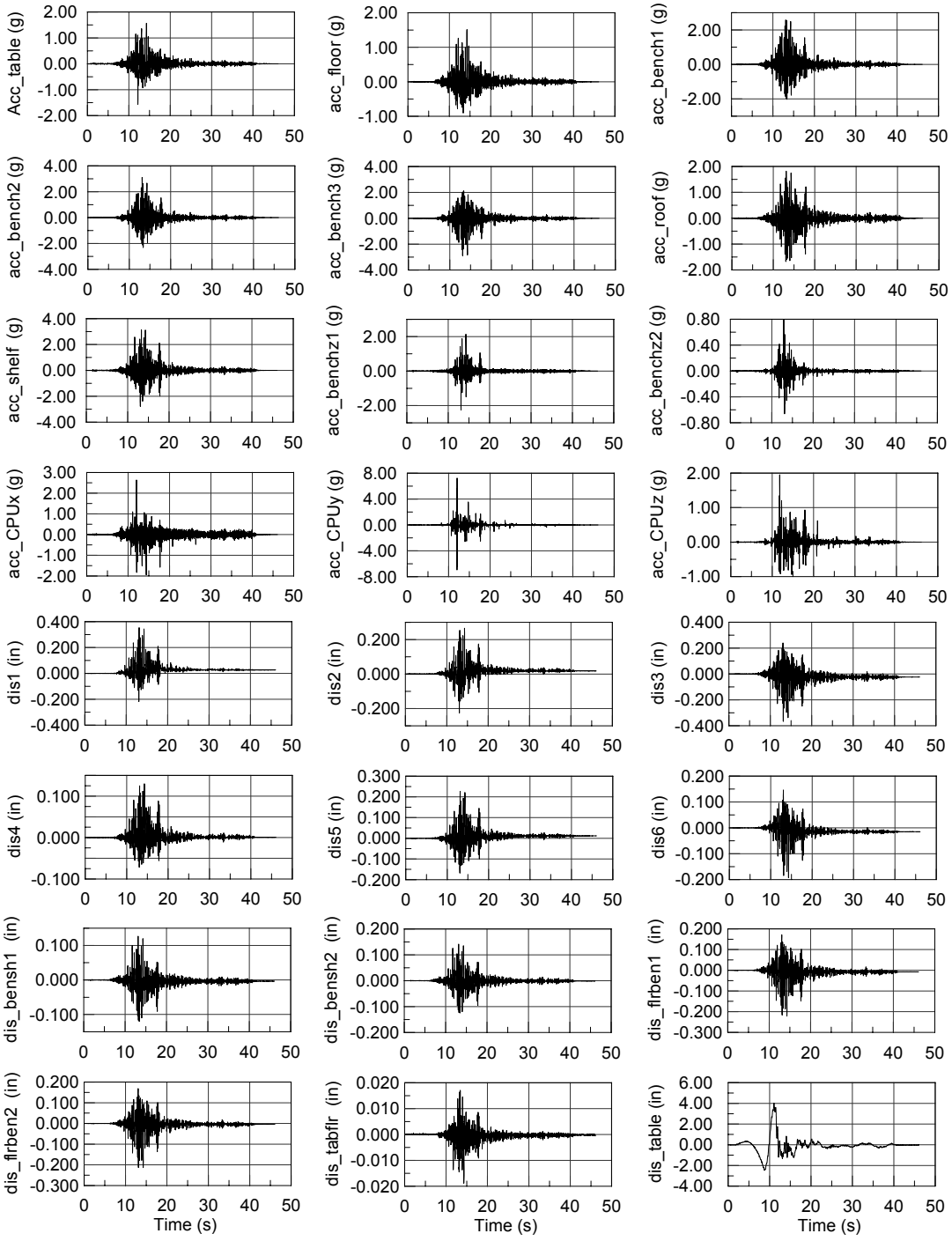

Figure B.32: Configuration 3A: Acceleration (upper four rows) and displacement (lower four rows) time histories for 2% in 50 years Tottori, Kofu, Japan (transverse) (GM - 10).

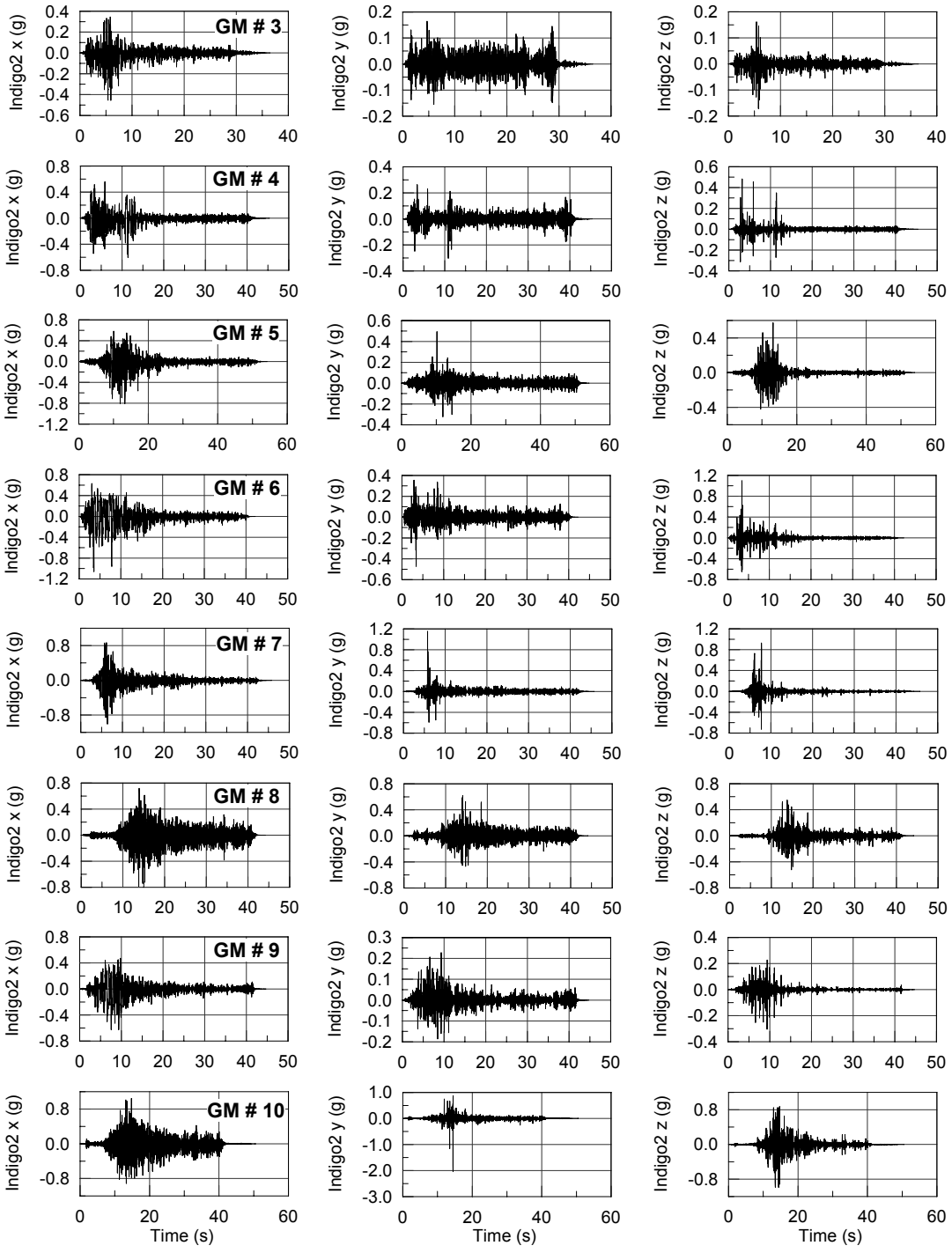

Figure B.33: Configuration 3B: Acceleration time histories of SGI CPU Indigo2 in three directions where each row represents GM - 3 through GM - 10.

B.4 CONFIGURATION 4

This configuration is a back to back double bench-shelf placed in the middle of the mock laboratory just perpendicular to Configuration 3, as shown in Figure B.34(a). Therefore, the direction of shaking, i.e., (x axis as used in the following figures) is along the transverse direction of the bench. The equipment tested in Configuration 4 are an Eppendoff centrifuge, a 15″ monitor (small), a 17″ monitor (medium), and a 19″ monitor (large), respectively, from left to right in Figure B.34(b). Figure B.35 shows the general analog instrument layout of the accelerometers and displacement transducers. Figures B.36–B.43 give the acceleration and displacement time histories for analog transducers. The y-axis label description (nomenclature) for these figures is given in Table B.4.

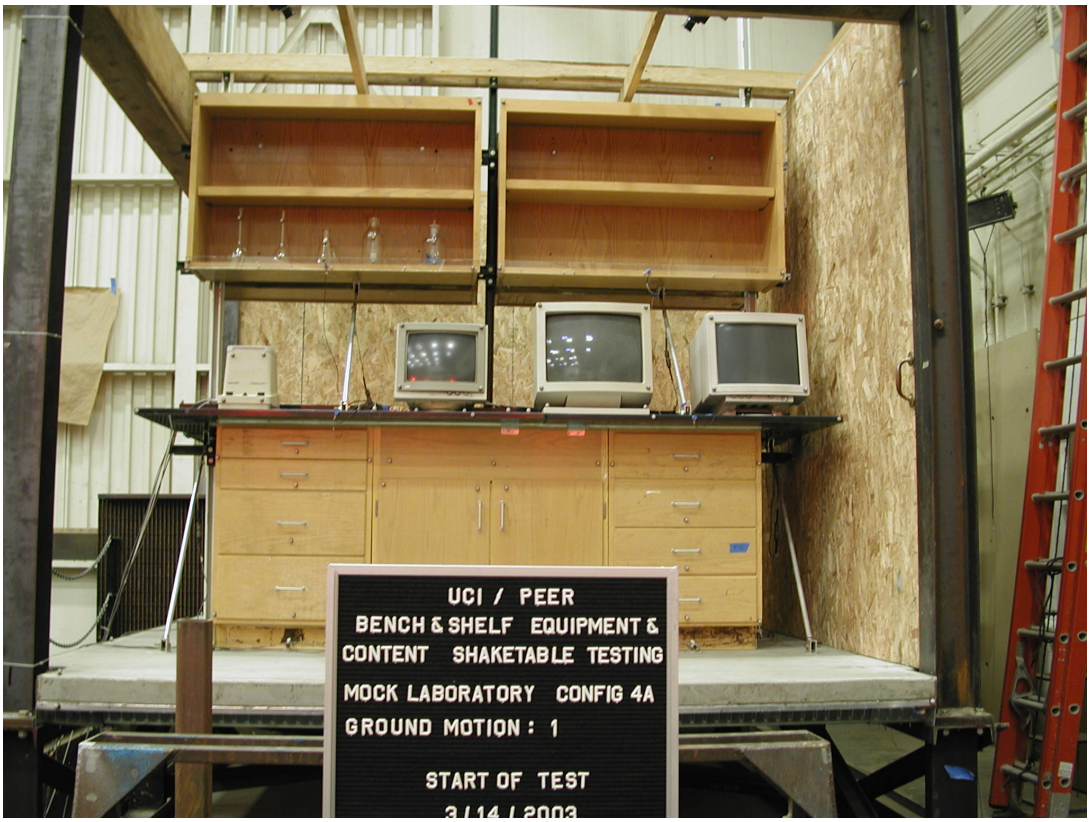

(a)

(b)

Figure B.34: (a) Mock-laboratory setup of Configuration 4 and (b) equipment tested in Configuration 4.

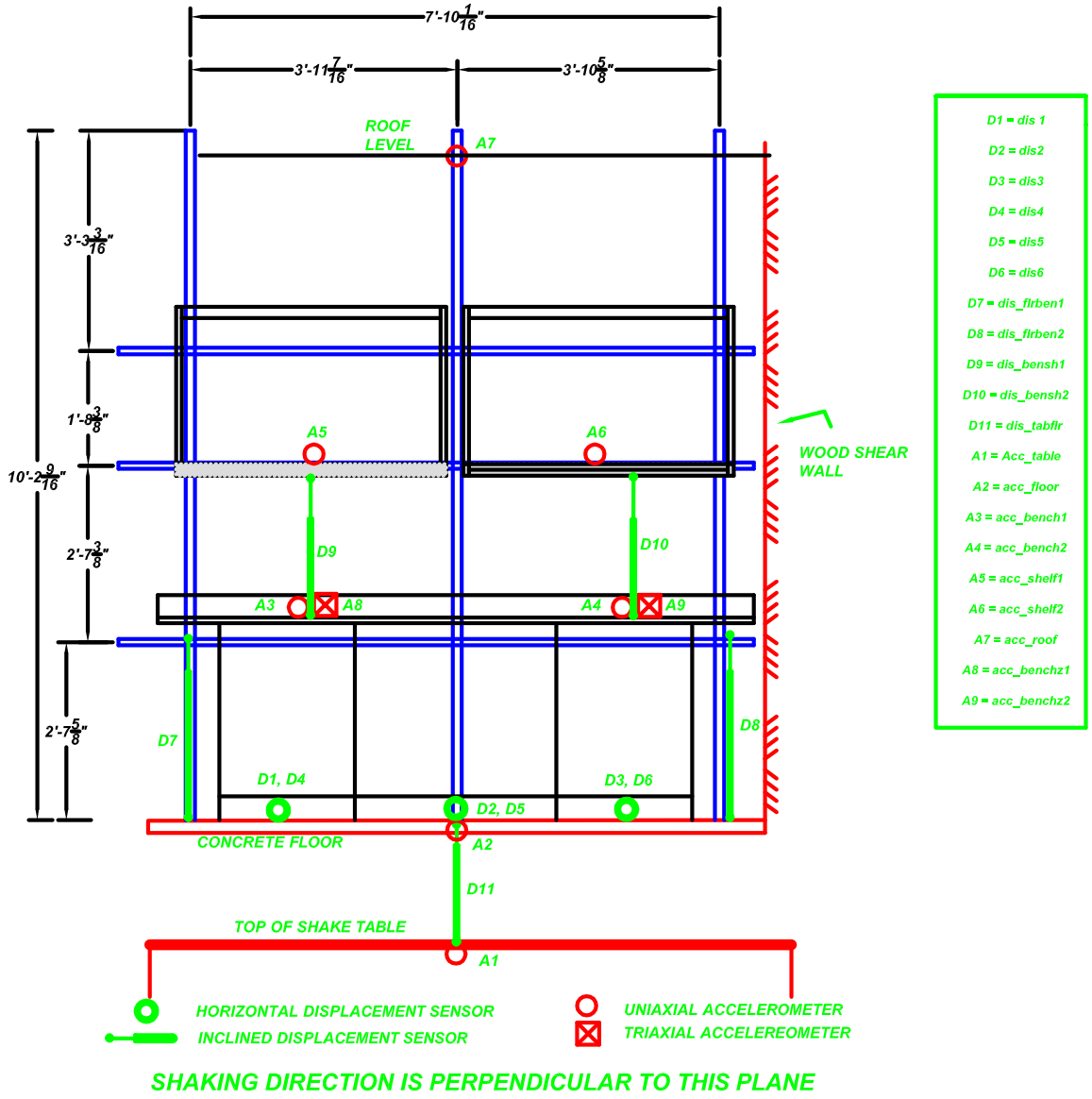

Figure B.35: Instrument layout for mock-laboratory setup Configuration 4.

Table B.4: Description of y-axis nomenclature used for the plots of Configuration 4 (Figures B.36– B.43). Refer to Figure B.35 for location of instruments.

Y axis title	Description
Acc_table	Shake table acceleration
acc_floor	Acceleration of concrete floor
acc_bench1	Acceleration of bench
acc_bench2	Acceleration of bench
acc_shelf1	Acceleration of shelf
acc_shelf2	Acceleration of shelf
acc_roof	Acceleration of beam at roof level
acc_benchz1	Acceleration of bench in the vertical direction
acc_benchz2	Acceleration of bench in the vertical direction
acc_smoni x	Acceleration of small (15”) monitor in the direction of shaking
acc_smoni y	Acceleration of small (15”) monitor in the direction perpendicular to shaking
acc_smoni z	Acceleration of small (15”) monitor in the vertical direction
dis1	Displacement of bench cabinet 1 w.r.t floor
dis2	Displacement of bench cabinet 2 w.r.t floor
dis3	Displacement of bench cabinet 3 w.r.t floor
dis4	Displacement of bench cabinet 4 (opposite to cabinet 1) w.r.t floor
dis5	Displacement of bench cabinet 5 (opposite to cabinet 2) w.r.t floor
dis6	Displacement of bench cabinet 6 (opposite to cabinet 3) w.r.t floor
dis_bensh1	Displacement of bench top w.r.t shelf bottom
dis_bensh2	Displacement of bench top w.r.t shelf bottom
dis_flrben1	Displacement of bench top w.r.t floor
dis_flrben2	Displacement of bench top w.r.t floor
dis_tabflr	Displacement of shake table w.r.t floor of the mock laboratory
dis_table	Shake table displacement

Unless otherwise mentioned, all the measurements are in the direction of shaking

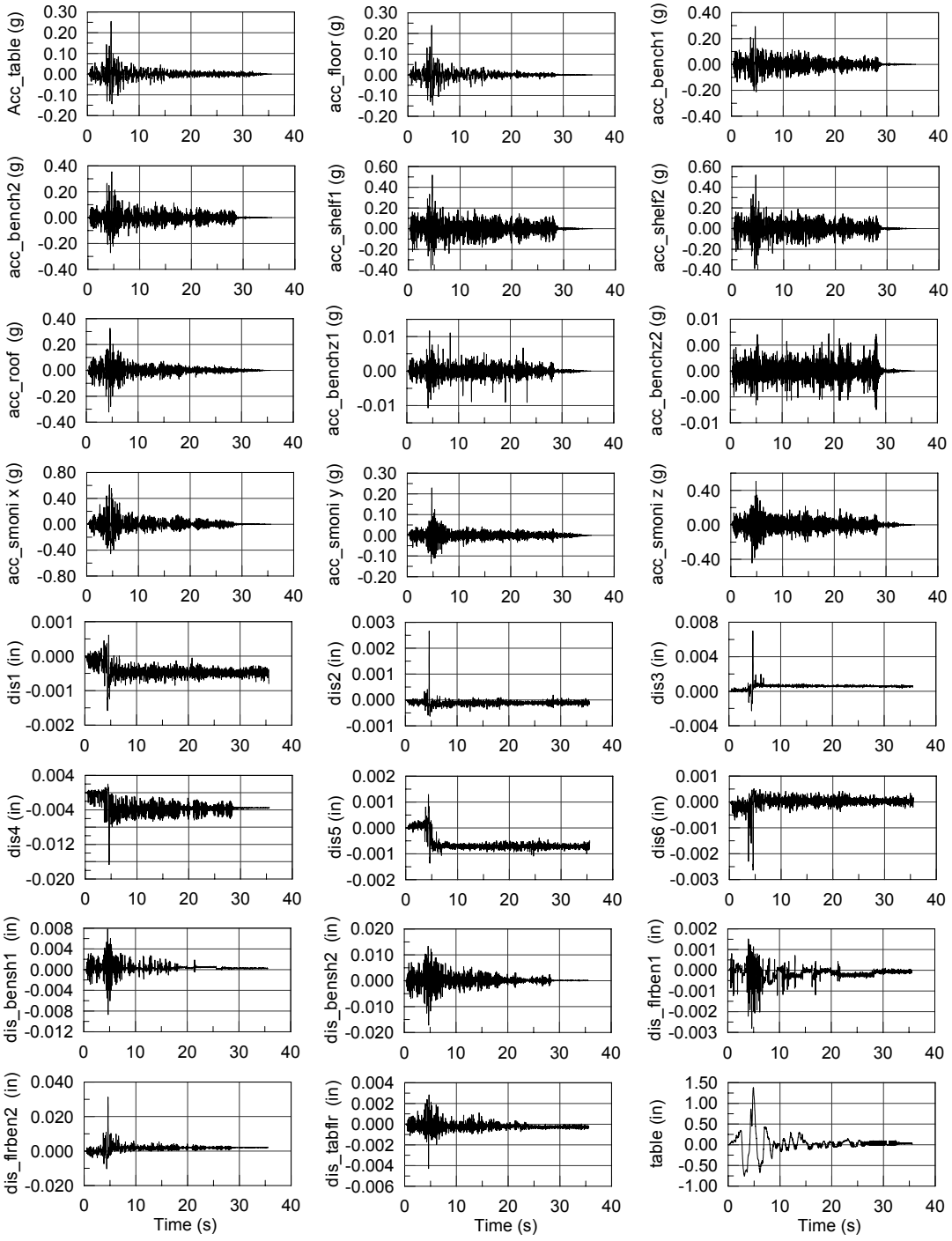

Figure B.36: Configuration 4: Acceleration (upper four rows) and displacement (lower four rows) time histories for 50% in 50 years Morgan Hill Anderson Dam Down (transverse) (GM - 3).

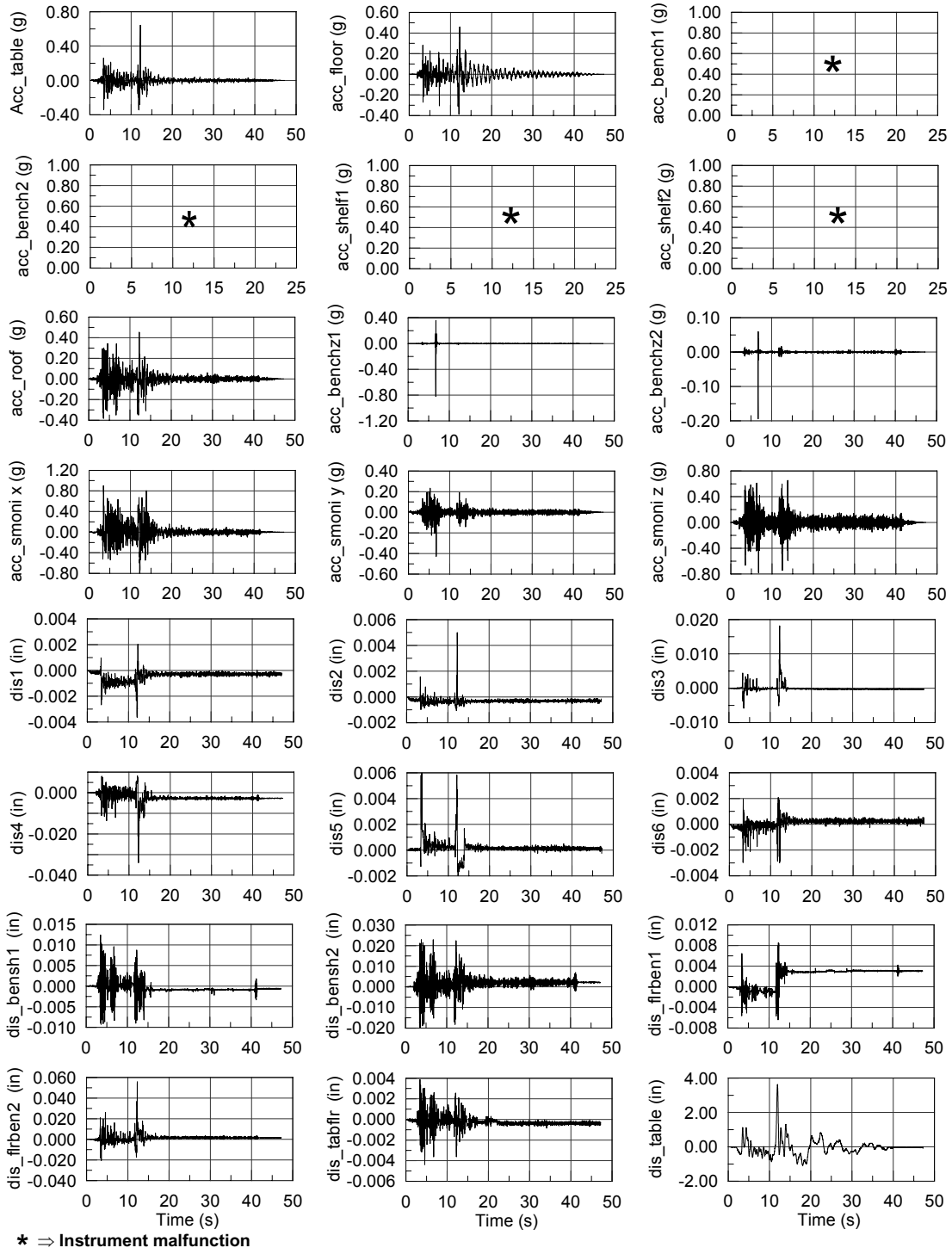

Figure B.37: Configuration 4: Acceleration (upper four rows) and displacement (lower four rows) time histories for 50% in 50 years Morgan Hill Halls Valley (transverse) (GM - 4).

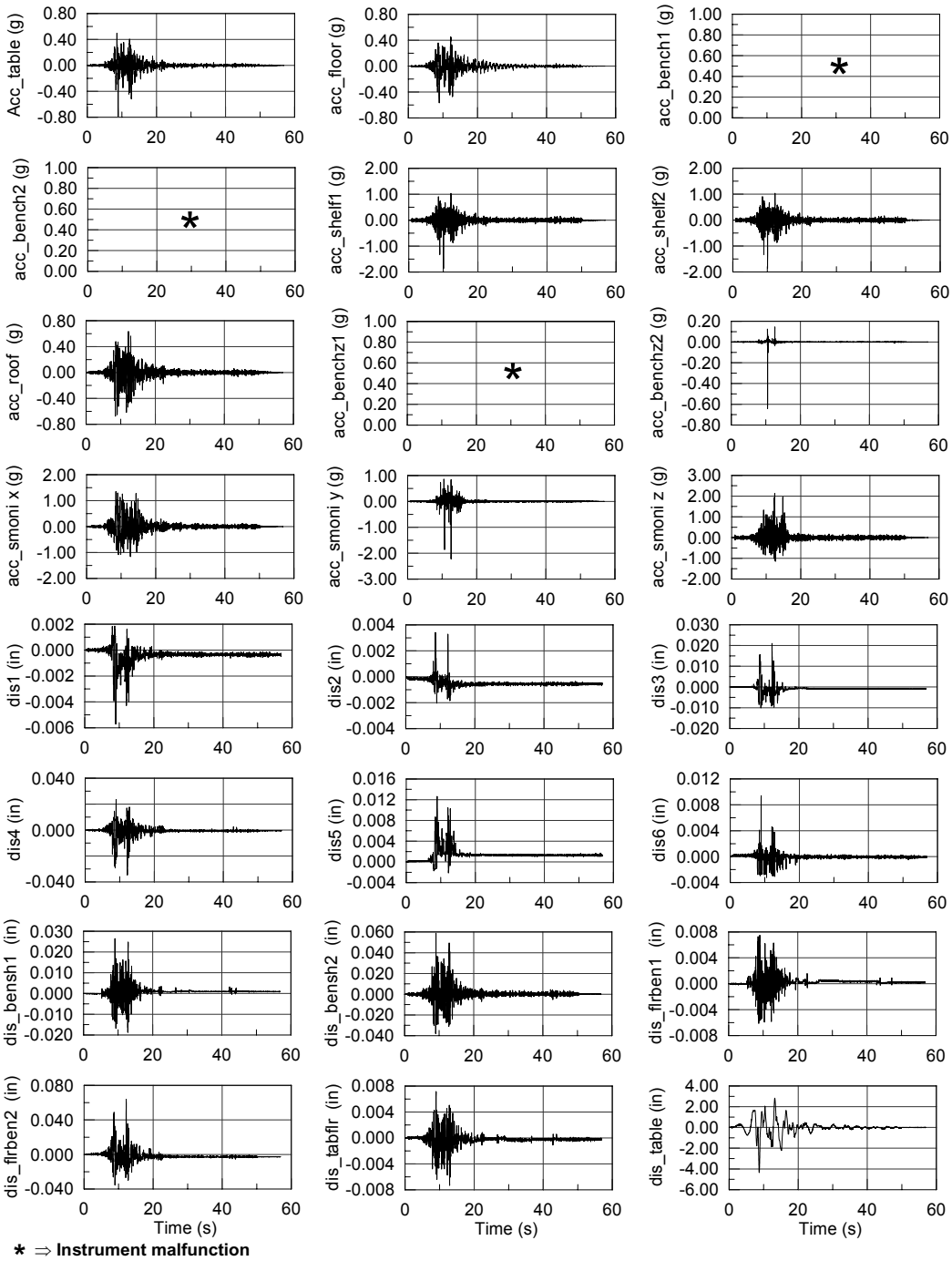

Figure B.38: Configuration 4: Acceleration (upper four rows) and displacement (lower four rows) time histories for 10% in 50 years Kobe, JMA, Japan (longitudinal) (GM - 5).

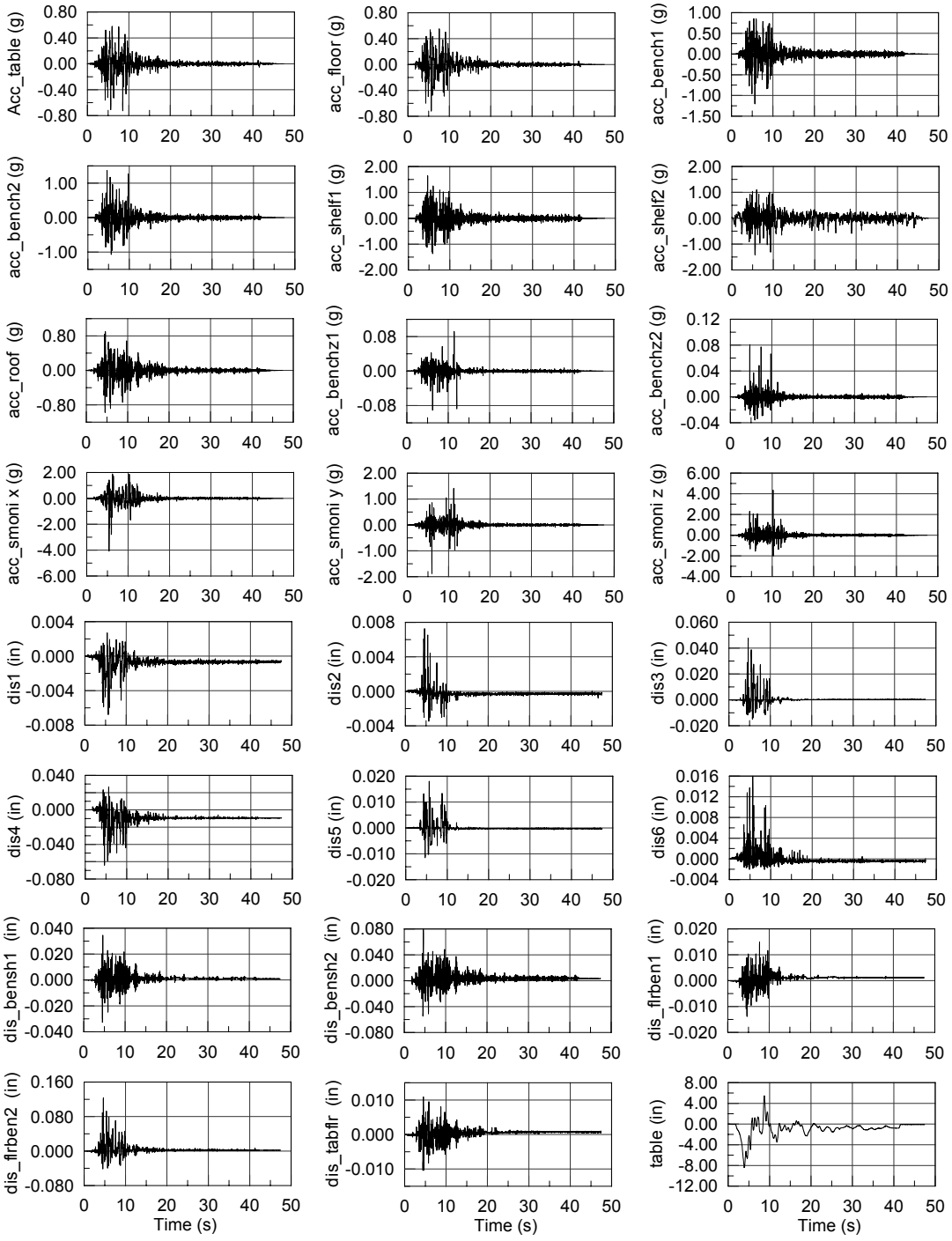

Figure B.39: Configuration 4: Acceleration (upper four rows) and displacement (lower four rows) time histories for 10% in 50 years Loma Prieta Corralitos (transverse) (GM - 6).

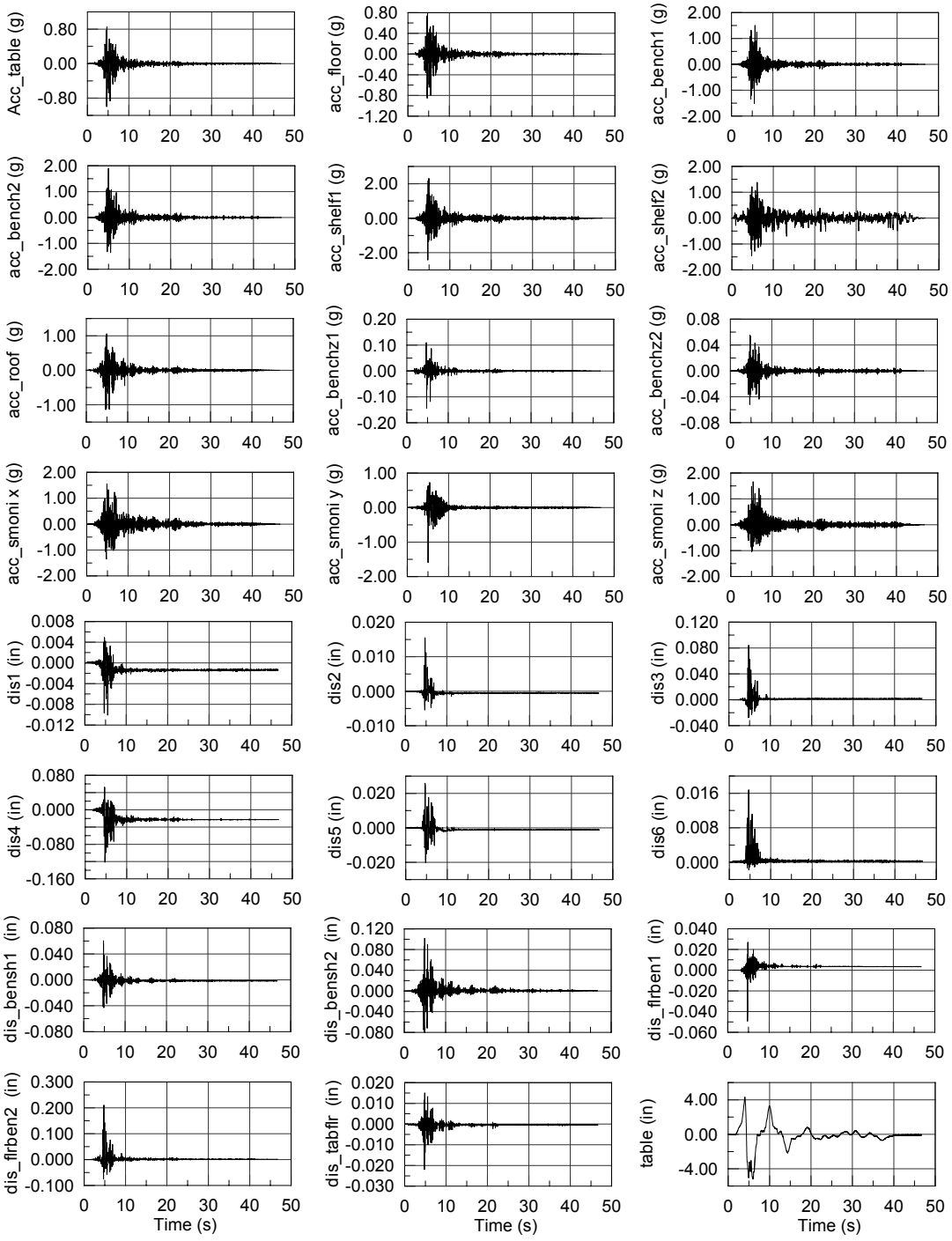

Figure B.40: Configuration 4: Acceleration (upper four rows) and displacement (lower four rows) time histories for 10% in 50 years Loma Prieta Gavilan College (transverse) (GM - 7).

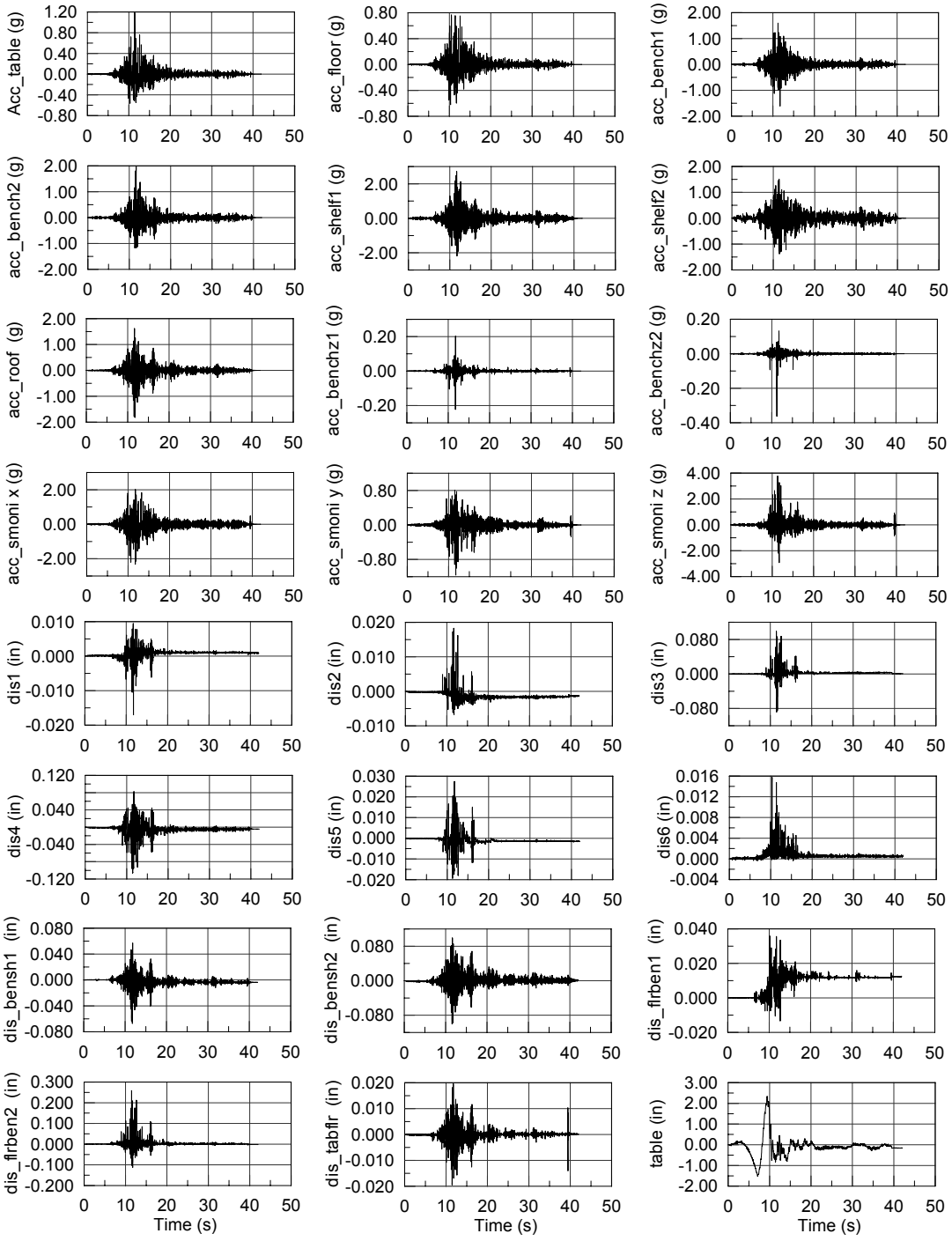

Figure B.41: Configuration 4: Acceleration (upper four rows) and displacement (lower four rows) time histories for 10% in 50 years Tottori, Kofu, Japan (transverse) (GM - 8).

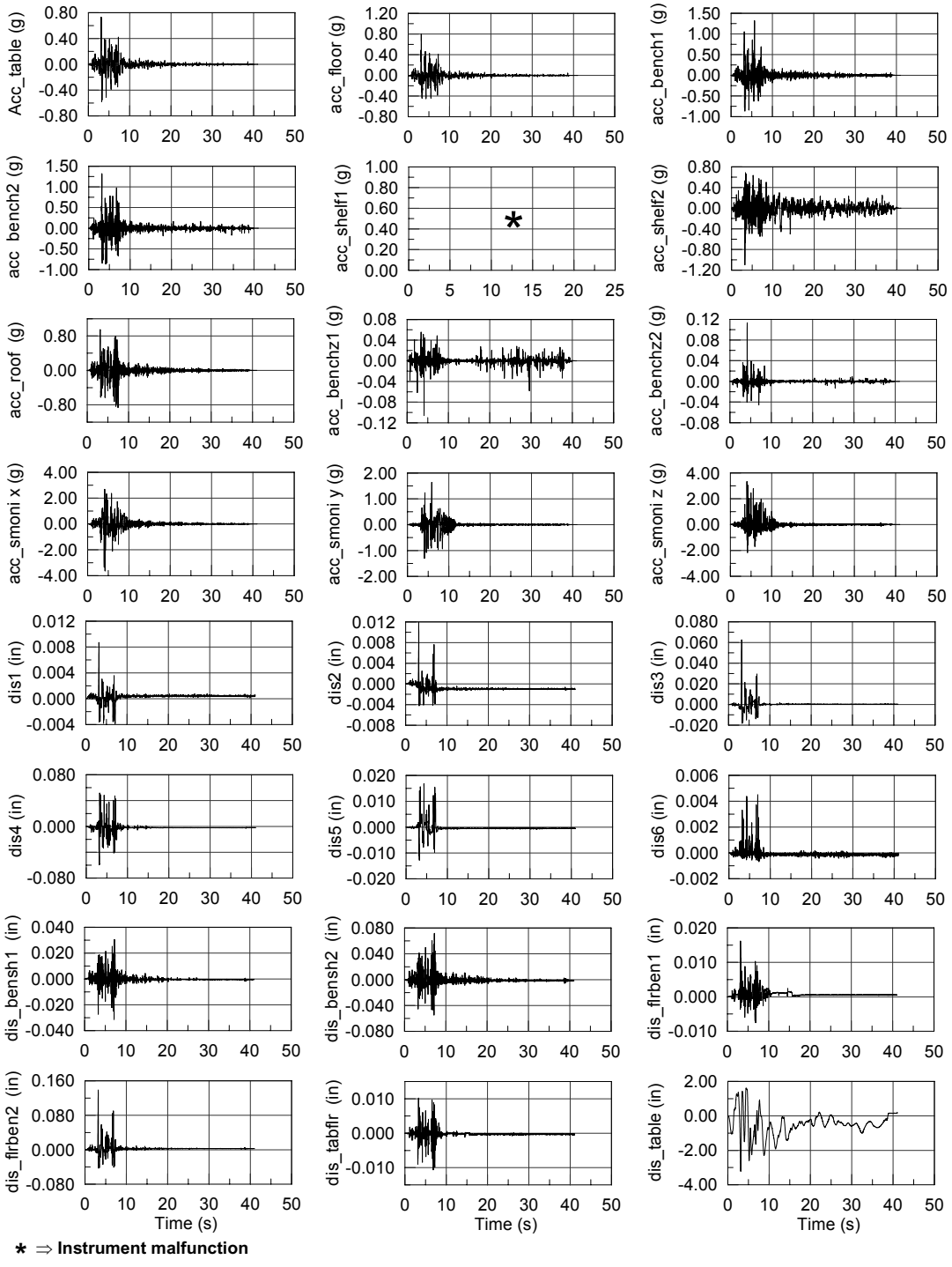

Figure B.42: Configuration 4: Acceleration (upper four rows) and displacement (lower four rows) time histories for 10% in 50 years Loma Prieta Lexington Dam (longitudinal) (GM - 9).

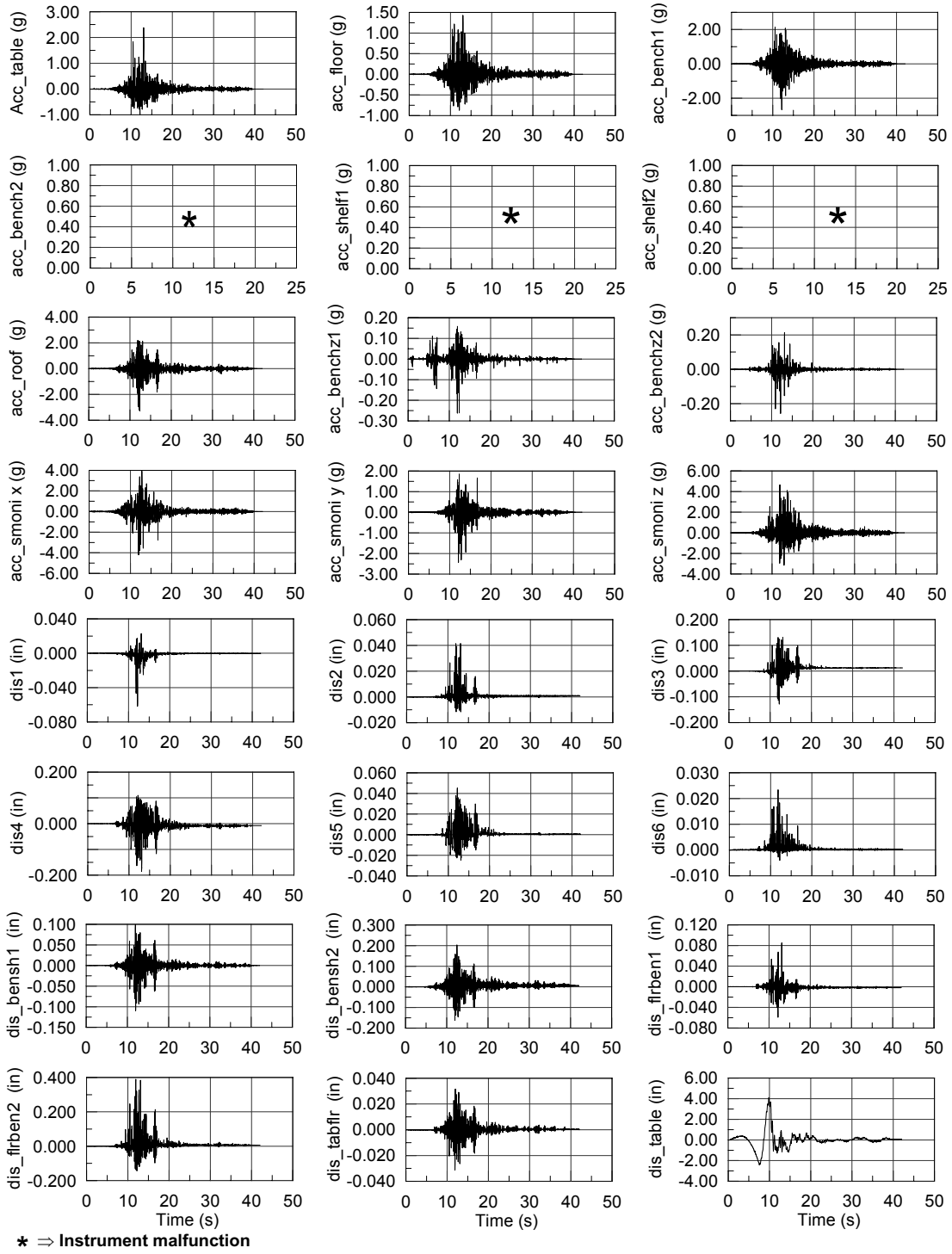

Figure B.43: Configuration 4: Acceleration (upper four rows) and displacement (lower four rows) time histories for 2% in 50 years Tottori, Kofu, Japan (transverse) (GM - 10).

Appendix C: Summary Equipment Response from Bare Shake Table Study

This appendix provides summary experimental results from bare shake table testing discussed in Chapter 5. Tables C.1 to C.10 show the maximum relative sliding distance of each piece of equipment for the different shake table trials, corresponding to different ground motions. Three different trials are conducted for any ground motion and any piece of equipment, if that equipment is observed to move under that ground motion shake table trial. Otherwise, a single trial is conducted for each ground motion. For each equipment, the average sliding response of the three trials and the percentage deviation of each trial with respect to the corresponding average are also given in these tables.

Table C.1: Maximum relative sliding displacement of scientific equipment– *Techtonic Autonalyzer* for different shake table trials in case of uniaxial and biaxial bare table tests.

Shake Table Trial #	Biaxial Excitation			Uniaxial Excitation		
	Relative Displacement (cm)	Average of 3 Trials (cm)	Deviation w.r.t Average (%)	Relative Displacement (cm)	Average of 3 Trials (cm)	Deviation w.r.t Average (%)
GM3-1	0.01	-	-	0.01	-	-
GM4-1	0.07	-	-	0.03	-	-
GM5-1	0.08	-	-	0.04	-	-
GM6-3	0.66	0.50	30.95	1.08	0.58	87.94
GM6-2	0.49	0.50	-2.04	0.41	0.58	-28.13
GM6-1	0.36	0.50	-28.91	0.23	0.58	-59.81
GM7-3	1.10	1.11	-0.38	1.68	1.72	-2.29
GM7-2	1.11	1.11	0.09	1.68	1.72	-1.97
GM7-1	1.11	1.11	0.29	1.79	1.72	4.26
GM8-3	0.96	1.01	-5.29	1.83	1.71	7.01
GM8-2	1.03	1.01	1.88	1.60	1.71	-6.21
GM8-1	1.05	1.01	3.40	1.70	1.71	-0.80
GM9-3	3.54	2.77	27.73	3.73	4.07	-8.21
GM9-2	2.70	2.77	-2.52	4.16	4.07	2.24
GM9-1	2.07	2.77	-25.21	4.31	4.07	5.97
GM10-3	11.19	10.16	10.16	12.35	11.58	6.69
GM10-2	9.96	10.16	-1.96	12.64	11.58	9.15
GM10-1	9.33	10.16	-8.20	9.74	11.58	-15.84

Table C.2: Maximum relative sliding displacement of scientific equipment– *Eppendoff centrifuge* for different shake table trials in case of uniaxial and biaxial bare table tests.

Shake Table Trial #	Biaxial Excitation			Uniaxial Excitation		
	Relative Displacement (cm)	Average of 3 Trials (cm)	Deviation w.r.t Average (%)	Relative Displacement (cm)	Average of 3 Trials (cm)	Deviation w.r.t Average (%)
GM3-1	0.01	-	-	0.02	-	-
GM4-1	0.09	-	-	0.07	-	-
GM5-1	0.08	-	-	0.08	-	-
GM6-1	0.11	-	-	0.10	-	-
GM7-1	0.22	-	-	0.33	-	-
GM8-3	0.32	0.29	7.99	0.43	0.38	12.30
GM8-2	0.29	0.29	0.35	0.45	0.38	19.91
GM8-1	0.27	0.29	-8.33	0.26	0.38	-32.22
GM9-3	0.18	0.20	-7.83	0.15	0.17	-11.62
GM9-2	0.21	0.20	4.30	0.17	0.17	3.14
GM9-1	0.21	0.20	3.53	0.18	0.17	8.47
GM10-3	12.41	9.55	29.97	13.46	11.92	12.90
GM10-2	9.26	9.55	-3.04	11.51	11.92	-3.40
GM10-1	6.98	9.55	-26.92	10.79	11.92	-9.50

Table C.3: Maximum relative sliding displacement of scientific equipment– *large microscope* for different shake table trials in case of uniaxial and biaxial bare table tests.

Shake Table Trial #	Biaxial Excitation			Uniaxial Excitation		
	Relative Displacement (cm)	Average of 3 Trials (cm)	Deviation w.r.t Average (%)	Relative Displacement (cm)	Average of 3 Trials (cm)	Deviation w.r.t Average (%)
GM3-1	0.16	-	-	0.17	-	-
GM4-1	0.37	-	-	0.36	-	-
GM5-3	7.81	7.18	8.83	7.10	5.46	29.97
GM5-2	8.47	7.18	18.01	5.28	5.46	-3.37
GM5-1	5.25	7.18	-26.84	4.01	5.46	-26.60
GM6-3	13.94	12.41	12.28	12.82	11.47	11.80
GM6-2	10.57	12.41	-14.81	9.06	11.47	-20.98
GM6-1	12.73	12.41	2.54	12.52	11.47	9.19
GM7-3	7.63	7.21	5.88	8.12	7.51	8.01
GM7-2	6.52	7.21	-9.55	7.92	7.51	5.37
GM7-1	7.47	7.21	3.67	6.51	7.51	-13.37
GM8-3	12.42	11.84	4.90	12.49	11.47	8.88
GM8-2	10.55	11.84	-10.92	10.05	11.47	-12.39
GM8-1	12.56	11.84	6.02	11.87	11.47	3.52
GM9-3	11.19	11.10	0.85	13.17	12.11	8.72
GM9-2	9.77	11.10	-11.99	12.73	12.11	5.08
GM9-1	12.33	11.10	11.15	10.44	12.11	-13.80
GM10-3	34.39	34.68	-0.84	30.64	31.94	-4.07
GM10-2	35.29	34.68	1.76	31.79	31.94	-0.47
GM10-1	34.36	34.68	-0.92	33.39	31.94	4.54

Table C.4: Maximum relative sliding displacement of scientific equipment– *small microscope* for different shake table trials in case of uniaxial and biaxial bare table tests.

Shake Table Trial #	Biaxial Excitation			Uniaxial Excitation		
	Relative Displacement (cm)	Average of 3 Trials (cm)	Deviation w.r.t Average (%)	Relative Displacement (cm)	Average of 3 Trials (cm)	Deviation w.r.t Average (%)
GM3-1	0.00	-	-	0.01	-	-
GM4-1	0.07	-	-	0.04	-	-
GM5-3	0.08	0.13	-41.41	0.14	0.20	-28.98
GM5-2	0.11	0.13	-15.75	0.19	0.20	-2.60
GM5-1	0.21	0.13	57.15	0.26	0.20	31.58
GM6-3	1.21	0.86	40.71	1.22	0.98	24.15
GM6-2	0.79	0.86	-7.98	0.84	0.98	-14.32
GM6-1	0.58	0.86	-32.72	0.89	0.98	-9.83
GM7-3	1.43	1.34	6.33	1.27	1.40	-9.32
GM7-2	1.33	1.34	-1.11	1.29	1.40	-7.75
GM7-1	1.27	1.34	-5.22	1.64	1.40	17.07
GM8-3	0.88	0.90	-2.30	0.87	0.87	-0.35
GM8-2	0.95	0.90	4.74	0.77	0.87	-10.81
GM8-1	0.88	0.90	-2.44	0.97	0.87	11.16
GM9-3	3.06	2.86	6.95	2.63	2.43	8.25
GM9-2	2.80	2.86	-2.01	2.30	2.43	-5.38
GM9-1	2.72	2.86	-4.94	2.36	2.43	-2.87
GM10-3	8.85	9.07	-2.46	10.28	9.34	10.04
GM10-2	9.34	9.07	2.94	8.14	9.34	-12.83
GM10-1	9.03	9.07	-0.48	9.60	9.34	2.79

Table C.5: Maximum relative sliding displacement of SGI CPU– *Indigo* for different shake table trials in case of uniaxial and biaxial bare table tests.

Shake Table Trial #	Biaxial Excitation			Uniaxial Excitation		
	Relative Displacement (cm)	Average of 3 Trials (cm)	Deviation w.r.t Average (%)	Relative Displacement (cm)	Average of 3 Trials (cm)	Deviation w.r.t Average (%)
GM3-1	0.02	-	-	0.05	-	-
GM4-1	0.20	-	-	0.24	-	-
GM5-3	2.16	1.85	16.61	2.94	3.06	-3.83
GM5-2	1.58	1.85	-14.88	3.59	3.06	17.20
GM5-1	1.82	1.85	-1.74	2.65	3.06	-13.37
GM6-3	4.35	3.94	10.66	5.28	5.08	3.86
GM6-2	3.62	3.94	-7.97	4.60	5.08	-9.45
GM6-1	3.83	3.94	-2.69	5.37	5.08	5.59
GM7-3	2.86	2.85	0.38	4.16	4.46	-6.52
GM7-2	3.06	2.85	7.35	4.58	4.46	2.88
GM7-1	2.63	2.85	-7.72	4.62	4.46	3.64
GM8-3	4.89	4.38	11.80	5.45	5.67	-3.80
GM8-2	4.23	4.38	-3.37	5.84	5.67	3.06
GM8-1	4.01	4.38	-8.43	5.71	5.67	0.75
GM9-3	5.05	4.90	3.08	7.34	7.21	1.69
GM9-2	5.06	4.90	3.18	7.12	7.21	-1.26
GM9-1	4.60	4.90	-6.26	7.18	7.21	-0.43
GM10-3	26.96	26.13	3.19	26.19	26.34	-0.55
GM10-2	25.81	26.13	-1.19	26.76	26.34	1.62
GM10-1	25.60	26.13	-1.99	26.06	26.34	-1.07

Table C.6: Maximum relative sliding displacement of SGI CPU– *Indy* for different shake table trials in case of uniaxial and biaxial bare table tests.

Shake Table Trial #	Biaxial Excitation			Uniaxial Excitation		
	Relative Displacement (cm)	Average of 3 Trials (cm)	Deviation w.r.t Average (%)	Relative Displacement (cm)	Average of 3 Trials (cm)	Deviation w.r.t Average (%)
GM3-1	0.00	-	-	0.08	-	-
GM4-1	0.09	-	-	0.04	-	-
GM5-3	0.78	0.82	-4.99	0.09	0.08	6.15
GM5-2	0.98	0.82	20.09	0.08	0.08	-6.16
GM5-1	0.69	0.82	-15.10	0.08	0.08	0.00
GM6-3	3.06	3.02	1.57	3.69	4.51	-18.09
GM6-2	2.93	3.02	-2.95	4.40	4.51	-2.33
GM6-1	3.06	3.02	1.38	5.43	4.51	20.42
GM7-3	2.32	2.44	-4.88	3.10	3.30	-6.06
GM7-2	2.59	2.44	5.93	3.31	3.30	0.09
GM7-1	2.42	2.44	-1.05	3.50	3.30	5.97
GM8-3	2.12	1.97	7.57	1.56	1.40	11.43
GM8-2	1.72	1.97	-12.60	1.43	1.40	2.06
GM8-1	2.07	1.97	5.03	1.21	1.40	-13.49
GM9-3	3.76	3.86	-2.54	4.72	5.64	-16.32
GM9-2	4.13	3.86	6.94	5.82	5.64	3.24
GM9-1	3.69	3.86	-4.40	6.38	5.64	13.08
GM10-3	15.69	15.07	4.15	12.84	12.87	-0.19
GM10-2	15.33	15.07	1.76	12.78	12.87	-0.68
GM10-1	14.18	15.07	-5.90	12.98	12.87	0.87

Table C.7: Maximum relative sliding displacement of SGI CPU– *Octane* for different shake table trials in case of uniaxial and biaxial bare table tests.

Shake Table Trial #	Biaxial Excitation			Uniaxial Excitation		
	Relative Displacement (cm)	Average of 3 Trials (cm)	Deviation w.r.t Average (%)	Relative Displacement (cm)	Average of 3 Trials (cm)	Deviation w.r.t Average (%)
GM3-1	0.01	-	-	0.01	-	-
GM4-1	0.11	-	-	0.08	-	-
GM5-3	0.43	0.36	20.68	0.08	0.07	11.49
GM5-2	0.33	0.36	-8.30	0.07	0.07	-6.39
GM5-1	0.31	0.36	-12.38	0.07	0.07	-5.10
GM6-3	1.35	1.56	-14.01	0.14	0.14	0.52
GM6-2	1.66	1.56	6.00	0.13	0.14	-4.68
GM6-1	1.69	1.56	8.01	0.14	0.14	4.17
GM7-3	1.08	1.18	-9.12	1.69	1.22	38.77
GM7-2	1.14	1.18	-3.79	1.08	1.22	-11.50
GM7-1	1.34	1.18	12.91	0.89	1.22	-27.27
GM8-3	1.13	1.02	10.88	2.05	1.89	8.40
GM8-2	1.02	1.02	0.12	1.94	1.89	2.89
GM8-1	0.90	1.02	-11.00	1.67	1.89	-11.29
GM9-3	3.94	3.36	17.30	4.76	4.52	5.35
GM9-2	3.49	3.36	3.71	4.57	4.52	1.30
GM9-1	2.66	3.36	-21.00	4.21	4.52	-6.65
GM10-3	10.78	11.67	-7.58	12.75	13.45	-5.19
GM10-2	13.19	11.67	13.05	14.36	13.45	6.77
GM10-1	11.03	11.67	-5.48	13.23	13.45	-1.59

Table C.8: Maximum relative sliding displacement of computer monitors– *19″ monitor* for different shake table trials in case of uniaxial and biaxial bare table tests.

Shake Table Trial #	Biaxial Excitation			Uniaxial Excitation		
	Relative Displacement (cm)	Average of 3 Trials (cm)	Deviation w.r.t Average (%)	Relative Displacement (cm)	Average of 3 Trials (cm)	Deviation w.r.t Average (%)
GM3-1	0.02	-	-	0.02	-	-
GM4-1	0.06	-	-	0.09	-	-
GM5-1	0.54	-	-	0.61	-	-
GM6-3	3.75	3.71	1.20	3.00	3.77	-20.44
GM6-2	3.63	3.71	-2.10	3.97	3.77	5.06
GM6-1	3.74	3.71	0.90	4.36	3.77	15.38
GM7-3	4.50	4.42	1.96	2.35	2.37	-1.00
GM7-2	4.44	4.42	0.51	2.27	2.37	-4.25
GM7-1	4.31	4.42	-2.47	2.49	2.37	5.25
GM8-3	0.64	0.61	4.66	0.61	0.69	-11.06
GM8-2	0.62	0.61	1.50	0.74	0.69	6.40
GM8-1	0.57	0.61	-6.17	0.72	0.69	4.67
GM9-3	2.16	6.59	-67.18	2.87	2.95	-2.57
GM9-2	1.81	6.59	-72.54	2.96	2.95	0.33
GM9-1	15.80	6.59	139.72	3.02	2.95	2.24
GM10-3	11.61	12.34	-5.91	13.67	12.78	6.96
GM10-2	13.33	12.34	7.98	12.68	12.78	-0.76
GM10-1	12.09	12.34	-2.07	11.99	12.78	-6.20

Table C.9: Maximum relative sliding displacement of computer monitors– *17″ monitor* for different shake table trials in case of uniaxial and biaxial bare table tests.

Shake Table Trial #	Biaxial Excitation			Uniaxial Excitation		
	Relative Displacement (cm)	Average of 3 Trials (cm)	Deviation w.r.t Average (%)	Relative Displacement (cm)	Average of 3 Trials (cm)	Deviation w.r.t Average (%)
GM3-1	0.16	-	-	0.11	-	-
GM4-1	0.41	-	-	1.04	-	-
GM5-3	1.85	2.03	-8.97	5.64	6.33	-10.85
GM5-2	1.83	2.03	-9.49	4.02	6.33	-36.42
GM5-1	2.40	2.03	18.46	9.32	6.33	47.27
GM6-3	5.86	6.24	-5.97	8.64	6.73	28.38
GM6-2	7.20	6.24	15.52	4.25	6.73	-36.90
GM6-1	5.64	6.24	-9.55	7.31	6.73	8.52
GM7-3	9.04	7.08	27.73	8.15	6.71	21.48
GM7-2	7.22	7.08	2.05	4.98	6.71	-25.75
GM7-1	4.97	7.08	-29.78	6.99	6.71	4.27
GM8-3	9.68	7.87	22.99	6.52	7.93	-17.77
GM8-2	6.74	7.87	-14.36	8.56	7.93	8.02
GM8-1	7.19	7.87	-8.64	8.70	7.93	9.75
GM9-3	12.21	12.96	-5.81	14.61	14.43	1.26
GM9-2	14.80	12.96	14.17	14.16	14.43	-1.85
GM9-1	11.88	12.96	-8.37	14.51	14.43	0.59
GM10-3	12.49	15.14	-17.51	22.70	20.15	12.63
GM10-2	13.28	15.14	-12.23	20.34	20.15	0.92
GM10-1	19.64	15.14	29.75	17.42	20.15	-13.55

Table C.10: Maximum relative sliding displacement of computer monitors– *15″ monitor* for different shake table trials in case of uniaxial and biaxial bare table tests.

Shake Table Trial #	Biaxial Excitation			Uniaxial Excitation		
	Relative Displacement (cm)	Average of 3 Trials (cm)	Deviation w.r.t Average (%)	Relative Displacement (cm)	Average of 3 Trials (cm)	Deviation w.r.t Average (%)
GM3-1	0.02	-	-	0.03	-	-
GM4-1	1.32	-	-	0.35	-	-
GM5-3	6.26	8.79	-28.75	9.17	7.17	27.88
GM5-2	12.52	8.79	42.40	5.55	7.17	-22.61
GM5-1	7.59	8.79	-13.65	6.80	7.17	-5.27
GM6-3	11.84	10.85	9.14	10.13	12.63	-19.81
GM6-2	13.62	10.85	25.56	9.92	12.63	-21.45
GM6-1	7.08	10.85	-34.70	17.85	12.63	41.25
GM7-3	6.83	6.76	0.91	3.91	4.04	-3.35
GM7-2	6.25	6.76	-7.55	4.25	4.04	5.03
GM7-1	7.21	6.76	6.64	3.98	4.04	-1.68
GM8-3	8.04	5.83	37.88	5.33	5.44	-2.14
GM8-2	4.15	5.83	-28.76	3.52	5.44	-35.22
GM8-1	5.30	5.83	-9.11	7.47	5.44	37.36
GM9-3	12.28	14.50	-15.30	17.10	15.87	7.72
GM9-2	19.98	14.50	37.78	11.75	15.87	-25.96
GM9-1	11.24	14.50	-22.47	18.77	15.87	18.25
GM10-3	9.42	10.10	-6.67	12.90	12.00	7.45
GM10-2	12.76	10.10	26.39	13.86	12.00	15.44
GM10-1	8.11	10.10	-19.72	9.25	12.00	-22.89

PEER REPORTS

PEER reports are available from the National Information Service for Earthquake Engineering (NISEE). To order PEER reports, please contact the Pacific Earthquake Engineering Research Center, 1301 South 46th Street, Richmond, California 94804-4698. Tel.: (510) 231-9468; Fax: (510) 231-9 461.

PEER 2006/01 *Bracing Berkeley: A Guide to Seismic Safety on the UC Berkeley Campus.* Mary C. Comerio, Stephen Tobriner, and Ariane Fehrenkamp. January 2006.

PEER 2005/12 *PEER Testbed Study on a Laboratory Building: Exercising Seismic Performance Assessment.* Mary C. Comerio, editor. November 2005.

PEER 2005/11 *Van Nuys Hotel Building Testbed Report: Exercising Seismic Performance Assessment.* Helmut Krawinkler, editor. October 2005.

PEER 2005/10 *First NEES/E-Defense Workshop on Collapse Simulation of Reinforced Concrete Building Structures.* September 2005.

PEER 2005/08 *Damage Accumulation in Lightly Confined Reinforced Concrete Bridge Columns.* R. Tyler Ranf, Jared M. Nelson, Zach Price, Marc O. Eberhard, and John F. Stanton. April 2006.

PEER 2005/07 *Experimental and Analytical Studies on the Seismic Response of Freestanding and Anchored Laboratory Equipment.* Dimitrios Konstantinidis and Nicos Makris. January 2005.

PEER 2005/06 *Global Collapse of Frame Structures under Seismic Excitations.* Luis F. Ibarra and Helmut Krawinkler. September 2005.

PEER 2005/05 *Performance Characterization of Bench- and Shelf-Mounted Equipment.* Samit Ray Chaudhuri and Tara C. Hutchinson. May 2006.

PEER 2005/04 *Numerical Modeling of the Nonlinear Cyclic Response of Shallow Foundations.* Chad Harden, Tara Hutchinson, Geoffrey R. Martin, and Bruce L. Kutter. August 2005.

PEER 2005/03 *A Taxonomy of Building Components for Performance-Based Earthquake Engineering.* Keith A. Porter. September 2005.

PEER 2005/02 *Fragility Basis for California Highway Overpass Bridge Seismic Decision Making.* Kevin R. Mackie and Bozidar Stojadinovic. June 2005.

PEER 2005/01 *Empirical Characterization of Site Conditions on Strong Ground Motion.* Jonathan P. Stewart, Yoojoong Choi, and Robert W. Graves. June 2005.

PEER 2004/09 *Electrical Substation Equipment Interaction: Experimental Rigid Conductor Studies.* Christopher Stearns and André Filiatrault. February 2005.

PEER 2004/08 *Seismic Qualification and Fragility Testing of Line Break 550-kV Disconnect Switches.* Shakhzod M. Takhirov, Gregory L. Fenves, and Eric Fujisaki. January 2005.

PEER 2004/07 *Ground Motions for Earthquake Simulator Qualification of Electrical Substation Equipment.* Shakhzod M. Takhirov, Gregory L. Fenves, Eric Fujisaki, and Don Clyde. January 2005.

PEER 2004/06 *Performance-Based Regulation and Regulatory Regimes.* Peter J. May and Chris Koski. September 2004.

PEER 2004/05 *Performance-Based Seismic Design Concepts and Implementation: Proceedings of an International Workshop.* Peter Fajfar and Helmut Krawinkler, editors. September 2004.

PEER 2004/04 *Seismic Performance of an Instrumented Tilt-up Wall Building.* James C. Anderson and Vitelmo V. Bertero. July 2004.

PEER 2004/03 *Evaluation and Application of Concrete Tilt-up Assessment Methodologies.* Timothy Graf and James O. Malley. October 2004.

PEER 2004/02 *Analytical Investigations of New Methods for Reducing Residual Displacements of Reinforced Concrete Bridge Columns.* Junichi Sakai and Stephen A. Mahin. August 2004.

PEER 2004/01 *Seismic Performance of Masonry Buildings and Design Implications.* Kerri Anne Taeko Tokoro, James C. Anderson, and Vitelmo V. Bertero. February 2004.

PEER 2003/18 *Performance Models for Flexural Damage in Reinforced Concrete Columns.* Michael Berry and Marc Eberhard. August 2003.

PEER 2003/17 *Predicting Earthquake Damage in Older Reinforced Concrete Beam-Column Joints.* Catherine Pagni and Laura Lowes. October 2004.

PEER 2003/16 *Seismic Demands for Performance-Based Design of Bridges.* Kevin Mackie and Božidar Stojadinovic. August 2003.

PEER 2003/15 *Seismic Demands for Nondeteriorating Frame Structures and Their Dependence on Ground Motions.* Ricardo Antonio Medina and Helmut Krawinkler. May 2004.

PEER 2003/14 *Finite Element Reliability and Sensitivity Methods for Performance-Based Earthquake Engineering.* Terje Haukaas and Armen Der Kiureghian. April 2004.

PEER 2003/13 *Effects of Connection Hysteretic Degradation on the Seismic Behavior of Steel Moment-Resisting Frames.* Janise E. Rodgers and Stephen A. Mahin. March 2004.

PEER 2003/12 *Implementation Manual for the Seismic Protection of Laboratory Contents: Format and Case Studies.* William T. Holmes and Mary C. Comerio. October 2003.

PEER 2003/11 *Fifth U.S.-Japan Workshop on Performance-Based Earthquake Engineering Methodology for Reinforced Concrete Building Structures.* February 2004.

PEER 2003/10 *A Beam-Column Joint Model for Simulating the Earthquake Response of Reinforced Concrete Frames.* Laura N. Lowes, Nilanjan Mitra, and Arash Altoontash. February 2004.

PEER 2003/09 *Sequencing Repairs after an Earthquake: An Economic Approach.* Marco Casari and Simon J. Wilkie. April 2004.

PEER 2003/08 *A Technical Framework for Probability-Based Demand and Capacity Factor Design (DCFD) Seismic Formats.* Fatemeh Jalayer and C. Allin Cornell. November 2003.

PEER 2003/07 *Uncertainty Specification and Propagation for Loss Estimation Using FOSM Methods.* Jack W. Baker and C. Allin Cornell. September 2003.

PEER 2003/06 *Performance of Circular Reinforced Concrete Bridge Columns under Bidirectional Earthquake Loading.* Mahmoud M. Hachem, Stephen A. Mahin, and Jack P. Moehle. February 2003.

PEER 2003/05 *Response Assessment for Building-Specific Loss Estimation.* Eduardo Miranda and Shahram Taghavi. September 2003.

PEER 2003/04 *Experimental Assessment of Columns with Short Lap Splices Subjected to Cyclic Loads.* Murat Melek, John W. Wallace, and Joel Conte. April 2003.

PEER 2003/03 *Probabilistic Response Assessment for Building-Specific Loss Estimation.* Eduardo Miranda and Hesameddin Aslani. September 2003.

PEER 2003/02 *Software Framework for Collaborative Development of Nonlinear Dynamic Analysis Program.* Jun Peng and Kincho H. Law. September 2003.

PEER 2003/01 *Shake Table Tests and Analytical Studies on the Gravity Load Collapse of Reinforced Concrete Frames.* Kenneth John Elwood and Jack P. Moehle. November 2003.

PEER 2002/24 *Performance of Beam to Column Bridge Joints Subjected to a Large Velocity Pulse.* Natalie Gibson, André Filiatrault, and Scott A. Ashford. April 2002.

PEER 2002/23 *Effects of Large Velocity Pulses on Reinforced Concrete Bridge Columns.* Greg L. Orozco and Scott A. Ashford. April 2002.

PEER 2002/22 *Characterization of Large Velocity Pulses for Laboratory Testing.* Kenneth E. Cox and Scott A. Ashford. April 2002.

PEER 2002/21 *Fourth U.S.-Japan Workshop on Performance-Based Earthquake Engineering Methodology for Reinforced Concrete Building Structures.* December 2002.

PEER 2002/20 *Barriers to Adoption and Implementation of PBEE Innovations.* Peter J. May. August 2002.

PEER 2002/19 *Economic-Engineered Integrated Models for Earthquakes: Socioeconomic Impacts.* Peter Gordon, James E. Moore II, and Harry W. Richardson. July 2002.

PEER 2002/18 *Assessment of Reinforced Concrete Building Exterior Joints with Substandard Details.* Chris P. Pantelides, Jon Hansen, Justin Nadauld, and Lawrence D. Reaveley. May 2002.

PEER 2002/17 *Structural Characterization and Seismic Response Analysis of a Highway Overcrossing Equipped with Elastomeric Bearings and Fluid Dampers: A Case Study.* Nicos Makris and Jian Zhang. November 2002.

PEER 2002/16 *Estimation of Uncertainty in Geotechnical Properties for Performance-Based Earthquake Engineering.* Allen L. Jones, Steven L. Kramer, and Pedro Arduino. December 2002.

PEER 2002/15 *Seismic Behavior of Bridge Columns Subjected to Various Loading Patterns.* Asadollah Esmaeily-Gh. and Yan Xiao. December 2002.

PEER 2002/14 *Inelastic Seismic Response of Extended Pile Shaft Supported Bridge Structures.* T.C. Hutchinson, R.W. Boulanger, Y.H. Chai, and I.M. Idriss. December 2002.

PEER 2002/13 *Probabilistic Models and Fragility Estimates for Bridge Components and Systems.* Paolo Gardoni, Armen Der Kiureghian, and Khalid M. Mosalam. June 2002.

PEER 2002/12 *Effects of Fault Dip and Slip Rake on Near-Source Ground Motions: Why Chi-Chi Was a Relatively Mild M7.6 Earthquake.* Brad T. Aagaard, John F. Hall, and Thomas H. Heaton. December 2002.

PEER 2002/11 *Analytical and Experimental Study of Fiber-Reinforced Strip Isolators*. James M. Kelly and Shakhzod M. Takhirov. September 2002.

PEER 2002/10 *Centrifuge Modeling of Settlement and Lateral Spreading with Comparisons to Numerical Analyses***.** Sivapalan Gajan and Bruce L. Kutter. January 2003.

PEER 2002/09 *Documentation and Analysis of Field Case Histories of Seismic Compression during the 1994 Northridge, California, Earthquake.* Jonathan P. Stewart, Patrick M. Smith, Daniel H. Whang, and Jonathan D. Bray. October 2002.

PEER 2002/08 *Component Testing, Stability Analysis and Characterization of Buckling-Restrained Unbonded Braces™*. Cameron Black, Nicos Makris, and Ian Aiken. September 2002.

PEER 2002/07 *Seismic Performance of Pile-Wharf Connections.* Charles W. Roeder, Robert Graff, Jennifer Soderstrom, and Jun Han Yoo. December 2001.

PEER 2002/06 *The Use of Benefit-Cost Analysis for Evaluation of Performance-Based Earthquake Engineering Decisions.* Richard O. Zerbe and Anthony Falit-Baiamonte. September 2001.

PEER 2002/05 *Guidelines, Specifications, and Seismic Performance Characterization of Nonstructural Building Components and Equipment*. André Filiatrault, Constantin Christopoulos, and Christopher Stearns. September 2001.

PEER 2002/04 *Consortium of Organizations for Strong-Motion Observation Systems and the Pacific Earthquake Engineering Research Center Lifelines Program: Invited Workshop on Archiving and Web Dissemination of Geotechnical Data, 4–5 October 2001*. September 2002.

PEER 2002/03 *Investigation of Sensitivity of Building Loss Estimates to Major Uncertain Variables for the Van Nuys Testbed.* Keith A. Porter, James L. Beck, and Rustem V. Shaikhutdinov. August 2002.

PEER 2002/02 *The Third U.S.-Japan Workshop on Performance-Based Earthquake Engineering Methodology for Reinforced Concrete Building Structures*. July 2002.

PEER 2002/01 *Nonstructural Loss Estimation: The UC Berkeley Case Study.* Mary C. Comerio and John C. Stallmeyer. December 2001.

PEER 2001/16 *Statistics of SDF-System Estimate of Roof Displacement for Pushover Analysis of Buildings.* Anil K. Chopra, Rakesh K. Goel, and Chatpan Chintanapakdee. December 2001.

PEER 2001/15 *Damage to Bridges during the 2001 Nisqually Earthquake.* R. Tyler Ranf, Marc O. Eberhard, and Michael P. Berry. November 2001.

PEER 2001/14 *Rocking Response of Equipment Anchored to a Base Foundation.* Nicos Makris and Cameron J. Black. September 2001.

PEER 2001/13 *Modeling Soil Liquefaction Hazards for Performance-Based Earthquake Engineering.* Steven L. Kramer and Ahmed-W. Elgamal. February 2001.

PEER 2001/12 *Development of Geotechnical Capabilities in OpenSees.* Boris Jeremi . September 2001.

PEER 2001/11 *Analytical and Experimental Study of Fiber-Reinforced Elastomeric Isolators*. James M. Kelly and Shakhzod M. Takhirov. September 2001.

PEER 2001/10 *Amplification Factors for Spectral Acceleration in Active Regions.* Jonathan P. Stewart, Andrew H. Liu, Yoojoong Choi, and Mehmet B. Baturay. December 2001.

PEER 2001/09 *Ground Motion Evaluation Procedures for Performance-Based Design.* Jonathan P. Stewart, Shyh-Jeng Chiou, Jonathan D. Bray, Robert W. Graves, Paul G. Somerville, and Norman A. Abrahamson. September 2001.

PEER 2001/08 *Experimental and Computational Evaluation of Reinforced Concrete Bridge Beam-Column Connections for Seismic Performance*. Clay J. Naito, Jack P. Moehle, and Khalid M. Mosalam. November 2001.

PEER 2001/07 *The Rocking Spectrum and the Shortcomings of Design Guidelines.* Nicos Makris and Dimitrios Konstantinidis. August 2001.

PEER 2001/06 *Development of an Electrical Substation Equipment Performance Database for Evaluation of Equipment Fragilities*. Thalia Agnanos. April 1999.

PEER 2001/05 *Stiffness Analysis of Fiber-Reinforced Elastomeric Isolators.* Hsiang-Chuan Tsai and James M. Kelly. May 2001.

PEER 2001/04 *Organizational and Societal Considerations for Performance-Based Earthquake Engineering.* Peter J. May. April 2001.

PEER 2001/03 *A Modal Pushover Analysis Procedure to Estimate Seismic Demands for Buildings: Theory and Preliminary Evaluation.* Anil K. Chopra and Rakesh K. Goel. January 2001.

PEER 2001/02 *Seismic Response Analysis of Highway Overcrossings Including Soil-Structure Interaction.* Jian Zhang and Nicos Makris. March 2001.

PEER 2001/01 *Experimental Study of Large Seismic Steel Beam-to-Column Connections.* Egor P. Popov and Shakhzod M. Takhirov. November 2000.

PEER 2000/10 *The Second U.S.-Japan Workshop on Performance-Based Earthquake Engineering Methodology for Reinforced Concrete Building Structures.* March 2000.

PEER 2000/09 *Structural Engineering Reconnaissance of the August 17, 1999 Earthquake: Kocaeli (Izmit), Turkey*. Halil Sezen, Kenneth J. Elwood, Andrew S. Whittaker, Khalid Mosalam, John J. Wallace, and John F. Stanton. December 2000.

PEER 2000/08 *Behavior of Reinforced Concrete Bridge Columns Having Varying Aspect Ratios and Varying Lengths of Confinement.* Anthony J. Calderone, Dawn E. Lehman, and Jack P. Moehle. January 2001.

PEER 2000/07 *Cover-Plate and Flange-Plate Reinforced Steel Moment-Resisting Connections.* Taejin Kim, Andrew S. Whittaker, Amir S. Gilani, Vitelmo V. Bertero, and Shakhzod M. Takhirov. September 2000.

PEER 2000/06 *Seismic Evaluation and Analysis of 230-kV Disconnect Switches.* Amir S. J. Gilani, Andrew S. Whittaker, Gregory L. Fenves, Chun-Hao Chen, Henry Ho, and Eric Fujisaki. July 2000.

PEER 2000/05 *Performance-Based Evaluation of Exterior Reinforced Concrete Building Joints for Seismic Excitation.* Chandra Clyde, Chris P. Pantelides, and Lawrence D. Reaveley. July 2000.

PEER 2000/04 *An Evaluation of Seismic Energy Demand: An Attenuation Approach.* Chung-Che Chou and Chia-Ming Uang. July 1999.

PEER 2000/03 *Framing Earthquake Retrofitting Decisions: The Case of Hillside Homes in Los Angeles.* Detlof von Winterfeldt, Nels Roselund, and Alicia Kitsuse. March 2000.

PEER 2000/02 *U.S.-Japan Workshop on the Effects of Near-Field Earthquake Shaking.* Andrew Whittaker, ed. July 2000.

PEER 2000/01 *Further Studies on Seismic Interaction in Interconnected Electrical Substation Equipment.* Armen Der Kiureghian, Kee-Jeung Hong, and Jerome L. Sackman. November 1999.

PEER 1999/14 *Seismic Evaluation and Retrofit of 230-kV Porcelain Transformer Bushings*. Amir S. Gilani, Andrew S. Whittaker, Gregory L. Fenves, and Eric Fujisaki. December 1999.

PEER 1999/13 *Building Vulnerability Studies: Modeling and Evaluation of Tilt-up and Steel Reinforced Concrete Buildings.* John W. Wallace, Jonathan P. Stewart, and Andrew S. Whittaker, editors. December 1999.

PEER 1999/12 *Rehabilitation of Nonductile RC Frame Building Using Encasement Plates and Energy-Dissipating Devices.* Mehrdad Sasani, Vitelmo V. Bertero, James C. Anderson. December 1999.

PEER 1999/11 *Performance Evaluation Database for Concrete Bridge Components and Systems under Simulated Seismic Loads.* Yael D. Hose and Frieder Seible. November 1999.

PEER 1999/10 *U.S.-Japan Workshop on Performance-Based Earthquake Engineering Methodology for Reinforced Concrete Building Structures.* December 1999.

PEER 1999/09 *Performance Improvement of Long Period Building Structures Subjected to Severe Pulse-Type Ground Motions.* James C. Anderson, Vitelmo V. Bertero, and Raul Bertero. October 1999.

PEER 1999/08 *Envelopes for Seismic Response Vectors.* Charles Menun and Armen Der Kiureghian. July 1999.

PEER 1999/07 *Documentation of Strengths and Weaknesses of Current Computer Analysis Methods for Seismic Performance of Reinforced Concrete Members.* William F. Cofer. November 1999.

PEER 1999/06 *Rocking Response and Overturning of Anchored Equipment under Seismic Excitations.* Nicos Makris and Jian Zhang. November 1999.

PEER 1999/05 *Seismic Evaluation of 550 kV Porcelain Transformer Bushings.* Amir S. Gilani, Andrew S. Whittaker, Gregory L. Fenves, and Eric Fujisaki. October 1999.

PEER 1999/04 *Adoption and Enforcement of Earthquake Risk-Reduction Measures.* Peter J. May, Raymond J. Burby, T. Jens Feeley, and Robert Wood.

PEER 1999/03 *Task 3 Characterization of Site Response General Site Categories.* Adrian Rodriguez-Marek, Jonathan D. Bray, and Norman Abrahamson. February 1999.

PEER 1999/02 *Capacity-Demand-Diagram Methods for Estimating Seismic Deformation of Inelastic Structures: SDF Systems.* Anil K. Chopra and Rakesh Goel. April 1999.

PEER 1999/01 *Interaction in Interconnected Electrical Substation Equipment Subjected to Earthquake Ground Motions.* Armen Der Kiureghian, Jerome L. Sackman, and Kee-Jeung Hong. February 1999.

PEER 1998/08 *Behavior and Failure Analysis of a Multiple-Frame Highway Bridge in the 1994 Northridge Earthquake.* Gregory L. Fenves and Michael Ellery. December 1998.

PEER 1998/07 *Empirical Evaluation of Inertial Soil-Structure Interaction Effects.* Jonathan P. Stewart, Raymond B. Seed, and Gregory L. Fenves. November 1998.

PEER 1998/06 *Effect of Damping Mechanisms on the Response of Seismic Isolated Structures.* Nicos Makris and Shih-Po Chang. November 1998.

PEER 1998/05 *Rocking Response and Overturning of Equipment under Horizontal Pulse-Type Motions.* Nicos Makris and Yiannis Roussos. October 1998.

PEER 1998/04 *Pacific Earthquake Engineering Research Invitational Workshop Proceedings, May 14–15, 1998: Defining the Links between Planning, Policy Analysis, Economics and Earthquake Engineering.* Mary Comerio and Peter Gordon. September 1998.

PEER 1998/03 *Repair/Upgrade Procedures for Welded Beam to Column Connections.* James C. Anderson and Xiaojing Duan. May 1998.

PEER 1998/02 *Seismic Evaluation of 196 kV Porcelain Transformer Bushings.* Amir S. Gilani, Juan W. Chavez, Gregory L. Fenves, and Andrew S. Whittaker. May 1998.

PEER 1998/01 *Seismic Performance of Well-Confined Concrete Bridge Columns.* Dawn E. Lehman and Jack P. Moehle. December 2000.